Radiation response and combination target discovery in a novel model of rectal cancer



Callum J. Beach

A thesis submitted for the degree of Doctor of Philosophy University of Oxford

Department of Oncology

Hilary term 2024

Abstract

Radiation response and combination target discovery in a novel model of rectal cancer.

Submitted for the degree of Doctor of Philosophy Callum Beach, St. Hugh's

College, Hilary Term 2024

Rectal cancer is typically treated with radiotherapy, with or without chemotherapy, prior to surgical resection of the tumour. However, in patients that respond poorly to radiation, tumours largely lack significant immune cells within the surrounding milieu and present with a CAF-rich stroma. We have recapitulated this radioresistant phenotype *in vivo* through the implantation of $Apc^{fl/fl}$, $Kras^{G12D/+}$, $Trp53^{fl/fl}$, $Tgfbrl^{fl/fl}$ (AKPT) organoids. Here, through the irradiation of the heterotopic AKPT model, we have identified two targets for inhibition to augment the anti-tumour effect of radiation: complement C5a receptor 1 (C5aR1) and transforming growth factor beta (TGF-β).

We demonstrated that inhibiting C5aR1 increased the effectiveness of irradiation in the AKPT model both *in vitro* and *in vivo*. Inhibiting C5aR1 *in vitro* had a direct impact on tumour cell radiosensitivity in the AKPT organoid model. *In vivo* we demonstrated that bolstering radiation through C5aR1 inhibition acts independently to the T-cell population, as shown in athymic mice bearing AKPT tumours heterotopically. Furthermore, we hypothesise that additional effects on the macrophage and cancer-associated fibroblast (CAF) populations could contribute to the augmentation of radiation anti-tumour effects when C5aR1 is inhibited. We demonstrate an increase in the inflammatory macrophage population, as well as a shift in the CAF phenotype. Interestingly, the modest radiosensitisation observed *in vitro* suggest that¸ in the *in vivo* AKPT model, mechanisms altering the macrophage and CAF populations may be of greater importance than increased intrinsic radiosensitivity.

We also demonstrate that the inhibition of TGF-β increased the effectiveness of radiation *in vivo* in the AKPT heterotopic model. Furthermore, we show that the inhibition of this multifunctional cytokine, when combined with irradiation, has a dramatic effect on both the immune cells and CAFs within the tumour milieu. These changes include a significant increase of cytotoxic T-cell infiltration of the tumour epithelium, a significant decrease in the Treg population, a shift in the macrophages toward a more inflammatory phenotype, and a shift in the CAF phenotype. These changes were reflected by the enrichment of immunogenic gene signatures in the AKPT model after treatment with radiation combined with TGF-β inhibition, with immunosuppressive signatures showing a corresponding negative enrichment. We hypothesise that the shift in the CAF population phenotype is directly linked to the increase immunogenic action against the tumour. We further suggest that in the AKPT rectal cancer model, the CAF population acts to orchestrate the sustained immune response after irradiation, provided TGF-β is inhibited.

Supervisors

Professor Simon J Leedham Dr.

Monica M. Olcina Professor

Timothy Maughan Dr.

Anderson J Ryan

Assessment committee

Professor Geoff S. Higgins

Professor Campbell Roxburgh

The study presented in this thesis was performed at the Old Road Campus Research building, Department of Oncology, University of Oxford and at the Wellcome Centre for Human Genetics, University of Oxford. The work was supported by the CRUK ACRCelerate studentship award.

Word count: 42522 (excluding references)

Acknowledgments

I would like to start by thanking my supervisors that I have had the pleasure of working with. I will always be grateful to Simon for his support and guidance during my DPhil experience. I have no doubt that Simon's insightful feedback and constructive criticism has been instrumental in shaping the trajectory of my research. The opportunity Simon has provided me to present my work to a wide-ranging audience has also helped me refine my research and helped me develop professionally. Thank you again Simon for all you have done over these years during my DPhil experience.

I would also like to say thanks to Monica for how her mentorship became such a cornerstone of my doctoral experience. She gave me the confidence to develop then pursue my ideas; and provided innumerable constructive suggestions and meaningful discussion. Consider me a convert to team complement now and I excited to see the direction your lab takes in the future!

Also, many thanks to Tim for his help over the course of my DPhil. His clinical insight was undeniably crucial in my development as a scientist. Also, the philosophy under which Tim carries out his research is something I have found inspiring, and I will be taking it with me in my future endeavours.

Many, many thanks to Andy for his assistance during my doctoral experience. Going above and beyond to help me wherever possible, with no obligation to do so. His insight has been invaluable to me and without a doubt played a massive role not just in my research but in my growth as a person over these four years.

I would also like to thank members of Simon's lab, who have been extraordinarily helpful over the course of my DPhil in more ways than they know. Gabriel's tireless work in helping with the RNAseq analysis of the mountains of mouse tissue I have collected over these four years has been critical for my research. This work will likely have implications for future work in multiple labs and I can not thank you enough for your help with this. Thank you also to Hayley, who's assistance with *in vivo* experiments during my time has been critical in my research. The hours spent together doing orthotopic implantations is something I will always remember, even when it was not always successful! Thanks to Eoghan also, taking time to teach me how to analyse multiplex stained tissue was crucial for my research. The generosity he had with his wealth of knowledge surrounding colorectal cancer, TGF-β, and fibroblasts is something I am thankful for also.

Key laboratory personal have also been invaluable to helping me with my research. Firstly, Karla and Magda have been indescribably helpful for all they have done assisting in my *in vivo* work. Also, I am thankful to Leticia and the THL team for all there help with sample analysis.

Over the course of my cancer research journey, I have had some key mentors that have pushed me to reach this point. Firstly, I'd like to thank Claire for introducing me to cancer research and providing mentorship during my undergraduate degree at Swansea. I have no doubt she was influential in my chosen research field. Also, I would like to thank James for the introduction to cancer immunology during my time at King's College London. He has helped shaped me as a research scientist and prepared me exceptionally for my time undertaking doctoral research.

I would also like to acknowledge the support I have received from my family during the undertaking of this DPhil. Their willingness to listen to me talk about my research helped me more than they know. Also, their optimism and long phone calls when times were challenging gave me a second wind to continue. I have no doubt they are as excited as I am for the next chapter in my career.

I struggle to find the words to express my gratitude to Lisa for all her incredible support and patience during my time working on my DPhil. I am supremely grateful being championed in my academic and professional endeavours by her. While writing my thesis Gus and herself have been an incredible team to support me in completing my DPhil. I am looking forward to seeing what the next chapter has in store for the both of you and myself.

Table of Contents

Abstract..... **ii**

Acknowledgments..... **iv**

List of Tables and Figures..... **x**

List of abbreviations..... **xiv**

Chapter 1 Introduction..... **1**

1.1 Cancer..... **1**

1.2 Rectal cancer..... **2**

1.2.1 Rectal cancer epidemiology..... 2

1.2.2 Surgical treatment options..... 3

1.3 Radiotherapy..... **4**

1.3.1 Radiotherapy in rectal cancer treatment..... 4

1.3.3 Radiation impact on tumour cancer cells..... 7

1.3.4 Radiation impact on tumour stroma and immune populations..... 9

1.4 Radiotherapy response in rectal tumours...... **13**

1.4.1 Rectal cancer stratification..... 13

1.4.2 Phenotypic links to poor radiotherapy response..... 16

Aims of the thesis..... **18**

Chapter 2 Methods and materials..... **19**

2.1 AKPT organoid culture..... **19**

2.2 Animal studies..... **20**

2.2.1Heterotopic rectal tumour model..... 20

2.2.2 Orthotopic AKPT tumour model 21

2.2.3 C5aR1 inhibitor dosing 21

2.2.4 TGF-β inhibitor dosing 22

2.3 In silico screen **22**

2.4 Tissue staining **23**

2.4.1 Formalin-fixed paraffin embedded processing 23

2.4.2 Immunohistochemistry staining of AKPT tumours 23

2.4.4 In situ hybridisation staining 23

2.5 Multiplex and HALO analysis **24**

2.7 Longitudinal biopsies from rectal adenocarcinoma patients **25**

2.8 Analysis on longitudinal biopsies from rectal adenocarcinoma patients 25

2.8.1 Staining on longitudinal biopsies from rectal adenocarcinoma patients 25

2.8.2 RNA-sequencing of longitudinal biopsies from rectal adenocarcinoma patients 26

2.9 RNA-sequencing **27**

2.9.1 Organoids RNA extraction for sequencing 27

2.9.2 AKPT tumour RNA extraction for sequencing 27

2.9 Statistics **28**

Chapter 3 Optimisation of a novel rectal tumour model and target discovery post-irradiation . **29**

3.1 Establishment of an organoid model to recapitulate rectal tumours with poor treatment response 29

3.1.1 Key TME phenotypes needed for organoid model to recapitulate poor-responding rectal tumours 29

3.1.2 Key mutations required in organoid model to recapitulate rectal tumour phenotypes 30

3.1.3 Establishment of the heterotopic AKPT rectal cancer model 31

3.2 Radiation response of the heterotopic organoid model 33

3.3 Target identification for potential neoadjuvant therapies 44

3.4 Discussion 51

Chapter 4 Investigating the impact of C5aR1 inhibition on the radiation response of rectal cancer 53

4.1 Background 53

4.2 C5aR1 expression in the AKPT rectal tumour model 57

4.3 AKPT rectal tumour model response to the combination of irradiation and C5aR1 inhibition 62

4.3.1 Efficacy of C5aR1 inhibition as a neoadjuvant therapy alongside irradiation to improve AKPT tumour survival 62

4.3.3 RNAseq analysis of AKPT tumours post treatment with irradiation + C5aR1 inhibition 71

4.4 Discussion 76

Chapter 5 Investigating the impact of TGF-β inhibition on the radiation response in rectal cancer. 82

5.1 Background 82

5.2 Heterotopic AKPT model response to the combination of irradiation and TGF-β inhibition 86

5.2.1 Efficacy of TGF-β inhibition as a neoadjuvant therapy alongside irradiation to improve survival in the heterotopic AKPT tumour model 86

5.2.2 Immune and stromal population changes post combination treatment 89

5.2.3 RNAseq analysis of AKPT tumour post treatment with irradiation + TGF-β inhibition 98

5.3 Impact of AKPT rectal tumour growing in situ versus heterotopically 106

5.3.1 Impact of rectal environment on AKPT immune and stromal changes post Impact of rectal environment on AKPT immune and stromal changes post irradiation…… ……...106

5.3.2 RNA-seq analysis of heterotopic versus orthotopic AKPT tumours post combination treatment 113

5.4 Discussion..... **120**

Chapter 6..... **129**

Summary and conclusions..... **129**

6.1 Aims of the thesis..... **129**

6.2 Further avenues for investigation..... **130**

Appendices..... **132**

Appendix A..... **132**

Appendix B..... **156**

References..... **157**

List of Tables and Figures

Figure 1.1 The hallmarks of cancer.....2

Figure 1.3.4 The impact of Irradiated CAFs on tumour cells and the stromal immune cell milieu.....11

Table 2.1 AKPT organoid culture media components.....20

Figure 3.1.1 Immune cell composition of AKPT tumour TME prior to treatment.....32

Figure 3.1.2 Stromal composition of AKPT TME prior to treatment.....33

Figure 3.2.1 Survival curves of mice bearing heterotopic AKPT tumours treated with 0Gy (A), 3x7Gy (B), or 15Gy (C).....35

Figure 3.2.2 Volume growth curves of mice bearing heterotopic AKPT tumour treated with 0Gy (A), 3x7Gy (B), or 15Gy (C).....36

Figure 3.2.3 $CD8^+$ T-cell population changes in heterotopic AKPT tumours post single- dose or after the final fraction of 3x7Gy irradiation.....38

Figure 3.2.4 $CD4^+$ T-cell population changes in heterotopic AKPT tumours post single- dose or after the final fraction of 3x7Gy irradiation.....39

Figure 3.2.5 Treg ($FOXP3^+$) T-cell population changes in heterotopic AKPT tumours post single-dose or after the final fraction of 3x7Gy irradiation.....41

Figure 3.2.6 Neutrophil population changes in heterotopic AKPT tumours post single- dose or after the final fraction of 3x7Gy irradiation.....42

Figure 3.2.7 Macrophage population changes in heterotopic AKPT tumours post single-dose or fractionated irradiation.....43

Figure 3.3.1 Identification of complement pathway upregulation post irradiation.....45

Figure 3.3.2 C5aR1 as a druggable target in rectal cancer.....46

Figure 3.3.3 C5aR1 expression (CPM) assessed by RNA-seq in wildtype (WT) or AKPT organoids grown *in vitro*......47

Figure 3.3.4 Prognostic factors in patient rectal tumours predicting response to radiotherapy 48

Figure 3.3.5 TGF-β signalling pathway upregulation in heterotopic AKPT tumours after receiving radiation and activin staining of AKPT tumours. 50

Figure 3.3.6 Heat map of the top 20 enriched genes after irradiating *in vivo* AKPT tumours with a 3x7Gy fractionation 51

Figure 4.1.1 Quantification of C5aR1 IHC staining in AKPT tumours 58

Figure 4.1.2 Changes to immune cell population within C5aR1^{+} stained areas after irradiation 59

Figure 4.1.3 C5aR1 staining of longitudinal rectal biopsies from patients with rectal adenocarcinoma 60

Figure 4.1.4 AKPT organoid survival after receiving radiation + PMX205. 61

Figure 4.3.2 Volume growth curves of mice bearing heterotopic AKPT tumour treated with PMX205 (A) or radiation + PMX205 (B) 63

Figure 4.3.3 Survival curves of athymic nude mice bearing heterotopic AKPT tumours treated with radiation + PMX205. 65

Figure 4.3.4 Volume growth curves of athymic nude mice bearing heterotopic AKPT tumour treated with PMX205 (A) or radiation + PMX205 (B) 66

Figure 4.3.7 Fibroblast population changes in heterotopic AKPT tumours post radiation + PMX205. 70

Figure 4.3.8 GSEA reactome network plot of top-level pathways enriched after AKPT tumour irradiation 71

Figure 4.3.9 GSEA reactome network plot of top-level pathways enriched after AKPT tumour C5aR1 inhibition. 72

Figure 4.3.11 Selected signature enrichment GSEA comparing M1-like macrophages in treated AKPT tumours. 74

Figure 4.3.12 Selected signature enrichment GSEA comparing CAF phenotypes in irradiated AKPT tumours......76

Figure 5.2.1 Survival curves of mice bearing heterotopic AKPT tumours treated with radiation + TGF-β inhibition.....87

Figure 5.2.2 Volume growth curves of athymic nude mice bearing heterotopic AKPT tumour treated with or without TGF-β (A) or radiation + TGF-β inhibition (B).....88

Figure 5.2.3 $CD8^+$ T-cell population changes in heterotopic AKPT tumours post treatment + radiation + TGF-βi.....90

Figure 5.2.4 Treg ($FOXP3^+$) T-cell population changes in heterotopic AKPT tumours post treatment + radiation + TGF-βi......92

Figure 5.2.7 GSEA reactome network plot of top-level pathways enriched after AKPT tumour irradiation.....99

Figure 5.3.1 $CD8^+$ T-cell population changes in between heterotopic and orthotopic AKPT tumours post treatment + radiation + TGF-βi.....107

Figure 5.3.2 Treg population changes in between heterotopic and orthotopic AKPT tumours post treatment + radiation + TGF-βi.....108

Figure 5.3.3 $CD4^+$ population changes in between heterotopic and orthotopic AKPT tumours post treatment + radiation + TGF-βi.....109

Figure 5.3.4 Neutrophil population changes in between heterotopic and orthotopic AKPT tumours post treatment + radiation + TGF-βi.....110

Figure 5.3.5 Macrophage population changes in between heterotopic and orthotopic AKPT tumours post treatment + radiation + TGF-βi.....111

Figure 5.3.6 Fibroblast population changes in between heterotopic and orthotopic AKPT tumours post treatment + radiation + TGF-βi.....112

Figure 5.3.7 GSEA reactome network plot of top-level pathways enriched in the orthotopic AKPT tumour versus the subcutaneous setting after irradiation.....114

Figure 5.3.9 GSEA reactome network plot of top-level pathways enriched in the orthotopic AKPT tumour versus the subcutaneous setting after irradiation and TGF-β inhibition.....116

Figure 5.3.10 Selected signature enrichment GSEA comparing immunogenicity and immunosuppression in treated AKPT orthotopic tumours.....117

Figure 5.3.11 Selected signature enrichment GSEA comparing M1-like macrophages in treated orthotopic AKPT tumours......118

Figure 5.3.12 Selected signature enrichment GSEA comparing CAF phenotypes in treated AKPT tumours......120

List of abbreviations

5-FU	5-Fluorourcil
AB/A-M	Antibiotic/Antimycotic
AKPT	*Apc$^{fl/fl}$, Kras$^{G12D/+}$, Trp53$^{fl/fl}$, Trgfbrl$^{fl/fl}$*
AKT	Protein Kinase B
ALDOA	Aldolase A
ALS	Amyotrophic Lateral Sclerosis
ANOVA	Analysis of Variance
APC	Adenomatous Polyposis Coli
ATM	Ataxia-telangiectasia
ATP	Adenosine Triphosphate
ATR	Ataxia Telangiectasia and Rad3-related
BED	Biologically Effective Dose
BST	Bone Marrow Stromal Cell Antigen 2
C4BPA	Complement Component 4 Binding Protein Alpha
CAF	Cancer-associated fibroblast
CCL	Chemokine Ligand
CD4	Cluster of Differentiation 4
CD8	Cluster of Differentiation 4
cGAS-STING	Cyclic GMP-AMP synthase- stimulator of interferon genes
CMS	Consensus Molecular Subtype
CPM	Counts per million
CR1	Complement Receptor 1
CRIS	Colorectal Cancer Intrinsic Subtypes

CRISPR	Clustered Regularly Short Palindromic Repeats
CSC	Cancer Stem Cells
CT	Computated Tomography
CTLA-4	Cytotoxic T-Lymphocyte Associated Protein 4
CXCR3	C-X-C Motif Chemokine Receptor 3
DAB	(3,3'-Diaminobenzidine)
DAMP	Danger-associated Molecular Patterns
DAPI	(4',6-diamidino-2-phenylindole)
DDR	DNA Damage Repair/Response
DFS	Disease-Free Survival
DMEM	Dulbecco's Modified Eagle Medium
DMSO	Dimethylsulfoxide
DNAPK	DNA-Dependent Protein Kinase
DSB	Double-strand Break
ECM	Extracellular Matrix
EGF	Epidermal Growth Factor
EGFR	Epidermal Growth Factor
EMT	Epithelial-Mesenchymal Transition
FCGR	FC-γ Receptor
FDR	False Discovery Rate
FFPE	Formalin-Fixed Paraffin-Embedded
FOLFOX	Folinic acid, 5-fluorouracil, oxaliplatin
FOXP3	Forkhead box P3
HEPES	(4-(2-hydroxyethyl)-1-piperazineethanesulfonic acid
HGSC	High-Grade Serous Carcinoma

IDO	Indoleamine 2,3-dioxygenase

IGF2	Insulin-Like Growth Factor
IHC	Immunohistochemistry
IL	Interleukin
ISH	*In situ* Hybridisation
KRAS	Kirsten Rat Sarcoma Virus
LDHA	Lactate Dehydrogenase-A
LGALS9	Galectin-9
MAPK	Mitogen-activated protein kinases
MDSC	Myeloid-derieved Stem Cells
MET	MNNG HOS Transforming Gene
MHC	Major Histocompatability Complex
MMP	Matrix Metalloproteinase
MSI	Microsatellite Instability
MYC	MYC Myelocytomatosis Oncogene
NCT	National Clinical Trial
NES	Normalised Enrichment Score
NET	Neutrophil Extracellular Traps
PARP	Poly (ADP-ribose) ploymerase
PBS	Phosphate-buffered Saline
pCR	Pathological Complete response
PD-1	Programmed Cell Death Protein 1
PDFGRα	Platelet-Derieved Growth Factor alpha
PD-L1	Programmed Death-Ligand 1
PI3K	Phosphoinositide 3-kinase
PPAR	Peroxisome Proliferator-Activated Receptors
RNA	Ribonucleic acid

SARRP	Small Animal Radiation Research Platform
SER	Sensitivity Enhancement Ratio
STAT	Signal Transducer and Activator of Transcription
SUMO	Small Ubiquitin-Like Modifier
TAM	Tumour-associated Macrophage
TAMIS	Transanal Minimally Invasive Surgery
TCA	Tricarboxylic Acid
TGF-β	Transforming growth factor beta
TIMP	TIMP Metallopeptidase inhibitor 1
TLR	Toll-Like Receptor
TME	Tumour microenvironment
TP53	Tumour Protein 53
Treg	Regulatory T-cell
TXN1	Thioredoxin 1
VEGF	Vascular Endothelial Growth Factor
VEGFR	Vascular Endothelial Growth Factor Receptor
VSIG4	V-set immunoglobulin-domain-containing 4
WNT	Wingless-related integration site
WT	Wildtype
α-SMA	Alpha Smooth Muscle Actin

Chapter 1

Introduction

1.1 Cancer

Cancer is a group of diseases in which cells undergo uncontrolled or aberrant growth that can then lead to the invasion of distant tissues (Hanahan & Weinberg, 2000). A landmark article illustrated six acquired characteristics that, when adopted by cells, directly lead to improved survival, increased inappropriate proliferation, and an invasive phenotype (Hanahan & Weinberg, 2000). These characteristics were then updated in to include two emerging hallmarks as well as two more enabling phenotypes (Hanahan & Weinberg, 2011). Both the deregulation of cellular metabolism and the proficiency that cancer cells demonstrate in evading detection and subsequent destruction by the immune system were the two new hallmarks. These hallmarks are summarised in Figure 1.1. Particularly relevant to this thesis, these hallmarks cover the dichotomy of tumour-promoting inflammation, paradoxically key in the early stages of tumorigenesis, and the evasion of immune destruction by the tumour, through the establishment of an immunosuppressive tumour microenvironment (TME) (Hanahan & Weinberg, 2011).

Moreover, the evasion of immune system facilitated destruction by the tumour lends itself to other important features in both cancer progression as well as treatment resistance. A characteristic of the evasion of immune destruction is the establishment of a specific millieu of cells with numerous and diverse roles within the TME (Gonzalez et al., 2018). The immune cell populations provide various inputs into the TME, both through crosstalk with each other and the tumour cells, that contribute to the adaptiveness of cancer as a disease (Gonzalez et al., 2018). Pivotal to the present work is the identification of druggable targets within this adaptive TME that can act to counteract the

immunosuppressive phenotype that forms within and around the tumour. The work in this thesis will also look to identify targets that act to assist in the recovery of the tumour post treatment, specifically radiotherapy.

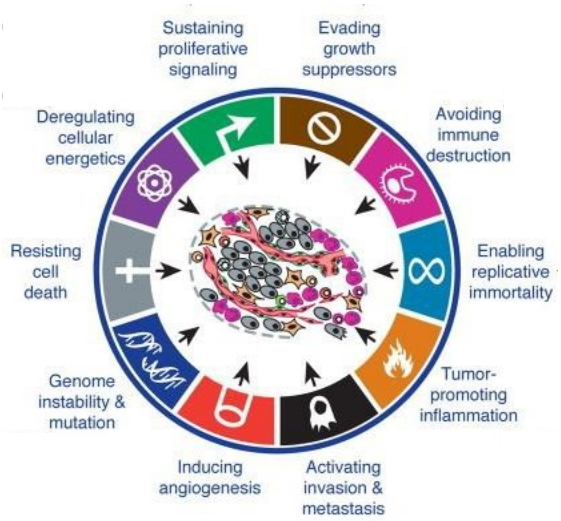


Figure 1.1 The hallmarks of cancer
An illustration of the combination of the original hallmarks of cancer as described in 2000 together with the updated emerging hallmarks and enabling capabilities as described by (Hanahan & Weinberg, 2011). Adapted and reprinted from Cell, vol 144 issue 5, 4 March 2011, Hanahan, D. and Weinberg, R., A., Hallmarks of Cancer: The next generation, 646-674, Copyright (2011).

1.2 Rectal cancer

1.2.1 Rectal cancer epidemiology.

Colorectal cancer is the third most common cancer and the second leading cause of cancer-related deaths globally (Xi & Xu, 2021). Rectal cancer accounts for one-third of these cases despite only accounting for 15-20% of the length of the combined colon and rectum (Ferlay et al., 2018). Despite a trend of decreased incidence and mortality from colorectal cancer, the incidence of the disease in patients under fifty years of age has increased markedly. In Europe incidence of disease increased at rates of 7.9% per year from 2004 to 2016 in patients aged 20 to 29; 4.9% per year from 2005 to 2016 in patients aged 30 to 39; and 1.6% per year from 2004 to 2016 in patients aged 40 to 49 with a lack of significant change to mortality (Vuik et al., 2019). This trend is mirrored for

patients within the United States, with the incidence estimated to rise by 124.2% for those aged 20 to 34 by 2030 (Bailey et al., 2015). With the increased incidence of rectal cancer in younger patient cohorts over the past ten years, combined with the failure to significantly reduce mortality rates over this timespan, improvements to current treatments are critical. With increased screening focusing on the over fifty age bracket (Cho et al., 2022), this increased incidence in younger patients is especially important as earlier onset disease may be missed by current screening methods. Additionally, functional outcomes and quality of life after rectal cancer surgery remains suboptimal (Gavaruzzi et al., 2014). This suboptimal quality of life experienced by patients has not significantly improved even with the improvement of surgical techniques. This is exemplified by the inability of the introduction of sphincter- preserving surgery to improve patient quality of life twenty-four months post-treatment (Pappou et al., 2022). Therefore, improvements to current rectal cancer treatments need to be developed both to increase treatment efficacy and to improve patient quality of life post-treatment.

1.2.2 Surgical treatment options.

Surgical treatment continues to play a key role in the treatment of rectal cancer. In 1982, Heald described the implementation of total mesorectal excision in surgically removing rectal tumours (Heald et al., 1982). Total mesorectal excision is performed through sharp dissection within the anatomical plane surrounding the mesorectal fascia to remove the entire mesorectal envelope, along with the venous and lymphatic drainage components of the rectum contained within. Depending on factors surrounding the patient and tumour size, total mesorectal excision can be performed either through open surgery or laparoscopically. An adapted approach to total mesorectal excision, Transanal total mesorectal excision, in which the majority of pelvic dissection is performed from the perineum rather than within the abdominal cavity. Although this updated take on total mesorectal excision surgery had positive results initially (Aubert et al., 2020) adoption of this technique has raised concerns regarding high local recurrence rates (Wasmuth et al., 2020). Stage 1 and 2 rectal cancer, with smaller tumours can be treated through transanal minimally invasive surgery (TAMIS) (Althumairi & Gearhart, 2015). The TAMIS

approach has similar efficacy to total mesorectal excision whilst providing much improved outcomes regarding quality of life. Therefore, it is critical when attempting to improve on existing surgical approaches of rectal cancer treatment to spare as much rectal tissue/function as possible in order to maintain a good patient quality of life. This can be attempted through the use of neoadjuvant treatments pre-operatively. In patients who demonstrate a complete clinical response to neoadjuvant therapies, the opportunity for adopting a “watch and wait” approach becomes available (Byun & Koom, 2023). To improve quality of life, patients who experienced a complete clinical response to neoadjuvant therapies underwent active surveillance rather than TME surgery. The effectiveness of this approach has been discussed (Byun & Koom, 2023) and is currently being tested in phase 3 clinical trials (NCT02704520 and NCT04095299). Therefore, improving current neoadjuvant therapies for rectal cancer could have a dramatic impact on the quality of life in patients and may spare some from radical rectal surgery. A consistent neoadjuvant therapy used in rectal cancer is radiotherapy, either in isolation or combined with chemoradiotherapy (Feeney et al., 2019), and is key in the adoption of the wait and see approach to treatment.

1.3 Radiotherapy

1.3.1 Radiotherapy in rectal cancer treatment.

Following the introduction of total mesorectal excision as the gold standard for surgical rectal cancer care, the role of radiotherapy was challenged (MacFarlane et al., 1993). However, the advantages of neoadjuvant radiotherapy were first recognised in 1997 (Swedish Rectal Cancer Trial et al., 1997). Crucially, the study found a significant decrease in in local recurrence rates when comparing a combined approach versus surgery in isolation (11% vs 27%). Though neoadjuvant therapy had little impact on postoperative mortality, 5-year survival was significantly improved in the radiotherapy group (58% vs 48%). Additionally, further short course (5 Gy x 5 days) trials have illustrated the importance of preoperative radiotherapy combined with total mesorectal excision in reducing local recurrence rate in patients (Kapiteijn et al., 2001; Marsh et al., 1994; Martling et al., 2005; Sebag-Montefiore et al., 2009; Swedish Rectal Cancer Trial et

al., 1997; van Gijn et al., 2011).

Currently there are two courses of radiotherapy used in the treatment of rectal cancer in the clinic: a short course of 5 Gy over 5 days with surgery usually performed within a week of the final fraction (Wo et al., 2021), and a long course of 45-50.4 Gy delivered in 25-28 daily fractions with surgery usually performed 4-6 weeks after the final fraction (Glynne-Jones et al., 2017). Typically, the use of a long course schedule of radiotherapy is combined with a concurrent chemotherapy regimen, such as 5-Fluorourcil (5-FU) (Minsky, 2012). The short course schedule of radiotherapy typically was performed without the concurrent use of chemotherapy currently within the clinic. However, following the results of the RAPIDO trial (Bahadoer et al., 2021) the use of chemotherapy after the completion of the radiation treatment is now considered, especially in locally advanced disease. When comparing these two modes of radiotherapy, randomized trials have demonstrated no significant differences with regard to local control, late toxicity, or survival (Bujko et al., 2006, 2016; Ngan et al., 2012).

Post-operative radiotherapy was implemented as a standard of care in locally advanced rectal cancer after demonstrating improved survival (Fisher et al., 1988; Krook et al., 1991; Thomas & Lindblad, 1988). However, with significant treatment-related side effects occurring in up to 61% of patients, (Sauer et al., 2004) the sequencing of radiotherapy with surgical intervention was investigated. This investigation culminated in the German Rectal Cancer Trial, testing preoperative versus postoperative radiotherapy (Sauer et al., 2004). This study concluded that efficacy and safety treatment outcomes were significantly improved in the preoperative group versus postoperative, with 5-year locoregional control (6% versus 13%) and 10-year cumulative recurrence rates (7.1% versus 10.1%), as well as improved quality of life for patients, with a higher rate of sphincter-sparing surgery (39% versus 19%). Overall survival was not significantly increased but due to the lower-rate of treatment-related toxicity, preoperative radiotherapy became the preferred standard of care.

Although preoperative radiotherapy has become a standard for neoadjuvant therapy in rectal cancer, there is still scope to improve the efficacy of this treatment and

potentially expand watch-and-wait approaches that could further improve patient quality of life.

1.3.2 Current landscape of neoadjuvant treatment in rectal cancer.

Improving radiotherapy through combination treatments is of great interest (H. H. W. Chen & Kuo, 2017). A current standard of neoadjuvant therapy prior to surgery involves a course of5-FU combined with radiotherapy. 5-FU acts to increase radiosensitisation when administered before or after radiation (Lawrence et al., 2003). 5-FU radiosensitisation mainly occurs through the inhibition of deoxythymidine monophosphate formation that leads to an imbalance in the deoxynucleotide pool, ultimately causing the arrest of *de novo* DNA synthesis and repair (Azwar et al., 2021). This impairment of DNA damage repair acts to sensitise tumours to irradiation. This use of 5-FU to augment the anti tumour effects of radiotherapy is the standard of care in the long course schedule of radiation delivery (Minsky, 2012).. This approach provides a pathological complete remission (pCR) of the disease in only 11-18% of patients (Deng et al., 2016; Haustermans et al., 2014; Rödel et al., 2015). However, the incorporation of other chemotherapy agents in addition to 5-FU is currently under investigation. Currently, the most compelling evidence provides some support for combining oxaliplatin treatment with standard 5-FU chemoradiotherapy. From the six phase III trials published so far, a significant increase in pCR rates has been found in two of these (Deng et al., 2016; Rödel et al., 2015), with one of these trials also demonstrating significantly improved survival (Rödel et al., 2015). However, all other trials failed to demonstrate improvements in major clinical outcomes and provided evidence for increased toxicity (Aschele et al., 2011; Gérard et al., 2010, 2012; O'Connell et al., 2014).

Following the results of the RAPIDO trial, patients with locally advanced rectal tumours can also be considered to receive chemotherapy following the completion of the short course of radiotherapy (Bahadoer et al., 2021). Typically, these patients receive capecitabine and oxaliplatin after the completion of radiotherapy (Bahadoer et al., 2021). After the administration of capecitabine, it is enzymatically converted to 5-FU (Walko & Lindley, 2005). This typically leads to the accumulation of 5-FU within the tumour and causes the impairment of DNA synthesis and repair as previously described (Walko &

Lindley, 2005). With tumours undergoing rapid mitosis, this inhibition of DNA synthesis especially impacts the cancerous cells (Levine & Holland, 2018). Oxaliplatin acts to exert its cytotoxic effect mainly through DNA damage through a number of different mechanisms including: the formation of DNA intra-strand and DNA-protein crosslinks; the arrest of DNA synthesis; and the inhibition of messenger RNA synthesis (Alcindor & Beauger, 2011).

The use of other chemotherapeutic agents, outside of the ones already in use for rectal cancer treatment in the clinic have also been investigated. Large-scale clinical trials looking to investigate the ability of other chemotherapeutic agents to improve the current standard chemoradiotherapy course include: irinotecan, with the phase III ARISTOTLE trial failing to improve pCR rate but increasing adverse events (Sebag-Montefiore et al., 2020); bevacizumab, demonstrating high rates of severe acute toxicities (Landry et al., 2013); and cetuximab, failing to significantly improve pCR rates (Bazarbashi et al., 2016; Gollins et al., 2017; Pinto et al., 2018).

Importantly, for the future of rectal cancer treatment, a pilot study in 2014 demonstrated that the use of preoperative fluorouracil, leucovorin, and oxaliplatin (FOLFOX) with bevacizumab, a vascular endothelial growth factor A (VEGF-A) inhibitor slowing tumour angiogenesis, was able to replicate the low local recurrence rates as found in a standard chemoradiotherapy regimen (Schrag et al., 2014). These findings were followed up by the PROSPECT trial, comparing chemotherapy alone versus chemoradiotherapy in the treatment of patients with locally advanced rectal cancer undergoing surgery (NCT01515787) (Schrag et al., 2023). This trial found that preoperative FOLFOX was noninferior to preoperative chemoradiotherapy with respect to disease-free survival. When considering toxic effects, severe post-operative events were more common in the chemoradiotherapy group (25.6% versus 32.6%). In the chemoradiotherapy group the most common sever adverse effects were neutropenia and diarrhea, whereas in the FOLFOX group the most common severe adverse effects were neutropenia, diarrhea, and hyponatremia. Conversely, patients receiving FOLFOX treatment demonstrated a greater incidence of toxic events during treatment than the

patients receiving chemoradiotherapy (41% versus 22.8%). However, the treatment period for the FOLFOX regimen was a minimum of 12 weeks versus the 5.5 weeks of chemoradiotherapy, therefore providing a rationale behind this significant increase in toxicity during the administration of FOLFOX treatment in comparison to chemoradiotherapy. . These findings, combined with a small-scale phase two trial demonstrating twelve of twelve patients with tumours containing high microsatellite instability respond completely using immunotherapy alone (NCT04165772) (Cercek et al., 2022), provides support for the idea of more customisable treatment in treating locally advanced rectal cancer.

For the scope of this thesis, there will be a specific focus on improving radiation treatment in isolation. The rationale behind this is the idea that improving radiotherapy outside of additional chemotherapeutic agents may lead to an improved preoperative anti- tumour effect whilst keeping toxic events within an acceptable threshold. Additionally, as radiotherapy acts as a local treatment rather than the systemic chemotherapy approach, further reduction of toxic side effects in patient treatment can be aspired to.

1.3.3 Radiation impact on tumour cancer cells.

Radiotherapy has a profound effect on the tumour and its surrounding environment, with irradiation beginning a cascade of an enormous number of different compensatory pathways. Specific to the tumour itself, a key aspect of radiotherapy is the arrest of cancer cell proliferation and induction of cell death (Baskar, 2010). This occurs through both direct action on tumour cells, through the damage of DNA (Baskar, 2010; Ward, 1988)., or indirectly through the ionisation of water in cells (about 80% of the cellular contents) to generate reactive oxygen species (ROS) that act to indirectly damage DNA (Baskar, 2010; Ward, 1988). Due to the abnormally high replication rate and defects in the DNA damage response machinery, tumours are left more vulnerable than the surrounding normal tissue to irradiation (Adjemian et al., 2020;

Srinivas et al., 2019). This damage to DNA leads to the induction of potentially lethal DNA double-strand breaks that can affect the fate of tumour cells (Table 1.3.3).

After the induction of DNA damage after irradiation, the most common form of cell death occurs through the mitotic catastrophe mechanism (Cohen–Jonathan et al., 1999). With dysfunctional cell cycle checkpoints being a common hallmark of cancer cells, radiation-damaged cells are able to enter mitosis prematurely with misrepaired DNA, leading to mitotic catastrophe (Cohen–Jonathan et al., 1999; Ross, 1999). Mitotic catastrophe is morphologically defined by unique nuclear changes including: multinucleation and micronucleation, both caused through the mis-segregation of uncondensed chromosones, as well as micronucleation, occurring through lagging chromosomes or chromosomal fragments during anaphase that remained outside of the daughter cell nuclei (Imreh et al., 2011). In cells undergoing the normal mitotic process, significant levels of DNA damage is detected by the G2 checkpoint leading to mitotic arrest and subsequent DNA damage repair or programmed cell death (Mc Gee, 2015). However, within a large number of cancer cell types there is an ineffective G2 checkpoint screening process prior to the entering mitosis (Vitale et al., 2011). Therefore, with irradiation of the cancer cells causing significant DNA damage, this mitotic entry in the presence of DNA strand breaks leads to a mitotic catastrophe. Following on from this cancer cells are met with three specific fates: death while undergoing mitosis within the presence of cyclin B following engagement of cell death machinery; during G1 of the next cell cycle after exiting the process of mitosis; and undergoing senescence after exiting mitosis (Mc Gee, 2015). In the cancer cell populations undergoing death during or after catastrophic mitosis, the eventual mode of mitotic cell death has been demonstrated to be determined by the presence of p53 (Mc Gee, 2015). Cancer cells with p53 expression undergo caspase-mediated apoptosis, whereas in the absence of p53 mitotic catastrophe causes cells to undergo necrosis (H et al., 2006, 2008; Imreh et al., 2011). Mitotic cell death of cancer cells refers to the regulated cell death driven by this mitotic catastrophe, with the p53 status of the tumours defining the mode of cellular execution (Galluzzi et al., 2018).

Table 1.3.3 Types of tumour cell death undergone after radiotherapy and the corresponding characteristics and features.

Type of cell fate	Characteristics	Features	References
Mitotic cell death	Lethal, immunogenic or nonimmunogenic	Cells with DNA damage entering mitosis,	(Cohen–Jonathan et al., 1999; Imreh et al., 2011; Mc Gee, 2015)
Apoptosis	Lethal, nonimmunogenic	Homeostatic cellular control, formation of apoptotic bodies	(Long et al., 2014; M. Wang et al., 2020)
Necrosis	Lethal, immunogenic	Cell swelling leading to rupture	(Hellevik & Martinez-Zubiaurre, 2014; Lauber et al., 2012)
Necroptosis	Lethal, immunogenic	Programmed cell death with necrotic morphology,	(Y. Yang et al., 2021)
Pyroptosis	Lethal, immunogenic	Gasdermin mediated pore formation with necrotic morphology	(Tan et al., 2022; T. Zhang et al., 2022)
Ferroptosis	Lethal, immunogenic	Lipid peroxide induced cell death with necrotic morphology, iron-dependent	(L. Feng et al., 2021; Lei et al., 2021)
Cuproptosis	Lethal, immunogenic	Copper and protein acylation in TCA cycle with necrotic morphology	(Jie et al., 2007; Oliveri, 2022)
Senescence	Non-lethal, immunogenic	Cellular loss of the ability to proliferate	(Marin et al., 2023; Tabasso et al., 2019)

Critically, while radiation has a significant impact on tumour cells through causing cell death or the cessation of cellular proliferation, there is also a significant impact on the surrounding TME. Compounding the impact of irradiation on the milieu within and around the tumour, a number of cell death fates are also highly immunogenic. This, combined with further cellular signalling (Barker et al., 2015) from the surviving irradiated tumour cells, causes further alterations to an already tumultuous setting post-irradiation.

1.3.4 Radiation impact on tumour stroma and immune populations.

The development of tumours requires the modulation of the immune system toward evade growth suppression (Dunn et al., 2004). This process of cancer immunoediting is a dynamic process composed of three key phases that must be passed through:

elimination of cancer through immunosurveillance, equilibrium, and escape (Dunn et al., 2004). Within the elimination stage, the innate immune cells, including natural killer cells and macrophages, as well as their adaptive counterparts, including dendritic cells as well as the $CD8^+$ and $CD4^+$ T-cells, interact with the highly immunogenic tumour cells present at the early stage of carcinogenesis (Dunn et al., 2004). This cohort of immune cells, forming the cancer surveillance network, typically act to eradicate growing tumours. However, due to the inherent genetic instability of the tumour, cells harbouring resistance to an immune attack may emerge but remain under control of the immune system, thereby entering a state of equilibrium. Within this state of equilibrium new populations of cancer cell variants may form that can then escape the immune system. At this point, cancer cells expressing fewer antigens and demonstrating the ability to edit the surrounding microenvironment can arise. After these cancer cells have adapted under constant immunological pressure, survival and subsequent growth of the tumours are supported by the through recruitment of immunosuppressive cells, such as regulatory T-cells or myeloid-derived suppressor cells (Dunn et al., 2004; Vesely et al., 2011). Within the newly established microenvironment, immunosuppressive metabolites such as arginase-1 and lactate, chemokines, and cytokines act to further aid in the evasion of immunosurveillance by the tumour. Additionally, these tumour cells that have escaped immune destruction can also express factors to avoid immunogenic cell death, such as programmed-death ligand 1 (PD-L1) (Yao et al., 2018). Typically the surrounding microenvironment in these growing tumours settles as: a deserted phenotype with anti-tumour immune cells becoming absent from both the tumour itself as well as its periphery; an exclusionary phenotype with anti-tumour immune cells being able to accumulate within the periphery but being unable to infiltrate the tumour itself; or an inflamed phenotype with anti-tumour immune cells being present within the tumour itself but their effectiveness having been inhibited (Liu & Sun, 2021). Typically tumours surrounded by a microenvironment with an inflamed phenotype are more sensitive to irradiation in comparison with tumours surrounded by a setting sparse in immune cells (Mortezaee & Najafi, 2021).

Within the stroma surrounding tumour cells, there are many different immune

populations that are all impacted by irradiation (de Andrade Carvalho & Villar, 2018). Additionally, irradiation typically triggers a network of crosstalk between these different populations to facilitate a response. The response of the stromal microenvironment is known to go through two phases of reaction to irradiation. Acutely, a strong immunogenic response is generated that temporarily increases anti-tumour immunity (Rückert et al., 2021). However, in patients who do not demonstrate a pCR to radiotherapy, radiation resistance is developed by the tumour. A key aspect of this resistance is the development of an immunosuppressive setting that quenches the newly established immunogenic response post-irradiation (Rückert et al., 2021). Historically the lethal biological effects of radiotherapy were attributed to its ability to induce DNA damage, primarily DNA double-strand breaks (DSBs) with the idea that this mechanism was immunosuppressive due to the killing of radio sensitive lymphocytes within the tumour stroma (Trowell, 1952). However, current evidence suggests that radiotherapy serves to deconstruct much of the immunosuppressive machinery within the stroma (Golden & Apetoh, 2015).

Radiotherapy is able to change the immunosuppressive microenvironment in favorable ways mainly through immunogenic cell death-related mechanisms (Ngwa et al., 2018). Generally, immunogenic cell death is characterised by the release of damage-associated molecular patterns (DAMPs) from cells after their membrane integrity is lost, typical in cells having undergone necrosis and necroptosis, but other types of cell death including apopotosis, pyroptosis, and ferroptosis also contribute to the release of DAMPs (Murao et al., 2021). DAMPs are typically located within cells under normal physiological conditions, however when they are detected by immune cells on the cell surface or in the intercellular space they indicate damaged tissue and induce an immunogenic response (Krysko et al., 2017). Well documented molecules that act as DAMPs include: the chromatin stabilisation protein high-mobility group box 1 (HMGB1); calreticulin; the energy transmitting molecule ATP; and chaperons of the family of the family of heat shock proteins such as HSP70 (Krysko et al., 2017). The expression of DAMPs by the tumour cells then act to both mediate chemotaxis of antigen-presenting cells (APCs) as well as a phagocytosis signal. This fosters antigen uptake by the APCs, the induction of

their maturation, and subsequent antigen presentation that leads to the priming of cytotoxic T-cells (Galluzzi et al., 2017). Expression of DAMPs on the tumour cell surface also act to directly activate and trigger the cytolytic activity of natural killer cells (Gaipl et al., 2014). Additionally, radiotherapy renders the tumour cell surface more immunogenic through the induction of both CD80 and major histocompatibility complex class I (MHC-I) alongside the upregulation of death receptors and stress ligands (Formenti & Demaria, 2013; Reits et al., 2006). These death receptors include CD95, and the tumour necrosis factor-related apoptosis-inducing ligand (TRAIL) receptors 1 and 2 (TRAIL-R1 and TRAIL-R2). Both death receptors, when activated, render tumour cells more vulnerable to apoptosis and can be used by cytotoxic T-cells as well as natural killer cells as a mechanism to kill cancer cells (Kroemer et al., 2013).

With MHC-I being downregulated in most cancers and being linked with poor patient prognosis (Cornel et al., 2020), the upregulation of this critical cytotoxic mediating receptor after radiotherapy plays a key role in the generation of an anti-cancer immune response. Following the upregulation of MHC-I on the tumour cell surface, the activation of the full T-cell repertoire is facilitated (X. Wang et al., 2016). Crucially, MHC-I upregulation after irradiation of tumour cells allows for improved targeting by cytotoxic T-cells. A key aspect of revolves around the generation of neoantigens after irradiation. Neoantigens are tumour-specific antigens that are expressed on the cell surface due to the accumulation of numerous DNA mutations. This accumulation of DNA mutations, and subsequent tumour-specific antigen formations, is further compounded by the irradiation of the tumour. With neoantigens being expressed on the tumour cell surface at an increased rate after irradiation, the upregulated MHC-I molecules act to bind to these proteins and facilitate the activation of cytotoxic T-cells (Mardis, 2019). This acts to further increase the rate of immunogenic cell death of the cancer cells after irradiation.

Additionally, within this immunogenic phase post- irradiation, pro-inflammatory signaling is also activated. This is critical in overcoming the immunosuppressive setting established by other cells within the tumour stroma, namely: Tregs, myeloid-derived stem cells, and M2-like tumour-associated macrophages (TAMs). After irradiation of

tumour cells, the subsequent increased presence of damaged DNA from the nuclei or mitochondria causes the activation of cGAS-STING pathway, a critical component of the innate immune pathway (Yang et al., 2023). The activated cGAS-STING pathway acts to upregulate the expression of type I interferons (IFN) (Q. Chen et al., 2016). Type I IFNs play a pivotal role in the increase in MHC-I expression and T-cell priming for an immunogenic response (Burnette et al., 2011). This family of interferons are also linked to the promotion of chemokine (C-X-C) motif ligands (CXCL) 9 and 10 by dendritic cells, thereby facilitating the recruitment of both APCs as well as the migration of cytotoxic T-cells (Padovan et al., 2002). Additionally, irradiation of the TME also orchestrates the passage of effector T-cells to the tumour through a variety of different means. These include: the induction of chemokine expression, including CXCL16 that assists in T-cell infiltration into the tumour epithelium (Matsumura et al., 2008); macrophage polarisation, with radiation acting to shift the TAM population toward an M1-like phenotype (Klug et al., 2013); and increased adhesion molecule expression by the tumour vasculature, exemplified by vascular cell adhesion protein 1 and intercellular adhesion molecule 1 expression improving lymphocyte infiltration of tumour cells (Chiriva- Internati et al., 2006; Rodriguez-Ruiz et al., 2017). Together, these factors collectively induce a system immunogenic response to the tumour post-irradiation. However, this immune response is quelled in tumours exhibiting radioresistance and the surrounding stroma makes a return to the immunosuppressive status quo (de Andrade Carvalho & Villar, 2018).

Following the immunogenic response mounted by radiotherapy, the tumour is also protected by the adaptions from the TME. A number of critical mechanisms for the reestablishment of an immunosuppressive setting are orchestrated by cancer-associated fibroblasts (CAFs). CAFs form a large proportion of cells within the stroma (Cordes & Meineke, 2004) and are further activated after irradiation of the tumour. Critically, CAFs within the tumour stroma demonstrate a radioresistance, with radiation unable to induce a cytolysis these cells (Z. Wang et al., 2019). CAFs typically enter a senescent state post high dose irradiation, with cell proliferation being arrested but the ability to express a host of different molecules remaining intact (Hellevik et al., 2012). The expression of a

wide range of signalling molecules in senescent CAFs has a broad impact on the tumour stroma post-irradiation with effects on multiple pro tumour growth functions including: tumorigenesis and proliferation; invasion and metastasis; ECM remodelling; angiogenesis; and radiotherapy resistance (Y. Zhang et al., 2023). Outside of direct effects on the tumour itself, CAF crosstalk with dendritic cells, T-cells, Natural Killer cells, MDSCs, and macrophages also allows for the establishment of an immunosuppressive TME (Y. Zhang et al., 2023).

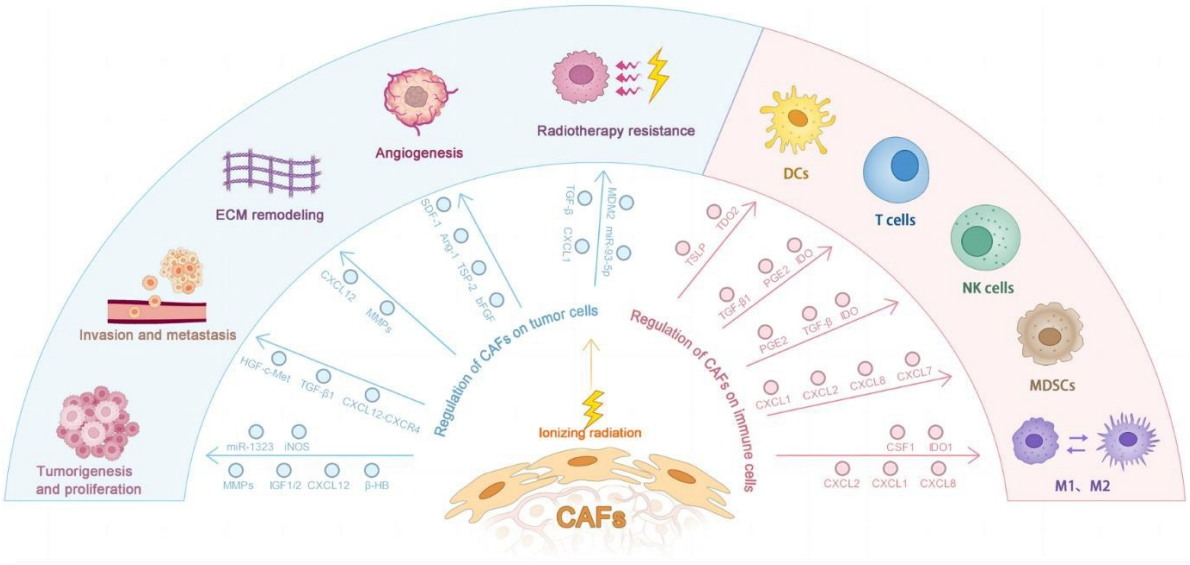


Figure 1.3.4 The impact of Irradiated CAFs on tumour cells and the stromal immune cell milieu.

Illustration of the broad impact of CAFs on the orchestration of tumour growth post irradiation and their crosstalk with the immune cell populations found within the stroma. Abbreviations: PGE2, prostaglandin E2; TDO2, tryptophan csf-dioxygenase; TSLP, thymic stromal lymphopoietin. Adapted and reprinted from Cell Death & Disease, vol 14 issue 541, 22 August 2023, Zhang, Y., Lv, N., Li, M., and Wu, C., Cancer-associated fibroblasts: tumour defenders in radiation therapy,

Another aspect of importance in the tumour TME post-irradiation is the regulatory T-cell (Treg) population. This $CD4^+$ $FOXP3^+$ T-cell population act to suppress immune responses and are critical for maintaining homeostasis as well as self-tolerance in normal tissues (Kondělková et al., 2010). This population of immune cells are linked with poor outcome in multiple different cancer types (Ladoire et al., 2011). Importantly, Tregs have been shown to be more radiotherapy resistance than the other T-cell populations, leading to a greater proportion of these immunosuppressive cells at the tumour site following irradiation (Balogh et al., 2013). Tregs proliferate at the tumour site after irradiation

(Muroyama et al., 2017) and therefore, post-irradiation the TME is poised ready for the T-cell populations to be skewed toward a dominant Treg presence. This is critical for the suppression of immunity within the TME due to the Treg expression of TGF-β and IL-10, IL-2 depletion, and ATP degradation into the immunosuppressive adenosine (Plitas & Rudensky, 2016). In support of a key role for Tregs in radioresistance, the depletion of the Treg population in combination with radiotherapy generated an improved antitumour response (Schoenhals et al., 2018).

Combined with the impact of these immunosuppressive cells, radiotherapy can induce $CD8^+$ cytotoxic T-cell exhaustion and the cessation of an antitumour response. Interferons have been found to play a key role in this, with IFNγ production after irradiation as part of the initial immunogenic response leading to increased expression of programmed-death ligand 1 (PD-L1) (Dovedi et al., 2014). The use of Durvalumab, an anti PD-L1 inhibitor, in patients with unresectable non-small-cell lung cancer after concurrent chemoradiotherapy demonstrated improved overall survival five years after the completion of the PACIFIC trial (NCT02125461) (Spigel et al., 2022).. Therefore, this concept of improving radiotherapy through the addition of immunotherapeutic has both a clear biological rationale as well as supportive evidence of efficacy in the clinic.

1.4 Radiotherapy response in rectal tumours.

1.4.1 Rectal cancer stratification.

When considering the response of rectal tumours to irradiation and defining prognostic markers, it is important to note that molecular stratification criteria have been developed within the field. Crucially, the molecular subtype of rectal cancer (described below), can have a marked impact on the tumour response to radiotherapy and the subsequent development of radioresistance.

In 2015, Guinney et al. published a seminal paper detailing a molecular classification system for colorectal cancer with clear biological interpretability, aiming to serve as a foundation for future clinical stratification of the disease. Stratification of colorectal cancer was completed through the coalescence of six distinct classification

systems from large-scale data into four consensus molecular subtypes (CMSs). Rectal tumours within the CMS1 phenotype are defined by their microsatellite instable status and high levels of mutation burden (Guinney et al., 2015). These tumours also have high levels of both immune cell infiltration as well as immune checkpoint expression. With the high level of mutational burden CMS1 tumours exhibit, the increase in neoantigen expression causes poor immunosurveillance evasion by these tumours (Roudko et al., 2021). Therefore, an equilibrium between immune cell activation and immunosuppressive factors within the microenvironment allow for tumour growth under these immunogenic conditions. The CMS1 tumours are also characterized by their higher rates of BRAF mutations, resistance to 5-FU treatment, and susceptibility to immunotherapies such as PD-L1 inhibition (Guinney et al., 2015). Additionally, these tumours constituted 14% of the samples analysed for the dataset and are typically found within the colon rather than the rectum. Tumours within the CMS2 classification are defined by their strong upregulation of targets downstream of the WNT and MYC signaling pathways (Guinney et al., 2015). Both of these pathways are tightly associated with carcinogenesis and are linked with poor patient outcomes (Gabay et al., 2014; Zhan et al., 2017). Interestingly, both these pathways are linked with the suppression of an anti-tumour immune response, with the CMS2 phenotype mirroring this with poor immune infiltration (Gabay et al., 2014; Zhan et al., 2017). In addition to the poor immune infiltration, CMS2 tumours also lacked any immune regulatory cytokines within the surrounding microenvironment (Guinney et al., 2015). Additionally, CMS2 colorectal tumours have high levels of somatic copy number alterations (SCNA) in comparison with the other phenotypes. CMS2 tumours constituted 37% of the samples analysed for the dataset and were formed both in the colon as well as the rectum (Guinney et al., 2015). CMS3 tumours are defined by their extensive metabolic adaptation that are in line with the occurrence of KRAS-activating mutations as described in the literature (Kamphorst et al., 2013; Ying et al., 2012). Tumours presenting with the CMS3 phenotype also had clear overrepresentation of KRAS mutations when compared to the other CMS types. CMS3 tumours were also found to be poorly immunogenic and lacked any immune regulatory cytokines within the surrounding microenvironment, akin to the CMS2 phenotype

(Guinney et al., 2015). Of the samples analysed, 13% of these were classified as CMS3 tumours and were located both in the colon as well as the rectum (Guinney et al., 2015). Tumours exhibiting the CMS4 phenotype are defined by their high levels of stromal infiltration (Guinney et al., 2015). These tumours also demonstrate large amount of transforming growth factor β activation (TGF-β) and upregulation of CXCL12. These factors act to regulate the immune response to these tumours. This is key due to the presence of macrophages within the surrounding microenvironment that can, without intervention by these immunosuppressive factors, act as APCs to prime an immunogenic response against these tumours (Lu et al., 2023). Additionally, the CMS4 phenotype demonstrates complement pathway activation, further increasing the necessity of immune regulation within the surrounding microenvironment. Within the stroma of these CMS4 tumours, greater levels of matrix remodelling were seen when compared to the other CMS groups. Additionally, the CMS4 tumours also demonstrated a greater ability to facilitate angiogenesis when compared to the other CMS groups. Of the samples analysed, 23% of the tumours were classified as CMS4 and these tumours were located both within the colon as well as the rectum (Guinney et al., 2015). When comparing patient outcomes between the CMS groups, patients with tumours defined as CMS4 had both the worst relapse-free as well as overall survival (Guinney et al., 2015).

Research has continued to find clear potential in the CMS classification system in predicting prognosis and response to systemic therapy (ten Hoorn et al., 2021). The CMS classification system additionally provided information on the anatomical location of colorectal tumours and their corresponding subtypes (Guinney et al., 2015). Within rectal cancer, Guinney et al. demonstrated the large majority of tumours fell outside of the CMS1 phenotype and typically presented with poor immune infiltration. When considering the classification of rectal tumours using CMSs, it is crucial to account for the heterogeneous nature of the tumours when *in situ*. Research looking to expand on the CMS stratification has found that, while able to provide prognostic benefit, sample heterogeneity contributes to a highly variable CMS assignment in multiregional biopsy samples (Ubink et al., 2017). This heterogenous nature of rectal tumours has been attributed to differing proportions of stromal and immune cells that make up the TME

within different biopsy samples (Alderdice et al., 2018). Additionally, it is worth noting that the CMS phenotype exhibited by the cancer cells is heavily influenced by the abundance and composition of the surrounding microenvironment (Calon et al., 2015; Isella et al., 2015; McCorry et al., 2018). Furthermore, CMS-related cell populations, specifically CMS1 paired with CMS4 and CMS2 paired with CMS3, have demonstrated plasticity within the tumour (L et al., 2021). Therefore, when considering the clinical application of the CMS stratification system of colorectal cancer, the inherent intra-tumour spatial heterogeneity of the disease must be considered. Interestingly, single cell RNA sequencing of colorectal tumours has demonstrated all tumours contained individual cells from each of the CMS phenotypes (S et al., 2021). Further implications from the research into tumour cell heterogeneity within colorectal cancer has also demonstrated that the CMS1 and CMS4 phenotypes are driven by immune and stromal cells respectively rather than the tumour cells (S et al., 2021). Interestingly, in colorectal tumours the specific combination of CMS phenotypes had a significant impact on patient outcomes .(L et al., 2021). All patients with tumours demonstrating a CMS4 component alongside another CMS phenotype had worse overall survival. When comparing the mixed CMS groups, the CMS4 and CMS1 phenotypes demonstrated the worst overall survival when compared. This combination of CMS phenotypes within the tumour was also overrepresent in patients with metastatic disease. Therefore, it is hypothesized that the CMS4 component of the tumour releasing TGF-β may assist in the immune escape of the highly genetically instable CMS1 component (L et al., 2021). It is critical, therefore, to take into account the impact of rectal cancer treatments on multiple CMS phenotypes simultaneously is this stratification system is to be used in profiling patient tumours.

In 2017, Isella et al. identified five different colorectal intrinsic subtypes: CRIS-A: mucinous, glycolytic, microsatellite instable; CRIS-B: TGF-β pathway enriched, active epithelial-mesenchymal transition, poor prognosis; CRIS-C: increased EGFR signalling and sensitivity to EGFR inhibition; CRIS-D: WNT activation, IGF2 gene overexpression and amplification; and CRIS-E: Paneth-like cell phenotype, and NU53 mutations (Isella et al., 2017). The establishment of the CRIS stratification of colorectal cancer looked to further investigate cancer cell intrinsic transcriptional features in isolation without the input of

lineage-dependent stromal components (Isella et al., 2017). Unfortunately, the CRIS classification system only provides an overview of colorectal stratification and lacks the establishment of specific rectal cancer subtypes. It is important to note that by establishing the CRIS stratification system, something also achieved by the development of CMS classification, numerous phenotypic links to patient outcomes have been identified (Isella et al., 2017).

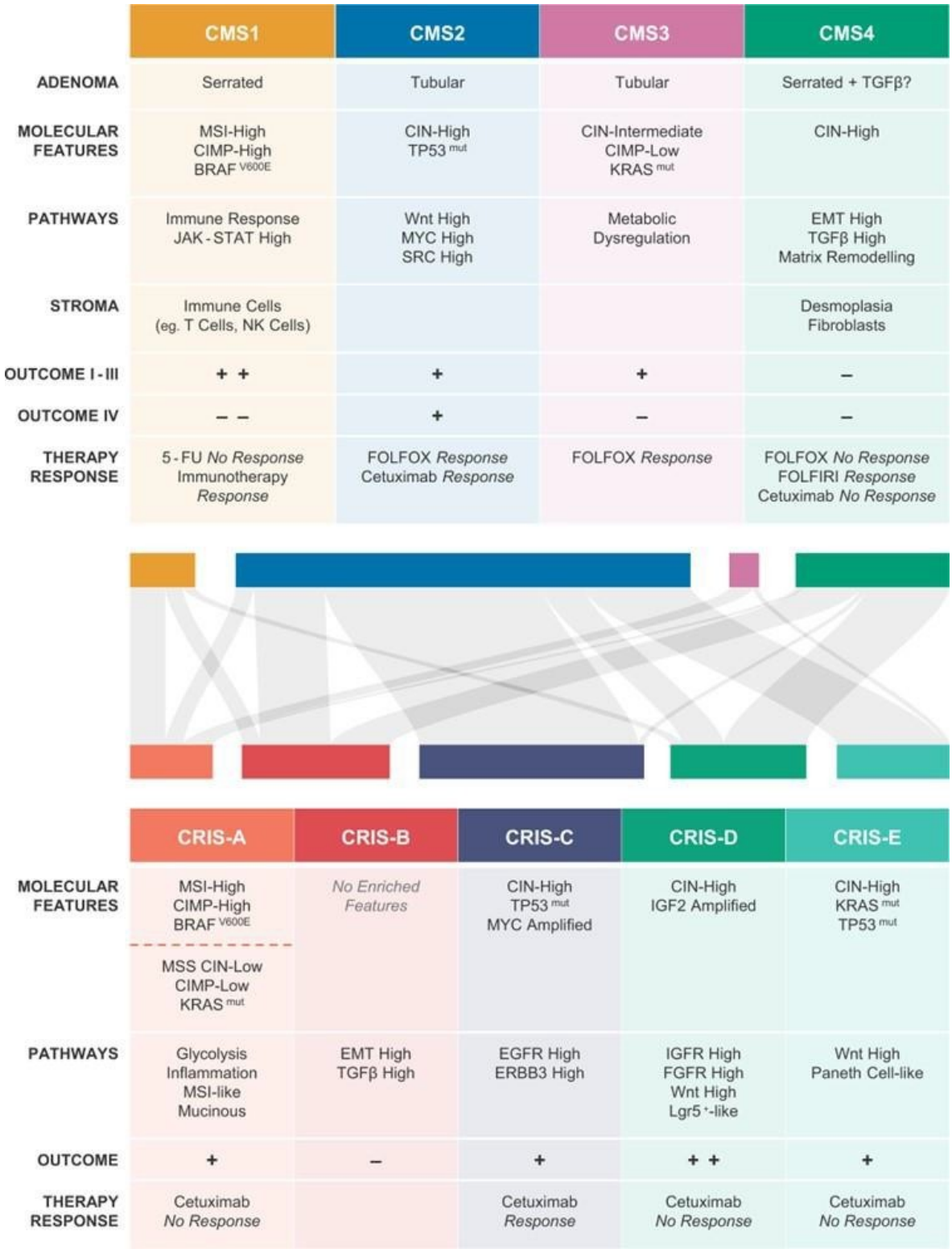


Figure 1.4.1 Summary of CMS and CRIS stratification for colorectal cancer

This diagram illustrates the key stratification markers for both the CMS and CRIS phenotypic groupings. The relationship between both classification systems is illustrated by the Sankey diagram and the colours of each node correspond to the respective subtypes. Sizes of the nodes align with the number of cultures adhering to that specific subtype. Adapted and reprinted from Oncogenesis, vol 9 issue 66, 9 July 2020, Buikhuisen, J., Torang, A., and Medema, J, Exploring and modelling colon cancer inter-tumour heterogeneity: opportunities and challenges.

1.4.2 Phenotypic links to poor radiotherapy response.

When examining both the CMS and CRIS stratification of colorectal cancer, specific subtypes appear to have worse prognosis. Specifically, patients with tumours classified as either CMS 4 or CRIS-B phenotypes demonstrated significantly worse disease-free survival (Guinney et al., 2015; Isella et al., 2017). These two phenotypes of rectal cancer share some similarities, namely their high expression of epithelium to mesenchymal transition (EMT) markers and upregulation of the TGF-β signalling pathway. EMT is associated with the acquisition and enhancement of radioresistance (Zhou et al., 2020). The different pathways related to EMT-mediated radioresistance are outlined in the table below along with their relevance to rectal cancer.

Table 1.4.2 Signalling pathways related to EMT and radioresistance in rectal cancer.

Abbreviations: CSC – Cancer Stem Cells, PPAR – Peroxisome proliferator-activated receptors (PPARs), DDR – DNA damage repair/response.

Target molecule	Function	Relevance in rectal cancer	Reference
TGF-β	EMT-mediated CSC, regulates expression of EMT markers	Link with poor prognosis, defining feature of CMS4 and CRIS-B	(J. Wang et al., 2017, 2021)
Wnt/β-catenin	Modulates EMT-related gene expression, alters PPAR signalling.	Defining feature of CMS2, CRIS-D/E, central role in tumourigenesis	(Emons et al., 2017; X.-Z. Yang et al., 2020)
PI3K/AKT	Regulation of EMT markers, promotion of CSC induction	Induction of rectal CSCs, promotes tumour regeneration post-radiation	(Park et al., 2021; Xu et al., 2015)
Notch	Enhancement of EMT process, DDR response, renewal of CSCs,	Promotion of CSCs, linked to rectal tumour radioresistance	(Brisset et al., 2023; Yahyanejad et al., 2015)
IL-6/STAT3	Regulation of mesenchymal markers, promotion of DDR	Negative correlation with post operation lymphocyte counts, tumour regeneration	(S. Feng et al., 2023; Hamada et al., 2016)

Additionally, the CMS4 phenotype of rectal cancer is also defined by stroma with a rich CAF population. These cells also play a key role in the development of radioresistance, the establishment of an immunosuppressive TME, and stimulating tumour cells to undergo EMT (Section 1.3.4). Following the results of the PROSPECT trial, comparing FOLFOX chemotherapy versus chemoradiotherapy (Schrag et al., 2023), it is worth noting that the CMS4 phenotype of rectal tumour typically failed to respond to the combination chemotherapy.

Outside of the CMS and CRIS stratification system, other rectal tumour features are also associated with a poor response to radiotherapy in patients. The immune cell populations within the stroma provide a key prognostic insight into how rectal tumours will respond to radiation. Key immune cell populations include positive markers of response such as tumour-infiltrating lymphocytes, especially key for cytotoxic T-cells (Fridman et al., 2017), the $CD8^+$ /$FoxP3^+$(Treg) ratio (Suzuki et al., 2010); natural killer cell infiltration (L. Zhang et al., 2018), and negative markers of response such as neutrophil to lymphocyte ratio in the peripheral blood (Pine et al., 2015) and a large MDSC population (Vasquez-Dunddel et al., 2013). Additionally, some systemic cytokines and chemokines have demonstrated prognostic potential to predict rectal tumour response to irradiation. IL-6 (table 1.4.2) has been shown to predict radiation response in rectal cancer. Il-8 has also shown promise as a prognostic tool (Jin et al., 2014), with the molecule acting to induce tumour cell proliferation, and later invasion in rectal cancer (Terada et al., 2005).

The current landscape surrounding the treatment of rectal cancer has opened avenues into the investigation of more customised treatment options, especially when considering the findings of the PROSPECT trial (Schrag et al., 2023). Therefore, gaining an understanding of therapeutics that may improve the efficacy of radiotherapy should, potentially, improve our current approach to rectal cancer treatment.

Aims of the thesis

The aims of this thesis are:

1. To identify potential neoadjuvant targets to compliment the anti-tumour effect of radiation.
2. To investigate the impact of inhibiting identified targets on the anti-tumour effect of radiation. Additionally, the impact inhibiting these targets have on the tumour microenvironment will also be examined.
3. To examine how the site of tumour implantation *in vivo* alters the surrounding tumour microenvironment. Also, how the location of the tumour alters the response to radiation augmented through inhibition of discovered targets will be explored.

Chapter 2

Methods and materials

2.1 AKPT organoid culture

Organoids were sourced from Eoghan Mulholland (Wellcome Trust Centre Human Genetics, University of Oxford) working within the ACRCelerator: Colorectal Cancer Stratified Medicine Network (A:CCSMN). These were generated from male mice with tumours from liver metastasis formed from a tamoxifen-induced colorectal cancer mouse model (with APC -/-, KRAS G12D, p53 -/-, TGFβR1-/-). Organoids were grown within 35 µl of Matrigel (Corning 356255), DMEM/F12 media mixture (2:1) with 500 µl of media overlaid within each well of a 24-well plate. Overlaid medium was supplemented with epidermal growth factor (EGF) and noggin at a concentration of 100 ng/ml and 50 ng/ml respectively. Organoids were maintained through passaging every three days.

Table 2.1 AKPT organoid culture media components.

	Company	**Cat. Number**	**Concentration**
Glutamax	*Gibco*	*35050-061*	*1:100*
Penicillin Streptomycin	*Gibco*	*15070-063*	*1:100*
N2 supplement	*Gibco*	*11520536*	*1:100*
B27 Supplement	*Gibco*	*11530536*	*1:50*
N-acetylcysteine	*Sigma*	*A9165*	*1:500*
HEPES	*Gibco*	*11560496*	*1:100*
AB/A-M	*Sigma*	*A5955*	*1:100*
Gentamicin	*Sigma*	*G1397*	*1:1000*
Fungizone	*Thermofisher Scientific*	*15290018*	*1:1000*

2.1.1 In vitro surviving fraction assay of AKPT organoids

For survival fraction studies, organoids were used 24 hours after passaging and plated into a 24-well plate. Vehicle or drug treatment was carried out as previously

described and added into the surrounding media 1 hour prior to irradiation. Organoid irradiation was carried out using an x-ray irradiator with lead shielding allowing for cumulative doses across a single plate (within a twenty-four well plate, two columns of four received 0Gy, two received 4Gy, and two received 9Gy). Organoids were imaged over the course of 3 days using a JuLi stage Real- Time Cell History recorder (NanoEnTek Inc., Korea) by using a 4x objective. Using the images, organoids were manually counted at day 0 and 3 with a surviving fraction subsequently calculated.

2.2 Animal studies

2.2.1 Heterotopic AKPT tumour model

Prior to commencing implantation of the AKPT organoids subcutaneously, the number of mice required for each was determined through power analysis as described by (Charan & Kantharia, 2013) to establish the treatment groups. Power analysis was performed using the G Power software (Faul et al., 2007), with group size calculated based on the assumption of an effect size considered large between the groups based on Cohen's principles (Charan & Kantharia, 2013). For heterotopic AKPT organoid-derived tumour models, male C57BL/6 or athymic nude (Crl:NU(NCr)-Foxn1nu) mice were purchased from Charles River at 5-6 weeks of age. Specifically male mice were used due to the AKPT organoids being sourced from a male tamoxifen-induced colorectal cancer model. This prevented any potential confounding factors when establishing the immunocompetent heterotopic AKPT tumour model. Mice were housed within a pathogen-free environment with a 12-hour light cycle at the RRI Biomedical Science Animal Unit at the University of Oxford. AKPT organoids were suspended in a PBS, Matrigel (Corning 356255) mixture (1:1) prior to subcutaneous injection. Resulting tumours were monitored once a day and their volume determined from: Length x Width x Height x 0.52 using calliper measurements. After the mean tumour volume across all mice was 150-200mm^3, mice were randomly assigned to treatment groups. For mouse survival curves, mice were euthanised once tumours reached a Length x Width value of 1200mm^3 by a Schedule 1 method (in line with UK Animals [Scientific Procedures] Act 1986 [ASPA]). For mice that experienced ulceration of the subcutaneous tumour, if the

wetness failed to resolve within 24 hours they were culled and not included as part of the experimental cohort.

All *in vivo* experiments adhered to the 3R's practice of animal research (replace, reduce, and refinement). Animal models were required for the experimental work for this thesis due to the lack of important features within *in vitro* organoid models, specifically the surrounding immune cell populations and stromal compartment. These aspects are critical for the investigation into the augmentation of radiotherapy. The experimental groups for all *in vivo* experiments were kept to a maximum size as dictated by optimized experimental design, with group size calculated through power analysis for a large effect size. By using the less invasive heterotopic model of rectal cancer initially, prior to the orthotopic model, the *in vivo* studies carried out during this thesis were refined to minimize animal pain, suffering, or distress.

For heterotopic experiments involving irradiation, once mean tumour volume across the mice reached 150-200mm^3, radiation was delivered using the Gulmay Medical RS320 irradiator (300kV, 10mA, 1.81Gy/min). For the irradiation of subcutaneous tumours, mice were anaesthetised with isoflurane and shielded by a lead semicylindrical shell with only the subcutaneous tumours being exposed to irradiation. In experiments using a fractionated radiation treatment scheme, all measurements are taken at the listed timepoint after the final fraction.

2.2.2 Orthotopic AKPT tumour model

For orthotopic AKPT organoid-derived rectal tumour models, male C57BL/6 mice were purchased from Charles River at 5-6 weeks of age and housed as described for the heterotopic counterparts. AKPT organoids were collected and incubated for 30min in cold PBS prior to implantation to break down any Matrigel (Corning 356255) without disrupting the organoid structure. 70µl of suspended organoids were then implanted under general anaesthesia via colonoscopy as described by *(Roper et al., 2017)*. Tumour formation was then confirmed by colonoscope before treatment commenced.

The submucosal rectal implantation of AKPT organoids formed an *in vivo* rectal cancer model that better mimicked the surrounding TME as found in patients, albeit at

the cost of a significant increase in complexity. The heterotopic model had a 100% take rate, with all mice that received AKPT organoids delivered subcutaneously developing heterotopic tumours. However, the orthotopic model with AKPT organoids delivered submucosally into the rectum had a take rate of 70%. For the orthotopic model, further humane endpoints were introduced to account for the more invasive procedures required. These included: checking for visible rectal bleeding after tumour implantation, with a failure to stop leading to sacrifice by schedule 1 method; and observation for signs of sepsis caused by bowel perforation, these signs include pyrexia, respiratory or circulatory distress, anorexia, dehydration, weakness, hunching, or other non-specific features of illness. In addition to the more complex organoid implantation required in the orthotopic model, delivery of radiation to rectal tumours also required an altered methodology compared to the heterotopic model.

For orthotopic experiments involving irradiation, after confirmation of tumour formation, radiation was delivered using the small animal radiation research platform (SARRP) (225kV, 2Gy/min, 10mm x 10mm field at the isocentre). Mice were anaesthetized with isoflurane, inverted and held in place on a movable gantry. The inversion of the mice allowed for the small intestine to fall outside of the field of radiation with the rectal portion of the bowel remaining inside. A computed tomography (CT scan) was used to aim radiation at the rectum and deliver the dose in an arc (-180^{o} to 180^{o}) to an inverted mouse under anaesthesia. Generated CT scans allowed for the use of anatomical landmarks, specifically the bladder, mouse tail vertebrate, and pelvic bones, to direct radiation doses to the rectum. Radiation was delivered through a 1cm x 1cm collimator. Generated CT scans for radiation delivery in the mouse model is illustrated in Appendix B.

2.2.3 C5aR1 inhibitor *dosing*

The C5aR1 inhibitor used for the experiments within this thesis was PMX205, a cyclic hexapeptide that acts as a potent noncompetitive inhibitor of the receptor (Kumar et al., 2020). Pharmacokinetic studies of PMX205 demonstrate that mice tolerate repeat dosing of the inhibitor well, even when considering that the drug is able to cross the blood-brain barrier (Kumar et al., 2020). Studies have also demonstrated that PMX205

fails to accumulate in the brain or spinal cord and undergoes efficient renal excretion (Kumar et al., 2020). Though the off-target effects of PMX205 are not well studied, it is worth noting that the ability of the inhibitor to readily cross the blood-brain barrier potentially opens avenues to neurological off-target effects.

For all *in vitro* experiments, organoids were treated with 10mg/ml PMX205 (Tocris, 5196) dissolved in 20% ethanol/water or water alone. Vehicle control in these experiments refers to 20% ethanol/water or water alone. Organoids were pretreated for one hour before irradiation.

For all *in vivo* experiments, PMX or vehicle was delivered by oral gavage once a day for 3 days. When combined with radiation, PMX/vehicle was delivered one day before, then on the day of (2 hours prior to radiation), and the day after irradiation of the AKPT tumours. For *in vivo* dosing of PMX205, 10mg/kg was administered orally. Vehicle in these experiments refers to 20% ethanol/water.

2.2.4 TGF-β inhibitor dosing

The TGF-β receptor inhibitor used for experiments within this thesis was vactosertib, a small molecule inhibitor of TGF-βR1 (also known as activin receptor-like kinase 5 (ALK5)). Pharmacokinetic studies of vactosertib have shown that the inhibitor is rapidly absorbed after being administered orally (Jung et al., 2020). Additionally, vactosertib reached a maximum plasma concentration at a median time of 1.2 hours after administration and subsequently was rapidly eliminated with the median half-life 3.2 hours (Jung et al., 2020). This trend of timings relating to vactosertib bioavailabilty was also observed after repeated doses of the inhibitor (Jung et al., 2020). Additionally, this study demonstrated that vactosertib had negative accumulation, even after repeated dosing (Jung et al., 2020). When considering potential off-target effects of vactosertib it is worth considering any adverse events observed in phase 1 clinical trials the inhibitor has been investigated in. When looking at these adverse events, vactosertib typically impacts the systemic immune system in patients that respond poorly to the inhibitor (Malek et al., 2023). Notably, this systemic immune system change includes the reduction in the

neutrophil and lymphocyte populations (Malek et al., 2023). This is reflected by the increase in both lung and upper respiratory tract infections seen in patients receiving vactosertib (Malek et al., 2023). Additionally, off target effects on the liver were rarely observed, with one patient having to cease vactosertib treatment due to high grade hepatotoxicity (Malek et al., 2023). However, the use of vactosertib in the *in vivo* AKPT tumour model was well tolerated in the mice with no evidence of toxicity. This is key as hepatotoxicity develops at a faster rate in mice than in humans, with it taking between 12 to 24 hours and 24 to 72 hours respectively (McGill & Jaeschke, 2019).

For all *in vivo* experiments, vactosertib or vehicle was delivered by oral gavage once a day for 10 days. When combined with radiation, vactosertib/vehicle treatment commenced 2 hours prior to irradiation. For *in vivo* dosing of vactosertib, 25mg/kg was administered orally after being dissolved in: 10% dimethylsulfoxide (DMSO); 45% polyethylene glycol 300; 5% Tween 80 (Sigma-Aldrich, CAS number: 9005-65-6); and 40% PBS. Vactosertib was first dissolved in DMSO before other components added. Vehicle in these experiments refers to these constituent parts missing vactosertib.

2.3 *In silico* screen

Data was accessed through the Depmap portal (https://depmap.org from 10th September 2020). Essentiality scores were calculated by dividing the number of dependent cell lines for each gene/total number of cell lines in either CRISPR-cas9 and RNAi screens. To identify stress- and cancer-specific dependencies, we applied stringent criteria and looked for 51 genes that were deemed non-essential across all cell lines (genes that when knocked-out/down under baseline conditions do not alter cell survival) while still being expressed across cell lines. Genes described as complement system components, receptors, proteases and regulators (as reported in (17)) were queried. The calculated essentiality score was presented as a colour in the heatmap. Green = No cell line is dependent on that gene and therefore the gene is not essential. Red = The majority of cell lines are dependent, or the gene is essential. Yellow/Orange = intermediate dependence or essentiality. The essentiality scale is shown at the bottom, left hand side of the heatmap. ATR was included in the screen a positive control. Target

tractability was assessed by accessing canSAR data as displayed on the Depmap portal. A gene was only considered a hit if it was “druggable” based on structural and ligand-based assessment. Genes that are hits and are druggable are shown in green. Red = not druggable based on structural or ligand-based assessment. C1R and CF1 were not included in the heatmap due to lack of CRISPR-Cas9 or RNAi data. C4A, C4B, VSIG4, C8A, C8B, CD93 and CR1 were not included due to their very low expression in the majority of tissues.

2.4 Tissue staining

2.4.1 Formalin-fixed paraffin embedded processing

Both heterotopic tumours, split to form equal hemispheres, and orthotopic rectal tumours, rolled into Swiss rolls and pinned, were fixed overnight in 10% neutral buffered formalin then transferred to 70% ethanol prior to processing. Tissue was then processed using an automatic tissue processor (Leica TP1020 Automatic Tissue Processor), dehydrating samples by passage through increasing ethanol concentrations and Citroclear (Leica Biosystems), then samples were embedded in paraffin wax using a paraffin embedding station (Histostar Tissue Embedding System). All tissues were sectioned at 4µm and placed on histology slides prior to IHC or multiplex staining.

2.4.2 Immunohistochemistry staining of AKPT tumours

Formalin-fixed paraffin-embedded (FFPE) 4µm sections of AKPT tumours were de-paraffinised in citroclear (Leica Biosystems) then rehydrated by passage through graded alcohol concentrations to water. Sections were stained with primary C5aR1 antibody (1:1000, Abcam, ab59390) using EnVision G2 Doublestain System (Dako) according to manufacturer’s instructions. Stained samples were scanned using Aperio CS scanner and ImageScope analysis software (Aperio technologies).

2.4.3 In situ hybridisation staining

For in situ hybridisation (ISH) of mouse FFPE samples, 4µm formalin-fixed, paraffin-embedded tissue sections were used. The sections were baked for 1 hour at 60^{o}C before dewaxing in xylene and ethanol. ISH was then performed using the

RNAscope HD assay-Brown kit (Bio-techne). Activin probe (Inhba, NBP1-33030) was purchase from Bio- techne.

2.5 Multiplex and HALO analysis

Multiplex immunofluorescence staining of AKPT tumours was performed on 4 µm thick FFPE sections using the OPAL protocol (Akoya Biosciences, Marlborough, MA). The Leica BOND RXm autostainer (Leica Microsystems, Wetzlar, Germany) was used to conduct this staining. Staining cycles were conducted six consecutive times using the following primary antibody-Opal fluorophore pairs:

Immune panel: (1) Ly6G (1:300, 551459; BD Pharmingen)–Opal 540; (2) CD4 (1:500, ab183685; Abcam)–Opal 520; (3) CD8 (1:800, 98941; Cell Signaling)– Opal 570; (4) CD68 (1:1200, ab125212; Abcam)–Opal 620; (5) FoxP3 (1:400, 126553; Cell Signaling)–Opal 650; and (6) E-cadherin (1:500, 3195; Cell Signaling)–Opal 690.

Stroma panel: (1) Gremlin 1 (1:750, AF956; R&D)–Opal 540; (2) CD34 (1:3000, ab81289; Abcam)–Opal 520; (3) CD146 (1:500, ab75769; Abcam)–Opal 570; (4) SMA (1:1000, ab5694; Abcam)–Opal 620; (5) Periostin (1:1000, ab227049; Abcam)–Opal 690; and (6) E-cadherin (1:500, 3195; Cell Signaling)–Opal 650. Tissues sections were incubated for 1 h in primary antibodies and detected using the BOND Polymer Refine Detection System (DS9800; Leica Biosystems, Buffalo Grove, IL) in accordance with the manufacturer's instructions, substituting DAB for the Opal fluorophores, with a 10-min incubation time and withholding the hematoxylin step. Antigen retrieval at 100°C for 20 min, in accordance with standard Leica protocol, with Epitope Retrieval Solution one or two was 43 performed prior to each primary antibody being applied. Sections were then incubated for 10 min with spectral DAPI (FP1490, Akoya Biosciences) and the slides mounted with VECTASHIELD Vibrance Antifade Mounting Medium (H- 1700-10; Vector Laboratories). Whole slide scans and multispectral images (MSI) were obtained on the Akoya Biosciences Vectra Polaris. Batch analysis of the MSIs from each case was performed with the inform 2.4.8 software provided. Finally, batched analysed MSIs were fused in HALO (Indica Labs) to produce a spectrally unmixed reconstructed whole-tissue

image. Cell density analysis was subsequently performed for each cell phenotype across the three MPIF panels using HALO. HALO Image Analysis Platform version 3.5.3577 and HALO AI version 3.5.3577 (Indica Labs, Inc.) were used. Analysis modules “Area Quantification 2.4.2”, “HighPlex FL 4.2.3” and “Random Forest Classifier” were used.

For C5aR1 and multiplex serial staining for comparison, cover slips were lifted post multiplex staining and C5aR1 (1:1000, Abcam, Cat: ab59390) antibody was stained for chromogenically on the Leica BOND autostainer. Antigen retrieval was carried out at 100ºC for 20 min with Epitope Retrieval Solution 2. Primary antibody incubation at 1:250 dilution for 30 minutes was followed by detection using the BOND™ Polymer Refine Detection System (DS9800, Leica Biosystems) as per manufacturer’s instructions.

2.6 Clinical dataset interrogation

Using the gene expression profiling interactive analysis (GEPIA) portal, Kaplan-Meier survival curves were constructed. These survival curves measured disease-free survival in the TCGA database of primary colorectal tumour biopsies. All TCGA data used was accessed through the cBioPortal (Cerami et al., 2012; de Bruijn et al., 2023; Gao et al., 2013).

For the interrogation of the stratification in colorectal cancer (S-CORT) dataset, the GRAMPIAN, patient biopsies of rectal tumours prior to treatment with radiotherapy $\pm$ additional chemotherapy, and ARISTOTLE, patient biopsies of rectal tumours prior to chemoradiotherapy treatment, cohorts were analysed. The combination of both datasets constituted a patient cohort of 363. Analysis of this dataset was performed by Enric Domingo as well as the construction of the resulting figures within this thesis.

2.7 Longitudinal biopsies from rectal adenocarcinoma patients

2.7.1 Analysis on longitudinal biopsies from rectal adenocarcinoma patients

Patients were receiving neoadjuvant chemoradiotherapy as part of their standard of care management. The gross rectal tumour and tumour involved lymph nodes were irradiated to a dose 50Gy in 25 fractions, and pelvis nodes to a dose of 45Gy in 25 fractions, over 5 weeks, concurrently with Capecitabine chemotherapy at 900mg/m^2, taken orally twice a day when receiving radiotherapy. Patients underwent sigmoidoscopy

at the described timepoints with direct visualisation and biopsies of the tumour.

2.7.2 Staining on longitudinal biopsies from rectal adenocarcinoma patients

C5aR1 staining was performed as described in 2.4 with C5aR1 antibody (Abcam, Cat: ab59390). For analysis the Indica Labs HALO 54 image analysis software (v3.6.4134.137 and HALO AI 3.6.4134) was used. Sections of biopsies were manually annotated by a trained pathologist as either cancer, normal/reactive or ulcer/granulation tissue. DenseNet V2 (HALO AI)" was then "taught" to discriminate between epithelium, stroma and glass. Within each annotation region, stroma and epithelium tissue compartments were analysed separately for 1) general tissue DAB intensity using "Indica Labs Area Quantification v2.4.2"; 2) Cell localised DAB intensity using "Indica Labs Multiplex IHC v3.4.9". Both analyses yielded the same overall results.

2.7.3 RNA-sequencing of longitudinal biopsies from rectal adenocarcinoma patients

RNA sequencing of the longitudinal biopises from rectal adenocarcinoma patients was performed by Lily Hilson and differentially expressed genes between baseline and post-treatment timepoints were identified. Gabriel Valbuena then carried out pairwise gene set enrichment analysis (GSEA)using the complement signature from (Ricklin et al., 2010). Subsequent figures formed from this data were also constructed by Gabriel Valbuena.

This study involves human subjects, and all samples were obtained following individual informed consent for research projects and subsequent ethical approval by the National Research Ethics Service in the UK (REC ref15/EE/0241, IRAS ref 169363 and REC ref 18WS00031). All samples were obtained by the Campbell Roxburgh lab group from the University of Glasgow.

2.8 RNA-sequencing

2.8.1 Organoids RNA extraction for sequencing

After the treatment, organoids were harvested by direct incubation in 350 µl RLT plus lysis buffer (Qiagen RNeasy® Plus Micro kit) in each well for 5 minutes and their RNA was extracted 53 using the Qiagen RNeasy® Plus Micro kit according to the manufacturer protocol. RNA quality and concentration were measured with Agilent

Bioanalyzer 2100 (Agilent) and Nanodrop (Thermo Fisher Scientific) respectively. RNA library preparation, sequencing, and data analysis were outsourced to Novogene (UK).

2.8.2 AKPT tumour RNA extraction for sequencing

Transcriptomic profiling was carried out by polyA RNAseq. RNA samples were quantified using Qubit 4.0 Fluorometer (Life Technologies, Carlsbad, CA, USA) and RNA integrity was checked with the RNA Kit on an Agilent 5300 Fragment Analyzer (Agilent Technologies, Palo Alto, CA, USA). RNA sequencing libraries were prepared using the NEBNext Ultra RNA Library Prep Kit for Illumina following manufacturer's instructions (NEB, Ipswich, MA, USA). Sequencing libraries were validated using NGS Kit on the Agilent 5300 Fragment Analyzer (Agilent Technologies, Palo Alto, CA, USA), and quantified by using Qubit 4.0 Fluorometer (Invitrogen, Carlsbad, CA). Libraries were sequenced using a 2x150bp paired end configuration on an Illumina NovaSeq 6000 instrument (Illumina).

Transcript abundance was mapped to the mouse transcriptome (Ensembl 96) and quantified from paired-end sequencing reads using Salmon v1.10.0 (Patro et al., 2017). Transcript counts were collapsed into gene-level quantifications using the tximport package in R.

Statistical analyses were carried out in the R statistical environment by Gabriel Valbuena. Differential expression analysis was performed using the limma package (v3.54.2). Gene set enrichment analyses were performed using the fgsea package (v1.24.0). GSEA network plots were created using the PPInfer package (v1.24.2), with edges and nodes laid out according to the Fruchterman-Reingold algorithm. In the GSEA network plots, the size of the nodes are proportional to the size of gene sets, and the more significant categories are, the less transparent their nodes are.

For the assessment of normalised enrichment scores in chapters 4 and 5, the following gene lists were used: immunogenic and immunosuppressive gene signature from (Nagarsheth et al., 2017; H. Wang et al., 2021); macrophage phenotype from (Coates et al., 2008); and fibroblast phenotype from (Grauel et al., 2020).

2.9 Statistics

Statistical analysis was performed using Graphpad Prism Software (version 9.2.0). P values were used to determine the significance of differences, and P values of less than 0.05 were considered significance. Log-rank tests and 1- or 2-way ANOVA were used as appropriate and as specified in the figure legend. All error bars for figures plot the standard error of the mean (SEM).

Chapter 3

Optimisation of a novel rectal tumour model and target discovery post-irradiation

---

3.1 Establishment of an organoid model to recapitulate rectal tumours with poor treatment response.

3.1.1 Key TME phenotypes needed for organoid model to recapitulate poor-responding rectal tumours.

To begin to study rectal cancer it is critical to develop a model that can recapitulate the phenotypes seen in tumours including those that respond poorly to the current chemoradiotherapy gold standard preoperative treatment. The use of organoids in cancer research has been attracting attention for their use in developing valuable preclinical models of the disease (Fang et al., 2023). Organoids are a three-dimensional cell culture *in vitro* that acts to model source tissue (Tuveson & Clevers, 2019). Importantly, the use of organoids *in vitro* has shown success in the evaluation of patient response to a number of therapies including chemoradiotherapy (Demyan et al., 2022), the current standard for preoperative rectal cancer treatment. The *in vivo* implantation of organoids to model cancer has been well established (Zhao et al., 2022). By harvesting tumours developed in genetically engineered mouse models (GEMMs), organoids can then subsequently be formed for *ex vivo* experimentation or *in vivo* reimplantation. Additionally, harvesting tumours from these models allows for specific mutations to be incorporated into future *in vivo* studies. While GEMMs are powerful tools in the study of cancer, the reimplantation of organoids harvested from these models allow for the rapid evaluation of treatment options.

As discussed within chapter 1, there is a myriad of factors that affect the response of rectal tumours to irradiation including the complex and ever-evolving TME surrounding the tumour. Therefore, when establishing an organoid model for the evaluation of current rectal cancer treatments, it is critical that the TME can recapitulate that seen in *in situ* patient tumours. Due to this, organoids derived from primary tumours in mice are relevant approach because of the natural formation of the TME around implanted tumours. Especially considering that patient-derived organoids, although a powerful tool in cancer research, require implantation into immunodeficient mice for growth to avoid elimination by the host immune system (Kdimati et al., 2023). Also key to the replication of rectal tumours with poor response to irradiation is the relatively specific stroma components that act as a defence for the cancer cells (Zhang et al., 2023). Therefore, tumours formed from implanted organoids must provide a TME with a rich CAF population (and should demonstrate a lack of immune cell infiltration, specifically $CD8^+$ infiltration (Demaria et al., 2016).

3.1.2 Key mutations required in organoid model to recapitulate rectal tumour phenotypes.

Colorectal cancer is known to form tumours through the stepwise accumulation of mutations (Fearon & Vogelstein, 1990). The seminal paper by Fearon and Vogelstein described the following mutations leading to the formation of tumours within the colorectal space: *Apc*, tumour suppressor gene; mitogen-activated protein kinase (MAPK); *Tp53*; and the TGF-β signalling pathway (Fearon & Vogelstein, 1990). Additionally, the progression of colorectal cancer is correlated with successive alterations to the following pathways: WNT, EGFR, p53, and TGF-β (Cancer Genome Atlas Network, 2012). This accumulation of stepwise mutations forms the basis of the classical route of rectal tumour formation, with an adenoma to carcinoma progression formed that accounts for around 70-80% of all colorectal cancer cases (Satorres et al., 2021).

The use of a genetically engineered mouse (GEM) model containing, *villinICreER* of $Apc^{fl/fl}$, $Kras^{G12D/+}$, $Trp53^{fl/fl}$, $Tgfbrl^{fl/fl}$ (AKPT) mice to form tumours for investigation has shown success (Nakayama et al., 2022; Tauriello et al., 2018). When these organoids have been implanted submucosally within the rectum, the resulting rectal tumours are

found to possess many of the characteristics of the CMS4 phenotype (Pennel et al., 2024). Additionally, the tumours formed by this orthotopic model of rectal cancer have been found to resemble the cancerous growths having undergone the classical route of colorectal carcinogenesis as described by (Fearon & Vogelstein, 1990) (Jackstadt et al., 2019; Vaquero-Siguero et al., 2022). The AKPT organoid-induced orthotopic model of rectal cancer has also shown to readily form liver and lung metastasis (Jackstadt et al., 2019). This suggests that, within the orthotopic space, this model of rectal cancer is able to recapitulate both late-stage and poor-responding rectal cancer as seen in patients. However, the use of AKPT organoids to form a heterotopic model has not been explored within the current literature. The use of a heterotopic model prior to moving into the orthotopic space will be explored within this thesis. This has the potential for the simpler heterotopic model to be used as a screen prior to the use of the more complicated orthotopic model. Additionally, the simplicity of the heterotopic model will allow for more in depth analysis of the resulting tumours and act to reduce the number of mice used for the orthotopic model on hypotheses disproven by this initial screening stage.

For the purpose of this thesis, it was also encouraging that the AKPT model demonstrated the formation of tumours containing a significant fibrotic niche rich in CAFs (Nakayama et al., 2022). Additionally, AKPT compound-mutant tumours displayed high levels of stromal TGF-β signalling within the stroma and an exclusion of T-cell infiltration into the cancerous epithelium (Tauriello et al., 2018). The combination of these factors suggests that the AKPT organoid model can provide an accurate recapitulation of rectal tumours that respond poorly to chemoradiotherapy, the current frontline treatment.

3.1.3 Establishment of the heterotopic AKPT rectal cancer model

To establish the AKPT rectal tumour model as a screening tool for potential TME-targeted therapies that could improve radiation efficacy, a heterotopic model was first developed. Through the subcutaneous implantation of AKPT organoids, a model of rectal cancer with a 100% take rate was formed. Additionally, the use of a heterotopic model allowed for the rapid formation and subsequent harvesting of AKPT tumours for further analysis. The simplicity of the model, in comparison to a more complex orthotopic

approach, also allow for a greater range of variables to be examined. Therefore, it is critical that the resulting heterotopic tumours are analysed to ensure the key TME features are recapitulated in this setting.

After implanting the AKPT organoids subcutaneously, we performed multiplex staining examining existing immune cell population and stromal landscape within the tumour microenvironment (TME). The overall immune cell population within these tumours was dominated by macrophages ($CD68^+$), whereas the more adaptive populations, including CD4 and CD8 T-cells were sparse throughout the tissue (Figure 3.1.1a-b).

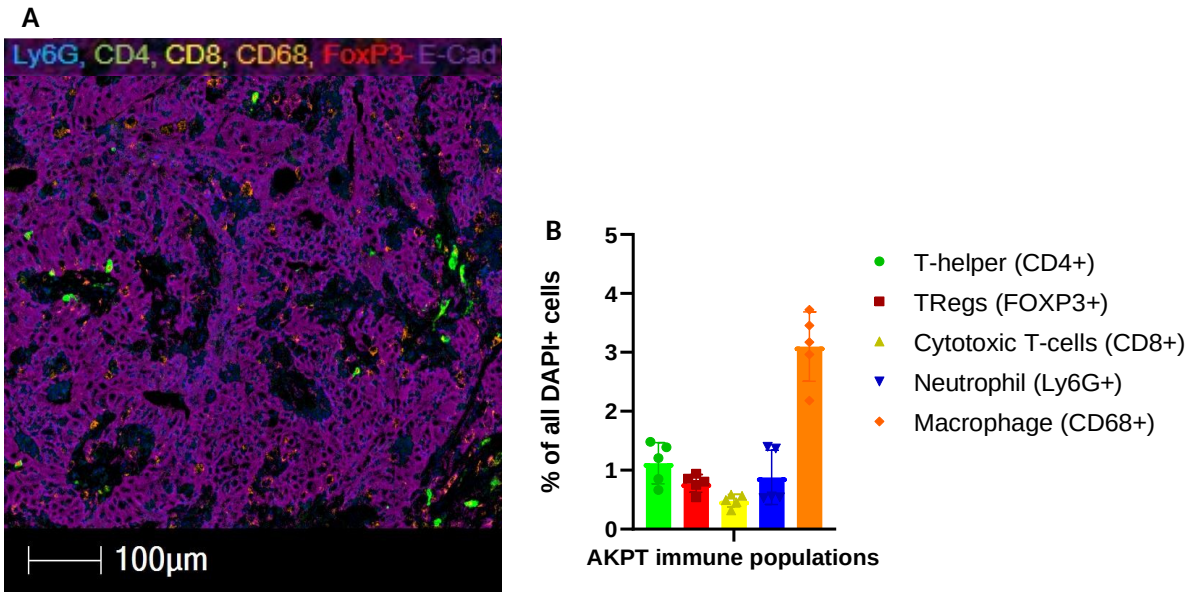


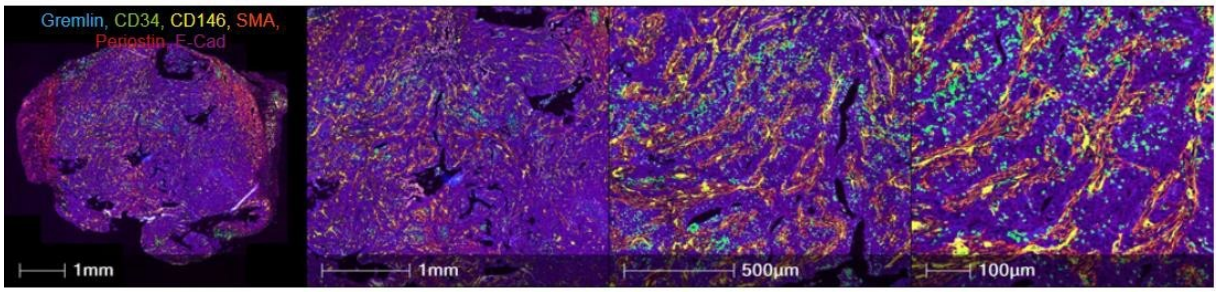
Figure 3.1.1 Immune cell composition of AKPT tumour TME prior to treatment.

(**A**) *VillinICreER* of *Apc*$^{fl/fl}$, *Kras*$^{G12D/+}$, *Trp53*$^{fl/fl}$, *Trgfbrl*$^{fl/fl}$ (AKPT) tumours implanted heterotopically then harvested and stained for multiple immune cells populations (Ly6G – neutrophil, CD4 – T-helper cells, CD8 – Cytotoxic T-cells, CD68 – macrophages, FoxP3 – Treg cells, E-cad – epithelium). (**B**) Using the HALO software, the number of immune cells within AKPT tumours was quantified based on the percentage of stained cells.

Crucially, the heterotopic AKPT-derived tumours featured a stroma rich in α-SMA^+ CAFs (Figure 3.1.2a-b). The CAF population acts as a significant contributor to the radiotherapy resistance demonstrated by poorly responding rectal tumours as described previously. However, this specific CAF phenotype, with α-SMA expression, has also been demonstrated to be the most frequent CAF biomarker (Rockey et al., 2013) and is correlated with increased tumour invasion in patients with rectal cancer (Nishishita et al., 2018). It is also important to note that the expression of α-SMA^+ by CAFs is linked with

TGF-β within the current literature (Ding et al., 2021; Putra et al., 2020). As described previously, TGF-β is an important factor in both the resistance of rectal tumours to radiation and the progression of the disease to metastasis.

A



B

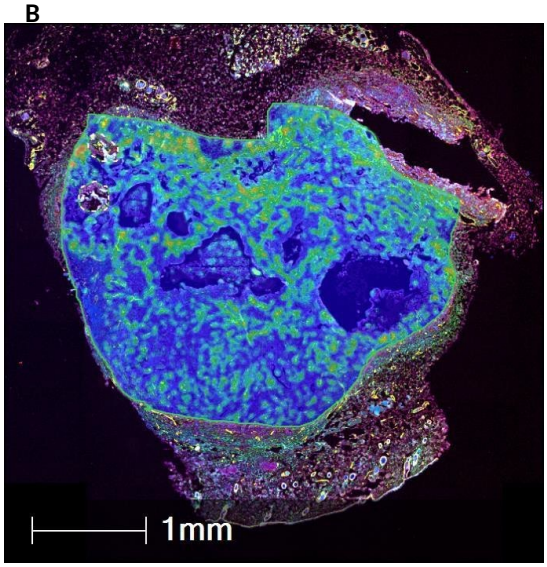


Figure 3.1.2 Stromal composition of AKPT TME prior to treatment

(**A**) Representative image of, *villinICreER* of *Apc*$^{fl/fl}$, *Kras*$^{G12D/+}$, *Trp53*$^{fl/fl}$, *Trgfbrl*$^{fl/fl}$ (AKPT) rectal tumour organoids grown subcutaneously. Multiplex staining of the harvested AKPT tumours for stromal markers and epithelium carried out. Stromal and epithelial stains for the full tumour shown in the whole tumour (left) and magnified regions.
(**B**) Using the HALO software location of α-SMA^{+} fibroblasts within the AKPT tumours were examined. From this a heat map was produced, with blue regions indicating an absence of the fibroblasts and green to red regions demonstrating the inverse.

Following the implantation of AKPT organoids subcutaneously, the immune cell population and stromal landscape demonstrated multiple similarities with rectal tumours found in patients who show the worst responses to typical treatment. The resulting heterotopic AKPT tumours formed a TME with CAF and macrophage stromal-rich regions. Additionally, these heterotopic tumours lacked significant adaptive immune cell populations, specifically the cytotoxic T-cell population. When comparing these findings to the literature regarding treatment resistant rectal tumours, this provided evidence that the heterotopic model was successful in recapitulating aspects of rectal cancer with poor outcomes.

3.2 Radiation response of the heterotopic organoid model

Following the establishment of the AKPT-derived heterotopic model we moved to investigate the response of resulting tumours to irradiation, due to its current use as a frontline treatment in patients. To investigate the use of radiation on heterotopic AKPT

tumours, we also looked to compare a single higher dose of irradiation against a fractionated treatment scheme. This is important for target discovery post-irradiation as differing doses of irradiation is known to have varying impacts on both the tumour itself and the surrounding TME. In rectal cancer, a greater pathological complete response has been linked with higher doses of irradiation (Appelt et al., 2013). Additionally, the use of higher doses of irradiation delivered in a smaller fractionation scheme, three doses rather than the minimum of five doses as prescribed as part of the short course treatment currently in use in clinic, is currently undergoing clinical trials in combination with immunotherapies (NCT02830594) (NCT02334709). Fractionated doses of irradiation have demonstrated a greater ability to exert immunomodulatory effects on the tumour TME (Demaria et al., 2021). Although single doses of irradiation have also demonstrated some ability to provide immunomodulation to the TME so it is critical to compare both when deciding on the radiation scheme to use *in vivo* (Demaria et al., 2021). Therefore, to investigate the impact of radiation fractionation on the AKPT tumours, the doses of 3x7Gy and 15Gy were chosen due to their similar biological effective dose (BED) on tumour epithelium, 35.7Gy and 37.5Gy respectively. The fractionation of 3x7Gy was chosen ahead of the more standard 3x8Gy due to issues with skin toxicity arising in the mice used.

Following irradiation, both the single-dose and fractionated treatment schedules demonstrated a significant increase in mouse survival with the AKPT tumour (Figure 3.2.1a). Additionally, both treatment schedules illustrated the same phenomena where a temporary arrest to tumour growth occurs before this is eventually overcome. When comparing the irradiation treatment schedules, there is no significant difference in mouse survival (Figure 3.2.1c).

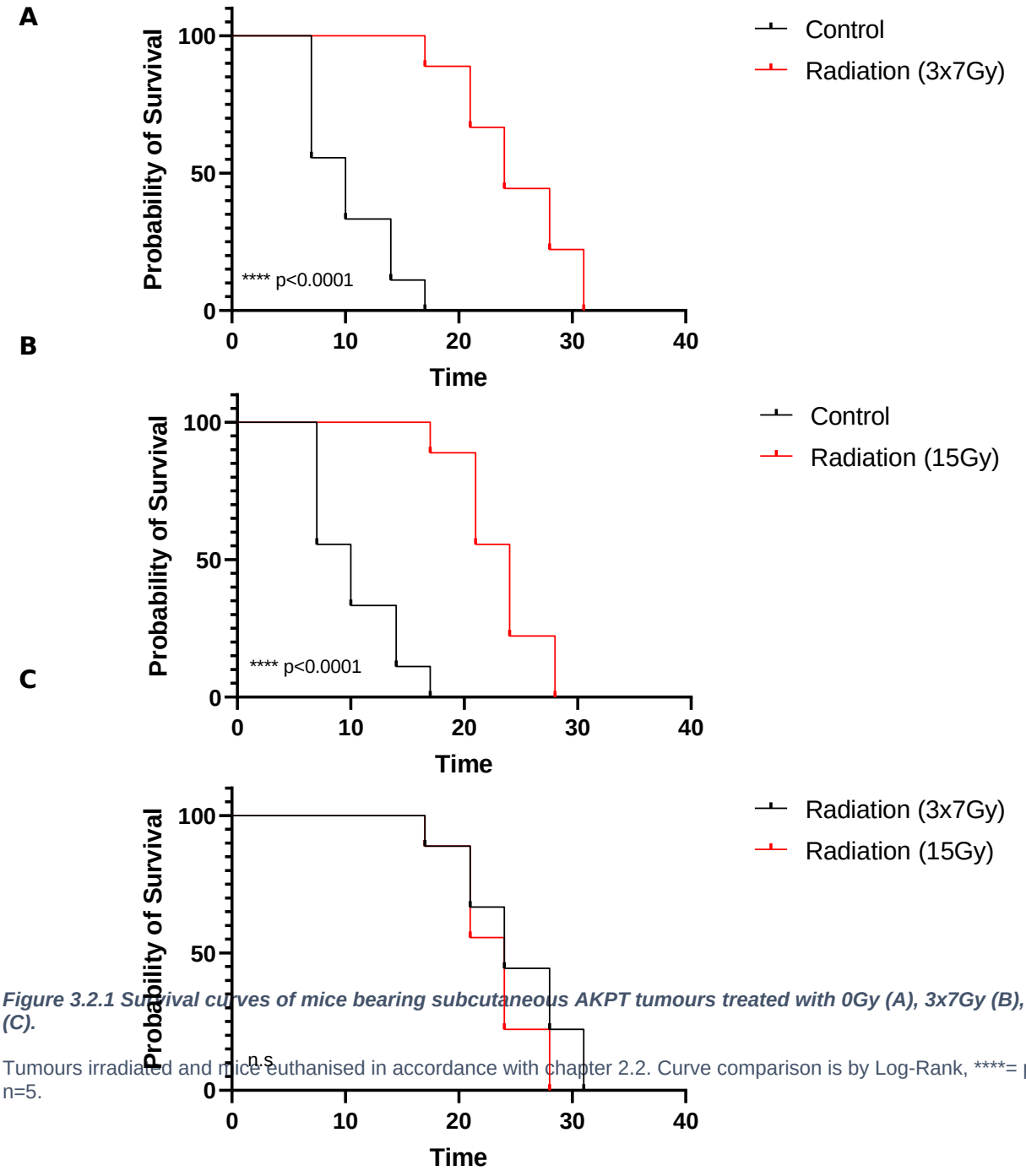
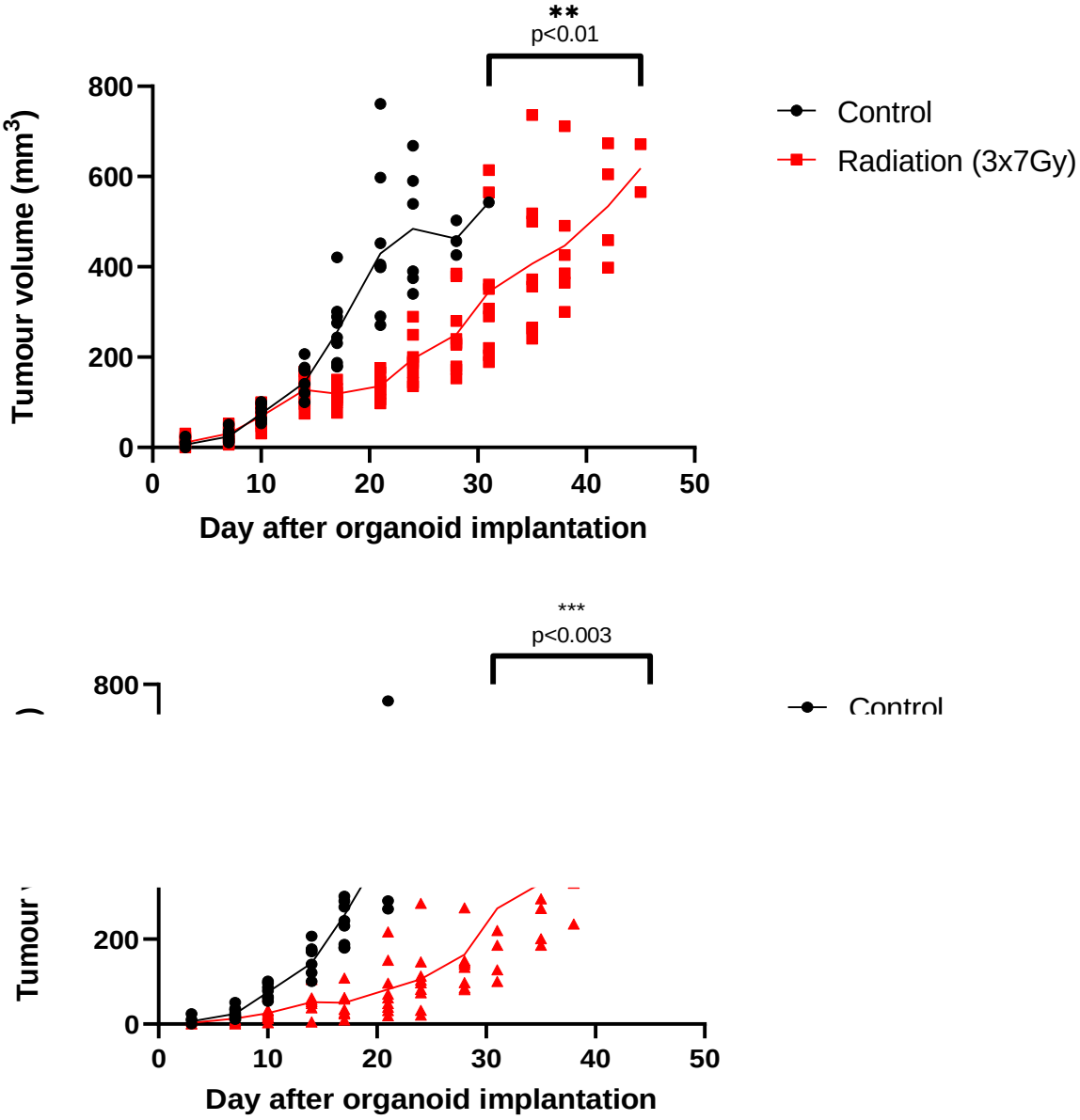


Figure 3.2.1 Survival curves of mice bearing subcutaneous AKPT tumours treated with 0Gy (A), 3x7Gy (B), or 15Gy (C).

Tumours irradiated and mice euthanised in accordance with chapter 2.2. Curve comparison is by Log-Rank, ****= p<0.001. n=5.

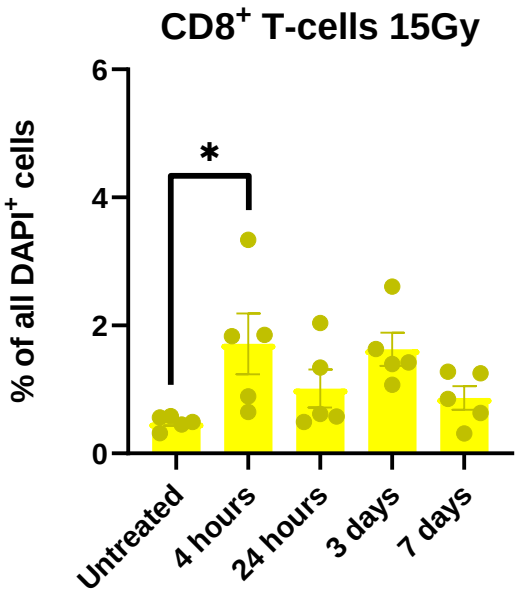
When comparing the tumour volumes over time post-irradiation, the heterotopic AKPT model demonstrated a temporary arrest to growth before progression resumed (Figure 3.2.2a-b). The ability of the AKPT tumours to regain the capacity for growth illustrates

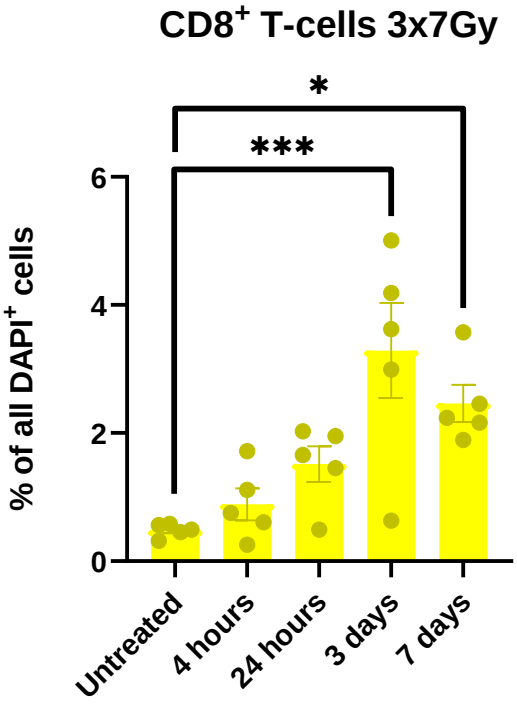
that post irradiation, may indicate that any immunogenic response is circumvented and that a change to the tumour TME facilitates the development of radioresistance.

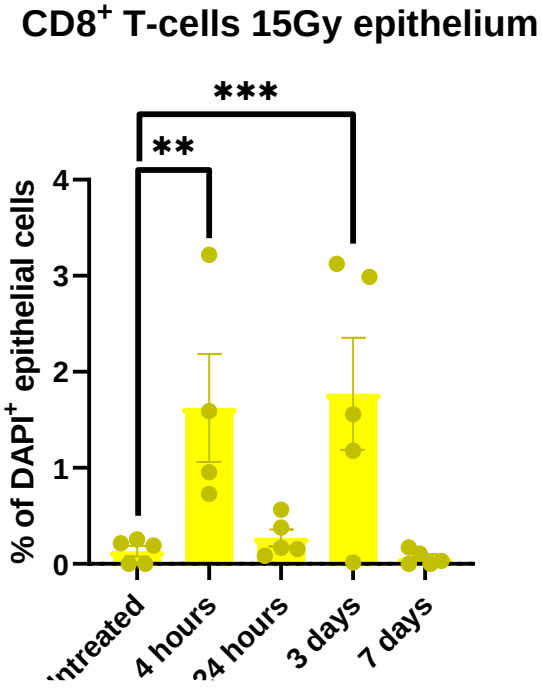


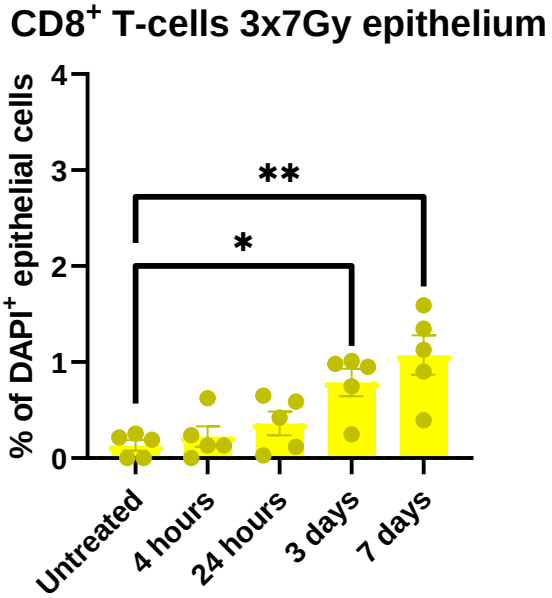
To elucidate the mechanism behind the pause in tumour growth, we investigated the AKPT tumour stromal and immune population changes post-irradiation for both treatment schedules. We performed this investigation by harvesting AKPT tumours at discrete timepoints after completing irradiation of the cancerous tissue.

Both the fractionated and single-dose treatment schedules demonstrated the ability to significantly increase the $CD8^+$ T-cell population four hours post-irradiation (Figure 3.2.3). This aligns with the current literature describing the acute immunogenic response post-irradiation. This is a key component in the initial reduction in tumour volume after irradiation, something mirrored by the AKPT model (3.2.2). However, the 3x7Gy treatment induced a more persistent effect, with the cytotoxic T-cells remaining significantly higher at later timepoints. This aligns with the current literature that outlines the increased immunogenic effect of irradiation when used in a fractionated treatment schedule to repeatedly rechallenge the tumour (Demaria et al., 2021). When we investigated the ability of the cytotoxic T-cells to infiltrate the tumour, interestingly we found that there was moderate success (Figure 3.2.3). In the 15Gy radiation treatment time course we saw significant infiltration four hours then three days post irradiation, with this infiltration being ablated by the latest timepoint (Figure 3.2.3). The use of the 3x7Gy fractionated treatment scheme also showed significant cytotoxic T-cell infiltration into the tumour epithelium at the later timepoints (Figure 3.2.3). Interestingly, we found that the $CD8^+$ T-cell infiltration was maintained up to a week after irradiation and potentially suggests immune evasion by the tumour post fractionated radiation.


CD8+ T-cells 15Gy
% of all DAPI+ cells
6
4
2
0
*
Untreated
4 hours
24 hours
3 days
7 days


CD8+ T-cells 3x7Gy
% of all DAPI+ cells
6
4
2
0
*
***
Untreated
4 hours
24 hours
3 days
7 days


CD8+ T-cells 15Gy epithelium
% of DAPI+ epithelial cells
4
3
2
1
0
**
***
4 hours
24 hours
3 days
7 days


CD8+ T-cells 3x7Gy epithelium
% of DAPI+ epithelial cells
4
3
2
1
0
*
**
Untreated
4 hours
24 hours
3 days
7 days

These results provide a potential rationale for the pause in tumour growth following the immunogenic effects of irradiation. The $CD4^+$ T-cell population mirrors some of the recruitment features following irradiation as seen by the cytotoxic T-cells (Figure 3.2.4). Following the single dose of irradiation, the $CD4^+$ T-cell population peaks acutely before reducing back to baseline in the later timepoints (Figure 3.2.4). However, following the fractionated 3x7Gy radiation treatment schedule the significant increase of the $CD4^+$ T-cell population peaks at the later timepoints (Figure 3.2.4).

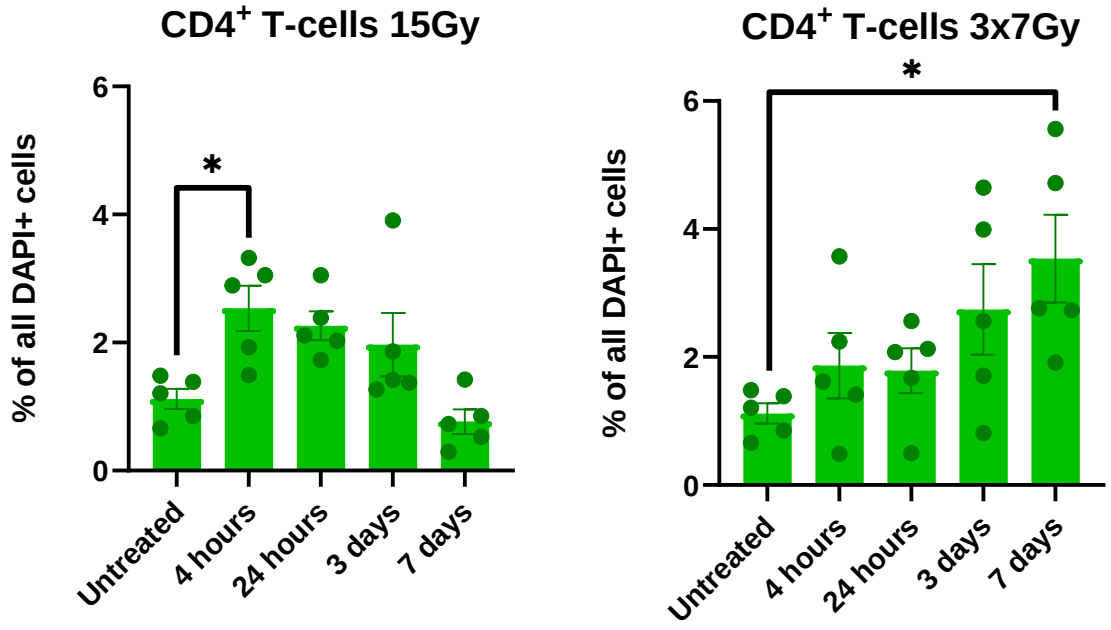


Figure 3.2.4 $CD4^+$ T-cell population changes as a proportion of $DAPI^+$ cells in subcutaneous AKPT tumours post single-dose or after the final fraction of 3x7Gy irradiation.

Using the HALO software, the changes to the $CD4^+$ T-cell population was analysed in the heterotopic AKPT tumour model were examined. All groups have n=5. Significance calculated by ordinary one-way ANOVA with Tukey's multiple comparisons (*P<0.05).

When investigating the immunosuppressive counterpart to these cells, Tregs, a significant increase is also observed in both treatment schedules (Figure 3.2.5). Following the single dose of irradiation, the Treg population was significantly increased three days after treatment, but this increase began to wane at the later timepoint (Figure 3.2.5). The fractionated irradiation demonstrated a sustained significant increase at the latter two timepoints in the Treg population (Figure 3.2.5). Interestingly, this pattern of increase in

the Treg population post fractionated irradiation mirrors the increase seen by the cytotoxic T-cells. It is well described in the literature that the increase of Treg infiltration into the tumour epithelium is strongly linked with poor rectal cancer patient prognosis (Aristin Revilla et al., 2022; Tanaka & Sakaguchi, 2017). When investigating Treg infiltration into the tumour epithelium post irradiation we found that it was increased at differing timepoints depending on the radiation treatment scheme. With the single-dose radiation dose, very little increase was observed with some infiltration occurring at the three-day timepoint (Figure 3.2.5). After irradiating the tumour with the fractionated dose, we saw a sustained increase in Treg infiltration that occurred at later timepoints (Figure 3.2.5). Although this increase failed to meet the threshold of statistical significance, this increase and its mirroring of the pattern of $CD8^+$ T-cell infiltration is notable.

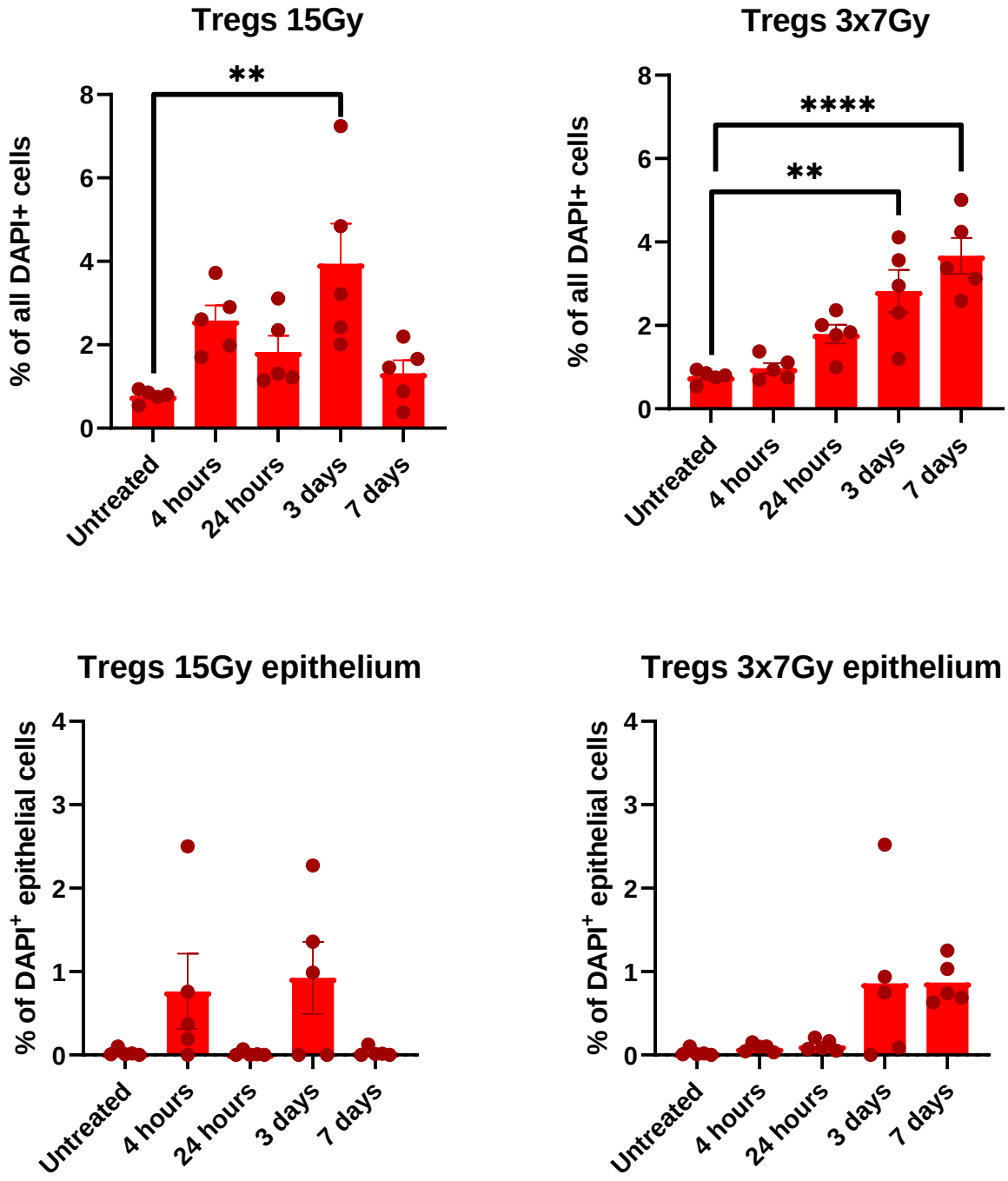


Figure 3.2.5 Treg (FOXP3$^+$) T-cell population changes as a proportion of DAPI$^+$ cells in subcutaneous AKPT tumours post single-dose or after the final fraction of 3x7Gy irradiation.

Using the HALO software, the changes to the Treg population was analysed in the heterotopic AKPT tumour model were examined. Machine learning-based quantification of AKPT epithelial infiltration by Treg post irradiation at a variety of timepoints was also carried out. All groups have n=5. Significance calculated by ordinary one-way ANOVA with Tukey's multiple comparisons (**P<0.01, ****P<0.001).

In accordance with data within the current literature, neutrophil ($Ly6G^+$) population significantly increased across the earlier timepoints following both single-dose and fractionated irradiation (Takeshima et al., 2016). However, this significant increase wassustained across all timepoints, specifically at seven days post-irradiation for both irradiation treatment schemes (Figure 3.2.6a-b).

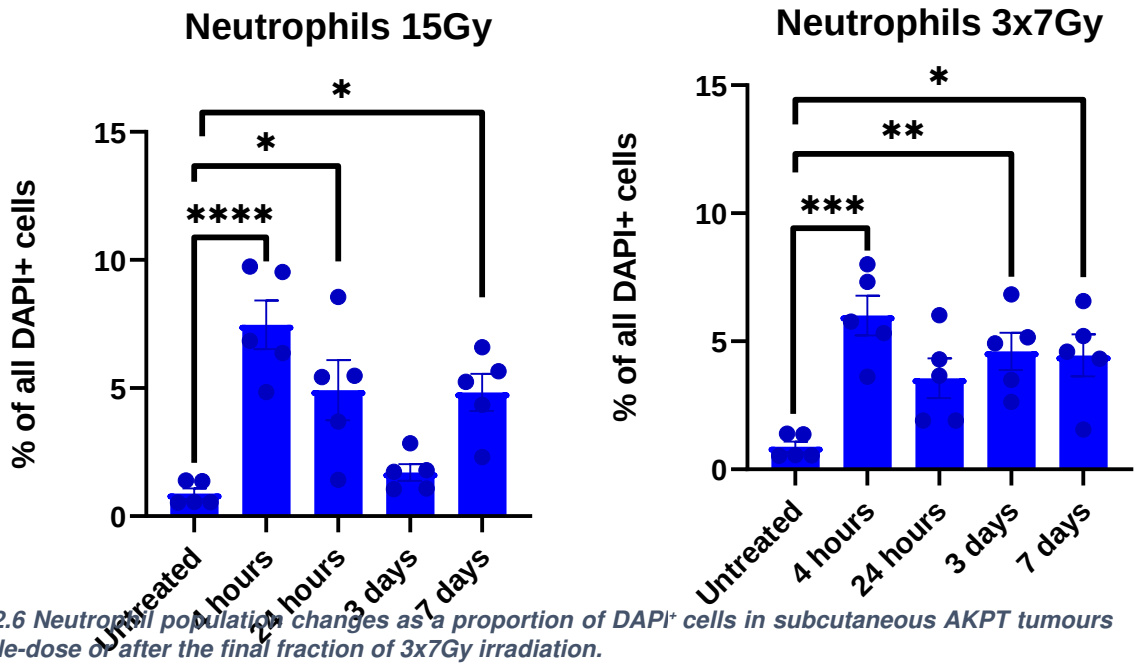


Figure 3.2.6 Neutrophil population changes as a proportion of DAPI⁺ cells in subcutaneous AKPT tumours post single-dose or after the final fraction of 3x7Gy irradiation.

Using the HALO software, the changes to the neutrophil population was analysed in the heterotopic AKPT tumour model were examined. Machine learning-based quantification of AKPT epithelial infiltration by neutrophils post irradiation at a variety of timepoints was also carried out. All groups have n=5. Significance calculated by ordinary one-way ANOVA with Tukey's multiple comparisons (*P<0.05, **P<0.01, ***P<0.001, ****P<0.0001).

Finally, when examining the macrophage population of the AKPT tumour post irradiation, we found that in the single-dose treatment scheme there was an acute increase in the population that trended back to baseline over time (Figure 3.2.7a). After tumours received the fractionated dose regimen, we observed no significant increase (Figure 3.2.7b). Importantly, the literature describes the recruitment of macrophages post irradiation of the tumour as a response to radiation injury to the cancer cells (Beach et al., 2022; Meziani et al., 2018). This disparity in macrophage recruitment may be explained due to a discrete population count being taken at specific timepoints. Therefore, the recruitment, and concurrent death of some macrophages, can result in an active change in the population that is not represented by the overall cell count.

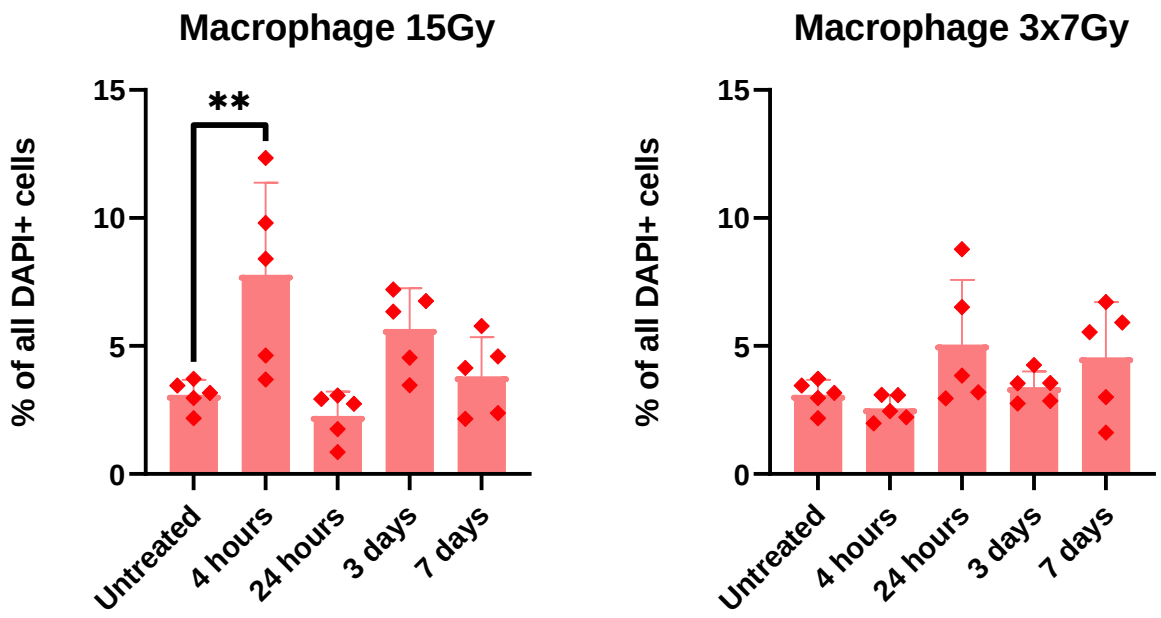


Figure 3.2.7 Macrophage population changes as a proportion of DAPI⁺ cells in subcutaneous AKPT tumours post single-dose or fractionated irradiation.

Using the HALO software, the changes to the macrophage population was analysed in the heterotopic AKPT tumour model were examined. All groups have n=5. Significance calculated by ordinary one-way ANOVA with Tukey's multiple comparisons (**P<0.001).

Interestingly, the specific changes of the immune cell populations within the tumour TME post-irradiation in combination with the current rectal cancer literature landscape, led us to consider the potential of TGF-β inhibition in improving tumour response to radiation. Aspects of the AKPT TME post irradiation reflects aspects of TGF- β involvement. The inability of $CD8^+$ T-cells to sustain an anti-tumour effect even after epithelial infiltration is well documented as a feature of TGF-β signalling. Specifically, TGF-β signalling is linked with the inhibition of granzyme B and IFNγ expression (Thomas & Massagué, 2005); the expression of chemokine receptor CXC motif 3 (CXCR3), key for effector T-cell function (Gunderson et al., 2020); and enhancement programmed cell death protein 1 (PD-1) as well as cytotoxic T-lymphocyte associated protein 4 (CTLA- 4) (Bao et al., 2021). Additionally, the significant sustained increase in the Treg population is a documented effect of TGF-β signalling. TGF-β acts to enforce the increase in a shift of the T-helper cell population to the immunosuppressive $FOXP3^+$ Treg phenotype (Chen et al., 2003; Fantini et al., 2004). The Treg population has been demonstrated to have a reduction in population size as well as influence on the cytotoxic T-cell population following TGF-β inhibition (Budhu et al., 2017). Interestingly the abnormal neutrophil population increase that is maintained after the acute phase post irradiation can be partially explained by the potent chemoattraction TGF-β imparts on peripheral

neutrophils to draw them into the tumour (Reibman et al., 1991). TGF-β also has a critical impact on blunting anti-tumour neutrophil activity, including the reduction in degranulation, thereby inhibiting some immunogenic aspects of irradiation (Fridlender et al., 2009; Shen et al., 2007). Additionally, the literature also outlines sources for TGF-β as including macrophages (Wynn & Barron, 2010), neutrophils (Grotendorst et al., 1989), Tregs (J. Wang et al., 2023), and α-SMA$^+$ fibroblasts (Liu et al., 2019). These immune cell populations all feature within the AKPT tumour stroma, with macrophages and α-SMA$^+$ fibroblasts being particularly abundant within the TME. With TGF-β becoming a molecule of interest to improve radiotherapy in the AKPT heterotopic model, we then sought to both rationalise this potential target and potentially discover other molecules of interest through further interrogation of these tumour samples.

3.3 Target identification for potential neoadjuvant therapies

To identify radiation-responsive pathways within these immunosuppressive tumours and isolate potential druggable targets RNA-seq analysis was undertaken by Gabriel Valbuena. Interestingly, network analysis of differentially expressed pathways post-irradiation indicated that the complement cascade was significantly upregulated and, crucially, was the top ranked pathway annotated as “Immune system pathway” in Reactome analysis at early timepoints post irradiation (Figure 3.3.1). Examining the most enriched “immune system pathways” after irradiation demonstrated a large, systemic change to the TME after irradiation. Four hours after irradiation the most enriched immune pathway was the complement cascade signalling pathway. Additionally, highly enriched immune pathways included: MHC-I and MHC-II antigen-presentation; T-cell receptor signalling; PD-1 signalling; neutrophil degranulation; immunoregulation between lymphoid and non-lymphoid cells; B-cell signalling; and IL-1 signalling, from most to least enriched. Twenty-four hours after irradiation, the most enriched immune pathways included: interferon signalling; MHC-I and MHC-II antigen cross-presentation; neutrophil degranulation; ROS production in phagocytes; activation of phagocytes; PD-1 signalling; the complement cascade; T-cell receptor signalling; and cytokine signalling, from most to least enriched. Three days after irradiation, the most enriched immune pathways included: neutrophil degranulation; interferon signalling; MHC-I and MHC-II antigen cross-presentation; ROS production in phagocytes; IL-20

signalling; cytokine signalling; IL-4 and IL-13 signalling; immunoregulatory interactions between lymphoid and non-lymphoid cells; the complement cascade; IL-6 signalling; and IL-1 signalling from most to least enriched. Seven days after irradiation, the most enriched immune pathways included: MHC-I and MHC-II antigen cross-presentation; CD28 stimulation of the T-cell receptor; interferon signalling; neutrophil degranulation; T-cell receptor signalling; immunoregulatory between lymphoid and nonlymphoid; PD-1 signalling; IL-2 signalling; cytokine signalling, Il-3, IL-5 and granulocyte-macrophage colony-stimulating factor; B-cell receptor signalling; cytotoxic T-lymphocyte associated protein 4 (CTLA-4) signalling; the complement cascade; phagocytosis pathway activation; IL-20 signalling; VEGF signalling; IL-6 signalling; IL-1 signalling; ROS production by phagocytes; and the toll-like receptor cascade, from most to least enriched. Interrogating the complement cascade pathway further illustrated that numerous members of the main complement functional categories (components, pattern recognition molecules, proteases, receptors, and regulators) showed transient enhanced expression (Figure 3.3.1). This transient increase was demonstrated by both the single dose and fractionated treatment schedules of radiation (Figure 3.3.1).

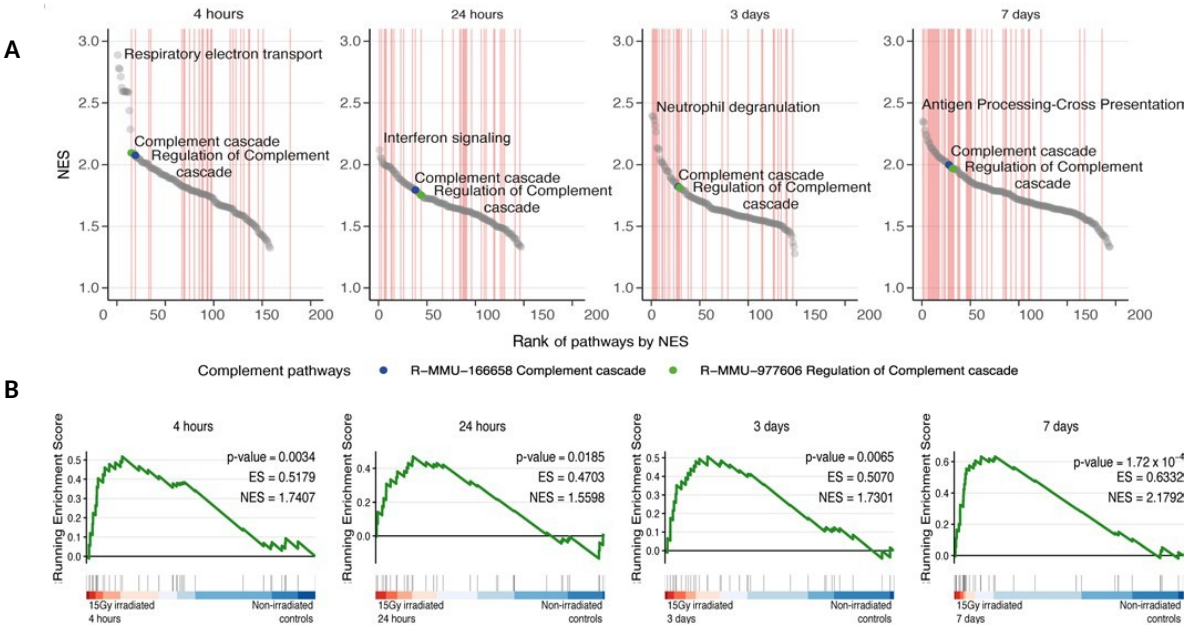


Figure 3.3.1 Identification of complement pathway upregulation post irradiation.

(A) Ranked normalised enrichment scores (NES) ordering the positively enriched pathways post irradiation of heterotopic AKPT tumours across a range of timepoints.

(B) Pairwise gene set enrichment analysis comparing irradiated heterotopic AKPT tumours across a range of timepoints compared with unirradiated controls.

Figures constructed by Gabriel Valbuena (Beach et. al. 2023).

To identify potential druggable targets within the complement cascade, the

DepMap database (a combination of CRISPR-Cas9 and RNAi screens in more than seven hundred cell lines) was interrogated to find any cancer-derived complement proteins. Additionally, a gene was only considered if it was “druggable” based on structural and ligand-based assessment (as shown in green, Figure 3.3.2a). Drug targets were only considered if they were non-essential as we reasoned this would lead to the discovery of genes providing stress-specific dependencies, thereby reducing the chance of mediating toxicity in normal tissue. From this approach of identifying complement targets for the

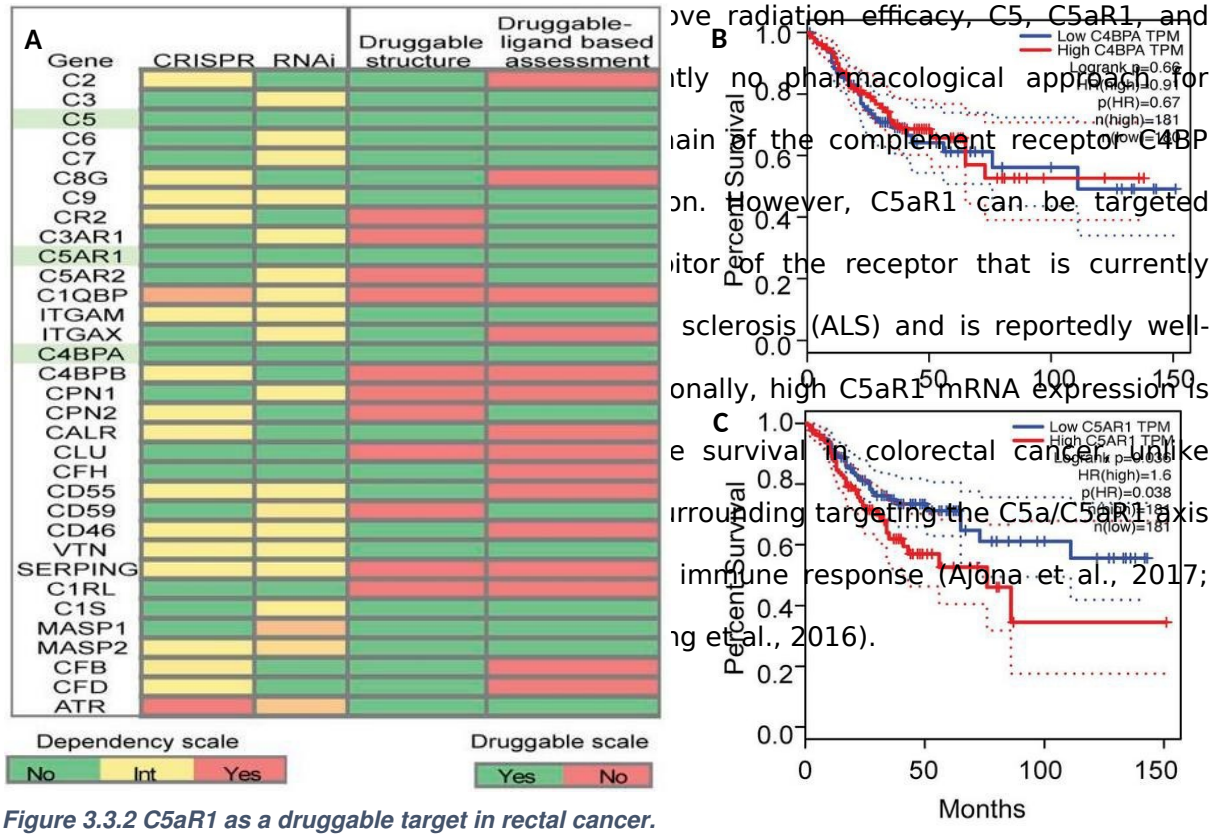


Figure 3.3.2 C5aR1 as a druggable target in rectal cancer.

Essential genes are shown in red and nonessential genes in green. Yellow or orange indicates intermediate dependence or essentiality. For target tractability, green represents a druggable structure, with red representing a non-druggable one.

Kaplan-Meier (KM) curve for disease-free survival (DFS) of TCGA patients with colorectal cancer with high (red) or low (blue) C4BPA mRNA expression. For all KM curves, group cutoff = median.

KM curve for DFS of TCGA colorectal cancer with high (red) or low (blue) C5aR1 mRNA expression. (Beach et.al. 2023).

Since C5aR1 is a druggable target with expression correlating with poor outcomes in colorectal cancer patients, we then looked at the expression of the receptor in the AKPT model. When looking for C5aR1 expression in *in vitro* AKPT organoids we found that the complement protein was significantly over expressed when compared with wild-type, non-tumour organoids.] (Figure 3.3.3).

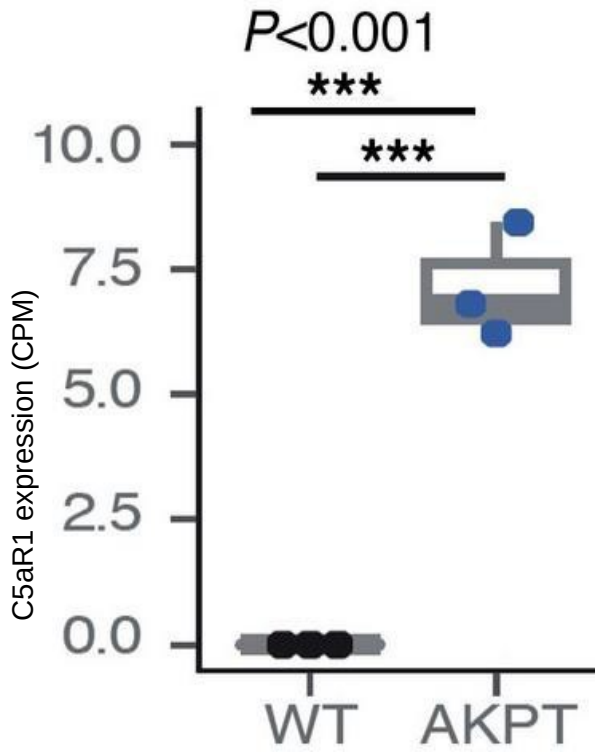


Figure 3.3.3 C5aR1 expression (CPM) assessed by RNA-seq in wildtype (WT) or AKPT organoids grown in vitro.

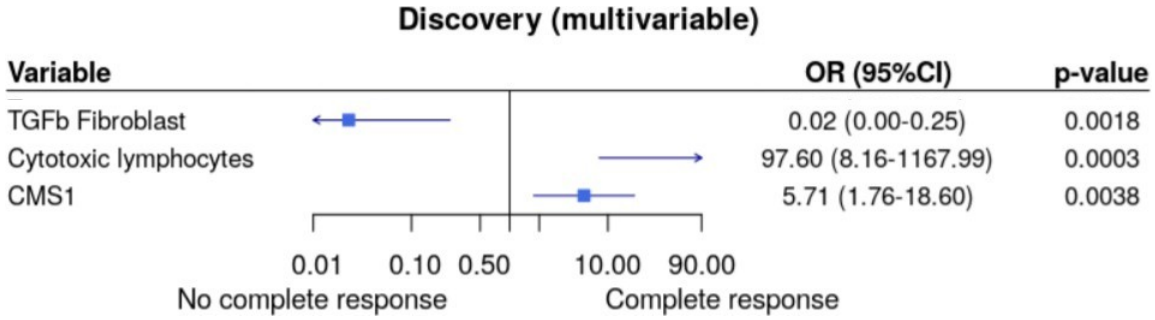
Empirical Bayes moderated t-statistic test (***P<0.001).

(Beach et. al. 2023)

Following on from this examination of AKPT tumours post irradiation, the data suggests that the complement system is a suitable pathway for targeting to improve the anti-tumour effect of radiation. With the data generated in chapter 3.2, in combination with the current literature surrounding rectal cancer, TGF-β appeared to be a clear candidate for targeting to improve radiotherapy efficacy when treating the AKPT tumours.

Access to the S-CORT rectal tumour biopsy dataset, previously analysed by Enric Domingo (Domingo et al., 2022) demonstrated that TGFβ-producing fibroblasts proved to be a significant marker for tumour radiotherapy response (Figure 3.3.4). Additionally, in line with current literature (Suzuki et al., 2010) the presence of $CD8^+$ cytotoxic T-cells predicted a better response to radiation patients (Figure 3.3.4).

Figure 3.3.4 Prognostic factors in patient rectal tumours predicting response to radiotherapy.



Forest plot of the GRAMPIAN and ARISTOTLE patient biopsy datasets from the S-CORT database. Predictive features of rectal tumours toward a complete response to radiotherapy in patients were identified by Enric Domingo.Figure constructed by Enric Domingo, (Domingo et al., 2022)

The identification of TGF-β as a druggable target is bolstered further by the work of Tauriello and colleagues, demonstrating that TGF-β plus PD-1 inhibition acted to inhibit metastasis whilst enhancing survival in an autochthonous colorectal tumour model (Tauriello et al., 2018). This combination of treatment, TGF-β plus PD-1 inhibition, has also entered in early clinical trials (NCT04515979). Combining these findings previously described with the data from mouse AKPT tumour tissue, including patterns of immune cell recruitment associated with TGF-β expression and presence of known sources of this molecule as described in chapter 3.2, led us to interrogate the RNAseq dataset further to investigate the TGF-β signalling pathway.

When comparing the single dose and fractionated radiation treatment schedules we observe that there is a lack of enrichment in the TGF-β signalling pathway across the timepoints in either radiation treatment schedule (Figure 3.3.5a). This was especially apparent when compared to the wide range of enriched immune system pathways as seen in Figure 3.3.1a. Interestingly, acutely the TGF-β signalling pathway appeared to be negatively enriched (Figure 3.3.5a). With irradiation having no impact on TGF-β

signalling we then decided to investigate any confounding factors within the AKPT TME that may have caused this, due to this data directly contradicting both the current literature as well as phenotypic changes seen with the AKPT tumours post irradiation. Crucially, we found that within the heterotopic AKPT tumours there was strong activin staining throughout (Figure 3.3.5b). Activin acts through the Smad pathway, causing the formation of Smad 2,3, and 4 complex through Alk4/7 receptor, to induce transcriptional changes (Bashir et al., 2015; Qiu et al., 2021; Wrana & Attisano, 2000). The well documented Smad signalling pathway is the canonical method of TGF-β signalling (Clayton et al., 2020), therefore we hypothesised that the presence of activin acts as a confounding factor when trying to examine TGF-β signalling in heterotopic AKPT tumours post irradiation.

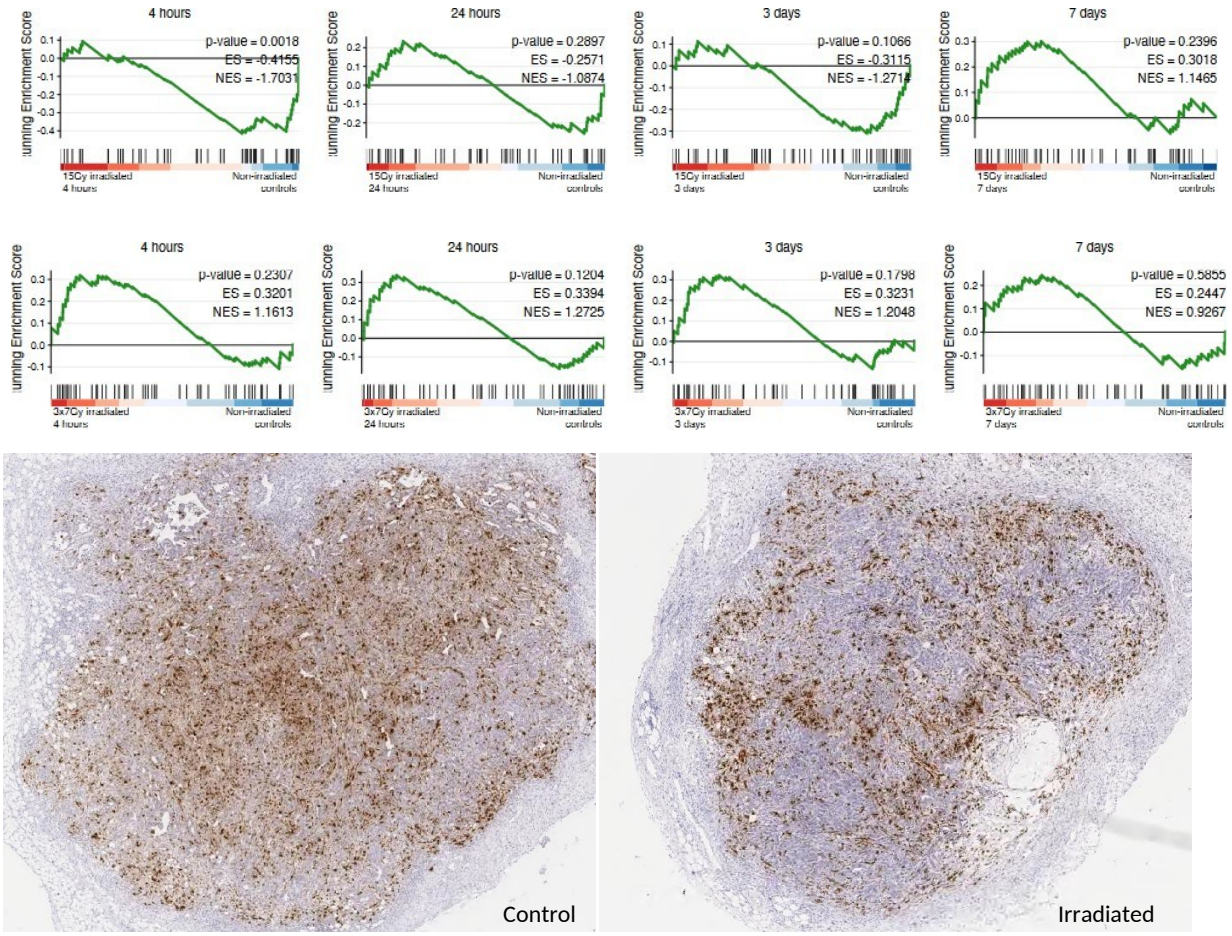


Figure 3.3.5 TGF-β signalling pathway upregulation in subcutaneous AKPT tumours after receiving radiation and activin staining of AKPT tumours.

(A) GSEA plots of AKPT tumours measuring the enrichment of the TGF-β signalling pathway at 4 hours, 24 hours, 3 days, and 7 days after irradiation with either a single or fractionated dose. Figure constructed by Gabriel Valbuena.

(B) *In situ* hybridisation staining of *Inhba*, a marker for the presence of activin, in both untreated and irradiated AKPT tumours (samples seven-days post irradiation).

In collaboration with Gabriel Valbuena, we then investigated the most significantly enriched genes post irradiation of the heterotopic AKPT tumours to observe changes to TGF-β signalling that may be hidden due to the amount of intrinsic Smad pathway activation. When examining the most significantly enriched genes, we found that the fractionated 3x7Gy irradiation had the greatest impact on altering TGF-β signalling within the TME. After fractionated irradiation, we found that out of the top twenty, nine of these were TGF-β specific through non-canonical signalling (Figure 3.3.6). When including TGF-β Smad signalling pathway, sixty five percent of the most enriched genes are all directly related to TGF-β (Figure3.3.6). The fractionated dose of irradiation provided both

more sustained enrichment of TGF-β specific genes as well as more upregulation at the acute timepoints than the single dose (Figure 3.3.6). Interestingly, *Hint1* acts to inhibit TGF-β2 function (L. Wang et al., 2009) and is also found to be significantly enriched (Figure 3.3.6) suggesting a potential negative feedback mechanism.

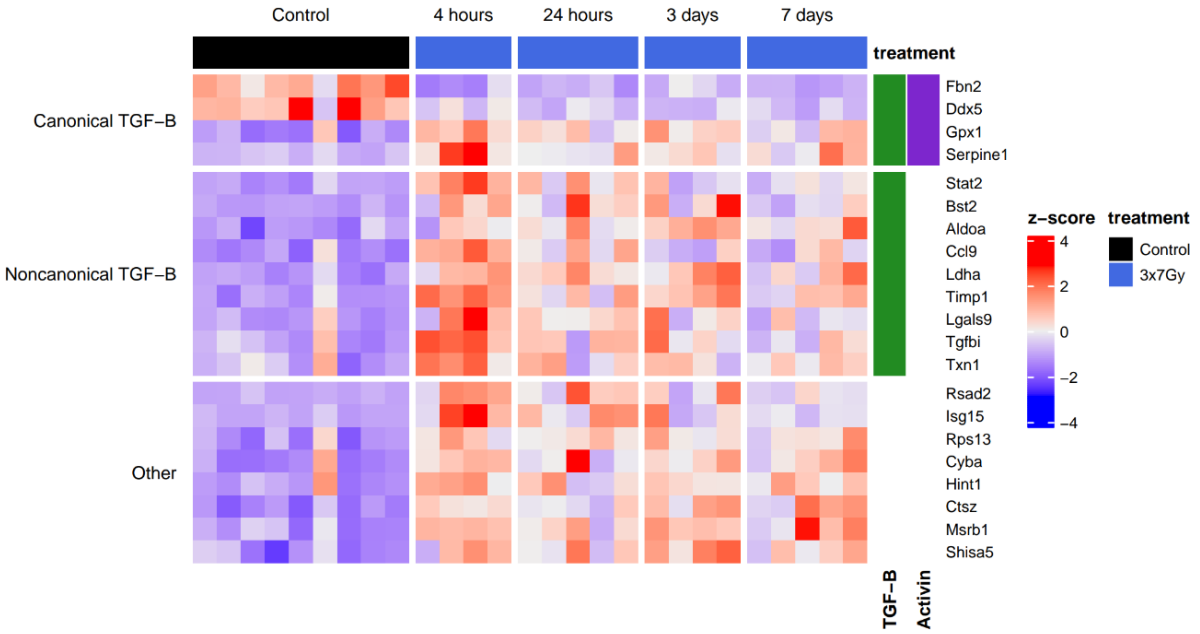


Figure 3.3.6 Heat map of the top 20 enriched genes after irradiating in vivo AKPT tumours with a 3x7Gy fractionation.

Upregulation is shown in red, as per the listed Z-score. Enriched genes catagorised by relation to TGF-β signalling pathway: canonical, noncanonical, and not related. Analysis of the extracted RNA and the construction of the figure were both performed by Gabriel Valbuena.

3.4 Discussion

We have demonstrated that the AKPT tumour model acts as a suitable heterotopic rectal cancer model that recapitulate key facets that predict poorer outcomes in patients (Figures 3.1.1-2). Furthermore, we observed that the heterotopic AKPT model proved to respond only modestly to irradiation, with tumour growth transiently inhibited rather than being arrested outright or regressing (Figures 3.2.1-2). This was the case both when irradiating these tumours with a single-dose or through a fractionated dosing schedule (Figures 3.2.1-2). Additionally, the changes in immune cell infiltration into the tumour

epithelium, specifically the modest increase in $CD8^+$ T-cells and Tregs, gave rise to the possibility of improving tumour treatment through incorporating immunomodulatory drugs. This is a concept that is relatively well understood within the field, and has shown success when using PD-1/PD-L1 or CTLA-4 inhibitor class of drugs within the clinic (Antonia et al., 2017; Bang et al., 2017; Ho et al., 2020; Lin et al., 2021; Mattes et al., 2021; Reardon et al., 2020; Spaas et al., 2021; Welsh et al., 2020; Yuan et al., 2021).

RNA-seq analysis of post irradiation AKPT tumours provided support for C5aR1 and TGF-β as promising therapeutic targets in rectal cancer that warranted further research. Therefore, we next investigated both potential signalling pathways as targets for improving the radiation response of AKPT tumours. Furthermore, we investigated potential mechanisms underlying any improvement in radiation response when inhibiting C5aR1 or TGF-β.

Chapter 4

Investigating the impact of C5aR1 inhibition on the radiation response of rectal cancer

4.1 Background

As described in chapter 3, C5aR1 demonstrated itself to be both highly upregulated in the AKPT tumour model in vivo as well as in patient samples. Importantly, data from the DepMap database also demonstrated that C5aR1 was a “druggable” target, that was involved with a non-essential stress-specific response. Current literature also demonstrates that high expression of complement system components play a major role in the inflammatory environment in rectal tumours that display the worst survival outcomes (Becht et al., 2016; Krieg et al., 2022). The complement system, an ancient component of the innate immune system, has recently come under increased scrutiny for its role in both autoimmunity and cancer (Daugan et al., 2021; Gros et al., 2008; Pio et al., 2014; Ricklin et al., 2010; Roumenina et al., 2019).

In accordance with the patient samples analysed in chapter 3, recent investigation into the role of the complement system within the TME has unveiled the importance of mechanisms mediated by this pathway. This includes the orchestration of multiple different functions assisting tumour growth (Kolev & Markiewski, 2018). Critically, although the complement system is able to mediate cytotoxicity toward tumour cells (Macor et al., 2018), this level of cell death remains insignificant in curbing the cancerous growth in part due to evasive mechanisms employed (Fishelson & Kirschfink, 2019). The complement system has also demonstrated an ability to organise the establishment of an immunosuppressive TME. Through the innate immune system, the complement system specifically acts to skew the TAM phenotype within the TME

towards an M2-like expression pattern (Bonavita et al., 2015). The complement system has also been documented to impact the adaptive arm of the tumour immune response. Within the tumour space, C5a expression causes a shift in the T-helper cell population to favour the TH2 phenotype that acts ineffectively to promote cytolytic $CD8^+$ T-cell function (Kochanek et al., 2018). Interestingly, an increase in the Treg population stemming from the original T-helper cell group has also been documented and linked with C5a expression (Kochanek et al., 2018). Outside of the surrounding TME, the complement family of proteins may also have a direct role in promoting tumour cell proliferation, migration, and EMT both inter and intracellularly (Fan et al., 2019; O'Brien et al., 2023; R. Zhang et al., 2019). Recently, current literature has identified the importance of the complement system in the progression of tumours within patients (Ajona et al., 2019; Daugan et al., 2021). Though the impact of the complement system on specific areas of TME orchestration and tumour cell-specific interactions have been outlined, this burgeoning field of research is yet to be fully investigated for future therapeutics.

The activation of C5aR1, a target identified during chapter three, has been reported as a central mediator of tumour promotion within the surrounding microenvironment, alongside C3aR (Ajona et al., 2019). When considering rectal cancer specifically, C5aR1 plays a relatively all-encompassing role in the promotion and subsequent progression of the disease. Within a newly forming TME, C5aR1 acts as a master regulator of tumorigenesis *in vivo*, through the modulation of immune function (Ding et al., 2020). C5aR1 activation was also found to be involved in the proliferation, migration and invasion of rectal cancer cells through the regulation of the Wnt/β-catenin pathway (Xu et al., 2023). Inhibition of C5aR1 has been shown to impact immunosuppressive TAMs leading to improved efficacy of PD-1 inhibition in gastric cancer (P. Zhang et al., 2023). This provides an exemplar of C5aR1 inhibition in combination therapy that impacts TME signalling and results in improved tumour response. Alongside the establishment of a pro tumour TME, C5aR1 expression is also linked with the enhancement of matrix metalloproteases (MMP's) thereby facilitating

cancer cell entrance into circulation and increased metastasis (Maeda et al., 2015).

In addition to complement components orchestrating the establishment of immunosuppression within the tumour microenvironment, this family of proteins play a key role in the tumour response to irradiation. Studies have demonstrated the association between tumour irradiation and the local, transient activation of complement pathways (Surace et al., 2015). Specifically, the generation of an immunogenic response against the tumour post-irradiation is linked with the production of C3a and C5a and subsequent binding with their respective receptors (Surace et al., 2015). Additionally, there may be a role for the complement system post tumour irradiation in facilitating the efficient mounting of an anti-tumour $CD8^+$ T-cell response (Regal et al., 2016; Surace et al., 2015). Furthermore, it has been found that complement inhibition, through C3a and C5a blockade, in combination with radiotherapy only improves survival in an *in vivo* model of head and neck squamous cell carcinoma when combined with specific anti-Treg therapy due to the T-helper cell phenotypic shift seen (Gadwa et al., 2021). However, a neutrophil- dependent modulation of T-cell tumour immunity post irradiation was demonstrated through the combination of complement inhibition and radiotherapy which significantly improved survival in an *in vivo* model of murine lymphoma (Elvington et al., 2014). An *in vivo* study in a murine model of glioblastoma demonstrated complement enhancement of radiotherapy anti-tumour efficacy through the indoleamine 2,3-dioxygenase (IDO) pathway (Li et al., 2014). This study outlining IDO pathway involvement is of note due to the well described involvement this pathway has in activating the Treg phenotype from the T-helper population (M. Liu et al., 2018). This combination of findings gives a potential exemplar of complement orchestration of the immunosuppressive TME through the expansion of the Treg population.

Although targeting the complement system is emerging as a promising therapeutic avenue in cancer, whether targeting this pathway will be a sum benefit is relatively unclear. In published studies, the anti-inflammatory glucocorticoid dexamethasone is typically used as the complement inhibitor due to its use in the clinic alongside radiotherapy, especially in studies demonstrating complement inhibition having a

potential reversing effect on the immunogenic response post irradiation. This method of inhibition acts to blockade both the C3a and C5a axis, therefore suggesting a specific approach to inhibiting complement, especially when considering notable success has been found when targeting C5aR1 specifically (Ajona et al., 2019; Ding et al., 2020). However, the question remains whether the inhibition of complement components will reduce the efficacy of the immunogenic response mounted post irradiation or help inhibit the establishment of an immunosuppressive TME. In the *in vivo* AKPT model, we see that irradiation of the tumour promotes a limited cytotoxic T-cell response with limited epithelial infiltration. This naturally lends itself to the idea that, at least within this tumour model and by extension rectal tumours exhibiting poor immune infiltration, the complement system is failing to initiate an anti-tumour immune response. Therefore, with C5aR1 revealing itself as a target of interest within this rectal tumour model, we hypothesised that the C5a/C5aR1 signalling axis is predominantly acting to form an immunosuppressive TME in this tumour setting. To test this hypothesis, it is critical we establish where within the tumour TME is C5aR1 being expressed. This importance of identifying C5aR1 expression areas is further compounded when considering that C5a is expressed by tumour cells outside of the canonical hepatocyte origin (Zwirner et al., 1999), and the corresponding C5aR1 is also expressed on rectal tumour epithelium (Xu et al., 2023) as well as intracellularly (Ding et al., 2022; O'Brien et al., 2023).

4.2 C5aR1 expression in the AKPT rectal tumour model.

With C5aR1 targeting having undergone clinical testing as a method to reinvigorate anti-tumour $CD8^+$ T-cell responses in advanced solid tumours (Massard et al., 2019), investigating what cell compartments were expressing the complement receptor, and thereby impacted by its inhibition, was critical. The importance of investigating the areas of C5aR1 expression within the tumour and its surrounding milieu was reinforced by the literature describing C5aR1 expression on a range of different innate immune cells, including monocytes, macrophages, and neutrophils (Dunkelberger et al., 2012; Karsten et al., 2015; Soruri et al., 2003; Werfel et al., 1992). Additionally, C5aR1 is also described as being well expressed on rectal tumour cells as well as

intracellularly. To investigate this, we harvested AKPT tumours at discrete timepoints post-irradiation, akin to the work done during target discovery, to investigate the constituent make-up of C5aR1 areas of expression over time.

Initial immunohistochemistry (IHC) staining for C5aR1 on heterotopic AKPT tumours that had undergone irradiation illustrated that, prior to treatment, the tumours expressed the receptor on the epithelium (Figure 4.1.1). After irradiation of the AKPT tumours, C5aR1 expression significantly increased twenty-four hours post radiation before returning to levels of expression seen pre-treatment (Figure 4.1.1).

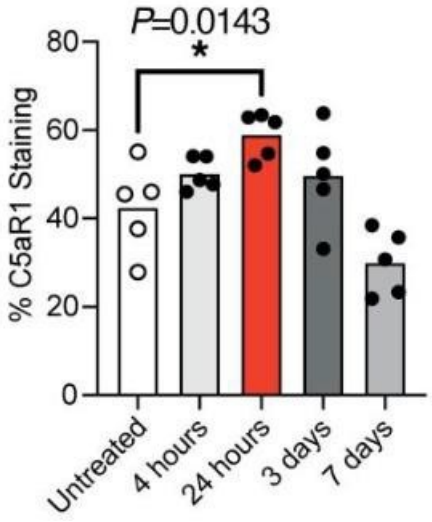


Figure 4.1.1 **Quantification of C5aR1 IHC staining in AKPT tumours.**

Percentage area of C5aR1 staining compared using ordinary one-way ANOVA, Dunnett's multiple comparisons (*p<0.05).

(Beach et. al. 2023)

We then used serial sections of AKPT tumours stained through the multiplex immune cell panel and C5aR1 IHC (Figure 4.1.2a). Using proximity-based machine learning-based quantification, the constituent immune populations within C5aR1 positive areas were quantified (Figure 4.1.2b). This examined what cells, both immune and epithelial, were found within areas that exhibited C5aR1 expression. From baseline to acute timepoints, up to seven days, C5aR1 expression is prominently found in the epithelium with little stromal contribution (Figure 4.1.2b). Interestingly, although a small population, $CD8^+$ T-cells were found in areas of positive C5aR1 expression significantly more pre-treatment than after irradiation (Figure 4.1.2b). Additionally, prior to treatment,

the heterotopic AKPT tumours have a TME containing very little $CD8^+$ T-cells (Figure 3.2.3). Therefore, although only a small constituent part of the C5aR1 positive area within AKPT tumours pre-treatment, the cytotoxic T-cells may be overrepresented there. Later timepoints, from three days onwards, saw a shift in from C5aR1 expression, with stromal C5aR1 significantly increasing (Figure 4.1.2b). The constituent components of stromal C5aR1 expression in the later timepoints demonstrating the greatest association with staining were the macrophages and neutrophils. Interestingly, after a single dose of irradiation the macrophage population within the TME was found to be significantly increased only at acute timepoints (Figure 3.2.7). This suggests that the increase of the macrophage population within areas positive for C5aR1 is not explainable by a general increase of this innate immune cell of tumour irradiation. Additionally, the significant increase in the neutrophil population within areas positive for C5aR1 may be explained by the TME-wide increase in the number of this innate immune cell after tumour irradiation (Figure 3.2.6). The expression of C5aR1 being predominantly found in the innate immune cell population, specifically macrophages and neutrophils has been described previously in the literature (Dunkelberger et al., 2012; Karsten et al., 2015; Soruri et al., 2003; Werfel et al., 1992).

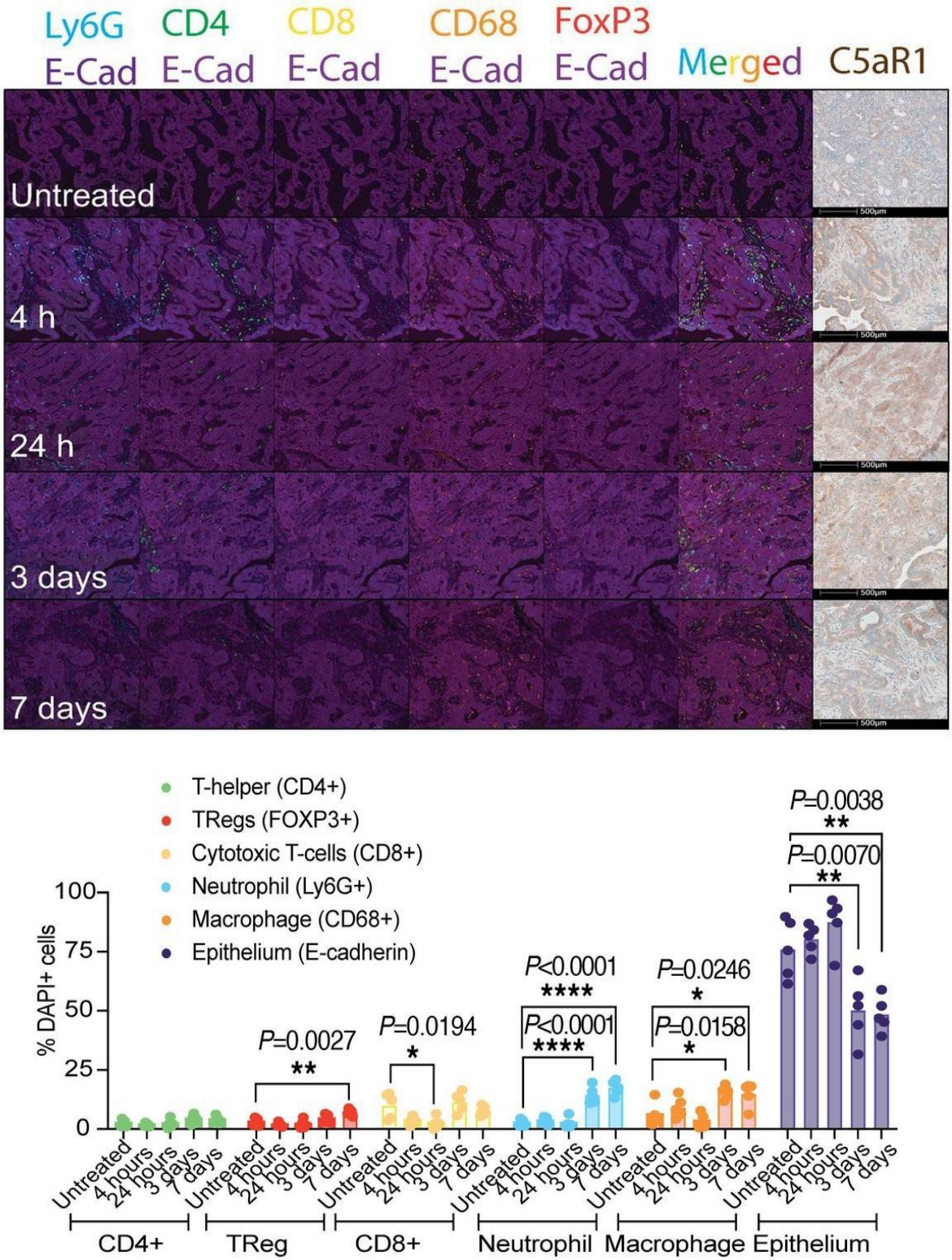


Figure 4.1.2 Changes to immune cell population within C5aR1+ stained areas after irradiation.

Machine learning quantification of the percentage of C5aR1 staining in the epithelium and stroma of AKPT tumours. **P* < 0.05, ***P* < 0.01, *****P* < 0.0001, ordinary 1-way ANOVA with Tukey's multiple comparisons. All other comparisons relative to untreated were not significant. *n* = 5 (Beach et. al. 2023)

Outside of the *in vivo* AKPT rectal cancer model, we also investigated C5aR1 expression in longitudinal biopsies of rectal adenocarcinoma from patients. These biopsies were sourced from the Campbell Roxburgh lab group at the University of Glasgow. C5aR1 staining was higher in the epithelium than the stroma across all patients (Figure 4.1.3a- b). Within three of the four patient samples analysed, C5aR1 staining remained at high levels or increased following post radiotherapy (Figure 4.1.3a-b). Across the patient cohort, heterogeneity was observed in C5aR1 staining was observed. One patient (P2) demonstrated high levels of C5aR1 staining at baseline, two patients (P3 and P6) demonstrated low levels of C5aR1 staining at baseline, and one patient (P15) had intermediate staining (Figure 4.1.3a-b).

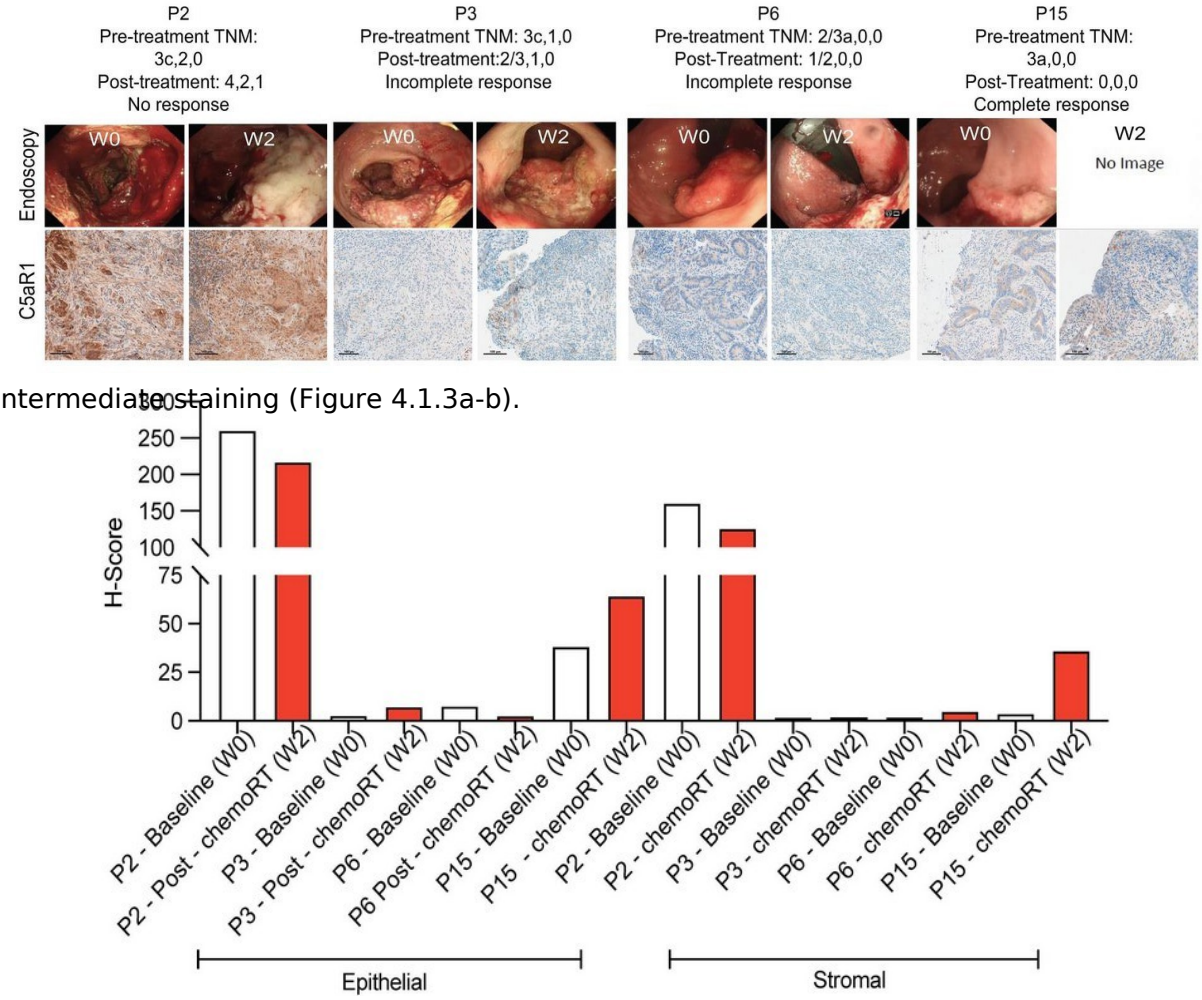


Figure 4.1.3 C5aR1 staining of longitudinal rectal biopsies from patients with rectal adenocarcinoma.

Endoscopy images and representative examples of C5aR1 staining at baseline (W0) compared with W2 in longitudinal biopsies from patients with rectal adenocarcinoma. W2, week 2 after treatment. Numbers refer to patient number, week after treatment, or TNM stage. Scale bar: 100 µm. (Beach et. al. 2023)

H-Scores of C5aR1 staining in epithelial and stromal areas of cancerous tissue from rectal adenocarcinoma longitudinal biopsies taken at W0 compared with W2. (H-scoring carried out by Alistair Easton) (Beach et. al. 2023)

Interestingly, the patient exhibiting the highest level of C5aR1 expression (P2) also had the poorest response to the chemoradiotherapy treatment. Conversely, the patient with an intermediate amount of C5aR1 expression (P15) completely responded to the chemoradiotherapy. Patients with very little C5aR1 expression demonstrated a partial response potentially suggesting a need for moderate expression for efficacious chemoradiotherapy. However, future studies incorporating additional samples will be needed to examine this hypothesis.

With the expression of C5aR1 being found predominantly on the tumour epithelium at acute timepoints post irradiation, we decided to investigate impact of C5aR1 inhibition *in vitro*. Using AKPT organoids we found that the selective C5aR1 inhibitor PMX205 caused reduced survival of AKPT organoids following treatment with increasing radiation doses (Figure 4.1.4). With the *in vitro* inhibition of C5aR1 reducing the survival of AKPT organoids post-irradiation we then moved examine the impact of PMX205 with or without radiation in the AKPT *in vivo* heterotopic model.

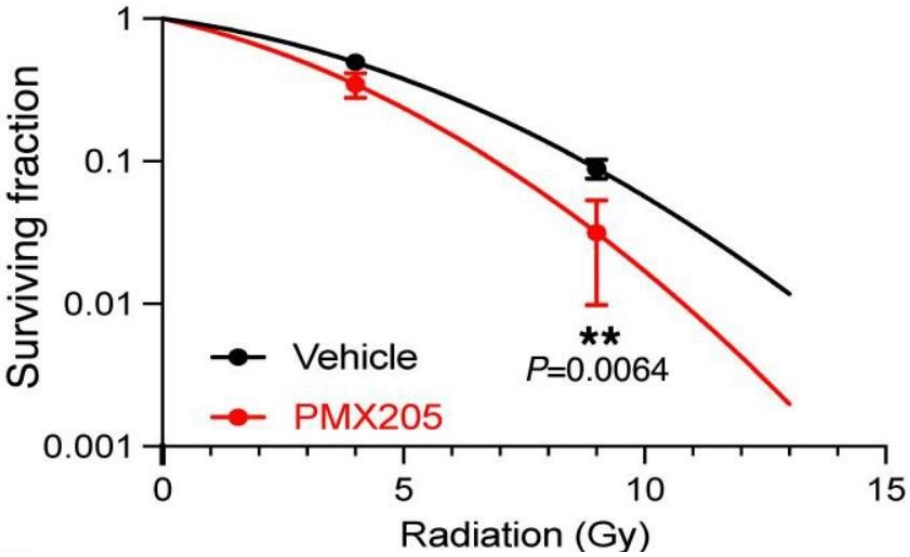


Figure 4.1.4 AKPT organoid survival after receiving radiation ± PMX205.

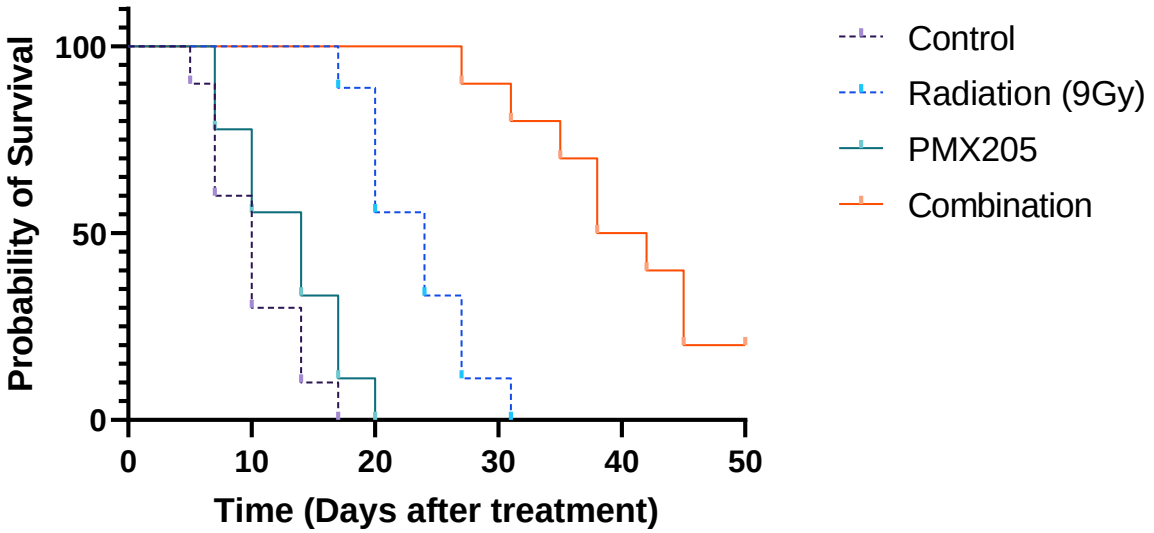
Curves show counted viable AKPT organoids vs. RT dose following treatment with vehicle or PMX205. **P < 0.01, Welch's t test. Data are shown as the mean. Error bars represent standard deviation. (Beach et. al. 2023)

4.3 AKPT rectal tumour model response to the combination of irradiation and C5aR1 inhibition

4.3.1 Efficacy of C5aR1 inhibition as a neoadjuvant therapy alongside irradiation to improve AKPT tumour survival.

With the inhibition of C5aR1 expression using PMX205 demonstrating an increase in AKPT organoid radiosensitivity *in vitro*, we then progressed to investigate the impact of PMX205 in the heterotopic model. For this avenue of investigation, a radiation dose of 9Gy was used rather than the previously described 15Gy or 3x7Gy. This is due to previous studies using the combination of PMX205 and radiation opted for a dose of 9Gy, something well tolerated in other heterotopic tumour models (Beach et al., 2023). Although outside the scope of this thesis, this will allow for the comparison between the heterotopic AKPT tumour model and other subcutaneous models when investigating the impact of C5aR1 inhibition on the radiotherapy response of rectal cancer. Additionally, the 9Gy dose of radiation has also demonstrated the ability to invoke an immunogenic response in *in vivo* cancer models (Kaur & Asea, 2012). Therefore, this dose of radiation able to act in an immunomodulatory manner and has sufficient tumour cell killing capacity, establishing it as appropriate for combination with C5aR1 inhibition to investigate changes to treatment efficacy.

Following the use of PMX205 in combination with irradiation, we found that there

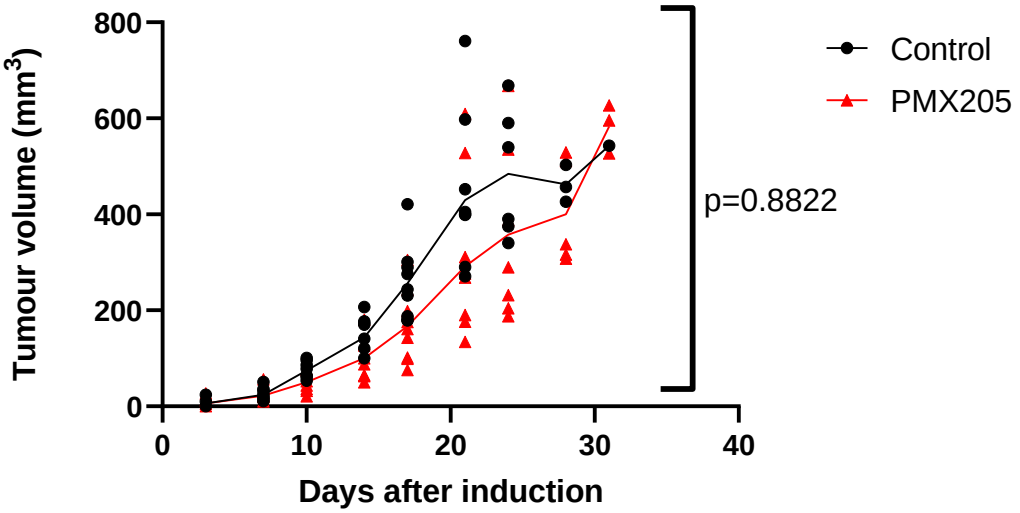


was a significant increase in mouse survival with heterotopic AKPT tumours compared to both control as well as irradiation alone (Figure 4.3.1). Interestingly, we discovered that C5aR1 inhibition alone had no significant improvement on mouse survival or reduction in tumour volume against mice receiving no treatment (Figure 4.3.1).

Figure 4.3.1 Survival curves of mice bearing subcutaneous AKPT tumours treated with radiation ± PMX205.

Curve comparison is by Log-Rank, ****= p<0.001. n=7 for all groups.

When comparing the tumour volumes over time in the different treatment groups, the temporary arrest to growth post irradiation is still observed (Figure 4.3.2a-b).Additionally, when using PMX205 alone, to treat the AKPT tumours we observe no significant impact on growth with the pattern of volume increase following a similar trend to the control group (Figure 4.3.2a). However, when AKPT tumours were treated with a combination of PMX205 and irradiation, we saw a sustained arrest to growth (Figure 4.3.2b).



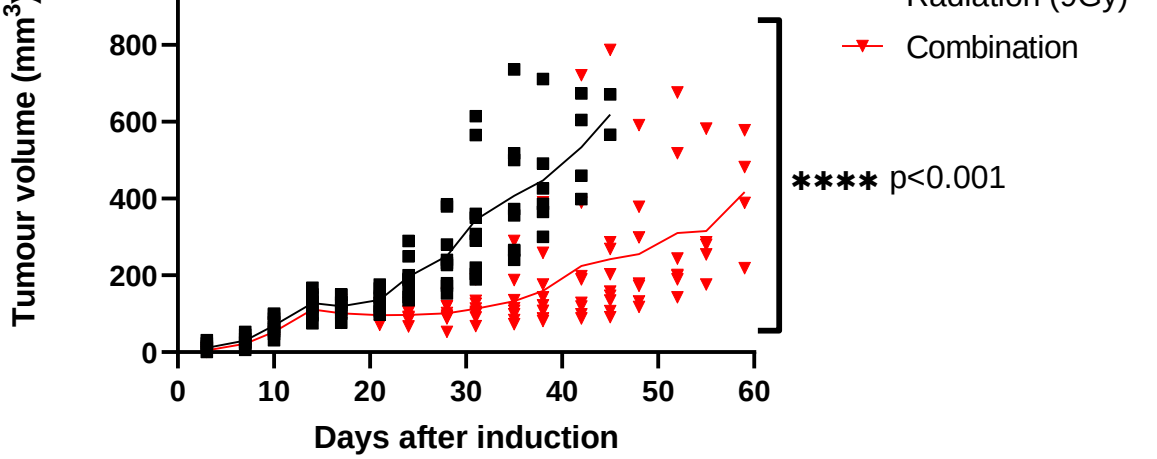


Figure 4.3.2 Volume growth curves of mice bearing subcutaneous AKPT tumour treated with PMX205 (A) or radiation ± PMX205 (B).

Volume growth curve comparison by repeated measure two-way ANOVA (with Geisser-Greenhouse correction), ****= p<0.001. n=7

With the inhibition of C5aR1 improving the anti-tumour effect of irradiation, we then undertook an investigation into the changes to the AKPT tumour TME. Although the data suggests a strong epithelial component to the improvement of irradiation efficacy in treating the tumours, the reduction in epithelial C5aR1 expression at later timepoints (Figure 4.1.2) may suggest further mechanisms that can be uncovered.

4.3.2 Immune and stromal population changes post combination treatment.

With epithelial C5aR1 appearing to be the major source of the complement receptor expression, we used PMX205 in combination with irradiation in heterotopic tumours in T cell deficient athymic nude mice. Work done by a collaborative group also demonstrated that targeting C5aR1 failed to increase the percentage of $CD8^+$ T-cells in the tumour following irradiation (Beach et al., 2023). Therefore, if the combination therapy of C5aR1 inhibition was able to improve the anti-tumour effect of irradiation in these athymic nude mice, it would suggest, and potentially confirm, a T-cell independent mechanism of action that has been observed in the recent literature.

Indeed, moving the heterotopic AKPT model into athymic mice had no impact on the efficacy of the combination treatment of PMX205 and irradiation. When investigating the survival of athymic mice bearing the heterotopic AKPT tumour, the combination treatment of C5aR1 inhibition and irradiation maintained its improved anti-tumour effect compared to radiation in isolation (Figure 4.3.3).

Figure 4.3.3 Survival curves of athymic nude mice bearing subcutaneous AKPT tumours treated with radiation ± PMX205

Curve comparison is by Log-Rank, ****= p<0.001. n=7.

Tumour growth curves in athymic nude mice showed a similar pattern of sustained growth arrest as immune competent mice when the combination treatment was employed (Figure 4.3.4a-b). The addition of PMX205 significantly improved the anti-tumour effect of irradiation on the AKPT tumours, akin to the effect seen in the immune competent model (Figure 4.3.4a). Additionally, the inability of C5aR1 inhibition alone to arrest the growth of the heterotopic AKPT tumours in immune competent mice was also observed in the athymic nude strain (4.3.4b).

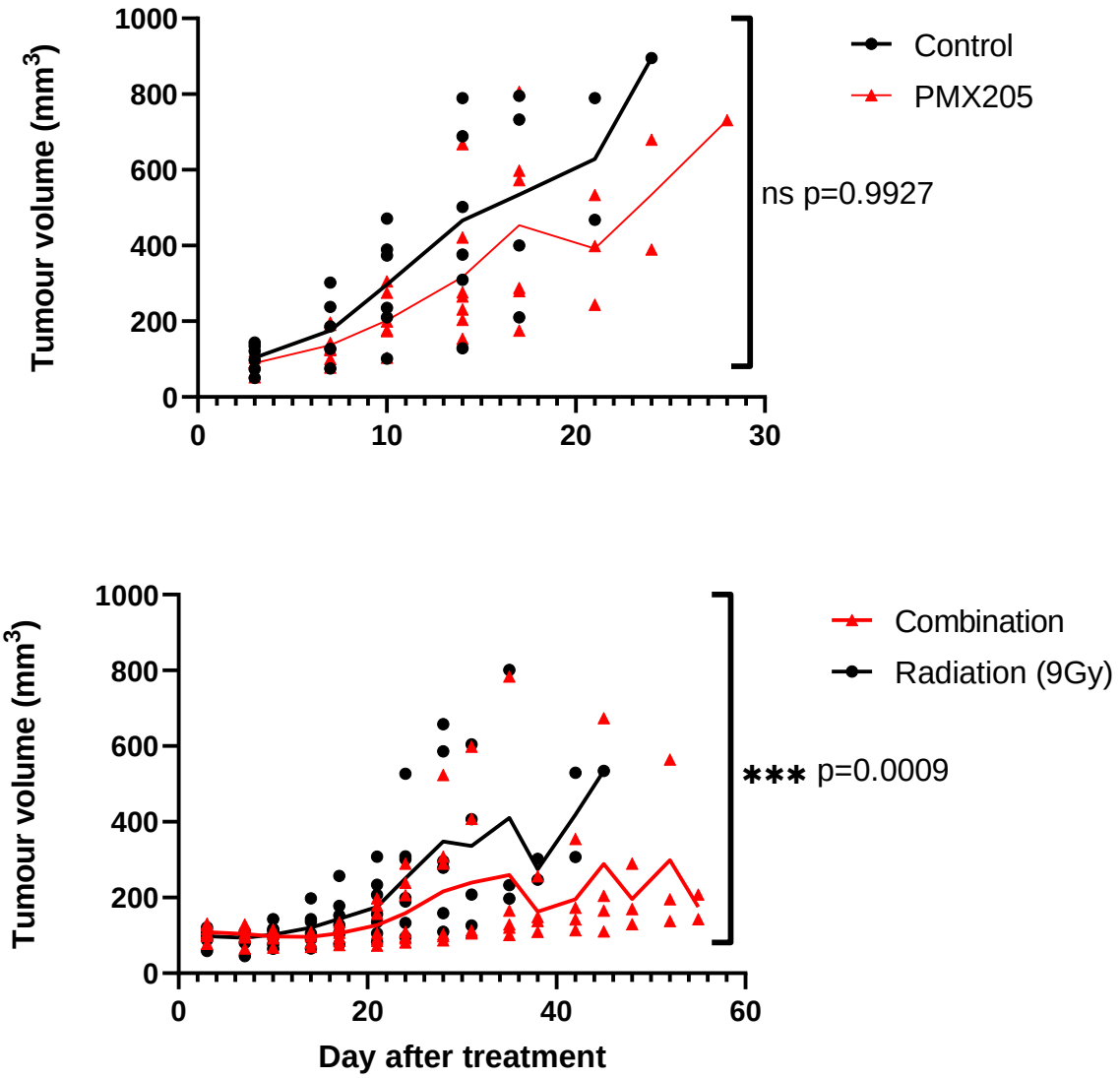


Figure 4.3.4 Volume growth curves of athymic nude mice bearing** subcutaneous **AKPT tumour treated with PMX205 (A) or radiation + PMX205 (B).

Volume growth curve comparison by repeated measure two-way ANOVA (with Geisser-Greenhouse correction), ****= p<0.0001. n=7

Since the effects of C5aR1 inhibition were not linked to a T-cell response, we then investigated the specific changes to the AKPT TME post-treatment. This was particularly key as, although C5aR1 expression is predominantly found on the epithelium at baseline and acutely after irradiation, a stromal component appears to emerge at later timepoints. Specifically, we examined the innate immune system

present using the established multiplex staining approach, as described in chapter 3.2, as well as the constituent stromal components.

Through the use of the multiplex staining approach described in chapter 3.2, we were able to examine the specific innate immune cell populations: neutrophils and macrophages. When examining the changes to the neutrophil population post C5aR1 inhibition, irradiation, or a combination of the two, significant differences in the group were observed. Twenty-four hours after irradiation, we saw a significant increase in the number of neutrophils present within the AKPT TME, as seen in chapter 3.2 (Figure 4.3.5). However, when PMX205 was used as a combination treatment with the irradiation this increase of neutrophils was lost within the acute timepoint (Figure 4.3.5).

Additionally, PMX205 alone also failed to induce an acute recruitment of neutrophils (Figure 4.3.5).

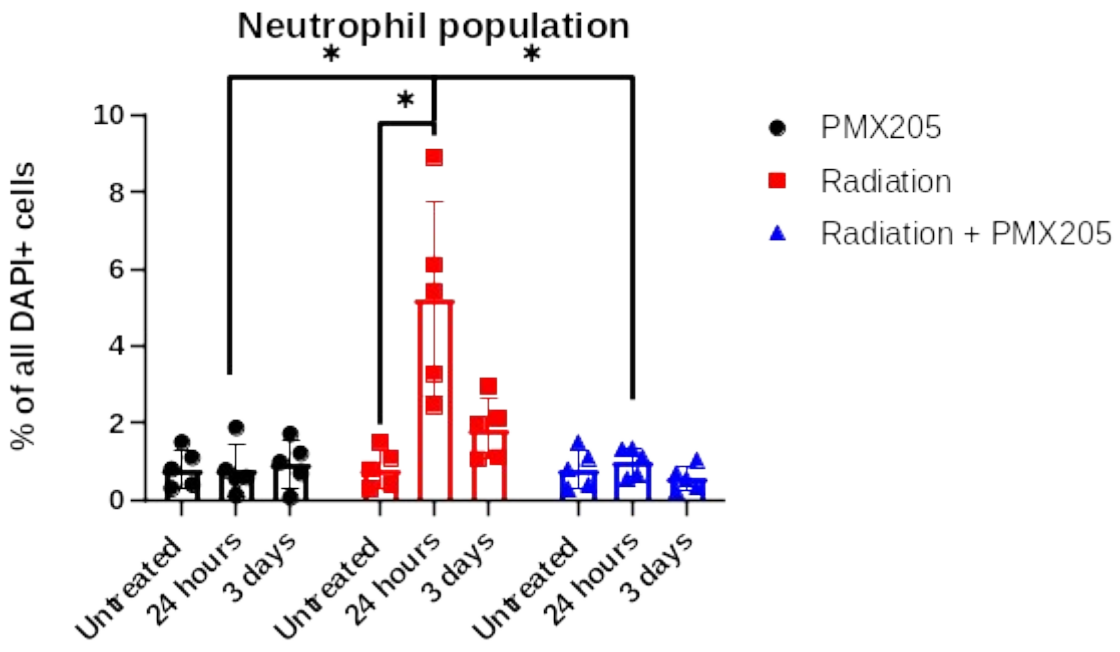


Figure 4.3.5 Neutrophil population changes as a proportion of DAPI^{+} cells in subcutaneous AKPT tumours post radiation ± PMX205.
Using HALO software, the changes to the neutrophil population was analysed in the heterotopic AKPT tumour model were examined. All groups have n=5. Significance calculated by two-way ANOVA with Geisser-Greenhouse correction and Tukey's multiple comparisons (*P<0.05).

When the tumours were irradiated in combination with C5aR1 inhibition, there was a significant decrease in the macrophage population post treatment compared with radiation treatment alone (Figure 4.3.6). This change occurred at later timepoints with the significant decrease being observed at the three-day timepoint (Figure 4.3.6). This decrease was not observed when C5aR1 was inhibited in isolation and only occurred in combination with irradiation (Figure 4.3.6).

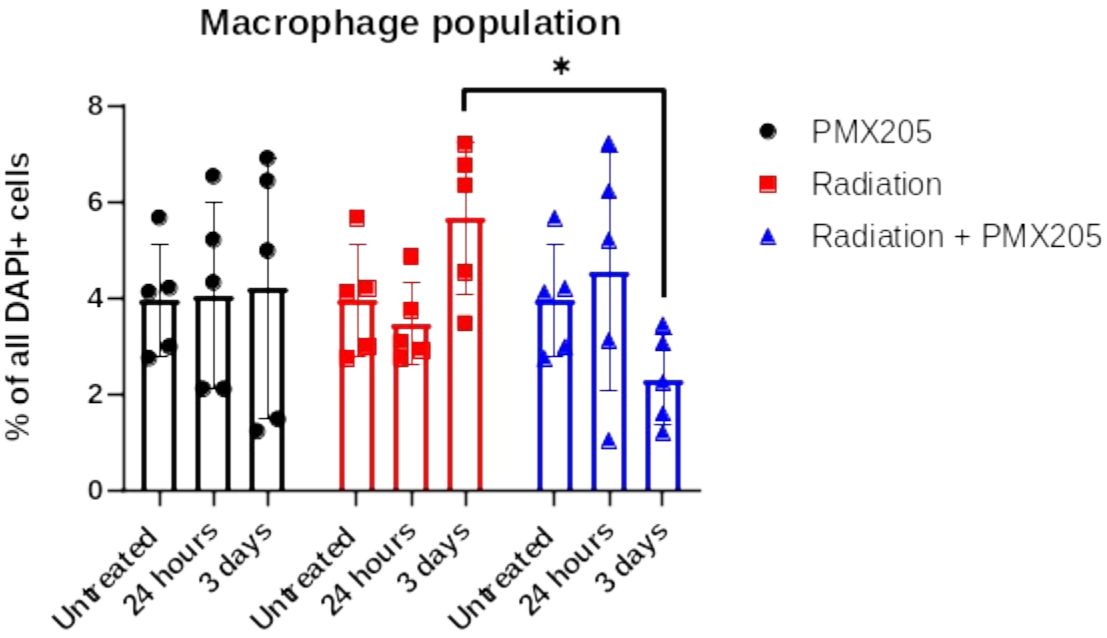


Figure 4.3.6 Macrophage population changes as a proportion of DAPI⁺ cells in subcutaneous AKPT tumours post radiation ± PMX205.

Using the HALO software, the changes to the macrophage population was analysed in the heterotopic AKPT tumour model were examined. All groups have n=5. Significance calculated by two-way ANOVA with Geisser-Greenhouse correction and Tukey's multiple comparisons (*P<0.05).

This change to the macrophage population is particularly interesting when considering the importance of this myeloid immune cell population in patient tumour response to radiotherapy (Beach et al., 2022). Therefore, we decided to investigate the changes to the phenotype of macrophages. This was performed through the interrogation of generated RNAseq data and is discussed further in section 4.3.3.

When examining the stromal compartment of the AKPT tumours post treatment, an interesting change to the fibroblast population within the stroma was observed. Through multiplex staining, fibroblasts expressing α-smooth muscle actin (α-SMA), a marker for myofibroblasts (Mao et al., 2021), demonstrated specific changes depending on the treatment experience by the AKPT tumour. Irradiation alone had no demonstrable impact on the myofibroblast population (Figure 4.3.7a). However, the inhibition of C5aR1, with or without irradiation, caused a reduction in this myofibroblast population (Figure 4.3.7a). Another marker for fibroblasts within the tumour stromal compartment is platelet-derived growth factor (PDFGRα) (Mao et al., 2021), also demonstrated interesting changes depending on the treatment received by the AKPT tumours. We saw that irradiation, with or without C5aR1 inhibition, led to a significant reduction in fibroblasts expressing PDFGR (Figure 4.3.7b).

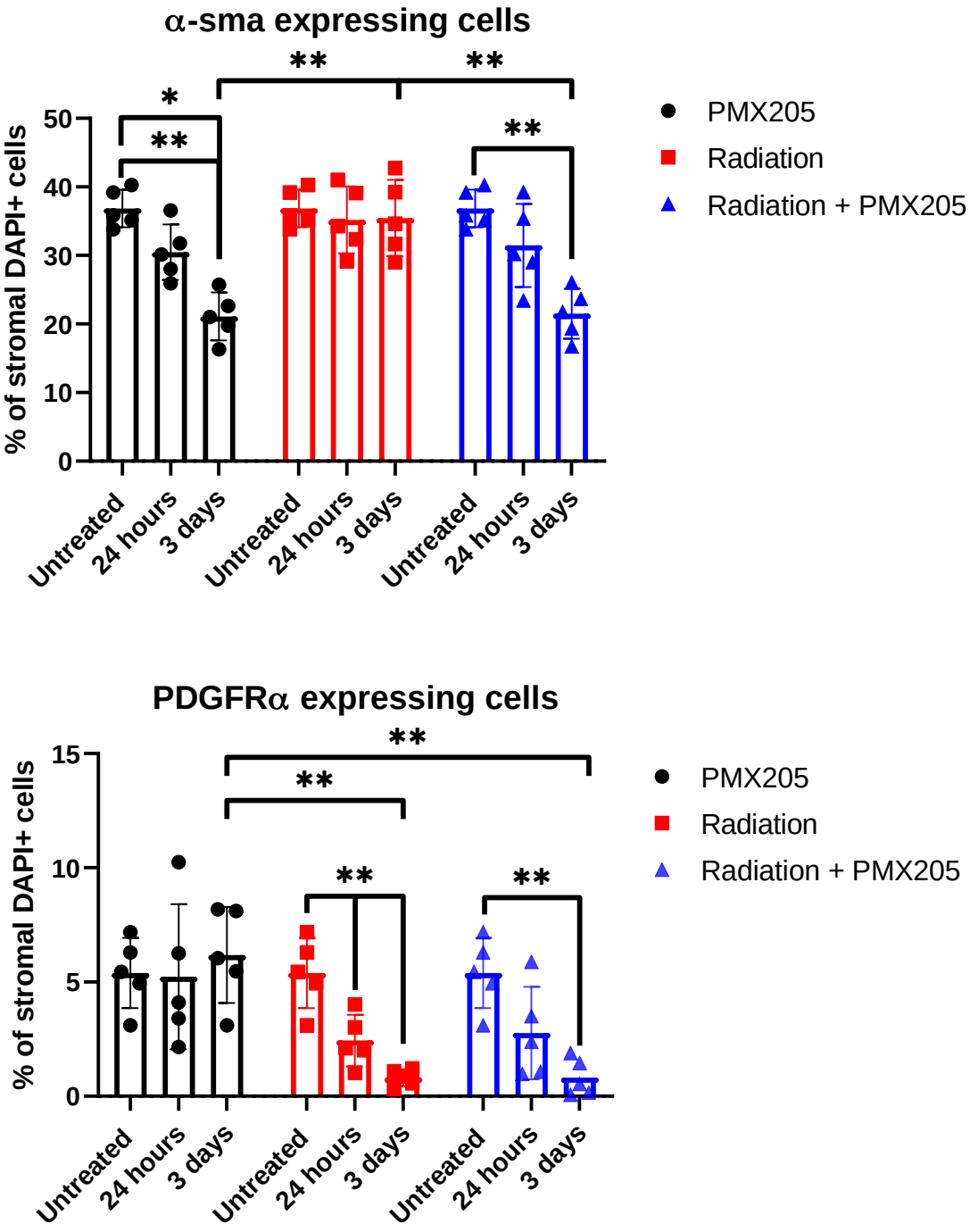


Figure 4.3.7 Fibroblast population changes in as a proportion of stromal DAPI^{+} cells in subcutaneous AKPT tumours post radiation ± PMX205.

Using HALO software, changes to the CAF population were analysed in the heterotopic AKPT tumour model. All groups have n=5. Significance calculated by two-way ANOVA with Geisser-Greenhouse correction and Tukey's multiple comparisons (*P<0.05).

With significant changes to the innate immune cell and CAF population depending on the treatment received by the AKPT tumours, we next investigated potential phenotypic changes. We did this through isolating RNA from the treated tumours in order to investigate both the immunogenic setting within the TME as well as phenotype changes specific cells within the TME have undergone.

4.3.3 RNAseq analysis of AKPT tumours post treatment with irradiation ± C5aR1 inhibition.

By sequencing the RNA from treated AKPT tumours, we began to investigate the impact of the different treatments on the tumour as well as its surrounding milieu. Analysis of RNA sequenced from AKPT tumours harvest from the heterotopic model was performed by Gabriel Valbuena. The data for the resulting GSEA plots, both the network plots as well as normalized enrichment score comparison, were also generated by Gabriel Valbuena. This investigation was carried out by examining the top-level enriched pathways within the AKPT tumours. In AKPT tumours receiving radiation alone, multiple pathways were enriched when compared to the untreated control. Specifically, a large network of DNA damage repair and cell cycle functions were enriched (Figure 4.3.8). Additionally, we also observed enrichment in pathways relating to the expression of hypoxia-inducible factors (Figure 4.3.8). Other notable pathways that were significantly enriched included: the toll like receptor nine (TLR9) cascade and signalling by MNNG HOS transforming gene (MET).

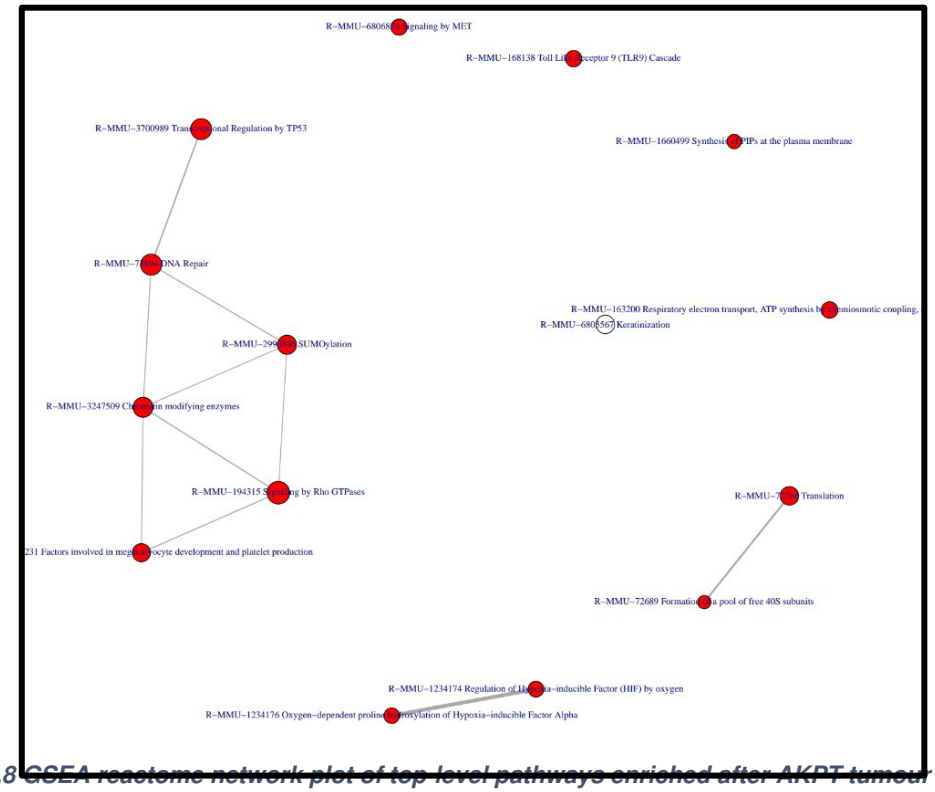


Figure 4.3.8 GSEA reactome network plot of top-level pathways enriched after AKPT tumour irradiation.

Red node colour represents an adjusted p value of <0.05, size of node represents level of enrichment. Redundant gene sets trimmed to plot top-level pathways, defined by having the largest amount of crossover with other pathways.

Figure constructed by Gabriel Valbuena

When performing the network analysis on top-level enriched pathways in AKPT tumours receiving only PMX205, several enriched pathways were observed. Notably, a network of enriched pathways revolving around genetic stability, through the degradation of securin and chromatin modification, as well as DNA damage repair and cell cycle regulation, through the small ubiquitin-like modifier (SUMO) pathway (Figure 4.3.9). Interestingly, pathways linked with an immunogenic response were also upregulated including the toll-like ligand four (TLR4) cascade and interferon signalling (Figure 4.3.9).

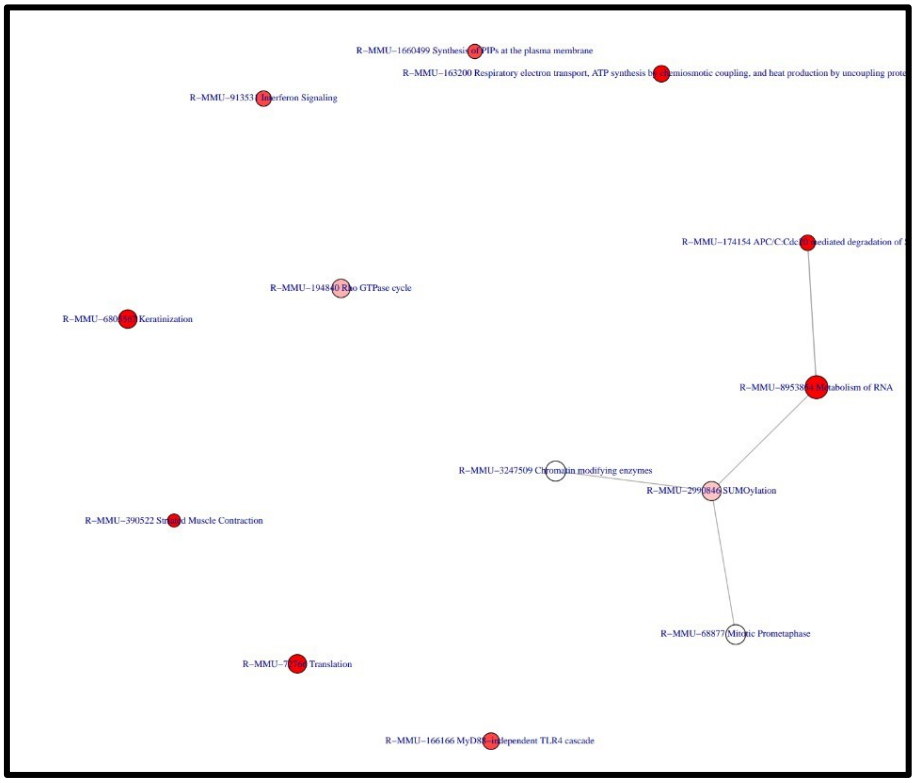


Figure 4.3.9 GSEA reactome network plot of top-level pathways enriched after AKPT tumour C5aR1 inhibition.

Red node colour represents an adjusted p value of <0.05, size of node represents level of enrichment. Redundant gene sets trimmed to plot top-level pathways, defined by having the largest amount of crossover with other pathways.

Figure constructed by Gabriel Valbuena

After combination treatment of PMX205 and irradiation, we see a significant network of enriched pathways in comparison to tumours receiving radiation alone. Importantly, we see a marked enrichment in a network of pathways involved in both DNA damage repair as well mitotic cell death (Figure 4.3.10). This network of enriched pathways also links to an upregulation of Fc-γ receptor (FCGR) dependent phagocytosis, a function performed by macrophages and neutrophils. Additionally, in line with the treatment of AKPT tumours with PMX205 alone, the combination treatment also demonstrated significant enrichment of the TLR4 cascade.

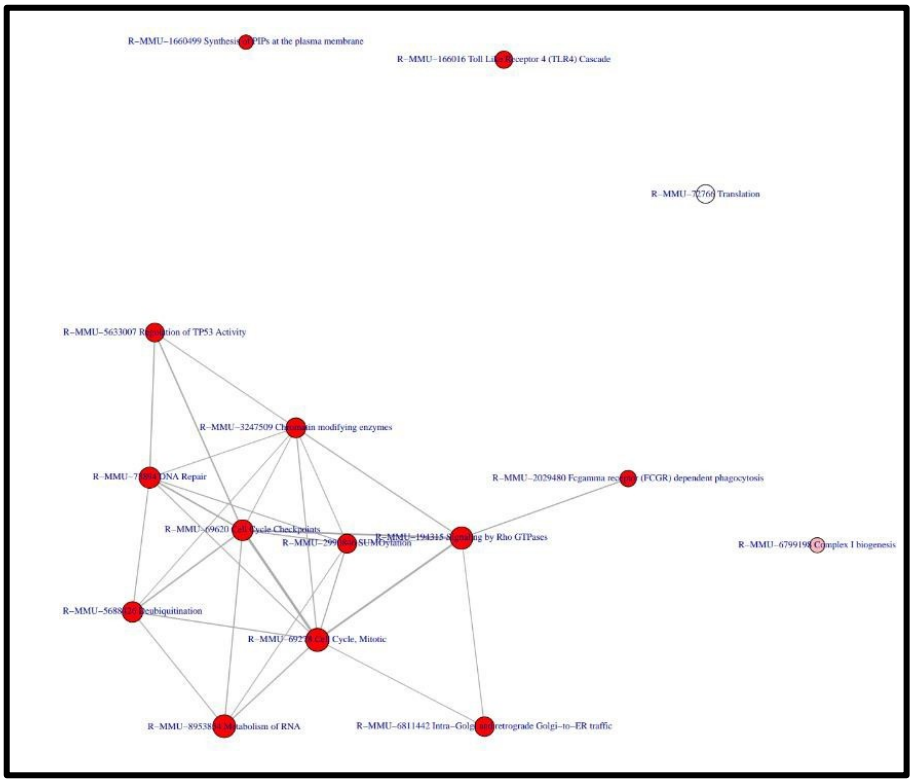


Figure 4.3.10 GSEA reactome network plot of top-level pathways enriched after AKPT tumour irradiation and C5aR1 inhibition.

Red node colour represents an adjusted p value of 0.05, size of node represents level of enrichment. Redundant gene sets trimmed to plot top-level pathways, defined by having the largest amount of crossover with other pathways.

Figure constructed by Gabriel Valbuena

When examining the enriched pathways, when PMX205 was used to treat the AKPT tumours, with or without irradiation, we saw upregulation in phagocytotic processes. This linked with the upregulation of TLR4 led us to investigate a potential change in the phenotype of the macrophages within the TME of the AKPT tumours post treatment. With macrophages being the dominant immune cell type within the TME, and a significant difference in population size being observed between irradiated and combination treated tumours (Figure 4.3.6), a change in phenotype would be critical toward treatment efficacy.

We found that post irradiation and when treating AKPT tumours with PMX205 alone, the macrophage population demonstrated negative enrichment in genes ascribed to an immunogenic, M1-like, phenotype (Figure 4.3.11). However, tumours treated with a

combination of PMX205 and radiation demonstrated a strong enrichment for M1-like macrophage specific genes when compared to solely irradiated tumours (Figure 4.3.11).

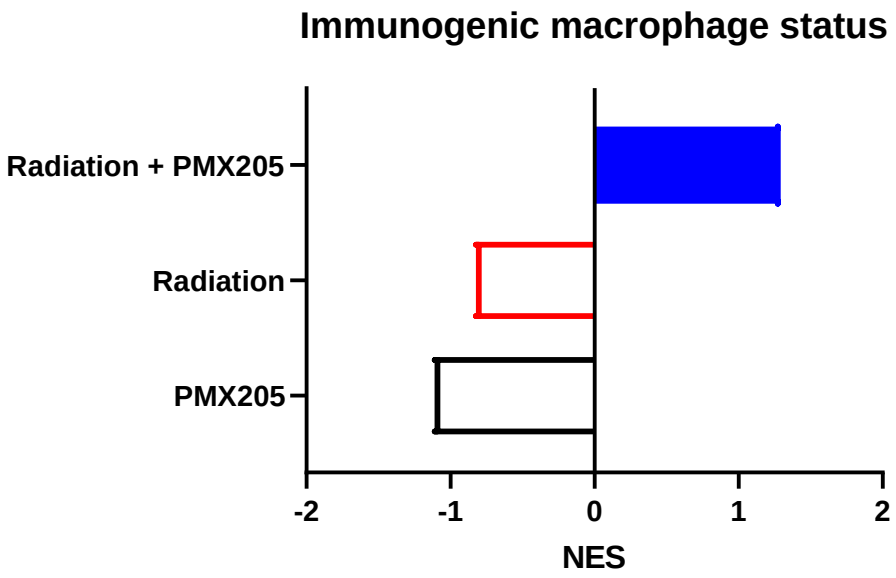


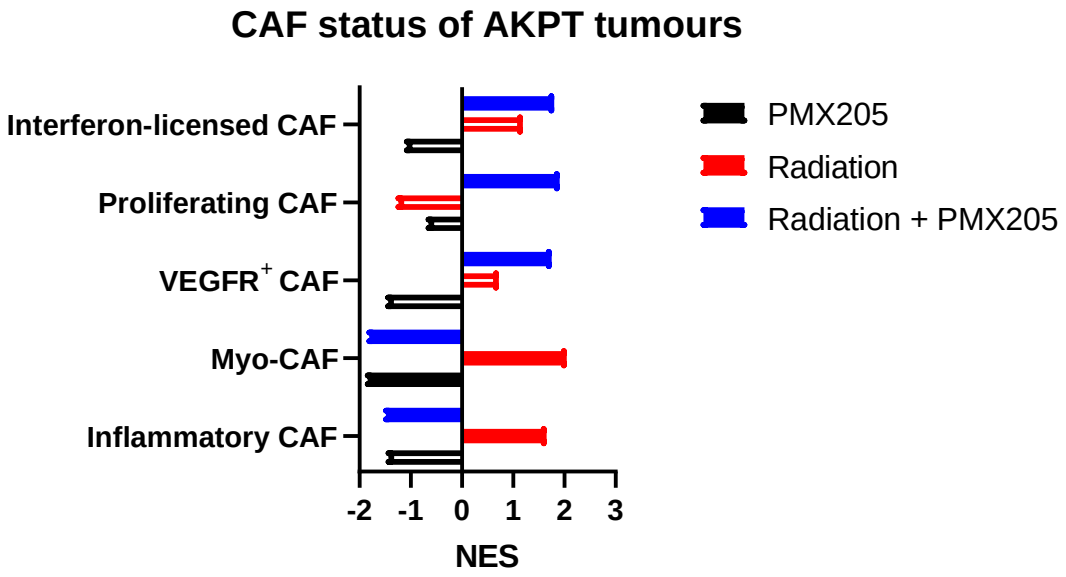
Figure 4.3.11 *M1-like macrophage gene list enrichment comparison* ***in treated AKPT tumours.***

The normalised enrichment score (NES) of selected gene signatures defining M1-like macrophages compared between: untreated vs irradiated; untreated vs PMX205; and irradiated vs irradiated and PMX205. Fully coloured bars represent a pFDR $\leq$ 0.1.

Although no enrichment of pathways relating to the ECM or CAFs were observed during the top-level GSEA analysis, multiplex staining had demonstrated a shift in the CAF population when PMX205 was incorporated as a treatment, either with or without irradiation (Figure 4.3.7). Therefore, we also investigated the phenotypic changes to CAFs within the tumour stroma.

Following the stratification of CAFs within the tumour stroma established by (Grauel et al., 2020), we implemented the published gene lists for further investigation into phenotypic changes in the AKPT tumour stroma post treatment. Genes ascribed to inflammatory CAFs (iCAF), defined by their immunomodulatory ability including IL6 and chemokine signalling, were found to be significantly enriched in the radiation alone group but the inverse was found when radiation was combined with PMX205 (Figure 4.3.12). The use of PMX205 alone also demonstrated, albeit not significantly, a reduction in the iCAF population (Figure 4.3.12). Genes identifying the canonical myofibroblast population

(myCAF), defined by their role in ECM remodelling, showed significant negative enrichment in both treatment groups including PMX205 (Figure 4.3.12). The vascular endothelial growth factor (VEGFR) positive CAF population (vCAFs), as defined by VEGF ligand-receptor interactions, demonstrated a modest, not significant, increase in tumours receiving radiation alone (Figure 4.3.12). PMX205 alone caused a modest negative enrichment for genes defining vCAFs, whereas PMX205 in combination with irradiation showed a significant enrichment (Figure 4.3.12). The proliferating CAF (prCAF) population, as defined by their enrichment of cell cycle pathways, are modestly negatively enriched in both the irradiation and PMX205 alone treatment groups (Figure 4.3.12). However, the combination of PMX205 and irradiation demonstrated a significant



enrichment in the prCAF set of genes (Figure 4.3.12). Finally, interferon-licensed CAFs (il-CAFs), defined by their upregulation of pathways enriched by interferon signalling, was positively enriched in all groups in which tumours received radiation. However, radiation alone only elicited a modest enrichment of the ilCAF gene set whereas the inclusion of PMX205 demonstrated a significant enrichment (Figure 4.3.12). PMX205 alone showed a modest negative enrichment of ilCAF defining genes (Figure 4.3.12).

Figure 4.3.12 CAF phenotype signature enrichment comparison in irradiated AKPT tumours.

The normalised enrichment score (NES) of selected gene signatures defining CAF phenotypes compared between: untreated vs irradiated; untreated vs PMX205; and irradiated vs irradiated and PMX205. Fully coloured bars represent a pFDR $\leq$ 0.1.

4.4 Discussion

We demonstrated that C5aR1 expression within the AKPT heterotopic tumour model increases after irradiation of the tumour site (Figure 4.1.1). Furthermore, we have shown that C5aR1 expression in irradiated AKPT tumours is more prominent on epithelial cells at baseline and acutely after irradiation, with a switch to a more stromal expression at later time points (Figure 4.1.2). This finding was reinforced through the irradiation of AKPT organoids *in vitro*. We demonstrated that the inhibition of C5aR1 was able to increase radiosensitivity (Figure 4.1.4). With the *in vitro* organoids lacking a surrounding TME, this implied a significant epithelial component to the ability of C5aR1 inhibition to improve the anti-tumour effect of radiation.

Encouragingly, the pattern observed in irradiation of AKPT tumours, with of C5aR1 expression increasing after radiation, was also demonstrated in rectal adenocarcinoma biopsies taken from patients (Figure 4.1.3). Interestingly, C5aR1 expression from patient biopsies suggested a potential “Goldilocks” effect for C5aR1 expression. In samples analysed, high baseline C5aR1 expression was observed in the patient tumours demonstrating strong radio resistance and continued progression while receiving treatment, whereas intermediate low expression in both patients with partial responses, and the patient with intermediate expression, concomitant with increased stromal expression following treatment, demonstrated high radiosensitivity and complete response to treatment (Figure 4.1.3). To ascertain how these clinical associations with C5aR1 expression can be manipulated for improved rectal cancer treatment, future studies with additional samples would be required.

After assessing the expression of C5aR1 in the AKPT tumour model we further demonstrated that inhibiting the receptor, using PMX205, was able to improve the survival of mice bearing heterotopic tumours (Figure 4.3.1-2). Literature investigating the impact of inhibiting the complement system on tumour radiotherapy response shows conflicting results when investigating any change to the anti-tumour effect witnessed (Elvington et al., 2014; Surace et al., 2015). Interestingly, in literature describing the importance of complement activation for radiotherapy response, signalling between

dendritic cells and $CD4^+$ T-cells through C5aR1 activation was found to promote the production of interferon-γ (IFNγ) (J. Liu et al., 2008). Additionally, this C5aR1-mediated interaction has been described as critical in counteracting the development of $FOXP3^+$ Treg cells through TGF-β signalling (Strainic et al., 2013). However, we have

demonstrated that athymic nude mice bearing heterotopic AKPT tumours show improved survival when radiation is combined with C5aR1 inhibition (Figure 4.3.3-4.3.4). This suggests that, at least within the AKPT heterotopic tumour model, the improvement to the anti-tumour effects of radiation is powered by interactions occurring without the T-cell population. It is worth considering that a study demonstrating the importance of complement signalling to a robust tumour radiation response, used heterotopic CT26 cell implantation to establish an *in vivo* colorectal tumour model (Surace et al., 2015). The *in vivo* CT26 model has been proven to be highly immunogenic at baseline, suggesting an increased importance in the T-cell population in treatment response (Zhong et al., 2020).

Intriguingly, literature describing improved anti-tumour effects when radiation is combined with complement inhibition, noted an absence of $CD8^+$ T-cells and Tregs (Elvington et al., 2014). The improved anti-tumour effect of radiation when combined with a complement inhibitor was directly linked with early neutrophil influx (Elvington et al., 2014). However, we demonstrate that although we found an improvement to the anti-tumour effect of radiation when C5aR1 was inhibited, there was a significant decrease in the neutrophil population when comparing tumours receiving radiation alone versus the combination treatment (Figure 4.3.5). Interestingly, investigation into the role of C5aR1 signalling in cancer has discovered that the activation of the complement receptor leads to the recruitment of myeloid cells to the tumour site and upregulates TGF-β production by these cells (Vadrevu et al., 2014). This idea of myeloid cell recruitment via C5aR1 signalling is further bolstered by our demonstration of a significant decrease in the macrophage population when radiation is augmented with C5aR1 inhibition (Figure 4.3.6). With the literature proving TGF-β as (Reibman et al., 1991; Shen et al., 2007) a potent chemoattractant for neutrophils this may provide an explanation. However, further investigation into this may be warranted as TGF-β is also known to diminish the anti-tumour activity of neutrophils following their recruitment to the tumour's stroma (Fridlender et al., 2009; Khan et al., 2021).

Through our investigation into the impact of C5aR1 inhibition on the CAF population within the stroma, we demonstrated significantly reduced numbers of

myofibroblasts (Figure 4.3.7a). Interestingly, the blockade of C5aR1 has been shown to downregulate the expression of α-SMA in a model of non-alcoholic steatohepatitis, an advanced form of fatty liver disease that is defined, in part, by increased fibrosis (Jiang et al., 2023). Additionally, in this precancerous liver setting we also see C5aR1 driving the recruitment of myeloid cells (Jiang et al., 2023). Interestingly, the recruitment of myeloid cells to the tumour TME through C5aR1 signalling has been described as fibroblast-mediated (Monteran et al., 2022). This study found that PDGFRα^{+} fibroblasts were the main source of complement within the tumour stroma (Monteran et al., 2022). Though we demonstrated that the PDGFRα^{+} fibroblast population within the tumour's stroma are significantly decreased following irradiation with or without PMX205 (Figure 4.3.7b), a large macrophage population remains after tumours receive radiation (Figure 4.3.6). A reduction in this myeloid cell population is only observed after radiation treatment is combined with C5aR1 inhibition.

Through examining the top-level enriched pathways following tumour treatment with radiation combined with PMX205, we demonstrated a significant increase in phagocytic signalling (Figure 4.3.8-10). Subsequently, we also illustrate when radiation is combined with C5aR1 inhibition, a more inflammatory phenotype is adopted by the macrophage population (Figure 4.3.11). Interestingly, this aligns with literature describing the significance of C5aR1^{+} M2-like macrophages have on maintaining an immunosuppressive TME (P. Zhang et al., 2023). Interestingly, this study also found that there was very little epithelial expression of C5aR1, contradictory to results we have demonstrated. However, it is worth considering the differences in the immune landscape between the AKPT rectal model against a model of high-grade serous carcinoma (HGSC). The AKPT rectal model is characterised by a TME lacking in any significant numbers of immune cells outside of macrophages, whereas HGSC tumours are typically "immune-excluded" with T-cells being present but unable to infiltrate the epithelium (Salas-Benito et al., 2020). Therefore, any disruption to the delicate balance of immunosuppression is likely to have greater effects due to their being no need for T-cell recruitment to occur.

Through the usage of the CAF stratification markers, as defined by (Grauel et al., 2020), we confirmed the large shifts in CAF population following treatment of the AKPT tumours. We demonstrated that the inhibition of C5aR1 caused a decrease in the iCAF and myCAF populations, with or without radiation (Figure 4.3.12). Interestingly, this reduction in both of these CAF populations suggest that there may be a loss of functionality for collagen degradation, MMP production, and ECM reorganisation in the stromal CAF population (Figure 4.3.12) (Grauel et al., 2020). Therefore, investigating how radiation combined with C5aR1 inhibition impacts tumour escape into circulation and potential metastasis could be a fruitful avenue of investigation.

The vCAF population that is also significantly increased in the AKPT tumour stroma post combination treatment could also prove to be an interesting avenue of research. With VEGF being a marker for poor prognosis in colorectal cancer (Baker et al., 2019) and inhibitors for the molecule currently employed in the clinic to treat metastatic colorectal cancer (Kanthou & Tozer, 2019), there may be potential in investigating this molecule further. Though the efficacy of radiation combined with VEGF inhibition has shown lower levels of efficacy than that demonstrated in preclinical *in vivo* models (Kanthou & Tozer, 2019) , the increase in the vCAF population post radiation and PMX2005 treatment may provide the ideal situation to employ a triplet therapeutic approach. However, *in vivo* tolerance studies would be required before any further research was undertaken. Interestingly, the combination of radiation and C5aR1 inhibition also significantly enriched the defining gene set of the ilCAF population (Figure 4.3.12). With this ilCAF population having significant involvement in antigen processing, presentation, and subsequent phagosome formation, this CAF phenotype may play a role in directing improved anti-tumour activity by the inflammatory macrophage population. It is worth noting that ilCAFs provide a significant amount of IFN-γ signalling to the tumour TME (Grauel et al., 2020). Therefore, although the combination of radiation and C5aR1 inhibition is able to induce an improved anti-tumour effect in the nude mouse model, there are likely a multitude of different immune effects to uncover. It would be fascinating to examine how C5aR1 activation is able to allow for tumour epithelial cells, CAFs, and macrophages to orchestrate the establishment of an immunosuppressive TME.

Investigating the interactions that the C5aR1^{+} populations of these cell types have with the other cell types within the TME would also potentially allow investigation into a potential triplet therapy to occur in order to improve patient outcomes.

Chapter 5

Investigating the impact of TGF-β inhibition on the radiation response in a rectal cancer

5.1 Background

TGF-β is able to predict the response of rectal cancer patients to the frontline treatment of chemoradiotherapy (See Chapter 3). Additionally, the combination of TGF-β inhibition alongside other immunomodulatory drugs has shown success (Tauriello et al., 2018) leading to the initiation of clinical trials (NCT04515979). The combination of TGF- β with an immunomodulatory approach has only been tested pharmacologically, such as with PD-1 inhibitors, but, hypothetically, the use of radiation as both tumour targeting an immunogenic tool may lend itself well to combination with TGF-β inhibition.

TGF-β signalling in cancer acts in an critical yet paradoxical manner in carcinogenesis and tumour progression (Lee, 2020). In normal tissue and the early stages of tumour development, TGF-β acts as a tumour suppressor through the inhibition of proliferation, induction of apoptosis of tumour cells, and immune cell modulation (Baba et al., 2022). TGF-β signalling inhibits the growth of tumours both through canonical SMAD-dependent signalling as well as the noncanonical pathway. Through the canonical pathway, TGF-β inhibits cell cycle progression through G1-arrest by activating cyclin-dependent kinase inhibitors and inhibiting the oncogene c-Myc, which stimulates cell proliferation (Katz et al., 2013; Mukherjee et al., 2010). TGF-β induces apoptosis through a number of different cell types by modulating the expression of B-cell lymphoma-2 (Bcl-2) family members, fibroblast associated antigen death receptors, death-associated kinases, and caspases (Zhang et al., 2017). Noncanonically, TGF-β promotes tumour suppression through p38-MAPK pathway, activating caspase-8-dependent programmed cell death. Additionally, TGF-β promotes tumour suppression through the regulation of

immune cell function in favour of tumour cell death (Schrantz et al., 2001).

In the later stages of cancer, TGF-β paradoxically results in tumour progression and metastasis (Katz et al., 2013). When considering rectal cancer specifically, the canonical pathway of carcinogenesis, as established by (Fearon & Vogelstein, 1990), demonstrated that mutations to TGF-β signalling pathway occurs at the later stages of the disease. In these later stages of disease TGF-β plays a key role in a wide range of tumour development processes including: EMT, cell proliferation, invasion and metastasis through ECM remodelling, angiogenesis, and evasion of immune surveillance (Dufour et al., 2018; Melzer et al., 2017).

When examining the role TGF-β plays within the AKPT tumour post irradiation we found that the majority of the most enriched genes were related to the noncanonical TGF-β signalling pathway. Although the canonical signalling pathway shows a lack of upregulation due to the prevalence of activin within the TME (Figure 3.3.5). Activin within the TME upregulates the Smad signalling pathway aking to the canonical TGF-β signalling pathway. Therefore, due to the canonical signalling pathway being upregulated prior to theirradiation of the AKPT tumour, enrichment of the TGF-β pathway appears to be relatively low and not significant (Figure 3.3.5).. In the tumour TME, non-canonical TGF- β signalling remains an encouraging avenue of neoadjuvant therapy development. Interestingly, when examining radiation-induced changes in gene expression, a clear pattern of immune and stromal modulating activity can be seen. When considering the AKPT tumour model, with the implanted organoids having TGFβR1 knocked out, the TGF-β signalling occurs namely within the surrounding stroma. Additionally, this stromal TGF-β signalling occurs through the noncanonical pathway, separate from the SMAD signalling pathway.

Over the entire irradiation time course, we observed that multiple upregulated genes were involved in CAF function within the AKPT TME (Chapter 3.3). These enriched genes included: tissue inhibitor of metalloproteinases 1 (TIMP1), found to promote the accumulation of CAFs (Gong et al., 2013) and increase tumour sensitivity to radiotherapy when inhibited (D'Costa et al., 2017); signal transducer and activator of transcription 2

(STAT2), found to influence a shift of CAF phenotype to a tumour protective phenotype (Pan et al., 2023) and linked to poor disease-free survival (DFS) in colorectal cancer (D. Li et al., 2022); and transforming growth factor beta induced (TGFβi), found to promote the accumulation of CAFs within the tumour TME (Y. Chen et al., 2021) and which is associated with poor prognosis in colorectal cancer (Chiavarina et al., 2021).

When examining enriched genes directly associated with non-canonical TGF-β signalling we also see a direct impact on a wide range of different immune cells, thereby impacting the AKPT tumour response to irradiation (Chapter 3.3). Notably, the cytotoxic T-cell population, critical for the implementation of an immunogenic effect post irradiation is curtailed by TGF-β signalling. Highly enriched genes involved with this include: TIMP1, with its expression being significantly correlated with negative presence of $CD8^+$ T-cells in colorectal tumours (Qiu et al., 2023); lactate dehydrogenase A (LDHA), with specific transient inhibition of the enzyme allowing for a more profound cytotoxic T-cell-mediated antitumour response through improved $CD8^+$ T-cell differentiation (Hermans et al., 2020); galectin-9 (LGALS9), a newly emerging immune checkpoint target implicated with the exhaustion of $CD8^+$ T-cells (Jin et al., 2023; Lv et al., 2023; Yang et al., 2021); and aldolase A (ALDOA), a marker for tumour progression in colorectal cancer (Y. Lu et al., 2023) as well as being negatively correlated with poor $CD8^+$ T-cell infiltration (G. Lu et al., 2021; Tian et al., 2022). The large range of cytotoxic T-cell impacting genes upregulated post irradiation of heterotopic AKPT tumours, linked with TGF-β signalling, suggest that the inhibition of this molecule may allow the temporary growth arrest (as seen in Figure 3.2.2), to be extended or made more permanent through the improvement of the immunogenic response.

When considering the ability of AKPT tumours to develop radioresistance and overcome the initial immunogenic response post irradiation, the Treg population is critical (Liu et al. 2015). Especially as TGF-β signalling has a large impact on this adaptive immune cell population, particularly the facilitation of the development of an immunosuppressive phenotype within the T-helper cell population through the increase

of FOXP3 expression (Battaglia et al., 2013; Strainic et al., 2013). The Treg population has also been shown to utilise TGF-β to suppress anti-tumour immune responses (M.-L. Chen et al., 2005; Mempel et al., 2006). From the genes demonstrating the highest enrichment post irradiation, multiple genes specifically upregulated by TGF-β are present (Chapter 3.3). These include: TIMP1, which acts to increase infiltration by Tregs (D'Costa et al., 2017); chemokine ligand 9 (CCL9), that acts to increase tumour infiltration by Tregs in multiple cancers including colorectal (Sarkar et al., 2021); and LGALS9, that reduces T-helper function through the promotion of FOXP3 acquisition to form the Treg phenotype (Pang et al., 2021).

Outside of the stromal and adaptive immune system response, TGF-β specific changes to the macrophage population within the AKPT TME are also critical to the response following irradiation. CCL9 acts to promote the recruitment of MDSCs post irradiation that then form a part of the immunosuppressive TAM population (B. Li et al., 2019); LDHA mediates the phenotypic switch toward an M2-like phenotype in TAMs associated with colorectal cancer following treatment (Hu et al., 2022); bone marrow stromal cell antigen 2 (BST2) has been discovered as a potential predictive marker in colorectal cancer due to its role in M2-like TAM polarisation; and TGFBi plays a role in the polarisation of TAMs to an M2-like phenotype that acts in a tumour protective role (Zhou et al., 2023). In addition to TAMs providing a radioprotective service to the AKPT tumours, as illustrated by the number of TAM-related genes being strongly enriched post irradiation, thioredoxin 1 (TXN1) is also strongly upregulated within the tumours. With TXN1 being upregulated specifically by TGF-β post irradiation of the AKPT tumour, it is particularly interesting that the gene as been implicated in the development of radioresistance in colorectal cancer (Yu et al., 2022).

The importance of TGF-β-mediated neutrophil infiltration in colorectal cancer, especially when considering disease progression, cannot be overlooked (Jackstadt et al., 2019). When examining the TGF-β specific upregulated genes post AKPT tumour irradiation, a few that exert an effect on the neutrophil population were present. These included: TIMP1, strongly associated with the formation of neutrophil extracellular traps

(NETs) that are linked with poor patient prognosis (Khan et al., 2021; Schoeps et al., 2021); TGFBi, which has a strong correlation with high levels of the protein and a large neutrophil constituency with the TME; and ALDOA, which is correlated with high levels of neutrophils in tumours (G. Lu et al., 2021).

With some of the most enriched genes within irradiated AKPT tumours being TGF-β mediated, it is critical that the immunomodulatory differences associated with these genes are mirrored by multiplex staining of the tumours. When observing the changes to the immune cell population post irradiation of heterotopic AKPT tumours we found that, aligning with the literature surrounding TGF-β as well as the RNAseq data (Figure 3.3.6), there was a relatively modest increase in the cytotoxic T-cell population and an inability for them to infiltrate the tumour epithelium (Figure 3.2.3). Additionally, we saw a significant increase in the Treg population at later timepoints post irradiation (Figure 3.2.5), matching the enriched genes found in after RNAseq of irradiated AKPT tumours (Figure 3.3.6). We also saw an increase in the neutrophil population that was maintained over the full-time course post irradiation, in line with the function of TGF-β upregulated genes.

With this background information on TGF-β, we hypothesised that the incorporation of an inhibitor would improve the anti-tumour effect of radiation on the heterotopic AKPT tumours through immunomodulation improving the immunogenicity of the treatment. We began investigating this through testing the ability of TGF-β inhibition to improve mouse survival post irradiation, and if there was any effect of using the inhibitor in isolation.

5.2 Heterotopic AKPT model response to the combination of irradiation and TGF-β inhibition

5.2.1 Efficacy of TGF-β inhibition as a neoadjuvant therapy alongside irradiation to improve survival in the heterotopic AKPT tumour model.

Unlike the studies involving the complement system (See Chapter 4), the phenotype of the AKPT organoids lent itself to the hypothesis that any improvement in

irradiation anti-tumour activity through TGF-β inhibition would occur through stromal interactions. This is because AKPT organoids lack TGFβR1 expression (as described in Chapter 3), therefore there will no direct impact of pharmacological TGF-β inhibition in tumour epithelial cells.

We found that inhibiting TGF-β, using the activin receptor-like kinase 5 (ALK5) inhibitor vactosertib), was able to significantly improve the survival of mice bearing heterotopic AKPT tumours when combined with irradiation compared with either control or irradiation alone groups (Figure 5.2.1). Interestingly, TGF-β inhibition alone was unable to improve mouse survival when compared to the control group (Figure 5.2.1).

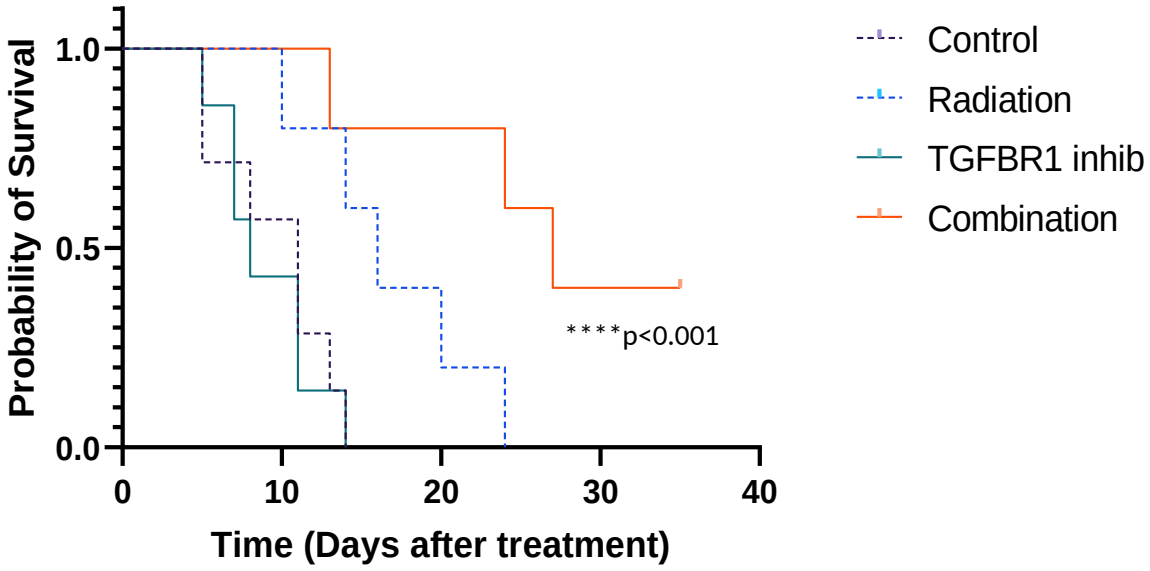


Figure 5.2.1 Survival curves of mice bearing subcutaneous AKPT tumours treated with radiation ± TGF-β inhibition.

Curve comparison is by Log-Rank, ****= p<0.001. n=7.

When comparing the tumour volumes over time in the different treatment groups, the findings from mouse survival are corroborated (Figure 5.2.2a-b). When comparing no treatment against TGF-β inhibition alone we observed no significant

improvement in halting tumour growth (Figure 5.2.2a). However, when this inhibition was combined with irradiation, we found that the arrest to tumour growth was significantly more pronounced and sustained (Figure 5.2.2b).

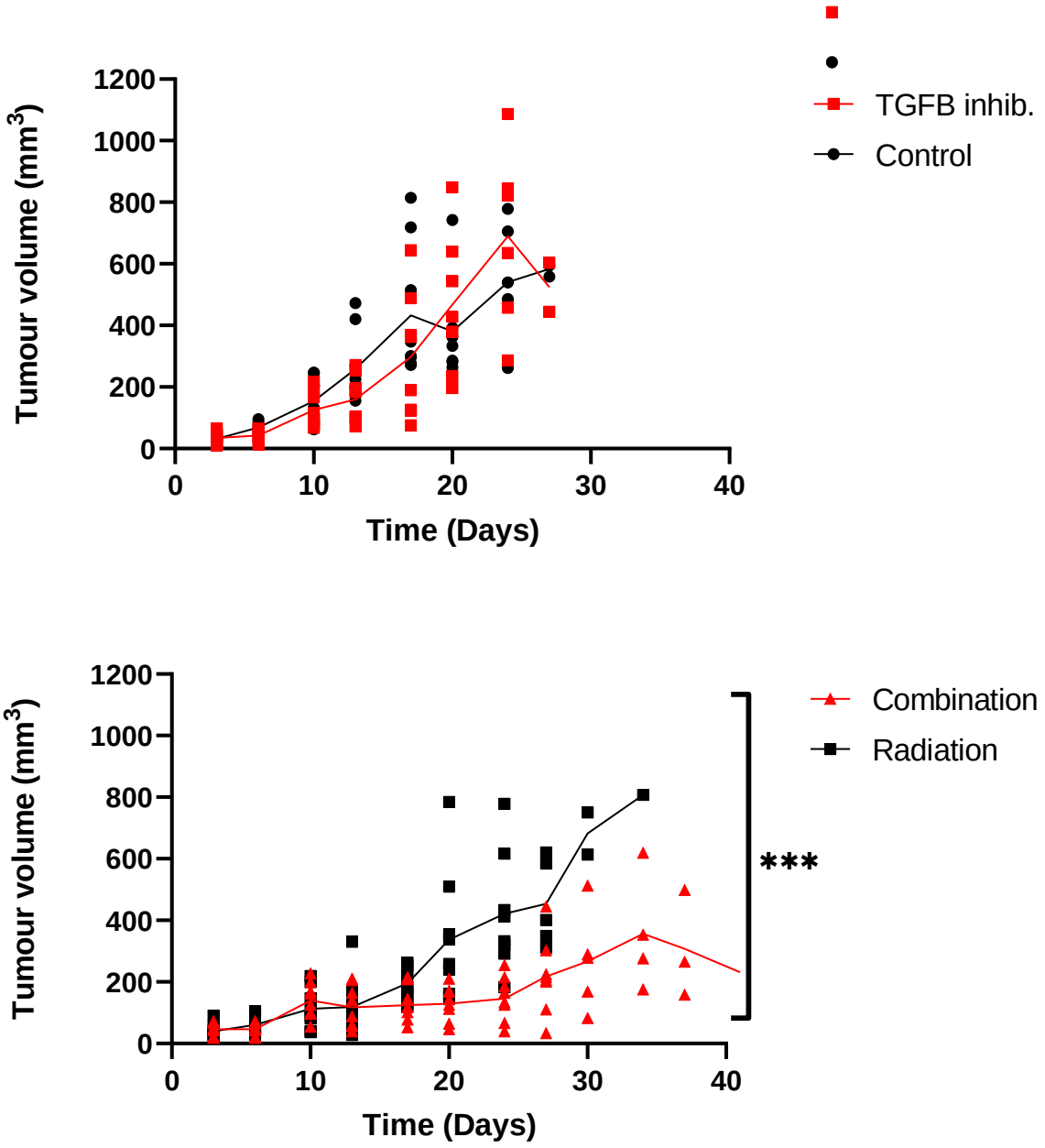


Figure 5.2.2 Volume growth curves of athymic nude mice bearing subcutaneous AKPT tumour treated with or without TGF-β (A) or radiation ± TGF-β inhibition (B).

Volume growth curve comparison by repeated measure two-way ANOVA (with Geisser-Greenhouse correction), ****= p<0.0001. n=7

Due to the inhibition of TGF-β improving the anti-tumour effect of irradiation on the heterotopic AKPT tumours, we looked to investigate the mechanism behind this. As described previously, due to the lack of TGFβR1 expression on the AKPT tumour

epithelium, we began our investigation into the components of the TME and how these changed depending on the treatment received.

5.2.2 Immune and stromal population changes post combination treatment

When examining cytotoxic T-cell populations post treatment in chapter three we found that although irradiation was able to significantly increase the number of these cells, the number able to infiltrate the tumour epithelium remained low (Figure 3.2.3). Therefore, due to this, combined with the importance of cytotoxic T-cells as a predictor of response to radiotherapy (Figure 3.3.4), the changes to this cell population may provide answers to the improved anti-tumour effect of irradiation when combined with TGF-β inhibition. Through the use of multiplex staining, we found that three days post treatment there was a significant increase in the $CD8^+$ T-cell population following combination treatment against all other groups (Figure 5.2.3a). Additionally, inhibiting TGF-β alone with no irradiation failed to significantly increase the number of cytotoxic T-cells against tumours receiving no treatment (Figure 5.2.3a). When investigating the ability of the cytotoxic T-cell population to infiltrate the epithelium, key for a functional immunogenic response to irradiation (H. Chen et al., 2018), we found that the addition of TGF-β inhibition alongside irradiation significantly increased this compared to radiation alone (Figure 5.2.3b). TGF-β inhibition alone was unable to increase the number of $CD8^+$ T-cells infiltrating into the tumour epithelium (Figure 5.2.3b). This increase in cytotoxic T-cells, both as a whole and within the tumour epithelium, may be a key facet in the increase of radiation dependent anti-tumour effects when combined with TGF-β inhibition.

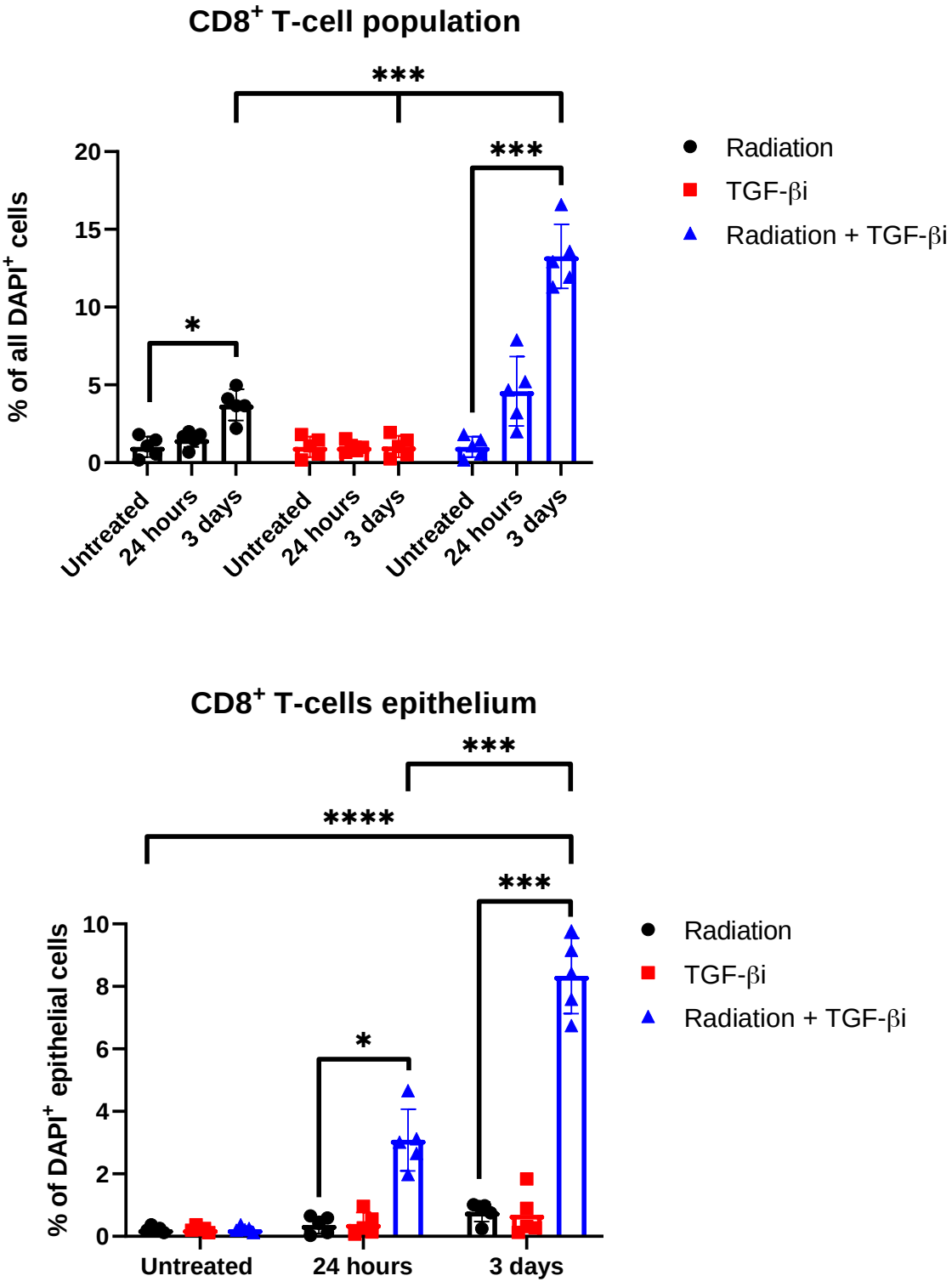


Figure 5.2.3 CD8+ T-cell population changes as a proportion of DAPI+ cells in subcutaneous AKPT tumours post treatment ± radiation ± TGF-βi

Using the HALO software, the changes to the $CD8^+$ T-cell population was analysed in the heterotopic AKPT tumour model were examined. Machine learning-based quantification of AKPT epithelial infiltration by $CD8^+$ T-cells post irradiation at a variety of timepoints was also carried out. All groups have n=5. Significance calculated by two-way ANOVA with Geisser-Greenhouse correction and Tukey's multiple comparisons (*P<0.05, **P<0.01, ***P<0.001).

The Treg population has been linked with the expression of TGF-β, through T-helper cells acquiring the immunosuppressive phenotype through the TGF-β signalling pathway (W. Chen et al., 2003; Fantini et al., 2004), and these are significantly more numerous post irradiation (Figure 3.2.5). Therefore, we employed the previously described multiplex staining approach to investigate the changes to the Treg population post irradiation with or without TGF-β inhibition. Our data showed that irradiation increased total numbers of Tregs in the tumour, but that this effect was fully inhibited by TGF-β inhibition (Figure 5.2.3a). In colorectal cancer, Treg infiltration into the tumour epithelium is a marker of poor prognosis (Aristin Revilla et al., 2022). Therefore, we sought to discover if the inhibition of TGF-β has an impact on the ability of Tregs to infiltrate the AKPT tumour epithelium. Consistent with the data in the whole tumour, TGF-β inhibition prevent the increased in Treg infiltration following irradiation (Figure 5.2.3b).

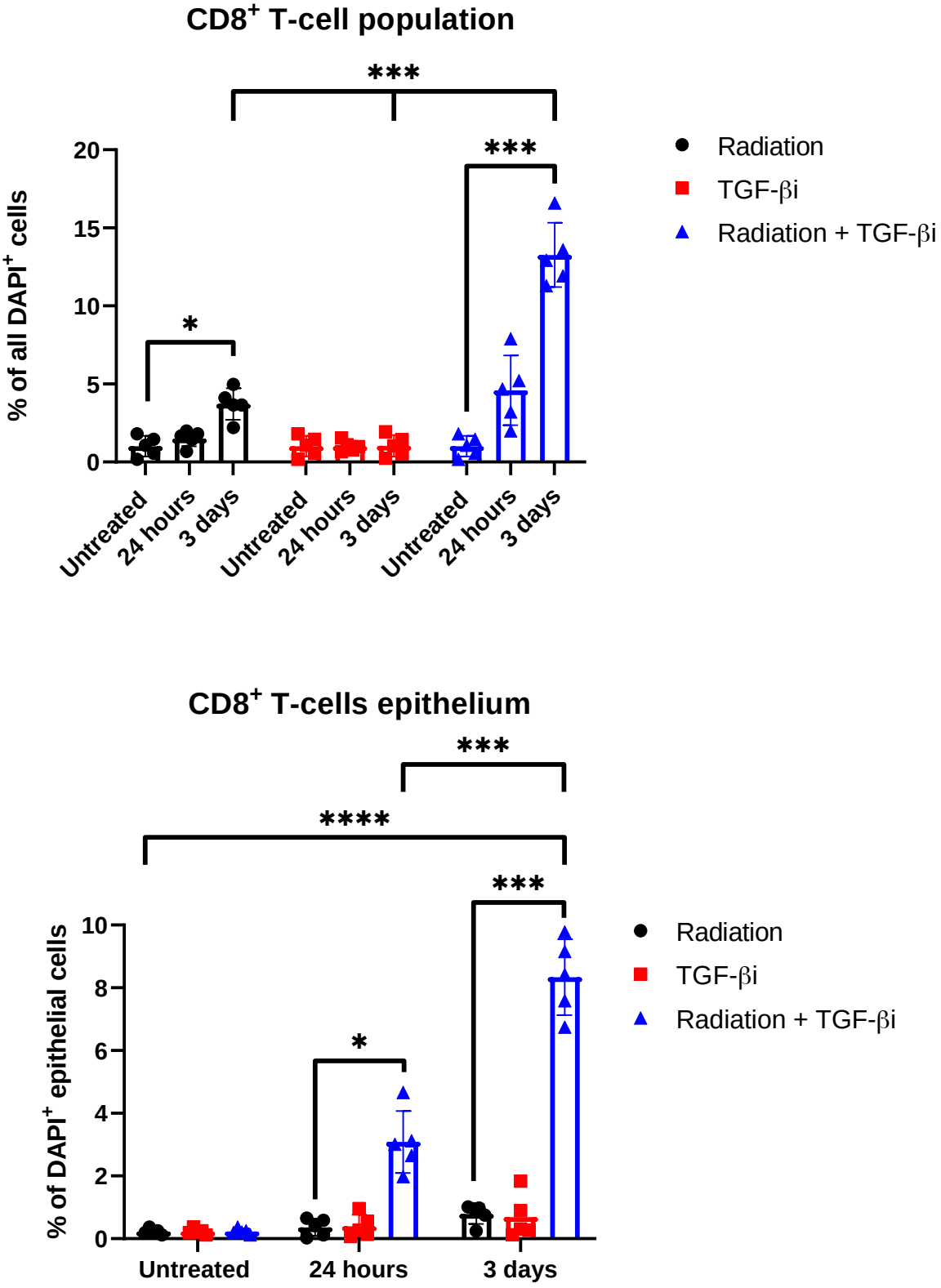


Figure 5.2.4 Treg (FOXP3$^+$) T-cell population changes as a proportion of DAPI$^+$ cells in subcutaneous AKPT tumours post treatment ± radiation ± TGF-βi.

Using the HALO software, the changes to the Treg population was analysed in the heterotopic AKPT tumour model were examined. Machine learning-based quantification of AKPT epithelial infiltration by

Treg post irradiation at a variety of timepoints was also carried out. All groups have n=5. Significance calculated by two-way ANOVA with Geisser-Greenhouse correction and Tukey's multiple comparisons (*P<0.05).

With TGF-β acting to induce T-helper cells to acquire the immunosuppressive phenotype and skew toward a Treg dominated immune population, we also decided to investigate the $CD4^+$ T-cell population. We found that the incorporation of TGF-β inhibition to the radiation treatment of the tumour significantly increased the number of $CD4^+$ T-cells (Figure 5.2.4). However, TGF-β inhibition alone did not lead to an increase in the recruitment of $CD4^+$ T-cells to the AKPT tumour (Figure 5.2.4).

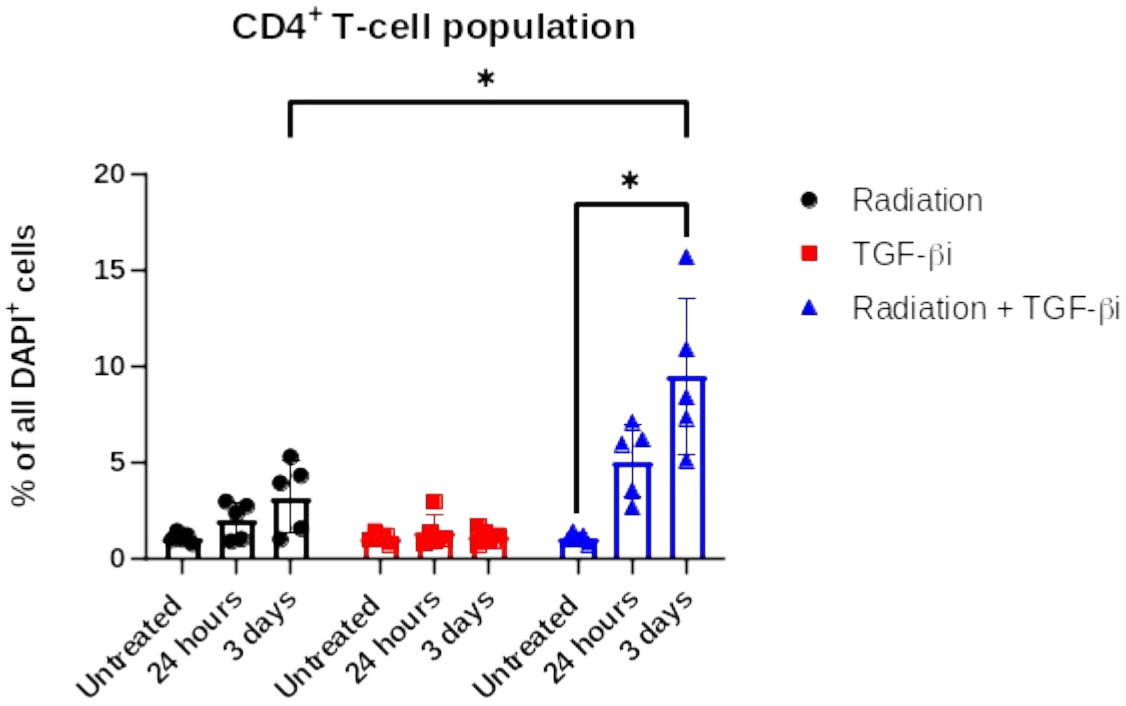


Figure 5.2.5 $CD4^+$ T-cell population changes as a proportion of $DAPI^+$ cells in subcutaneous AKPT tumours post treatment ± radiation ± TGF- βi.

Using the HALO software, the changes to the $CD4^+$ T-cell population was analysed in the heterotopic AKPT tumour model were examined. All groups have n=5. Significance calculated by two-way ANOVA with Geisser-Greenhouse correction and Tukey's multiple comparisons (*P<0.05).

This increase of T-helper cells within the tumour site, in combination with the significant decrease of the Treg and increase in the cytotoxic T-cell populations, suggests that the incorporation of TGF-β inhibition acts to improve the overall immunogenic effects of irradiating the tumour. The changes in the functionality of the T-cell portion of the adaptive immune response will be further investigated in Section 5.2.3 through

analysis of AKPT tumour RNA.

When examining the changes to the innate immune response when TGF-β is inhibited in combination with tumour irradiation, the neutrophil population is critical. This is due both the significant effect TGF-β signalling has on neutrophils (Fridlender et al., 2009, 2009; Reibman et al., 1991) as well as their link to poor prognosis in colorectal cancer (Jackstadt et al., 2019; Khan et al., 2021; Pine et al., 2015). Through staining for neutrophils in treated AKPT tumours we found that irradiation caused a significant acute increase of these immune cells post irradiation, both with and without TGF-β inhibition (Figure 5.2.5). TGF-β in isolation was unable to induce neutrophil recruitment to the tumour site (Figure 5.2.5).

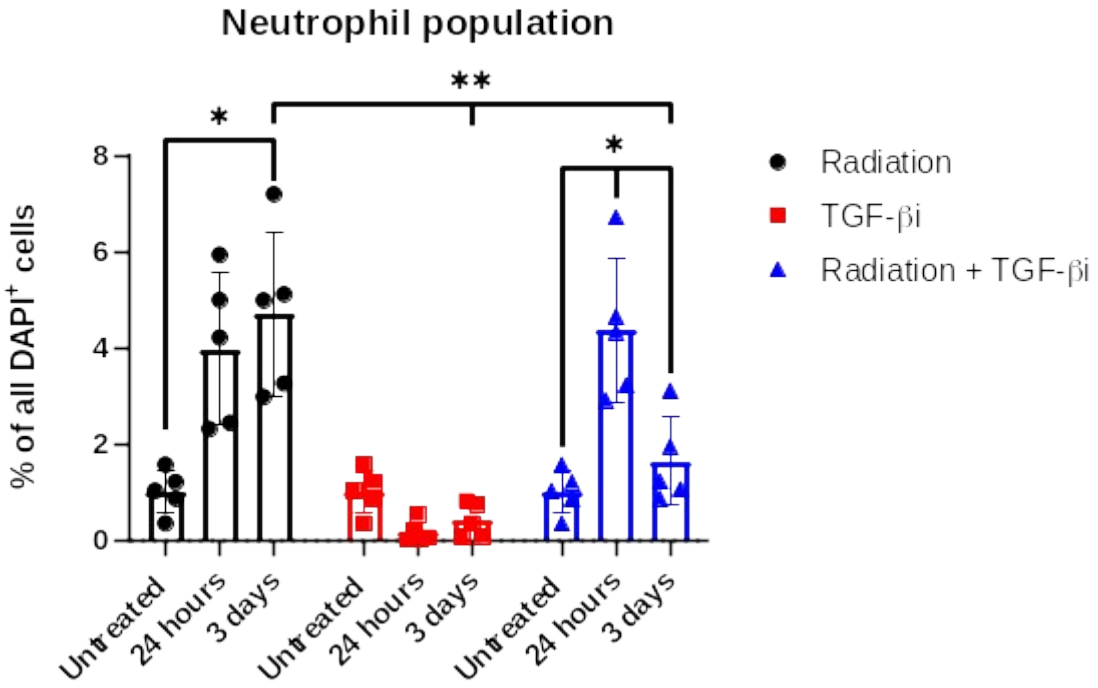


Figure 5.2.6 Neutrophil population changes as a proportion of DAPI+ cells in subcutaneous AKPT tumours post treatment ± radiation ± TGF-βi.

Using the HALO software, the changes to the neutrophil T-cell population was analysed in the heterotopic AKPT tumour model were examined. All groups have n=5. Significance calculated by two-way ANOVA with Geisser- Greenhouse correction and Tukey's multiple comparisons (*P<0.05, **P<0.01).

In addition to neutrophils, we also examined the changes to the macrophage population post irradiation. We found no significant changes to the macrophage population in any of the treatment groups between each other (Figure 5.2.5). However, when considering the importance of macrophages in the tumour's milieu when responding to irradiation there is a possibility of changes to the phenotype post treatment. Therefore, this will be further examined in section 5.2.3 through analysis of RNA acquired from the AKPT tumours.

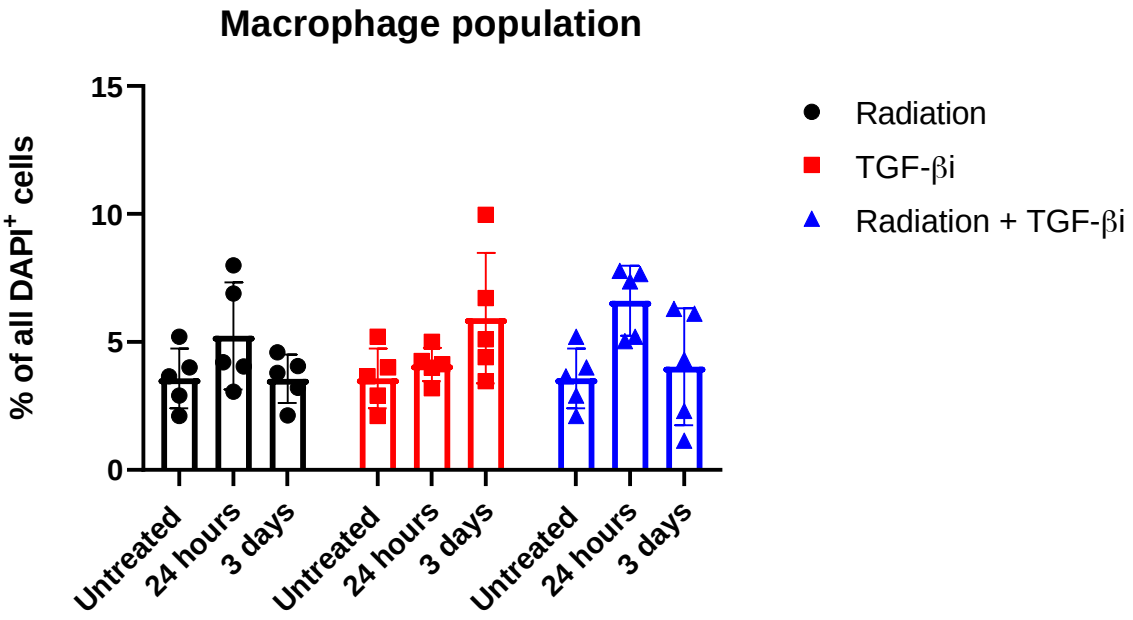


Figure 5.2.7 Macrophage population changes as a proportion of DAPI⁺ cells in subcutaneous AKPT tumours post treatment ± radiation ± TGF-βi.

Using the HALO software, the changes to the macrophage population was analysed in the heterotopic AKPT tumour model were examined. All groups have n=5. Significance calculated by two-way ANOVA with Geisser-Greenhouse correction and Tukey's multiple comparisons.

Outside of the immune population changes to the AKPT tumour post treatment, interesting changes to the fibroblast population within the stroma were observed. The α-SMA fibroblasts within the stroma changed in number depending on the treatment received. After irradiation this CAF population remained as one of the dominant populations within the tumour's stroma (Figure 5.2.6). TGF-β inhibition led to a significant decrease in the α-SMA^{+} cell population in both irradiated and unirradiated treatment groups (Figure 5.2.6). With the α-SMA^{+} CAF constituting a large component of the heterotopic AKPT tumour's stroma, this demonstrates that the inhibition of TGF-β has

a significant stromal effect. Another CAF marker within the tumour's stroma is PDGFRα, which we also examined concurrently with α-SMA. Interestingly, we found that the population of PDGFRα expressing CAFs demonstrated different trends than the α-SMA population. Specifically, the PDGFRα$^+$ population demonstrated a significant increase in the presence of TGF-β inhibition (Figure 5.2.6). The change to this CAF population demonstrates the significant effect the inhibition of TGF-β has on the tumour stroma, with the CAF population undergoing phenotypic changes. However, there was no significant difference in the PDGFRα$^+$ CAF population between the irradiated and combination treatment groups (Figure 5.2.6). Although a modest decrease of the PDGFRα$^+$ CAF population was seen in the radiation alone group, this was not significant.

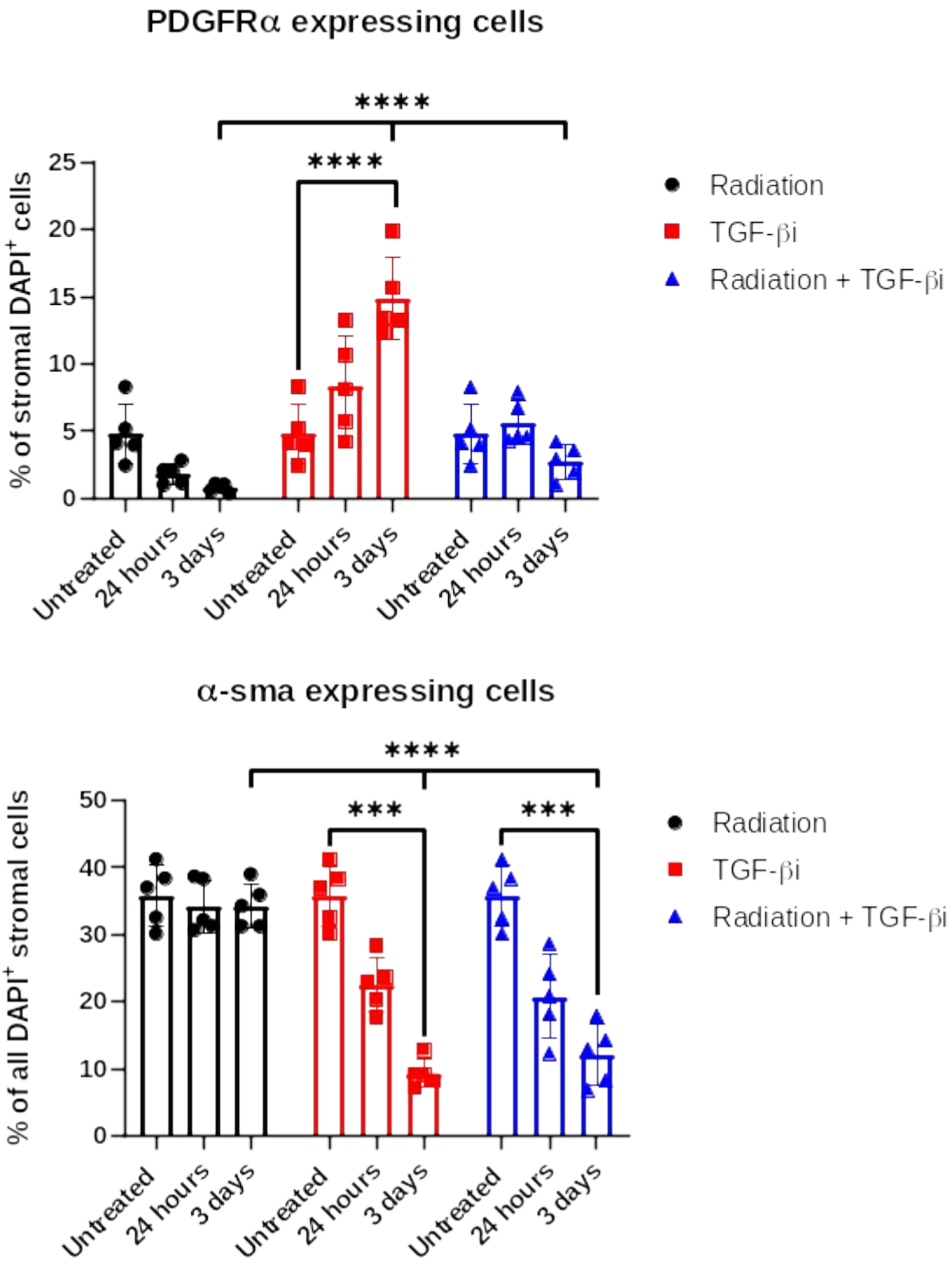


Figure 5.2.6 Fibroblast population changes in heterotopic AKPT tumours post± radiation ± TGF-βi.

Using the HALO software, the changes to the CAF population was analysed in the heterotopic AKPT tumour model were examined. All groups have n=5. Significance calculated by two-way ANOVA with Geisser-Greenhouse correction and Tukey's multiple comparisons (***P<0.005, ****P<0.001).

With there being a clear change in the CAF population depending on the treatment received by the AKPT heterotopic tumour, as illustrated by the changes in fibroblasts

expressing α-SMA and PDGFRα, further investigation into the changing phenotypic landscape of the CAFS was warranted. Therefore, the phenotypic changes of the CAFs will be investigated further through the RNA extracted from treated AKPT tumours in the subsequent chapter.

With significant changes to both the immune cell population and the stromal fibroblast population, investigating the phenotypic changes occurring was critical. Therefore, we next investigated the RNA from treated AKPT tumours.

5.2.3 RNAseq analysis of AKPT tumour post treatment with irradiation ± TGF-β inhibition.

Through sequencing the RNA of treated heterotopic AKPT tumours we began investigating the impact of the different treatments on the surrounding tumour milieu by examining the top-level enriched pathways. Analysis of RNA sequenced from AKPT tumours harvest from the heterotopic model was performed by Gabriel Valbuena. The data for the resulting GSEA plots, both the network plots as well as normalized enrichment score comparison, were also generated by Gabriel Valbuena. When examining the most enriched pathways in the irradiated AKPT tumours, we find that a strong network of interconnected DNA damage repair and cell cycle functions are enriched (Figure 5.2.7). Additionally, other pathways enriched post irradiation include metabolic changes and other cell protective measures, such as detoxification of reactive oxygen species (Figure 5.2.7). However, outside of these pathways, there is a lack of immune or stromal specific pathways upregulated after the irradiation of the AKPT tumours.

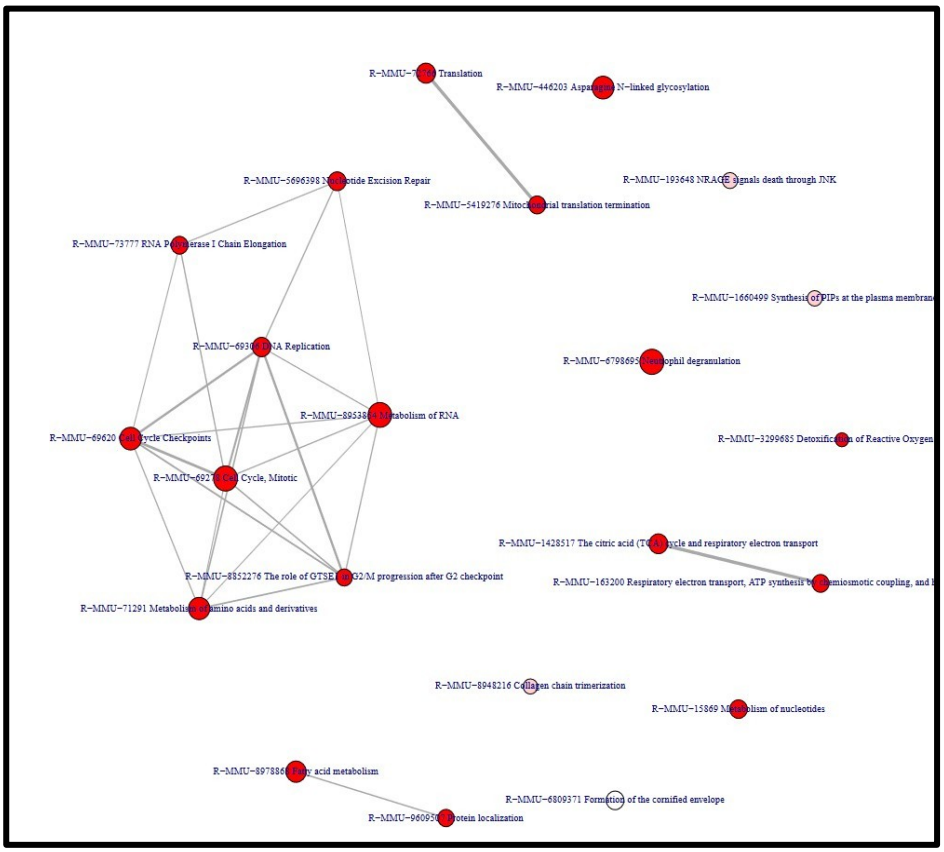


Figure 5.2.7 GSEA reactome network plot of top-level pathways enriched after AKPT tumour irradiation.

Red node colour represents an adjusted p< 0.05, size of node represents level of enrichment. Redundant gene sets trimmed to plot top-level pathways, defined by having the largest amount of crossover with other pathways. Figure constructed by Gabriel Valbuena.

When performing network analysis on AKPT tumours treated with the TGF-β inhibitor in isolation, several enriched pathways can be observed. A key network of pathways upregulated post inhibition of TGF-β are directly involved with both the innate immune system as well as the stromal component of the tumour (Figure 5.2.8). We see a significant enrichment in the neutrophil degranulation pathway, suggesting an improvement in anti-tumour activity (Figure 5.2.8). Additionally, this degranulation process undergone by the neutrophils is inhibited by TGF-β (Shen et al., 2007). Therefore, this suggests that the inhibition of TGF-β may induce more an anti-tumour role within the neutrophil population. Additionally, pathways involved in phagocytosis are upregulated, specifically the formation of the phagocytic cup (Figure 5.2.8). This suggests an improvement in the phagocytic activity from innate immune system that may act in an anti-tumour capacity. Within the stroma, we also see an increase in ECM

organisation that may be linked to the CAF population changes we previously observed through α-SMA and PDGFRα staining (Figure 5.2.8).

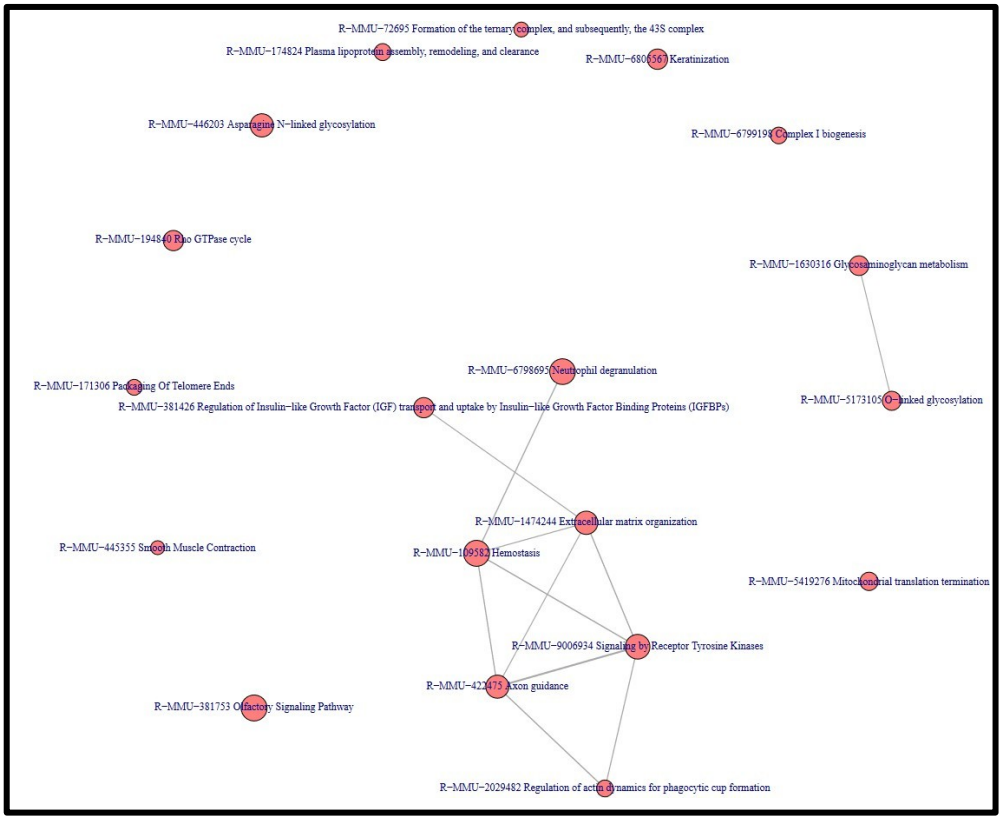


Figure 5.2.8 GSEA reactome network plot of top-level pathways enriched after AKPT tumour TGF-β inhibition.

Red node colour represents an adjusted p <0.05, size of node represents level of enrichment. Redundant gene sets trimmed to plot top-level pathways, defined by having the largest amount of crossover with other pathways. Figure constructed by Gabriel Valbuena.

In AKPT tumours treated with a combination of radiation and TGF-β inhibition, we see a unique set of enriched top-level genes in comparison to radiation alone. Specifically, a network of pathways indicating both stromal remodelling and the induction of a strong immunogenic response can be observed (Figure 5.2.9). Specifically, regarding the stroma, we see an upregulation of ECM organisation. Immunogenically, we see an upregulation of MHC-II and Fc-γ receptors suggesting an increase in the ability of innate immune cells within the TME to carry out phagocytosis (Figure 5.2.9). Additionally, the increase in interleukin 2 (IL2) signalling suggests a sustained induction of an immunogenic response post treatment (Figure 5.2.9). This is due to the IL2 signalling pathway forming a positive feedback loop with T-helper and cytotoxic T-cells. This loop

acts to enhance the survival of these cells, mediate the differentiation of T-helper cells, and enhance the cell killing activity of cytotoxic T-cells (Ross & Cantrell, 2018).

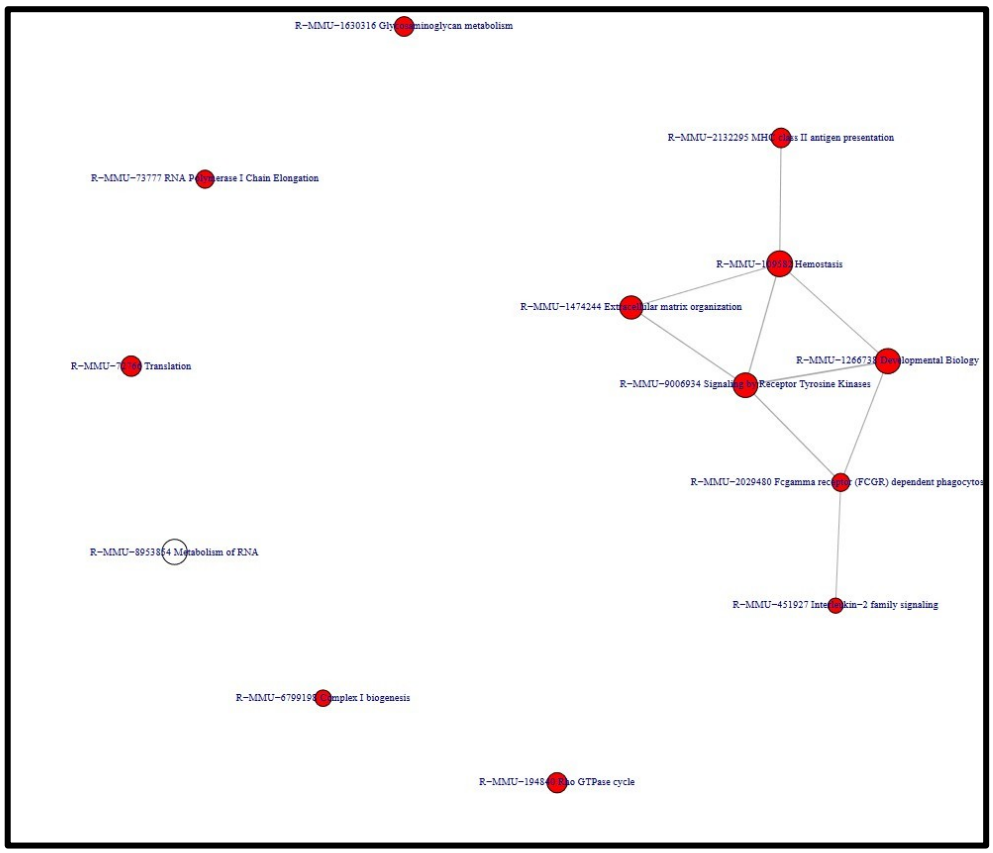


Figure 5.2.9 GSEA reactome network plot of top-level pathways enriched after AKPT tumour radiation and TGF-β inhibition when compared to AKPT tumours treated with radiation alone.

Red node colour represents an adjusted p<0.05, size of node represents level of enrichment. Redundant gene sets trimmed to plot top-level pathways, defined by having the largest amount of crossover with other pathways. Figure constructed by Gabriel Valbuena.

With the combination of irradiation and TGF-β inhibition enriching several immunogenic pathways, we then used the literature to establish gene lists to further interrogate how different treatments induced differing immunogenic responses against the AKPT tumours. Initially we examined the overall immune landscape of the tumours post treatment. We did this through investigating the state of enrichment in genes linked to an active immune response within the TME and genes linked with an immunosuppressive setting.

In the radiation alone setting we discovered that, in line with staining done on

irradiated AKPT tumours (Figures 3.2.3 to 3.2.5), a significant competing immunogenic and immunosuppressive response arose (Figure 5.2.10). Although not statistically significant, we also saw an increase in immune checkpoint expression thereby providing further explanation toward the ability of AKPT tumours to overcome irradiation (Figure 5.2.10). When investigating TGF-β inhibition alone we saw that there was an inability to establish a significant change to the immune landscape of the AKPT tumour. However, the modest enrichment seen suggested a reversal in the enrichment of immunosuppressive setting found after irradiation (Figure 5.2.10). When combining TGF-β inhibition with irradiation we compared the enrichment of genes following combination treatment of the tumour against tumours receiving radiation alone. We found that there was a modest increase, although not significant, of the immunogenic response (Figure 5.2.10). This is particularly interesting as the data suggests inhibiting TGF-β causes a modest further increase to the already significant enrichment of genes relating to the mounting of an immune response post irradiation. Critically, we saw a dramatic and significant decrease in the enrichment of genes encoding for immune checkpoints (Figure 5.2.10). This suggests that this may be a potential function of TGF-β inhibition, when combined with irradiation, that allows for the increase anti-tumour activity of cytotoxic T-cells.

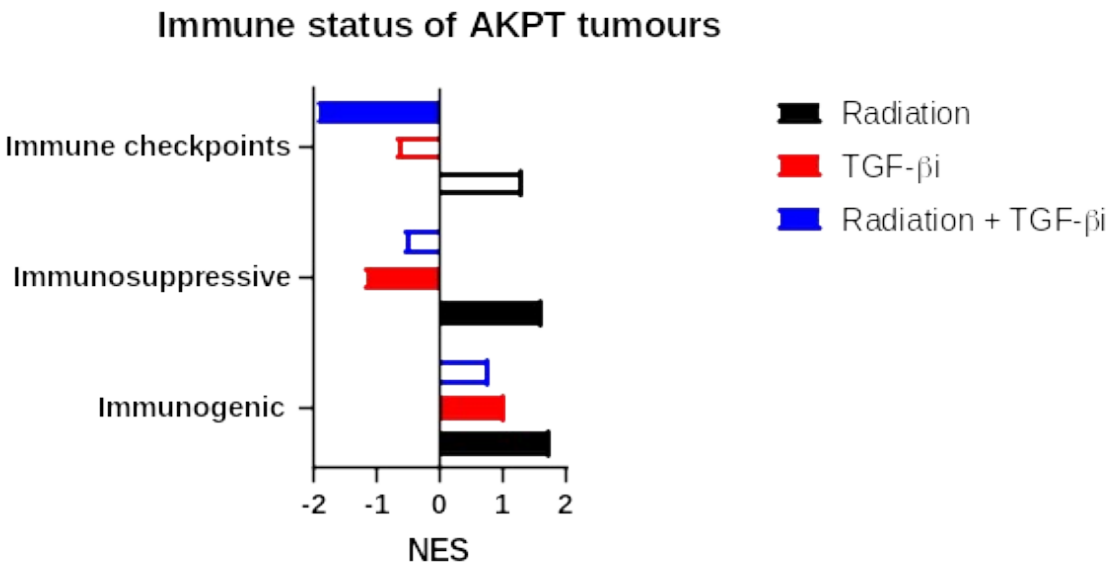


Figure 5.2.10 Immunogenic, immunosuppressive, and immune checkpoint gene signature enrichment comparison in treated AKPT tumours.

The enrichment of selected gene signatures defining immunogenicity, immunosuppression, and immune checkpoints compared between: untreated vs irradiated; untreated vs TGF-βi; and irradiated vs irradiated and TGF- βi. Filled bars represent a pFDR ≤ 0.1. NES = Normalised Enrichment Score. Data analysed by Gabriel Valbuena

As mentioned in chapter 5.2.2, although we did not find a significant change to the macrophage population between any of the treatment groups, any changes to the phenotype of this myeloid immune cell population may have been missed. Examining the shift of macrophages between the immunogenic M1-like and immunosuppressive M2-like phenotype may lead to further answers on how TGF-β inhibition alters the immune landscape of the AKPT tumour. We found that after irradiation, macrophages showed a negative, though not statistically significant, enrichment of genes linked to an immunogenic macrophage phenotype (Figure 5.2.11). When TGF-β was inhibited in isolation we found that there was a modest enrichment in immunogenic macrophage-specific genes (Figure 5.2.11). Interestingly, the combination of radiation and TGF-β inhibition caused a significant enrichment in immunogenic macrophage-specific genes when compared to tumours receiving radiation alone (Figure 5.2.11).

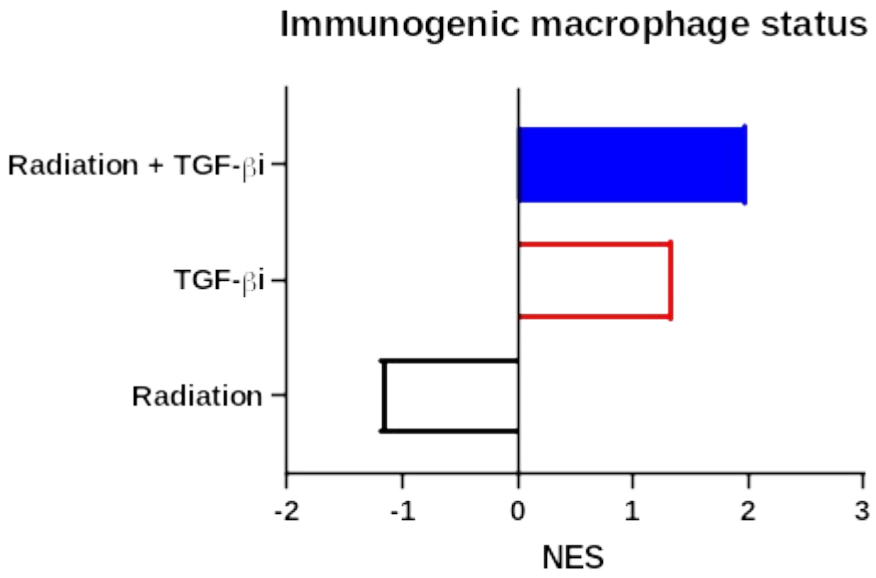


Figure 5.2.11 M1-like macrophage gene list enrichment comparison in treated AKPT tumours.

The enrichment of selected gene signatures defining M1-like macrophages compared between: untreated vs irradiated; untreated vs TGF-βi; and irradiated vs irradiated and TGF-βi. Filled bars represent a pFDR ≤ 0.1. NES = Normalised Enrichment Score. Data analysed by Gabriel Valbuena

With interesting shifts in the CAF population being observed depending on the treatment received by the AKPT tumours (Figure 5.2.6), we further investigated the phenotypic changes occurring in this stromal cell population. Following the stratification of CAFs within the tumour stroma established by (Grauel et al., 2020), we implemented the published gene lists to allow us to investigate the CAF phenotype within the AKPT tumour stroma. Genes ascribed to inflammatory CAFs (iCAF), defined by their immunomodulatory ability including IL6 and chemokine signalling, where found to be significantly enriched in the radiation alone group but the inverse was found when TGF-β was inhibited (Figure 5.2.12). When combining radiation and TGF-β inhibition the iCAF population was significantly negatively enriched when compared to irradiation alone (Figure 5.2.12). Genes identifying the canonical myofibroblast population (myCAF), defined by their role in ECM remodelling, showed a modest negativeenrichment in both treatment groups including TGF-β inhibition (Figure 5.2.12). The vascular endothelial growth factor (VEGFR) positive CAF population (vCAFs), as defined by VEGF ligand-receptor interactions, have their defining gene set significantly enriched through irradiation whereas the inverse is true when combined with TGF-β inhibition (Figure 5.2.12). The proliferating CAF (prCAF) population, as defined by their enrichment of cell cycle

pathways, are significantly negatively enriched in both treatment groups that include irradiation (Figure 5.2.12). Finally, interferon-licensed CAFs (il-CAFs), defined by their upregulation of pathways enriched by interferon signalling, was positively enriched in all treatment groups by different amounts (Figure 5.2.12). Irradiation and TGF-β inhibition in isolation showed a very modest enrichment of il-CAF defining genes. However, radiation combined with TGF-β inhibition showed a significant enrichment in the ilCAF genes when compared to tumours receiving radiation alone.

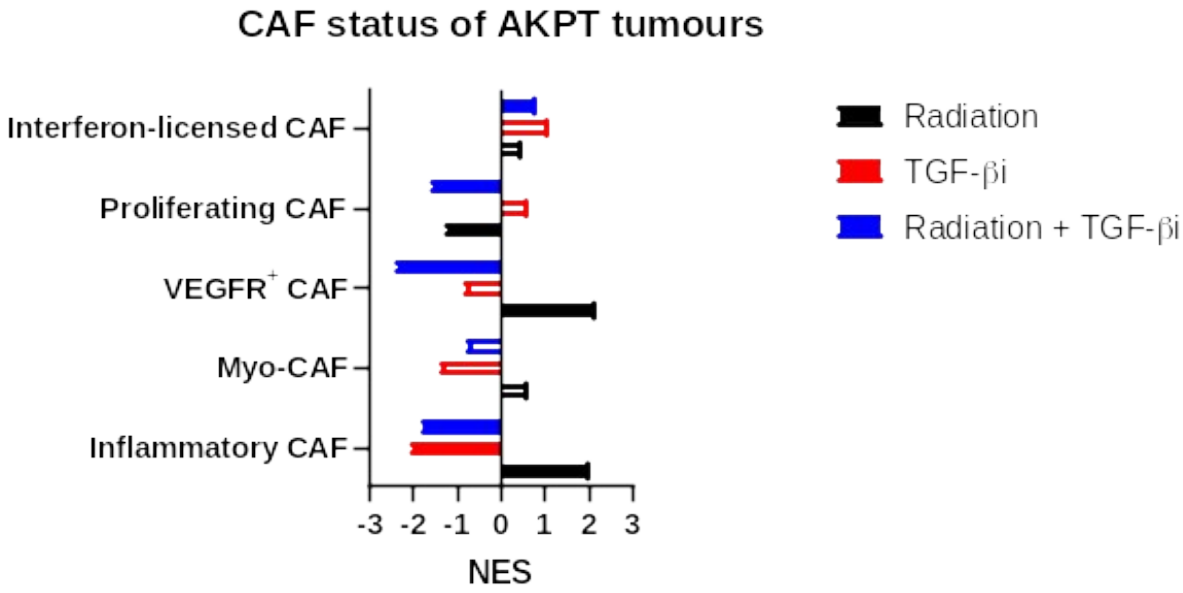


Figure 5.2.12 CAF genetic phenotype enrichment comparison in treated AKPT tumours.

The enrichment of selected gene signatures defining CAF phenotypes compared between: untreated vs irradiated; untreated vs TGF-βi; and irradiated vs irradiated and TGF-βi. Filled bars represent a pFDR ≤ 0.1.NES= Normalised Enrichment Score. Data analysed by Gabriel Valbuena

Following on from the data gathered through multiplex staining and RNA sequencing of treated AKPT tumours, it became clear the constituent components of the TME surrounding the cancer cells played a vital role in the efficacy of treatment. The combination of TGF-β inhibition with radiotherapy demonstrated an increase in the immune system response to the AKPT tumour, exemplified by the increase in $CD8^+$ T-cell infiltration into the tumour epithelium (Figure 5.2.3). Additionally, we saw that TGF-β inhibition, with or without radiation, has a significant impact on the tumour's stroma. This was demonstrated by the shift in CAF phenotypes after treatment, both when looking at α-SMA and PDGFRα markers (Figure 5.2.6) as well as markers within the RNAseq data (Figure 5.2.12). With the AKPT tumours

investigated so far being implanted subcutaneously there may be specific treatment responses that are specific to the tumour location. Therefore, to investigate this we moved to compare the heterotopic model with an orthotopic one, with AKPT organoids being implanted submucosally into the rectum. We then directly compared these orthotopic tumours with the heterotopic model to investigate whether AKPT tumours would respond differently to the treatments when implanted *in situ*.

5.3 Impact of AKPT rectal tumour growing *in situ* versus heterotopically.

5.3.1 Impact of rectal environment on AKPT immune and stromal changes post irradiation combined with or without TGF-β inhibition.

To compare the differences in immune populations depending on the implantation site of the AKPT organoids, we used the same orthogonal approach as described in prior chapters combining multiplex staining with RNA sequencing. When comparing immune cell staining in the heterotopic and orthotopic model, some notable differences were observed.

When comparing the changes to the cytotoxic T-cell population depending on the implantation site of the AKPT organoids, we saw some significant changes (Figure 5.3.1). Examining the $CD8^+$ T-cell population demonstrated a significantly higher level in the orthotopic AKPT tumours after treatment with irradiation and TGF-β inhibition when compared to identically treated subcutaneous tumours (5.3.1a). When examining the ability of the cytotoxic T-cells to infiltrate the tumour epithelium a similar trend was observed (Figure 5.3.1b). Significantly more $CD8^+$ T-cells infiltrating the tumour epithelium was also observed in the irradiated orthotopic AKPT tumours in comparison to subcutaneous tumours receiving the fractionated dose of radiation (3x7Gy).

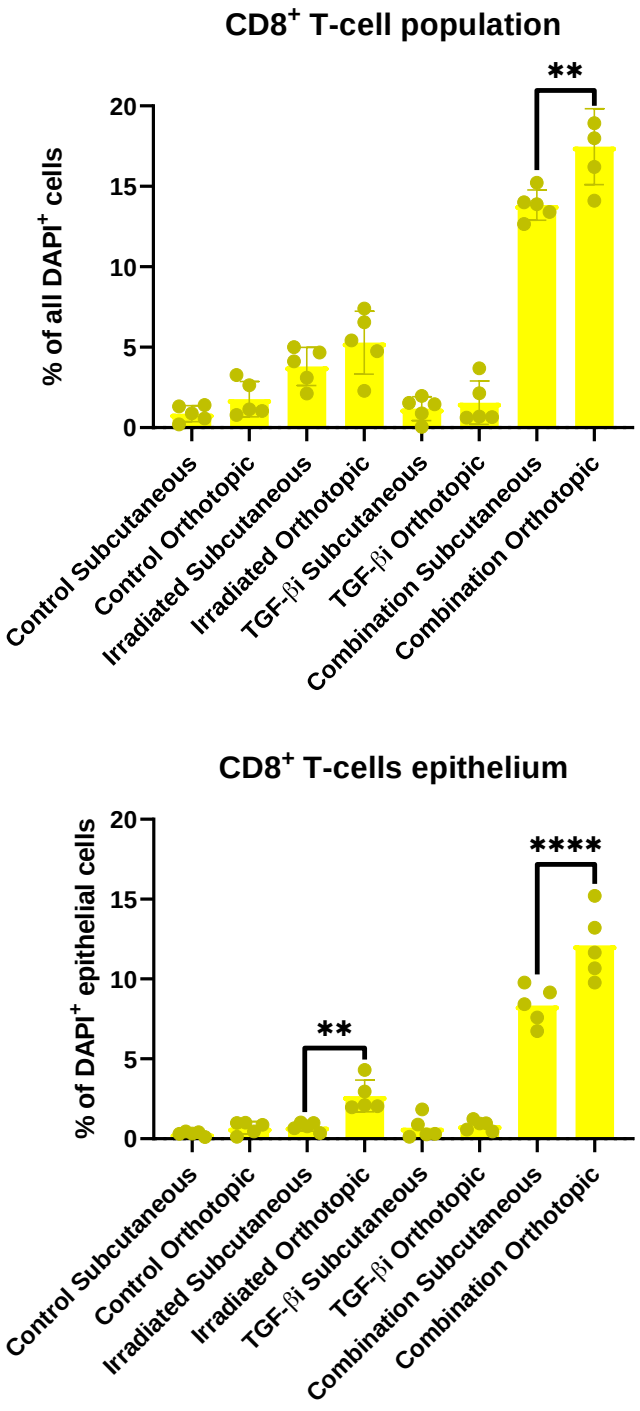


Figure 5.3.1 CD8+ T-cell population changes as a proportion of DAPI+ cells in subcutaneous and orthotopic AKPT tumours post treatment ± radiation ± TGF-βi

Using the HALO software, the changes to the CD8+ T-cell population was analysed in both heterotopic and orthotopic AKPT tumour model were examined. Machine learning-based quantification of AKPT epithelial infiltration by CD8+ T-cells post treatment at a variety of timepoints was also carried out. All groups have n=5. Significance calculated by two-way ANOVA with Geisser-Greenhouse correction and Tukey's multiple comparisons (**P<0.01, ****P<0.001).

The regulatory Treg population also demonstrated some significant differences depending on the AKPT tumour site of implantation. When tumours were treated with TGF-β inhibition, with or without radiation, the Treg population was reduced both as a whole and within the tumour epithelium (Figure 5.3.2a-b). However, following irradiation, orthotopic AKPT tumours demonstrated a larger number of Tregs both as a whole as well as within the tumour epithelium (Figure 5.3.2a-b). AKPT tumours receiving no treatment also demonstrated significantly more Tregs within the tumour epithelium when implanted orthotopically versus subcutaneously (Figure 5.3.2b).

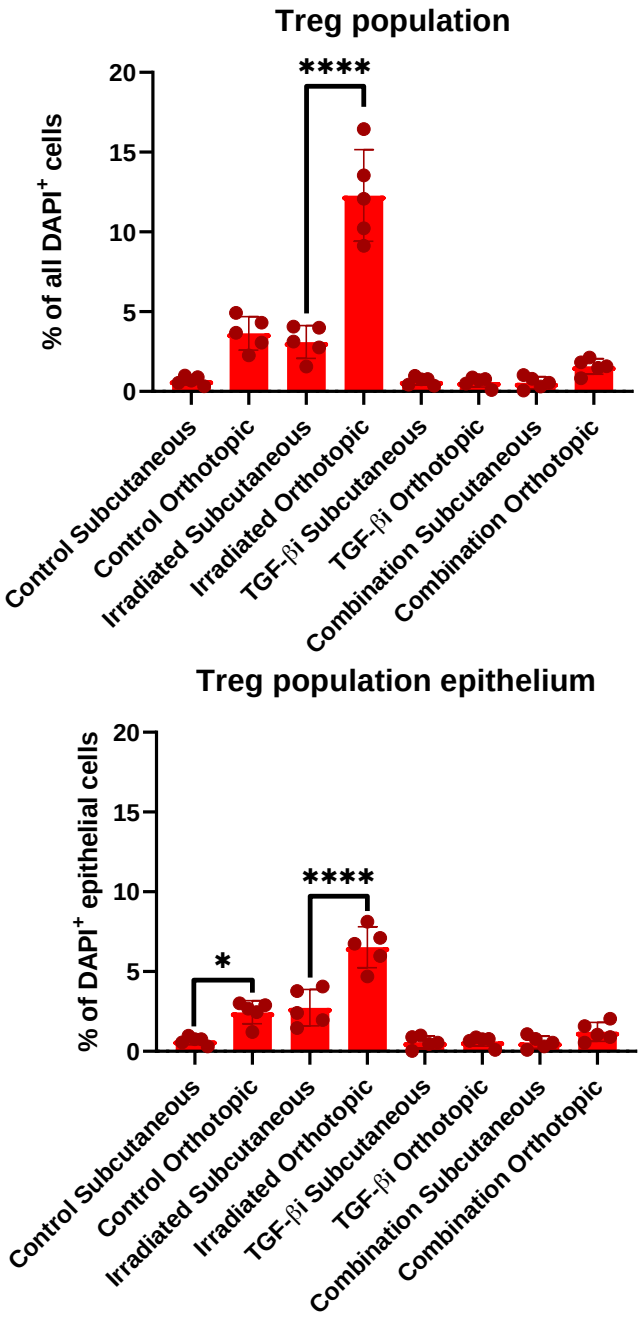
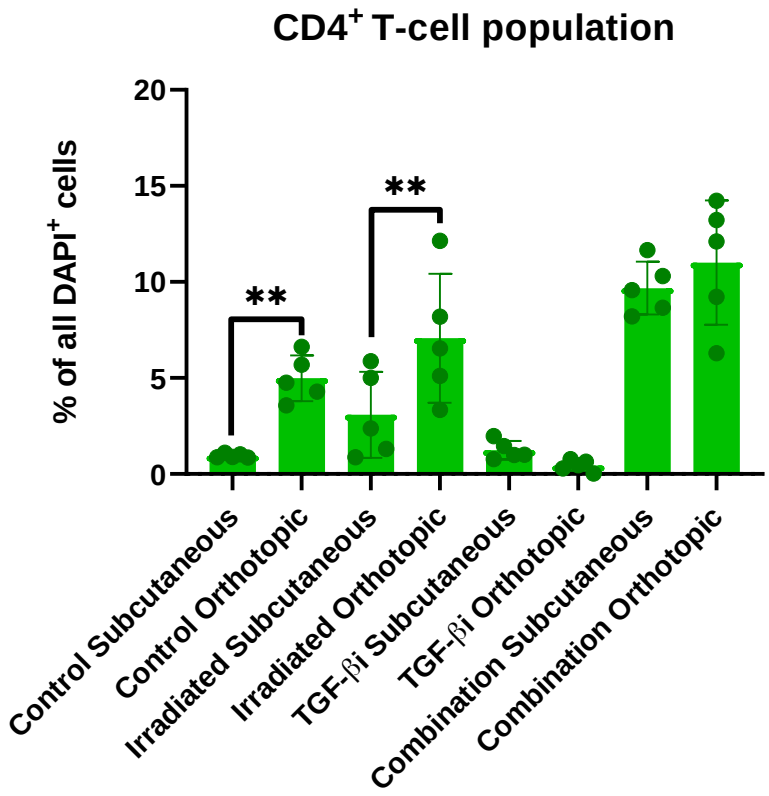


Figure 5.3.2 Treg population changes as a proportion of DAPI+ cells in subcutaneous and orthotopic AKPT tumours post treatment ± radiation ± TGF-βi

Using the HALO software, the changes to the Treg population was analysed in both heterotopic and orthotopic AKPT tumour model were examined. Machine learning-based quantification of AKPT epithelial infiltration by Treg post treatment at a variety of timepoints was also carried out. All groups have n=5. Significance calculated by two- way ANOVA with Geisser-Greenhouse correction and Tukey's multiple comparisons (*P<0.05, ****P<0.001).

When comparing the T-helper cell population between the subcutaneous and orthotopic AKPT tumours, significant differences in the populations are seen.

Specifically, orthotopic AKPT tumours demonstrate a great number of $CD4^+$ T-cells in both the untreated and irradiated groups in comparison to their subcutaneous equivalent (Figure 5.3.3). After the incorporation of TGF-β inhibition, this difference in T-helper population size within the AKPT tumours is lost and no significant difference was



observed (Figure 5.3.3.).

Figure 5.3.3 $CD4^+$ population changes as a proportion of $DAPI^+$ cells in subcutaneous and orthotopic AKPT tumours post treatment ± radiation ± TGF-βi

*Using the HALO software, the changes to the Treg population was analysed in both heterotopic and orthotopic AKPT tumour model were examined. All groups have n=5. Significance calculated by two-way ANOVA with Geisser-Greenhouse correction and Tukey's multiple comparisons (**P<0.01)*

Examining the differences in the innate immune cell components between AKPT tumours grown subcutaneously versus orthotopically also demonstrated some significant differences. In tumours treated with TGF-β inhibition there was no change in the number of neutrophils between subcutaneous or orthotopic tumours (Figure 5.3.4). However, in

both the control and irradiated treatment groups, orthotopic AKPT tumours demonstrated significantly greater number of neutrophils within the tumour site (Figure 5.3.4).

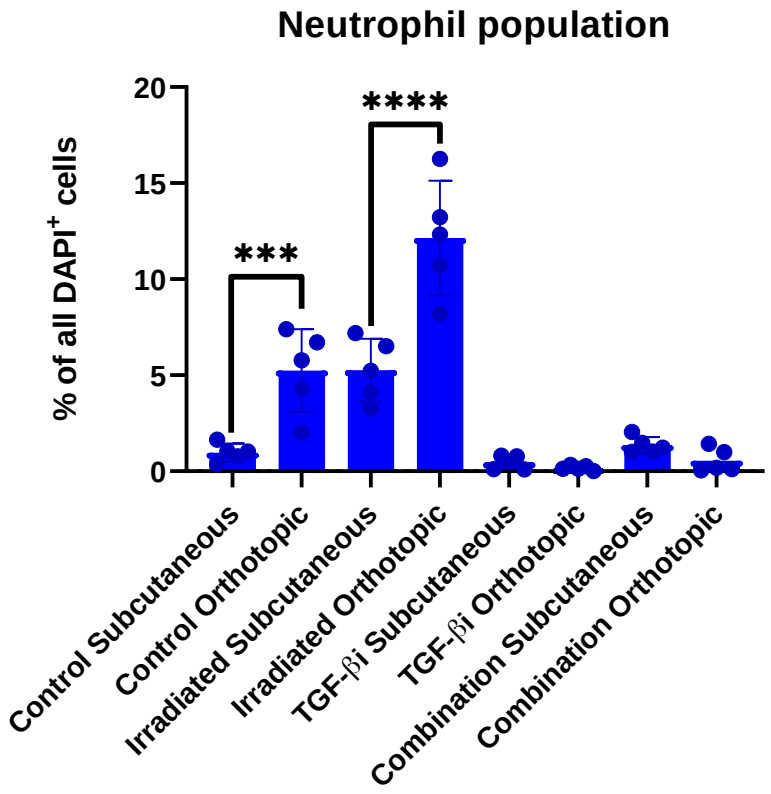


Figure 5.3.4 Neutrophil population changes as a proportion of DAPI⁺ cells in subcutaneous and orthotopic AKPT tumours post treatment ± radiation ± TGF-βi.

Using the HALO software, the changes to the neutrophil population was analysed in both heterotopic and orthotopic AKPT tumour model were examined. All groups have n=5. Significance calculated by two-way ANOVA with Geisser-Greenhouse correction and Tukey's multiple comparisons (***P<0.005, ****P<0.001)

When comparing the macrophage population in subcutaneous and orthotopic tumours we saw significant differences depending on the location of the tumour implantation site. Within the control and the irradiated tumour groups, the orthotopic setting demonstrated a significantly greater macrophage population (Figure 5.3.5). Additionally, when AKPT tumours were treated with the TGF-β inhibitor in isolation, we saw this trend continues with macrophages remaining to be a significantly larger population in the orthotopic model (Figure 5.3.5). However, when TGF-β inhibition was combined with irradiation, there was no significant difference in the size of the

macrophage population when comparing orthotopic tumours against tumours implanted subcutaneously.

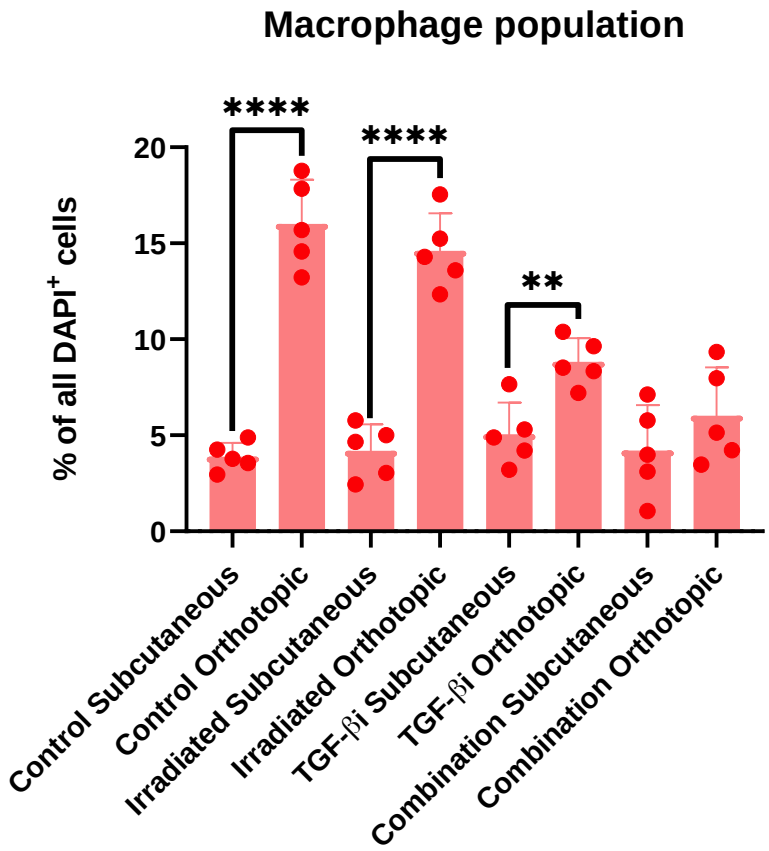


Figure 5.3.5 Macrophage population changes as a proportion of DAPI⁺ cells in subcutaneous and orthotopic AKPT tumours post treatment ± radiation ± TGF-βi

*Using the HALO software, the changes to the Macrophage population was analysed in both heterotopic and orthotopic AKPT tumour model were examined. All groups have n=5. Significance calculated by two-way ANOVA with Geisser-Greenhouse correction and Tukey's multiple comparisons (**P<0.01, ****P<0.001)*

When comparing the differences found in the stromal CAF components of the AKPT tumour depending on implantation site, we saw some specific changes. As described before, we stained for CAFs using α-SMA and PDGFRα to ascertain the size of the population. Interestingly, the only significant difference found between α-SMA expressing CAFs was between tumours receiving irradiation alone (Figure 5.3.6a). In this setting, the subcutaneous AKPT tumour demonstrated a significantly greater amount of α-SMA expression. When staining for PDGFRα we only saw a significant difference in

tumours receiving TGF-β inhibition alone, suggesting that TGF-β inhibition may have an greater effect on the orthotopic CAF population and therefore its stroma (Figure 5.3.6b).

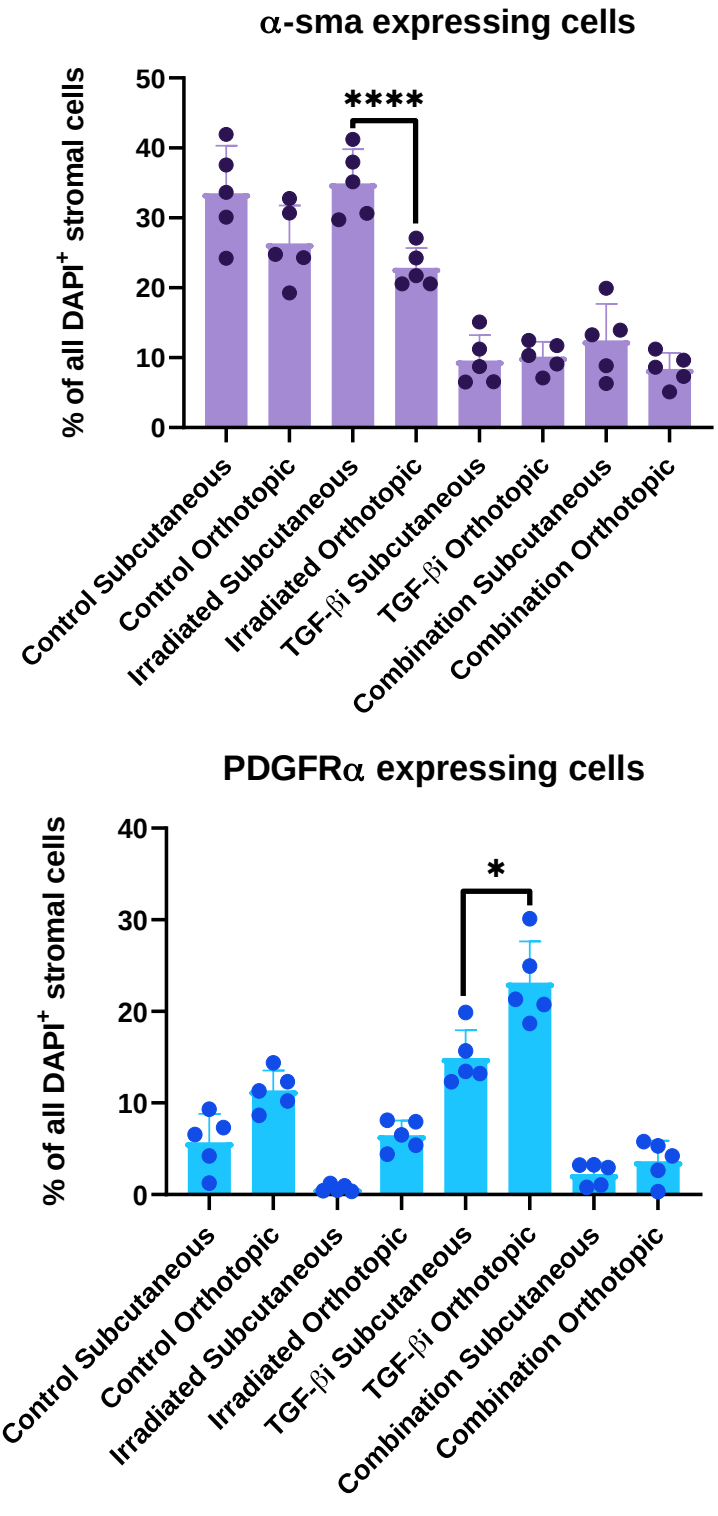


Figure 5.3.6 Fibroblast population changes as a proportion of $DAPI^+$ cells in subcutaneous and orthotopic AKPT tumours post treatment ± radiation ± TGF-βi

Using the HALO software, the changes to the Treg population was analysed in both heterotopic and orthotopic AKPT tumour model were examined. All groups have n=5. Significance calculated by two-way ANOVA with Geisser-Greenhouse correction and Tukey's multiple comparisons (**P<0.01).

To further compare the differences between AKPT tumours in the orthotopic and subcutaneous models, we carried out RNAseq analysis. This analysis was carried out using the methodology developed in chapter 5.2.2. We then examined additional effects imparted on AKPT tumour samples, after receiving treatment, that the location of the organoid implantation imparted.

5.3.2 RNA-seq analysis of heterotopic versus orthotopic AKPT tumours post combination treatment.

Akin to chapter 5.2.2, we began through sequencing RNA from treated subcutaneous and orthotopic tumours. Analysis of RNA sequenced from AKPT tumours harvest from the heterotopic model was performed by Gabriel Valbuena. The data for the resulting GSEA plots, both the network plots as well as normalized enrichment score comparison, were also generated by Gabriel Valbuena. Then we investigated the impact of the tumour location by examining the top-level enriched pathways in the orthotopic tumours directly compared to their subcutaneous counterparts.In AKPT tumours receiving radiation alone there we observed some significantly enriched pathways in the orthotopic model when compared to irradiated subcutaneous tumours. Specifically, we saw an enrichment in pathways relating to the regulation of hypoxia-inducible factor (HIF) (Figure 5.3.7) suggesting a change in oxygenation status when comparing irradiated subcutaneous and orthotopic tumours. Additionally, aligning with the modest increase of PDGFRα^{+} expressing cells seen through comparative multiplex staining, we saw an enrichment in pathways linked to PDGFRα signalling (Figure 5.3.7).

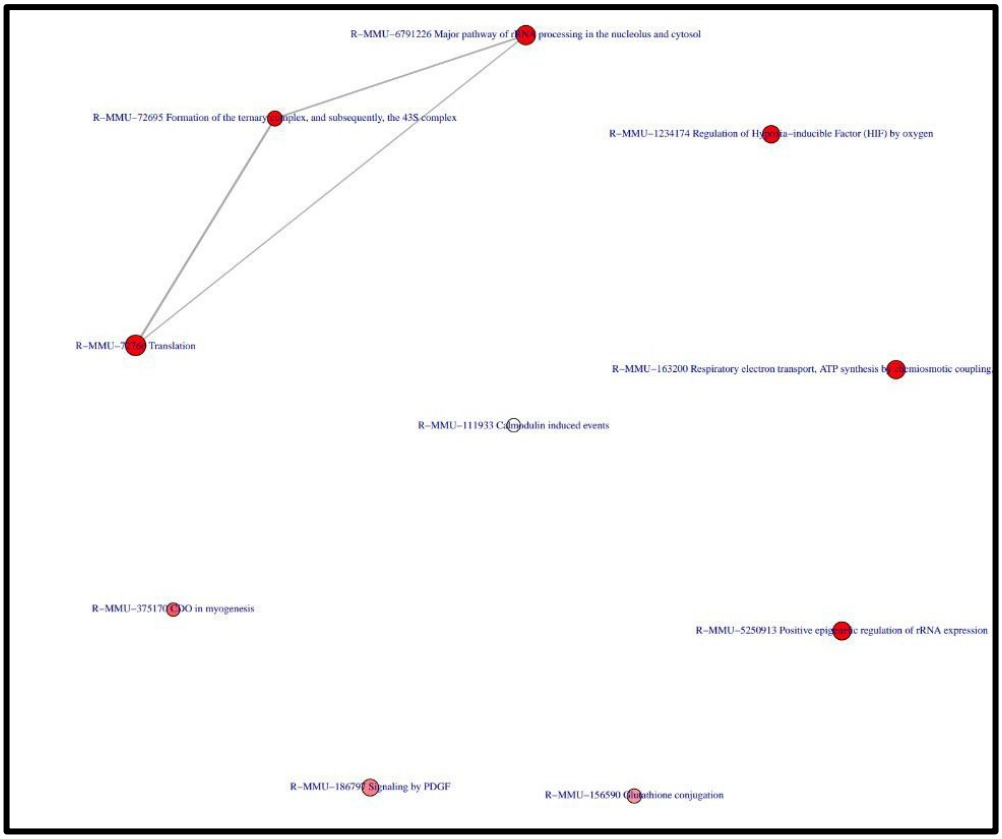


Figure 5.3.7 GSEA reactome network plot of top-level pathways enriched in the orthotopic AKPT tumour versus the subcutaneous setting after irradiation.

Red node colour represents an adjusted p value of 0.05, size of node represents level of enrichment. Redundant gene sets trimmed to plot top-level pathways, defined by having the largest amount of crossover with other pathways. Figure constructed by Gabriel Valbuena.

Comparing subcutaneous and orthotopic AKPT tumours receiving TGF-β inhibition also demonstrated some significantly enriched, top-level pathways. Interestingly we saw an enrichment in a network of pathways related to macrophages, FC-γ dependent phagocytosis and VEGFR signalling pathways (Figure 5.3.8). Additionally, an enrichment of the pathway involved with the formation of collagen fibrils suggest an increase in ECM remodelling occurring in the orthotopic model after receiving TGF-β inhibition in comparison to the heterotopic model (Figure 5.3.8).

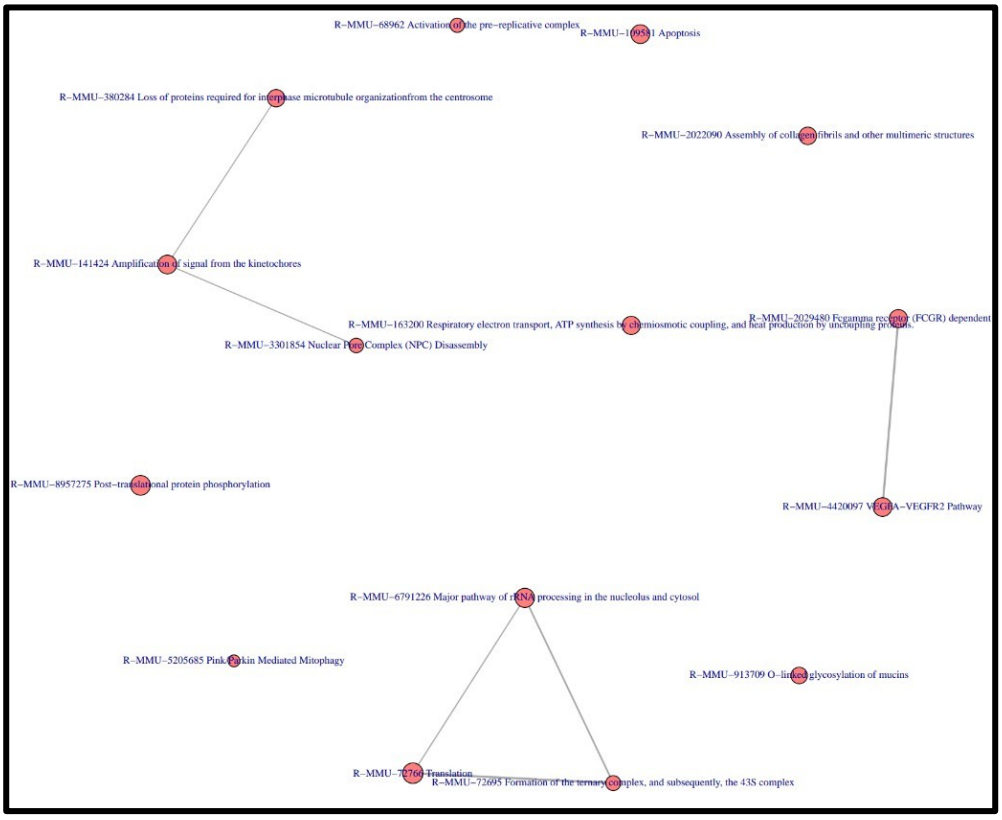


Figure 5.3.8 GSEA reactome network plot of top-level pathways enriched in the orthotopic AKPT tumour versus the subcutaneous setting after TGF-β inhibition.

Red node colour represents an adjusted p value of 0.05, size of node represents level of enrichment. Redundant gene sets trimmed to plot top-level pathways, defined by having the largest amount of crossover with other pathways. Figure constructed by Gabriel Valbuena.

Comparing orthotopic with heterotopic AKPT tumours demonstrated a large number of enriched pathways in rectal tumours were found after treatment with radiation combined with TGF-β inhibition. Notably, a network of pathways linked to VEGF and phagocytic pathways were significantly enriched (Figure 5.3.9). Additionally, pathways linked to the immunoregulatory interactions between lymphoid and non-lymphoid immune cells are significantly enriched (Figure 5.3.9). A network of enriched pathways involved with cell mitosis, including SUMO pathway that is involved in regulating the stability of mitotic proteins (Figure 5.3.9).

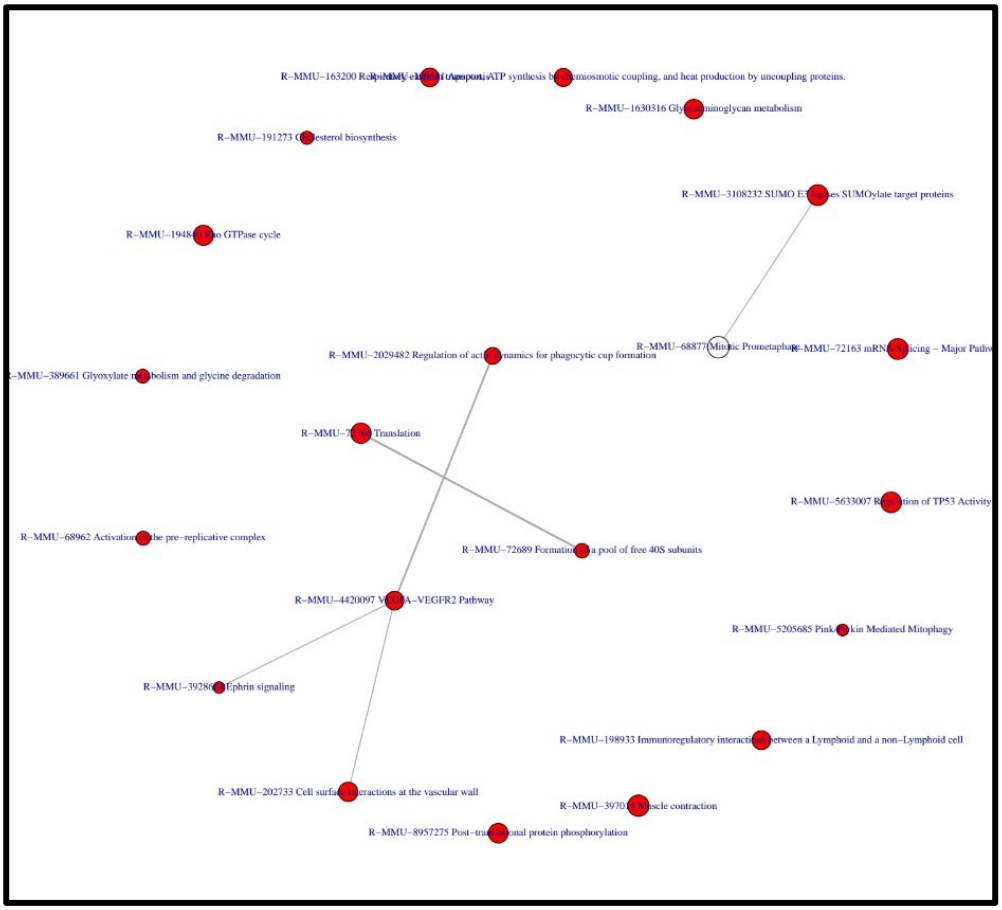


Figure 5.3.9 GSEA reactome network plot of top-level pathways enriched in the orthotopic AKPT tumour versus the subcutaneous setting after irradiation and TGF-β inhibition.

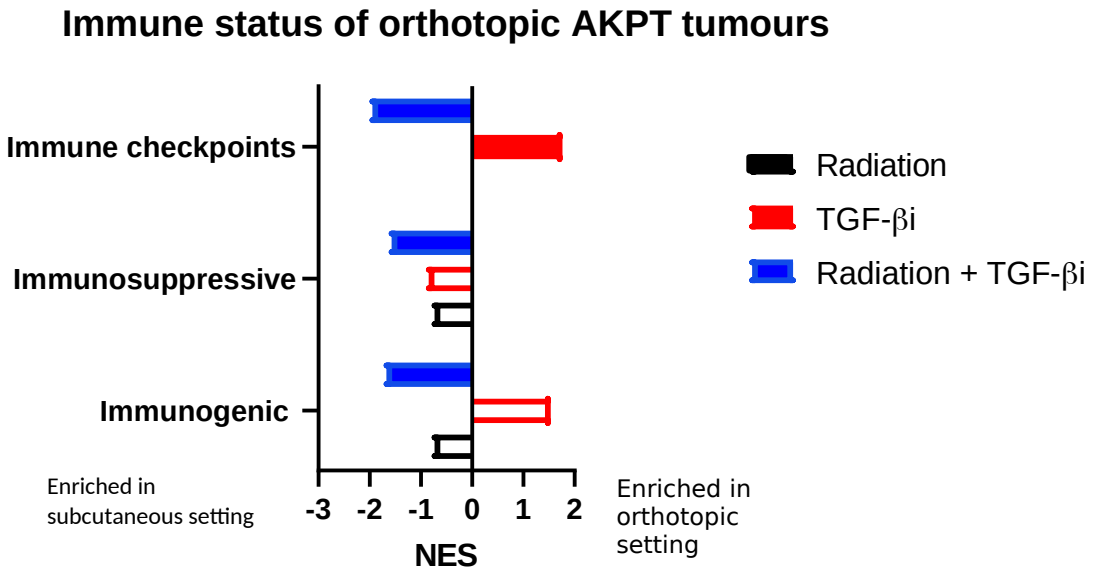
Red node colour represents an adjusted p value of 0.05, size of node represents level of enrichment. Redundant gene sets trimmed to plot top-level pathways, defined by having the largest amount of crossover with other pathways. Figure constructed by Gabriel Valbuena.

After investigating the enriched pathways between the heterotopic and orthotopic AKPT tumours we then used the literature to establish gene lists to further interrogate how different treatments induced differing immunogenic responses against the AKPT tumours. This was carried out using the same methodology as employed in chapter 5.2.3. Therefore, we initially investigated the changes to the overall immune landscape in AKPT tumours forming from differing implantation sites, after receiving identical treatment.

When comparing the impact of tumour site on the enrichment of genes relating the overall immune setting of the AKPT tumour we saw differences

between the heterotopic and orthotopic model. After irradiation, we failed to see any significant changes in

enrichment (Figure 5.3.10). However, the modest effects suggested that while there was a slightly more immune checkpoint gene expression in the orthotopic model, the immunosuppressive and immunogenic signatures seemed to be moderately increased in the heterotopic model (Figure 5.3.10). Comparing the different tumour locations after receiving TGF-β inhibition did demonstrate some significant differences, however. Specifically, there was a significant increase in the expression of immune checkpoint genes in the orthotopic model when compared to the heterotopic tumour (Figure 5.3.10). Interestingly, comparing heterotopic tumours and orthotopic tumours receiving the combination treatment, there was a significant increase in gene expression in the heterotopic model for the immunogenic, immunosuppressive, and immune checkpoint



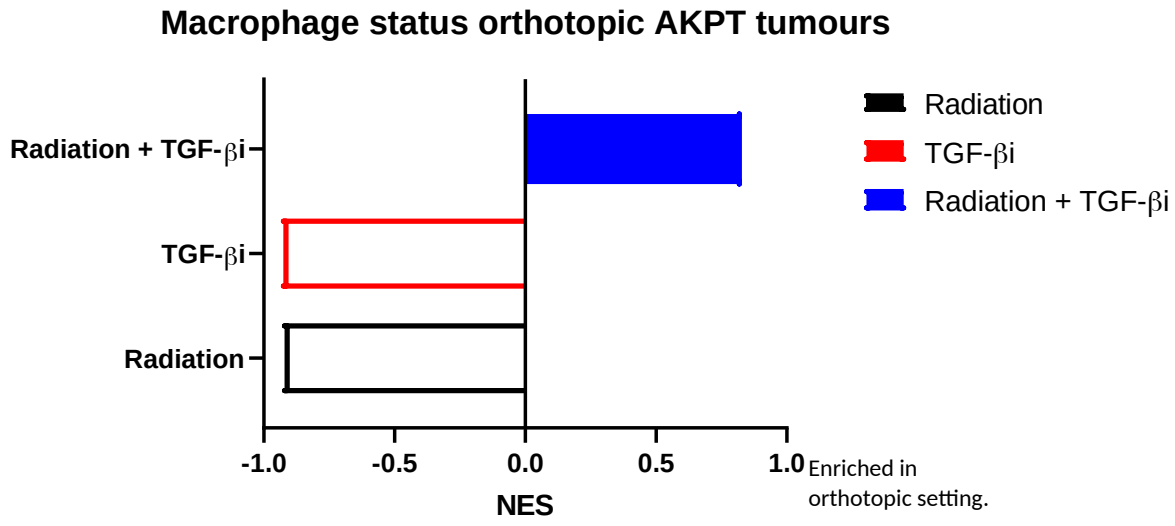
signatures (Figure 5.3.10).

Figure 5.3.10 Immunogenic, immunosuppressive, and immune checkpoint gene signature enrichment comparison between subcutaneous and orthotopic AKPT tumours.

The enrichment of selected gene signatures defining immunogenicity, immunosuppression, and immune checkpoints comparing heterotopic and orthotopic tumours after receiving equivalent treatment. Filled bars

represent a pFDR $\leq$ 0.1. NES = Normalised Enrichment Score. Data analysed by Gabriel Valbuena.

When comparing the enrichment of genes specific to M1-like macrophages, only one of the treatment groups demonstrated a significant change. When treating AKPT tumours with radiation and TGF-β inhibition, we found that the orthotopic model possessed a significantly higher expression of genes specific to the immunogenic macrophage phenotype (Figure 5.3.11). Interestingly, this enrichment pattern was reversed in tumours receiving radiation or TGF-β inhibition alone, with a modest



enrichment found in the heterotopic model (Figure 5.3.11).

Figure 5.3.11 M1-like macrophage gene list enrichment comparison in treated subcutaneous and orthotopic AKPT tumours.

The enrichment of selected gene signatures defining M1-like macrophages comparing heterotopic and orthotopic tumours after receiving equivalent treatment. Filled bars represent a pFDR ≤ 0.1. NES = Normalised Enrichment Score. Data analysed by Gabriel Valbuena.

We then examined the changes in the CAF phenotype depending on the AKPT tumour location. When examining the iCAF population, we saw that radiation in combination with TGF-β inhibition showed a modest amount of enrichment of the defining genes in the orthotopic model (Figure 5.3.12). However, this modest effect was inverted in tumours receiving radiation or TGF-β inhibition in isolation, with a moderate enrichment toward the heterotopic model being observed (Figure 5.3.12). In the myCAF population we saw similarly modest changes to gene enrichment, with radiation and TGF-β in isolation demonstrating moderate enrichment toward the orthotopic model, with the combination treatment showing the same but toward the heterotopic model (Figure 5.4.12). The

vCAF population showed modest, nonsignificant differences between the two tumour models. TGF-β inhibition, with or without radiation, showed a moderate increase in the vCAF population, whereas radiation alone showed modest enrichment toward the heterotopic model. The prCAF population demonstrated some significant differences depending on the AKPT tumour site of implantation. Radiation showed a small enrichment toward the heterotopic model whereas TGF-β alone demonstrated a significant and large enrichment in the orthotopic model (Figure 5.3.12). When tumours were treated with a combination of radiation and TGF-β inhibition, prCAF genes were significantly enriched toward the heterotopic model (Figure 5.3.12). Finally, the ilCAF phenotype demonstrated some modest, nonsignificant differences. Radiation, with or without TGF-β inhibition, showed a modest enrichment of ilCAF genes toward the heterotopic model, whereas treatment with TGF-β inhibitor alone demonstrated a modest enrichment toward the orthotopic model (Figure 5.3.12).

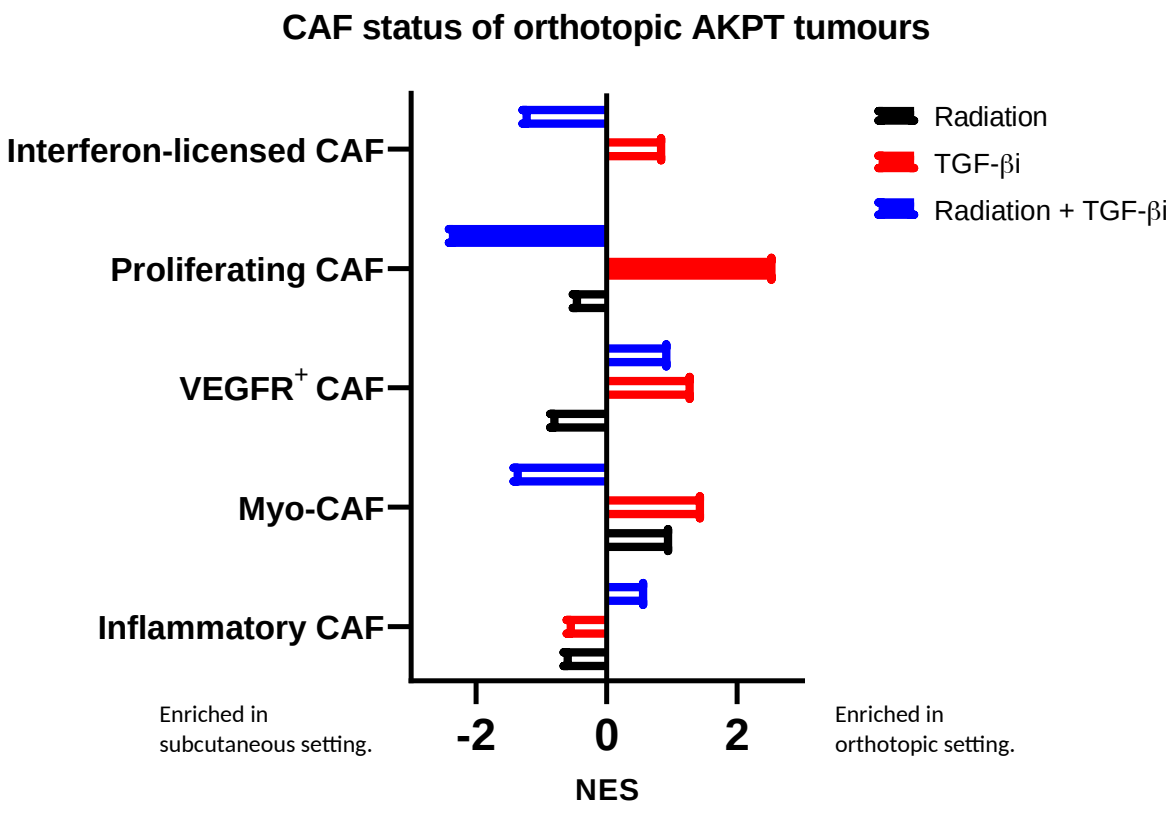


Figure 5.3.12 CAF genetic phenotype enrichment comparison in treated subcutaneous or orthotopic AKPT tumours.

The enrichment of selected gene signatures defining CAF phenotypes comparing heterotopic and orthotopic

tumours after receiving equivalent treatment. Filled bars represent a pFDR $\leq$ 0.1. NES = Normalised Enrichment Score. Data analysed by Gabriel Valbuena.

5.4 Discussion

We demonstrated that the addition of TGF-β inhibition was able to improve the anti-tumour effect of radiation when treating heterotopic AKPT tumours (Figure 5.2.1-2). In the heterotopic model, by implementing multiplex staining, we observed significant modulation of the immune response post irradiation when TGF-β was inhibited (Figure 5.2.3-5). This is critical due to the AKPT model lacking TGFβR1, meaning any functional effects the inhibitor had on improving tumour response to radiation occurred within the surrounding milieu.

In the heterotopic model we demonstrated a significant increase in the number of cytotoxic T-cells as a whole as well as within the tumour epithelium (Figure 5.2.3). The concept of TGF-β inhibition increasing the number of, and effector function, of cytotoxic T-cells is increasingly being understood within the literature (W. Chen, 2023; Gunderson et al., 2020; Tauriello et al., 2018). Interestingly, we found that TGF-β inhibition alone was unable to generate a significantly increased cytotoxic T-cell response, with radiation being required for this (Figure 5.2.3). This suggests that, at least within the AKPT model, a method of cytotoxic T-cell recruitment is required in tandem with TGF-β inhibition to generate a lasting anti-tumour effect. Interestingly, we also demonstrate that as well as enhancing the immunogenic $CD8^+$ offensive against the tumour when radiation is combined with TGF-β, the immunosuppressive Treg defensive is simultaneously compromised (Figure 5.2.4).

The role of the Treg population is well described in the literature as increasing post irradiation (Liu et al., 2015), something we also demonstrate in the AKPT heterotopic model (Figure 5.2.4). We also demonstrated that the inhibition of TGF-β causes a significant reduction in the Treg population, even when combined with irradiation. This is in accordance with the literature surrounding Treg biology, with TGF-β playing a critical role in the differentiation of $CD4^+$ cells to this immunosuppressive $FOXP3^+$ population (Fantini et al., 2004; Strainic et al., 2013; Wang et al., 2023; Windhagen et al., 1995). The importance of our demonstration of a reduction in the Treg population both as a whole

and within the epithelium (Figure 5.2.4), through the combination TGF-β and irradiation, also has potential clinical applications, with Treg epithelial infiltration being strongly associated with poor patient outcomes (Aristin Revilla et al., 2022).

Interestingly, with the Treg population being formed, in part, due to the differentiation of $CD4^+$ T-cells through TGF-β signalling (Fantini et al., 2004; Strainic et al., 2013; Wang et al., 2023; Windhagen et al., 1995), we also demonstrated that the combination treatment caused a significant increase in the T-helper cell population (Figure 5.2.5). Though we saw an increase in the overall $CD4^+$ $FOXP3^-$ T-cell population through the combination of radiation and TGF-β inhibition, to more fully understand the impact this has on the tumour itself would require further investigation. With the complexity of $CD4^+$ T-cell lineage and subpopulations becoming an increasing area of focus due to their varying roles regarding tumour immunity (Al-Mterin et al., 2022; DiToro & Basu, 2021; Zheng et al., 2023), further investigation into this immune cell subset may prove fruitful.

Through the treatment of the AKPT tumours, we also demonstrated a significant change to the neutrophil population depending on the treatment administered (Figure 5.2.6). We showed that after irradiation there was a sustained influx of neutrophils to the tumour site, whereas when radiation was combined with TGF-β inhibition this increase only occurred acutely (within 24 hours) and was reverted by 3 days (Figure 5.2.6). It is well established that TGF-β is a potent chemoattractant for neutrophils and inhibits anti-tumour effects from these innate immune cells (Reibman et al., 1991; Shen et al., 2007). Interestingly, TGF-β-mediated neutrophil infiltration has also been linked to driving metastasis in colorectal cancer models *in vivo* (Jackstadt et al., 2019).

When examining the macrophage population, we saw no significant changes in the population size between the different treatment options (Figure 5.2.5). However, when examining the specific macrophage phenotype, we demonstrated that the combination of radiation with TGF-β inhibition was able to enrich genes defining the inflammatory M1- like phenotype (Figure 5.2.11). This skewing of the macrophage

population toward a more inflammatory phenotype could act as the removal of another line of tumour defence against the immunogenic response mounted after irradiation, akin to the shift in the Treg population (Figure 5.2.4). Interestingly, though not statistically significant, we saw a shift in the macrophage population away from the M1-like phenotype in the other two treatment groups. This shift after irradiation this has been described in the literature (Beach et al., 2022; Becherini et al., 2023; Wu et al., 2017). However, we demonstrated that inhibiting TGF-β also skewed the macrophage population away from the M1-like phenotype, contradicting literature describing TGF-β playing a critical role in reducing the inflammatory macrophage population (Bose et al., 2019; Zhang et al., 2016). Therefore, with the polarisation state of macrophages becoming increasingly acknowledged as a spectrum within the literature (Opzoomer et al., 2021; Xue et al., 2014), a specific investigation into the specific phenotypic changes of the macrophages within the AKPT model after treatment may prove enlightening.

Through the interrogation of the sequencing data after isolating RNA from treated AKPT tumours, we demonstrate that the addition of TGF-β inhibition to irradiation has a profound impact on the immune landscape within the TME (Figure 5.2.10). In accordance with the multiplex staining data (Figures 5.2.3-5.2.7), we demonstrate a modest enrichment of genes associated with an immunogenic response when comparing radiation alone with radiation combined with TGF-β inhibition (Figure 5.2.10). This increase in immunogenicity when examining gene enrichment provides orthogonal confirmation of the increase in the mounting of both an adaptive and innate immune response against the tumour post combination treatment. Additionally, we demonstrate that genes associated with an immunosuppressive setting within the TME were more highly enriched in tumours having only received radiation rather than the combination treatment (Figure 5.2.10). This also aligns with our findings thus far staining treated tumours, with this decrease in immunosuppressive gene enrichment in combination treated AKPT tumours corroborating the decrease in the Treg population (Figure 5.2.4) as well as shift to a more inflammatory macrophage phenotype (Figure 5.2.7). Interestingly, we also saw a significant decrease in genes encoding for immune checkpoints when radiation was combined with TGF-β inhibition (Figure 5.2.10). This effect has been

indirectly confirmed by the literature with the inhibition of TGF-β causing a significant change to the fibroblast population within the tumour's stroma (Zhao et al., 2018). These fibroblasts have been described to facilitate the matrix metalloproteinase-9 cleavage of PD-L1 cell surface expression (Aguirre et al., 2019; Zhao et al., 2018).

In accordance with the previous literature (Aguirre et al., 2019; Zhao et al., 2018), we demonstrated that the use of TGF-β inhibition, with or without radiation, had a profound impact on the CAF populations within the stroma of heterotopic AKPT tumours (Figure 5.2.6 and Figure 5.2.12). We demonstrated that the inhibition of TGF-β causes a decrease in the α-SMA^{+} population of fibroblasts within the tumour stroma (Figure 5.2.6). Additionally, radiation significantly decreased the PDGFRα^{+} population within the stroma with or without TGF-β inhibition (Figure 5.2.6). Therefore, we interrogated the sequenced RNA extracted from treated AKPT tumours. To do this we implemented the CAF stratification system established by (Grauel et al., 2020), to further investigate the phenotypic changes of the fibroblasts.

In accordance with published findings (Grauel et al., 2020), we found that the inhibition of TGF-β, with or without irradiation, led to a marked decrease in iCAF gene enrichment whilst promoting enrichment of ilCAFs (Figure 5.2.12). This finding suggests that in AKPT tumours treated with a combination of radiation and TGF-β inhibition, the ilCAF population may play a role in orchestrating the revitalised immunogenic response against the cancer cells.

Perhaps unsurprisingly, we also demonstrate that radiation, with or without TGF- β inhibition, has a significant impact on the prCAF population (Figure 5.2.12). This is likely due to the sensitivity of cells undergoing the cell cycle (Pawlik & Keyomarsi, 2004). However, whether the prCAFs experience cell death or undergo differentiation toward one of the other CAF phenotypes is something that requires further exploration. Finally, we also demonstrate that in the heterotopic AKPT model, the addition of TGF-β inhibition to irradiation caused a significant decrease in gene enrichment for the vCAF population (Figure 5.2.12).VEGF is known to act as a marker for poor prognosis in colorectal cancer

(Baker et al., 2019), due to its ability to foster radioprotection of the tumour (Kanthou & Tozer, 2019).With VEGF being implicated with radioprotection through its ability to nurture improved tumour vasculature, investigating the blood supply of tumours post combination treatment may provide further insight into how TGF-β inhibition improves the anti-tumour effect of radiation.

We investigated whether implantation subcutaneously or submucosally into the rectum impacts the response of AKPT tumours and demonstrated that, prior to treatment, the orthotopic tumour had significantly different immune cell populations (Figure 5.3.2- 5). We demonstrated that the T-cell population, specifically T-helper and Treg cells, were greater in the orthotopic tumours when compared to AKPT organoids growing subcutaneously (Figure 5.3.2-3). Within the tumour epithelium of the orthotopic model, there was a significant increase in Treg infiltration in comparison to the subcutaneous setting (Figure 5.3.2). This increase is potentially borne out of necessity due to the colorectal environment containing tissue-resident memory T-cells (Trm) (Lin et al., 2023). Additionally, Trm cells predominantly express cytotoxic activation and are a positive survival marker in patients with colorectal cancer (Kitakaze et al., 2023). Therefore, the formation of the orthotopic tumour after implantation submucosally may require the recruitment of Treg cells to escape resident immune surveillance. Additionally, a significantly larger macrophage population was observed in the untreated orthotopic AKPT tumour (Figure 5.3.5). With a large pool of resident macrophages to recruit from, there is possibility macrophages are recruited and subsequently differentiated toward a more immunosuppressive phenotype to overcome the innate immune surveillance of the rectum. Future research implementing knock-out mouse models lacking macrophages or Treg cells may assist in ascertaining the necessity of these immune cells to the growth of the orthotopic AKPT tumour.

After irradiation, we see a more significant increase in the recruitment of immune cells in the orthotopic model when compared to the subcutaneous setting. Most notably, we see a significantly larger increase in Treg cell recruitment in the orthotopic model when compared to the subcutaneous setting (Figure 5.3.2). The Treg population is well

described in the literature to be able to form from the differentiation of $CD4^+$ T-cells following TGF-β signalling (Wang et al., 2023). With a larger initial population of $CD4^+$ T-cells present prior to treatment, this improvement to Treg recruitment may be caused by the increased differentiation pool available with their existing a larger T-helper cell component (Figure 5.3.3). The larger population of macrophages present may also play a role in this increase in immune cell response to irradiation. Specifically, we demonstrated a significantly higher rate of neutrophil recruitment in the orthotopic model versus tumours grown subcutaneously. Macrophages are described in the literature to be adept in recruiting neutrophils through IL-8 signalling, especially in the gut (Prame Kumar et al., 2018).

When comparing the changes in the immune cell landscape between subcutaneous and orthotopic tumours, we demonstrated only the recruitment of cytotoxic T-cells were significantly different (Figure 5.3.1). We hypothesise that after irradiation combined with TGF-β inhibition recruitment of $CD8^+$ T-cells occurs from two pools in the orthotopic model: from circulation and from the rectal tissue itself. After irradiation we demonstrated a slight increase in $CD8^+$ T-cells but this is potentially blunted by the presence of a large fraction of immunosuppressive cells within the tumour milieu. However, through the addition of TGF-β inhibition, the tumour is less able to evade immune detection so both circulating and Trm $CD8^+$ cells can act to exert a cytolytic on the growing tumour. With Trm $CD8^+$ T-cells within the gut expressing CD103, investigating tumours for $CD8^+/CD103^+$ co-staining would allow us to unpick the source of cytotoxic T-cells recruited to the tumour post treatment.

Interestingly, when we investigated the immunogenic landscape of subcutaneous and orthotopic tumours after treatment using extracted RNA we demonstrated some significant differences to the previous results. When TGF-β was inhibited in isolation, we observed a modest enrichment of genes defining an immunogenic response in the orthotopic model as well as genes defining immune checkpoint molecules (Figure

5.3.10). However, the combination treatment of radiation and TGF-β inhibition showed a significant enrichment of immunogenic, immunosuppressive, and immune checkpoint genes in the subcutaneous setting (Figure 5.3.10). A potential explanation for this is the lack of spatial information gained from the RNA sequencing analysis. For example, in the subcutaneous tumours, the peri-tumour regions typically contained a large number of lymphocytes that failed to enter the tumour itself or the stroma (Appendix figure) but this peri-tumour tissue forms part of the material analysed for the RNA-Seq data. Typically, this is not the case for orthotopic tumours, which sit within non-diseased rectal tissue. Consequently, data contributed from the peri-tumour regions in subcutaneous tumours has the potential to mask significant changes in gene expression occurring within the tumour, in particular where the number of immune cells within the tumour is relatively small. To examine and potentially overcome this, future work could take a combinational approach of single-cell RNA sequencing and spatial transcriptomics to account for confounding spatial effects.

Interestingly, the combination of radiation with TGF-β inhibition demonstrated a significant enrichment of inflammatory macrophage-specific genes in the orthotopic model when compared to subcutaneous tumours. We have demonstrated this effect occurring in the subcutaneous model (Figure 5.2.11), therefore this is potentially a result of the larger macrophage population present in the orthotopic setting (Figure 5.3.5).

Comparing the CAF population between subcutaneous and orthotopic tumours, we demonstrated that the trend of α-SMA expression decreased in the same pattern between models, after the incorporation of TGF-β inhibition, and PDGFRα expression was increased in a similar fashion also, increase after TGF-β was inhibited (Figure 5.3.6). Interestingly, when investigating the CAF phenotypic changes post treatment, we demonstrated a large degree of similarity between the tumour models (Figure 5.3.12). Both the iCAF and vCAF phenotype demonstrated small, non-significant enrichments. Interestingly, we saw a significant difference in the prCAF population depending on the tumour model. With TGF-β inhibition treatment, we demonstrate that within the rectal environment has a significantly larger enrichment of prCAF defining genes (Figure

5.3.12). This may be linked to the significant difference of PDGFRα expression between the two tumour models after treatment with TGF-β inhibition (Figure 5.3.6).

Chapter 6

Summary and conclusions

6.1 Aims of the thesis.

A major aim of this thesis was to identify novel neoadjuvant targets to enhance the anti-tumour effect of radiation. In chapter 3 we identified, through the irradiation of the AKPT rectal cancer model, two promising targets in C5aR1 and TGF-β, and demonstrated that both these targets were upregulated after irradiation of AKPT tumours.

When investigating these targets, C5aR1 inhibition increased the effectiveness of radiation both *in vitro* and *in vivo* in the heterotopic tumour model. Inhibiting C5aR1 *in* vitro using AKPT organoids suggested a direct effect on tumour cell radiosensitivity. This mechanism has been further explored and a working model is established in our recent publication (Beach et al., 2023). Interestingly, we demonstrated that bolstering radiation through C5aR1 inhibition occurred in the absence of T-cells in the athymic nude model. Furthermore, we suggest that additional effects on both the macrophage and CAF population could contribute to the augmentation of radiation anti-tumour efficacy when C5aR1 is inhibited. Interestingly, the modest radiosensitisation observed *in vitro* suggests that, in the *in vivo* AKPT model, other mechanisms such as the alteration of the macrophage and CAF population may be of greater importance than increased intrinsic radiosensitivity.

Exploration of TGF-β demonstrated that the inhibition of this multifunctional cytokine increased the effectiveness of radiation *in vivo* in the AKPT heterotopic model of

rectal cancer. We also demonstrated that the inhibition of TGF-β, combined with irradiation, had a marked impact on both immune and other stromal cell types within the tumour milieu. Changes to the immune cell population when TGF-β inhibition was combined with irradiation included: an increase to the cytotoxic T-cell population with the ability to infiltrate the tumour epithelium; a decrease in the Treg population; a prevention of chronic increase in the neutrophil population and a change to the macrophage population, causing a skew toward the inflammatory phenotype. These changes to the immune cell populations were reflected by enrichment of immunogenic gene signatures and a corresponding negative enrichment in the immunosuppressive signatures. Within the stroma, we also observed significant changes to the CAF populations including increases in CAF phenotypes directly linked to immunogenic action against the tumour, suggesting that fibroblasts within the stroma can act to orchestrate a sustained immune response to tumours when TGF-β is inhibited alongside irradiation.

6.2 Further avenues for investigation.

The AKPT model of rectal cancer recapitulates important features linked to poor radiotherapy response in patients and is a highly relevant model for future investigation into the mechanisms underpinning C5aR1 inhibition combined with irradiation, Critically, the most important mechanisms behind the increased radiosensitivity after inhibiting C5aR1 *in vitro* and *in vivo* remain unclear. *In vitro*, further RNAseq analysis of irradiated organoids would potentially improve the understanding of the mechanisms behind the increased radiosensitisation when C5aR1 is inhibited. Additionally, a comparison in the AKPT models of C5aR1 inhibition and other approaches under clinical investigation as novel radiosensitisers, e.g. inhibitors of proteins involved in the DNA damage responses such as ataxia telangiectasia mutated (ATM), poly (ADP-ribose) polymerase (PARP), and DNA-dependent protein kinase (DNAPK), would provide insights into the importance of increased intrinsic radiosensitivity in combination with

the potentially broader tumour cell-specific effects of complement inhibition toward improving radiation response.

Though we have demonstrated the radiosensitising effects of C5aR1 inhibition in another immune-competent model of colorectal cancer, through the implantation of the colorectal cancer cell line MC38 (Beach et al., 2023), exploring the impact of inhibiting the complement system in combination with radiation in other, more clinically relevant, mouse models is warranted. For example, future models could include *Kras*$^{G12D/+}$, *Trp53*$^{fl/fl}$, *Rosa26*$^{N1icd/+}$ (KPN) organoids. This organoid model, defined by increased NOTCH signalling recapitulates an additional subset of colorectal tumours with poor prognosis, with extensive stromal infiltration and serrated tumour formation (Jackstadt et al., 2019).

When considering future work on TGF-β inhibition, further investigation into the differences between the orthotopic and subcutaneous models is warranted. Specifically, the efficacy of combining TGF-β inhibition and radiation in the orthotopic model fell outside of the scope for this thesis. For future exploration of drug-radiation combinations, careful evaluation of the differences between the two models could provide a rationale for evaluating targets and testing compounds first in the simpler heterotopic model before evaluating in the more complex orthotopic model. Additionally, in the AKPT model, experiments presented in this thesis demonstrated that augmenting radiation, with TGF-β inhibition, significantly improves tumour control. However, a proportion of the mouse cohort receiving the combination treatment only experience a temporary arrest to tumour growth. Therefore, there may be room to further improve the efficacy of this doublet therapy, with aims to fully eradicate the tumour or permanently arrest its growth. This suggests that more efficacious radiation doses/schedules may need to be identified, and/or that more effective/prolonged stimulation of the immune responses is required, possibly by combining TGF-β/ C5aR1 with other immune-oncology approaches.

Appendices

Appendix A

Published papers

1) **Reprinted with permission from the Journal of Clinical Investigation. Beach, C.,** MacLean, D., Majorova, D., Melemenidis, S., Nambiar, D. K., Kim, R. K., Valbuena, G. N., Guglietta, S., Krieg, C., Darvish-Damavandi, M., Suwa, T., Easton, A., Hillson, L. V. S., McCulloch, A. K., McMahon, R. K., Pennel, K., Edwards, J., O'Cathail, S. M., Roxburgh, C. S., … Olcina, M. M. (2023). Improving radiotherapy in immunosuppressive microenvironments by targeting complement receptor C5aR1. *The Journal of Clinical Investigation*, *133*(23). https://doi.org/10.1172/JCI168277 [1]

2) **Beach, C.,** Mulholland, E., Belnoue-Davis, H., Valbuena, G., Molino, M. O. del, Maughan, T., & Leedham, S. (2022). O40 Impact of TGFβ inhibition and radiotherapy in a heterotopic rectal cancer mouse model. *Gut*,*71*(Suppl1),A24–A24. https://doi.org/10.1136/gutjnl-2022-BSG.40[2]

3) **Beach, C.,** MacLean, D., Majorova, D., Arnold, J. N., & Olcina, M. M. (2022). The effects of radiation therapy on the macrophage response in cancer. *Frontiers in Oncology*, *12*. https://doi.org/10.3389/fonc.2022.1020606

[1] Most of data used in Chapter 3 and 4.

[2] Some data used in Chapter 5

JCI The Journal of Clinical Investigation

Improving radiotherapy in immunosuppressive microenvironments by targeting complement receptor C5aR1

Callum Beach, … , Amato J. Giaccia, Monica M. Olcina

J Clin Invest. 2023;133(23):e168277. https://doi.org/10.1172/JCI168277.

Research Article | Cell biology | Oncology

An immunosuppressive microenvironment causes poor tumor T cell infiltration and is associated with reduced patient overall survival in colorectal cancer. How to improve treatment responses in these tumors is still a challenge. Using an integrated screening approach to identify cancer-specific vulnerabilities, we identified complement receptor C5aR1 as a druggable target, which when inhibited
improved radiotherapy, even in tumors displaying immunosuppressive features
+
and poor CD8 T cell infiltration. While C5aR1 is well-known for its role in the immune compartment, we found that C5aR1 is also robustly expressed on malignant epithelial cells, highlighting potential tumor cell–specific functions. C5aR1 targeting resulted in increased NF-κB–dependent apoptosis specifically in tumors and not normal tissues, indicating that, in malignant cells, C5aR1 primarily regulated cell fate. Collectively, these data revealed that increased complement gene expression is part of the stress response mounted by irradiated tumors and that targeting C5aR1 could improve radiotherapy, even in tumors displaying
immunosuppressive features.

Improving radiotherapy in immunosuppressive microenvironments by targeting complement receptor C5aR1

Callum Beach,[1] David MacLean,[1] Dominika Majorova,[1] Stavros Melemenidis,[2] Dhanya K. Nambiar,[2] Ryan K. Kim,[2] Gabriel N. Valbuena,[3] Silvia Guglietta,[4,5] Carsten Krieg,[5,6] Mahnaz Darvish-Damavandi,[7] Tatsuya Suwa,[1] Alistair Easton,[1] Lily V.S. Hillson,[8] Ashley K. McCulloch,[8] Ross K. McMahon,[8] Kathryn Pennel,[8] Joanne Edwards,[8] Sean M. O'Cathail,[8] Campbell S. Roxburgh,[8] Enric Domingo,[1] Eui Jung Moon,[1,2] Dadi Jiang,[9] Yanyan Jiang,[1] Qingyang Zhang,[1] Albert C. Koong,[9] Trent M. Woodruff,[10] Edward E. Graves,[2] Tim Maughan,[1] Simon J.A. Buczacki,[7] Manuel Stucki,[11] Quynh-Thu Le,[2]

Simon J. Leedham,[3] Amato J. Giaccia,[1,2] and Monica M. Olcina[1,2,11]

[1]Department of Oncology, University of Oxford, Oxford, United Kingdom. [2]Department of Radiation Oncology, Stanford University, Stanford, California, USA.

[3]Wellcome Centre for Human Genetics, University of Oxford, Oxford, United Kingdom. [4]Department of Regenerative Medicine and Cell Biology, [5]Hollings

Cancer Center, and [6]Department of Pathology and Laboratory Medicine, Medical University of South

Carolina, Charleston, South Carolina, USA. [7]Nuffield Department of Surgical Sciences, University of Oxford, Oxford, United Kingdom. [8]School of Cancer Sciences, University of Glasgow, Glasgow, United Kingdom. [9]The University of Texas MD Anderson Cancer Center, Houston, Texas, USA. [10]School of Biomedical Sciences, Faculty of Medicine, The University of Queensland, Brisbane, Queensland, Australia.

[11]Department of Gynecology, University of Zurich, Schlieren, Switzerland.

An immunosuppressive microenvironment causes poor tumor T cell infiltration and is associated with reduced patient overall survival in colorectal cancer. How to improve treatment responses in these tumors is still a challenge. Using an integrated screening approach to identify cancer-specific vulnerabilities, we identified complement receptor C5aR1 as a druggable target, which when inhibited improved radiotherapy, even in tumors displaying immunosuppressive features and poor $CD8^+$ T cell infiltration. While C5aR1 is well-known for its role in the immune compartment, we found that C5aR1 is also robustly expressed on malignant epithelial cells, highlighting

potential tumor cell–specific functions. C5aR1 targeting resulted in increased NF-κB–dependent apoptosis specifically in tumors and not normal tissues, indicating that, in malignant cells, C5aR1 primarily regulated cell fate. Collectively, these data revealed that increased complement gene expression is part of the stress response mounted by irradiated tumors and that targeting C5aR1 could improve radiotherapy, even in tumors displaying immunosuppressive features.

Introduction

The composition of the tumor microenvironment (TME) affects treatment responses in cancer (1–3). Immunosuppressive TME features, which act as a barrier to extensive $CD8^+$ T cell infiltration typically characterize immune cold tumors, which are associated with poor prognosis (4–6). Indeed, low density of total T lymphocytes ($CD3^+$) at the center or invasive margins of tumors is associated with reduced overall survival in colorectal cancer (CRC)
(5). Improving treatment responses for those patients with poor tumor lymphocyte infiltration remains a challenge.

Approximately one-third of all CRCs arise in the rectum. Locally advanced rectal cancers are typically treated with neoadjuvant chemoradiotherapy (nCRT) prior to surgery. Unfortu-

Authorship note: CB, D MacLean, and D Majorova are co–first authors.

Conflict of interest: TMW has consulted previously with Alsonex Pty Ltd., which is commercially developing PMX205.

Copyright: © 2023, Beach et al. This is an open access article published under the terms of the Creative Commons Attribution 4.0 International License.

Submitted: January 11, 2023; **Accepted:** October 5, 2023; **Published:** December 1, 2023.

Reference information: *J Clin Invest*. 2023;133(23):e168277. https://doi.org/10.1172/JCI168277.

nately, despite nCRT leading to complete pathological response in 15%–20% of these patients, 75%–80% will fail to achieve complete responses (7, 8). There is therefore a need to further improve responses in a significant portion of patients receiving nCRT (9–11). Identifying targets that modulate radiosensitivity, particularly in tumors displaying immunosuppressive features, could improve treatment outcomes for the most resistant tumors.

High expression of complement system components is part of the inflammatory environment of colon and rectal tumors displaying the worst survival outcomes (4, 12–14). The complement system is an ancient component of innate immunity, and both canonical and noncanonical functions are increasingly being recognized as important for infection control, autoimmunity, and cancer (15–19). In the context of cancer treatment, complement proteins can be expressed and may function independently of their role in the

inflammatory environment; however, this remains to be fully understood.

In this study, we found that, in murine models that recapitulate an immunosuppressive TME, the complement system was the first immune response pathway to be upregulated at early time points following irradiation (RT). Importantly, an enrichment in complement signatures following CRT was also observed in longitudinal biopsies from patients with rectal adenocarcinoma. Through an integrated screening approach, we identified complement receptor C5aR1 as a druggable target, which inhibited radiation-induced cell death/apoptosis through regulation of tumor cell fate. Interestingly, these effects were not observed in untransformed intestinal organoids or normal intestinal tissues in vivo. Consequently, targeting C5aR1 with a clinical grade and orally active C5aR1 antagonist, PMX205, resulted in improved tumor radiation responses in vivo. Importantly, PMX205 improved response in several murine models, including those displaying high radiation-induced complement expression and immunosuppressive features associated with $CD8^+$ T cell exclusion.

Results

Identification of radiation-responsive targets in immunosuppressive tumors. When grown subcutaneously, tumor organoids originally derived from *villin*Cre^{ER}; *Apc*$^{fl/fl}$; *Kras*$^{G12D/+}$; *Trp53*$^{fl/fl}$ *TgfbrI*$^{fl/fl}$ (AKPT) mice displayed TME features resembling those of CRC samples from patients that typically have poor outcomes (Figure 1, A–C). These features include stromal-rich regions with high numbers of fibroblasts and macrophages but relatively few $CD8^+$ T cells (Figure 1, A–C). Interestingly, we found that although RT was able to moderately enhance infiltration of Tregs, macrophages, neutrophils, and $CD4^+$ and $CD8^+$ T cells into these tumors, such infiltration was limited to stromal regions and did not increase numbers of intraepithelial immune cells (Figure 1, A–C, and Supplemental Figure 1, A–G; supplemental material available online with this article; https://doi.org/10.1172/JCI168277DS1). To identify radiation- responsive pathways in the immunosuppressive microenvironment of these tumors, we performed RNA-Seq analysis. Network analysis of differentially expressed pathways following RT indicated that the complement cascade was significantly upregulated and, in fact, was the top-ranked pathway, annotated as an “immune system pathway,” in Reactome at early time points after RT (Figure 1, D and E; Supplemental Figure 1H; and Supplemental Table 1). Examples of members across all the main complement functional categories were induced following RT, with most individual genes showing transient enhanced expression (Supplemental Figure 1, I–M). Analysis of enriched pathways in rectal adenocarcinoma biopsies taken at baseline, 2, 6, or 12 weeks during/following nCRT indicated that complement system genes were also significantly upregulated (compared with baseline, Figure 1F and Supplemental Figure 1N). As an example, analysis of the top 50 enriched pathways at week 6 (compared with baseline) indicated that the complement hallmark pathway was ranked fourth. Overall, these data indicate that complement gene expression was induced following RT in both a murine tumor model of an immunosuppressive TME and in patients with rectal cancer undergoing nCRT.

C5aR1 is a radiation-responsive druggable target. To identify potential targets within the complement cascade that could be therapeutically inhibited, we queried the CanSAR database (https://cansar.ai/; ref. 20). A gene was only considered a hit if it was "druggable" based on structural and ligand-based assessment (Figure 2A and Supplemental Table 2, as shown in green). We also interrogated the DepMap database (https://depmap.org/portal/) (which combines data from CRISPR/Cas9 and RNAi screens in more than 700 cell lines) to identify cancer-derived complement proteins that may have autocrine functions specifically affecting cell fate under stress conditions. We reasoned that looking for nonessential hits would allow the identification of genes providing stress-specific dependencies and, therefore, potential therapeutic targets less likely to mediate toxicity in normal tissues. Following the combined CanSAR and DepMap analysis, we found 3 hits: *C5*, *C5AR1*, and *C4BPA* (Figure 2A and Supplemental Table 2). *ATR* was included in the screen as a positive control for essential genes because its deletion is lethal in several cell lines due to its role in replication and the DNA damage response (21, 22). Interestingly, *C1QBP*, a complement gene that was recently shown to play a role in the DNA damage response by modulating DNA resection, was essential in a number of cell lines, further validating our screening approach (23) (Figure 2A and Supplemental Table 2).

C5 encodes a complement component, which when cleaved will form C5a. C5aR1 is the main signaling receptor for the C5a ligand.

C4BPA encodes the α chain of complement regulator C4BP (24). There are currently no known pharmacological approaches for targeting C4BPA. To further narrow down which hit would be the best therapeutic target, we assessed the association of C5, C5aR1, and C4BPA mRNA expression with prognostic outcomes and found that only high C5aR1 mRNA expression was associated with significantly poor disease-free survival in CRC (Figure 2, B–D). We confirmed that high C5aR1 mRNA expression was correlated with decreased overall survival in a further independent data set (Supplemental Figure 2A).

In vivo we found that C5aR1 was robustly expressed in AKPT tumors at baseline. A transient induction in C5aR1 expression was also observed after RT (Figure 2E and Supplemental Figure 2, B and C, for negative control C5aR1 staining). We next used multiplex staining and machine learning–based image analysis software to investigate the cellular compartments expressing C5aR1 in greater detail (Figure 2, F and G). Interestingly, we found that at baseline and earlier time points after RT, C5aR1 expression was more prominent in the epithelium, while stromal C5aR1 expression appeared to increase at later time points after RT. Within the immune populations, macrophages and neutrophils were associated with the greatest C5aR1 staining (especially at 3 and 7 days after RT) (Figure 2G). The dominance of stromal C5aR1 expression at these later time points may reflect increased infiltration of C5aR1-expressing immune cells following RT, although this remains to be formally assessed. AKPT tumors harbor stromal infiltration features comparable to those of patients with tumors that could be classified as consensus molecular subtype 4 (CMS4) (4). We therefore asked whether C5aR1 expression might be differentially expressed across

subtypes (CMS1–CMS4). Analysis of pretreatment rectal tumor biopsies identified that those classified as CMS4 had the highest RNA levels of C5aR1 compared with the other subtypes (Supplemental Figure 2D). Furthermore, in previously analyzed RNA-Seq of longitudinal biopsies from patients with rectal adenocarcinoma, we noted that C5aR1 expression was significantly increased following treatment (Supplemental Figure 2, E and F). Analysis of C5aR1 staining in these biopsies indicated that C5aR1 expression was higher in malignant, cancerous tissue than in normal, reactive tissue (Figure 2, H and I; Supplemental Figure 2, G and H; and Supplemental Table 3). Within the

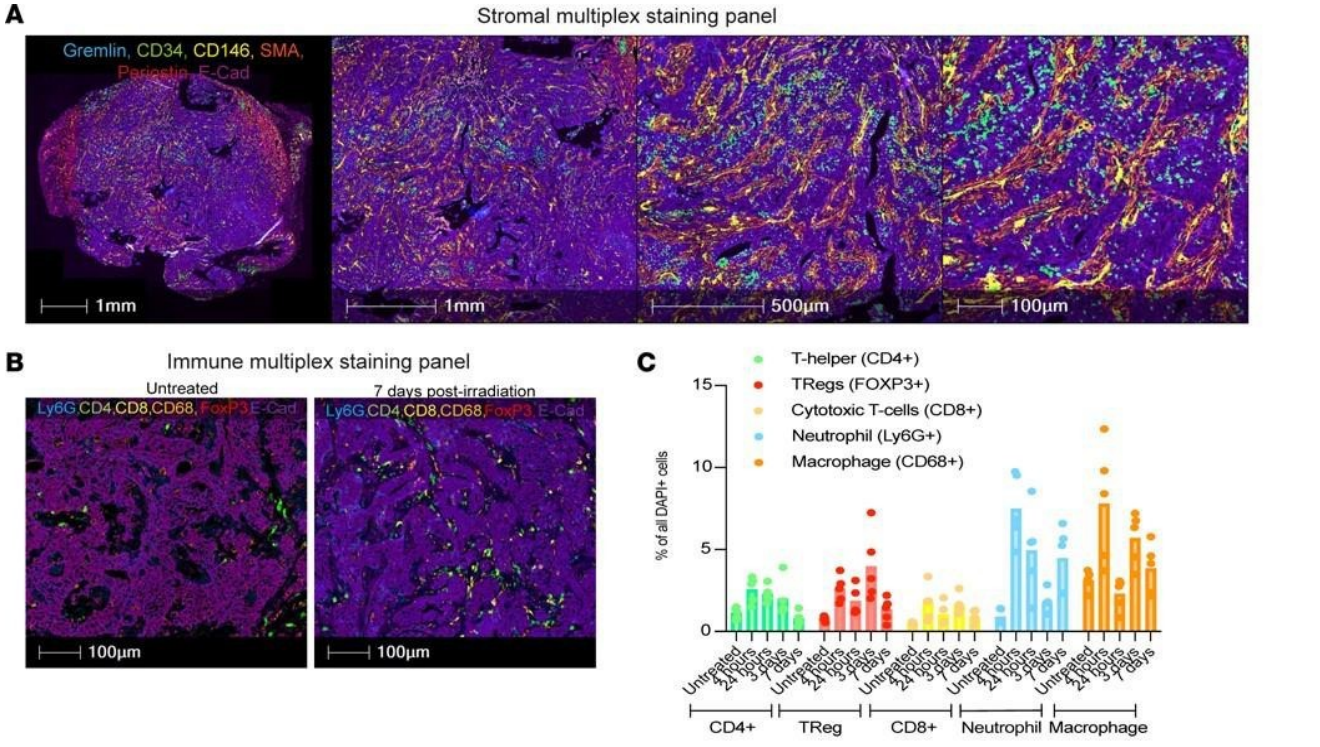

A
Stromal multiplex staining panel
Gremlin, CD34, CD146, SMA,
Periostin, E-Cad
1mm
1mm
500µm
100µm
B
Immune multiplex staining panel
Untreated
7 days post-irradiation
Ly6G,CD4,CD8,CD68,FoxP3,E-Cad
100µm
100µm
C
T-helper (CD4+)
TRegs (FOXP3+)
Cytotoxic T-cells (CD8+)
Neutrophil (Ly6G+)
Macrophage (CD68+)
% of all DAPI+ cells
CD4+
TReg
CD8+
Neutrophil
Macrophage
D
4 hours
24 hours
3 days
7 days
Respiratory electron transport
Complement cascade
Regulation of Complement cascade
Interferon signaling
Neutrophil degranulation
Antigen Processing-Cross Presentation
NES
Rank of pathways by NES
Complement pathways
R-MMU-166658 Complement cascade
R-MMU-977606 Regulation of Complement cascade
E
4 hours
p-value = 0.0034
ES = 0.5179
NES = 1.7407
24 hours
p-value = 0.0185
ES = 0.4703
NES = 1.5598
3 days
p-value = 0.0065
ES = 0.5070
NES = 1.7301
7 days
p-value = 1.72 x 10^-4
ES = 0.6332
NES = 2.1792
Running Enrichment Score
15Gy irradiated
Non-irradiated controls
F
Week 2
padj = 3.33e-05
ES = 0.687
NES = 1.86
Week 6
padj = 0.00243
ES = 0.604
NES = 1.64
Week 12
padj = 0.0131
ES = 0.54
NES = 1.46
Running Enrichment Score

Figure 1. Identification of radiation-responsive targets in immunosuppressive tumors. (**A**) Representative images of *villin*Cre^{ER}; *Apc*$^{fl/fl}$; *Kras*$^{G12D/+}$; *Trp53*$^{fl/fl}$ *Tgfbrl*$^{fl/fl}$ (AKPT) colorectal tumor organoids grown subcutaneously. Multiplex staining of epithelial and stromal cells is shown in whole tumor (left; scale bar: 1 mm) and zoomed in regions (scale bar: 1 mm, 500 μm, and 100 μm [left to right]). (**B**) Representative images of AKPT colorectal tumor organoids grown subcutaneously and treated with either 0 Gy (left) or 15 Gy (right) (scale bar: 100 μm). Multiplex staining of epithelial and immune cells is shown. (**C**) Machine learning–based quantification of immune cell infiltration in AKPT tumors following multiplex staining at different time points following RT. *n* = 5 per group. (**D**) Ranked normalized enrichment scores (NES) are shown below the network graphs for the significant positively enriched pathways. The complement pathways appear among the top most enriched pathways at each time point after 15 Gy radiation treatment. The top enriched pathway for each plot is also shown for comparison. Ranks of pathways annotated as immune system pathways in Reactome are denoted by the vertical lines in red. *n* = 5 (control, *n* = 9). (**E**) Pairwise gene set enrichment analysis comparing irradiated AKPT tumors at 4 hours, 24 hours, 3 days, or 7 days after 15 Gy compared with unirradiated controls. *P* values, enrichment scores (ES), and NES scores are also provided. Complement gene signatures (described in ref. 17) are shown. *n* = 5 (control, *n* = 9). (**F**) Pairwise gene set enrichment analysis comparing baseline samples to samples collected 2 weeks, 6 weeks, or 12 weeks after starting RT in longitudinal biopsies from patients with rectal adenocarcinoma. *P* values, ES, and NES scores are also provided. Complement gene signatures (described in ref. 17) are shown.

cancerous tissue, in 3 of 4 patients analyzed, C5aR1 staining remained either high (with >90% of the epithelium staining for C5aR1) or increased following RT (Figure 2, H and I). Heterogeneity in C5aR1 staining was observed with 1 patient showing very high levels of C5aR1 at baseline (P2), 2 patients showing low baseline staining (P3 and P6), and 1 showing intermediate levels of staining (P15). In all patients C5aR1 staining was higher in the epithelium compared with the stroma (Figure 2, H and I, and Supplemental Figure 2, G and H).

To directly assess whether radiation could impact tumor cell– intrinsic expression of C5aR1 or C5, we turned to an in vitro system. Following RT of mouse and human CRC cells, we found a modest but reproducible increase in C5aR1 (but not C5) across cell lines (Figure 2, J–L, and Supplemental Figure 2, I–M). We also noted that GFP-tagged C5aR1 mostly colocalized with phalloidin-labeled cytoskeletal actin filaments, indicating that C5aR1 is likely present at the plasma membrane (Supplemental Figure 2N).

C5aR1 regulates tumor cell survival under stress. PMX205 is a selective inhibitor of C5aR1 currently undergoing clinical testing for ALS; it is reportedly well-tolerated (25). We assessed the effects of treating CRC cells with PMX205. As anticipated, given the fact that C5aR1 is a GPCR, we found reduced ERK1/2 and RelA phosphorylation (as a readout for NF-$_K$B signaling) in PMX205- treated human and mouse cells (Figure 3A and Supplemental Figure 3A). However, PMX205 had negligible effects on AKT

phosphorylation (at threonine 308) (Supplemental Figure 3, B and C).

Changes in MAPK signaling could impact cell cycle distribution, which, in turn, could impact cellular radiosensitivity. However, we did not note any significant differences in cell cycle profiles or in cell proliferation in cells treated with or without PMX205 with or without RT (Supplemental Figure 3, D–G). We also did not note significant

changes in γH2AX levels or 53BP1 foci between treatment groups, suggesting that DNA damage and repair are likely unaffected by PMX205 (Supplemental Figure 3, H and I). Functional annotation analysis of differentially expressed proteins following reverse-phase protein array (RPPA) analysis indicated that the top differentially expressed pathways at the protein level clustered around apoptosis/cell death with negative regulators of apoptosis being repressed following PMX205 treatment and positive regulators of apoptosis being upregulated (Supplemental Figure 3J and Supplemental Tables 4 and 5). Protein phosphorylation and MAPK cascade were also differentially expressed, consistent with reduced GPCR activity downstream of C5aR1 inhibition and our Western blotting data (Figure 3A). In line with the RPPA data, PMX205 treatment or C5aR1 depletion resulted in increased apoptosis in tumor cells following RT as well as 5-FU and Oxaliplatin treatment (Figure 3, B and C, and Supplemental Figure 3, K–P). Targeting C5aR1 did not result in increased apoptosis in the absence of RT, in agreement with a stress-specific role in modulating cell death. Supporting this, in HCT116 xenografts, we observed increased apoptosis in PMX205- and RT-treated tumors (Figure 3D).

To investigate whether apoptosis of PMX205-treated tumor cells occurred downstream of attenuated GPCR-associated signaling, we

first depleted NF-κB inhibitor, IκBα, as a means of interrogating the

NF-κB dependence of the effects observed. If PMX205-mediated

apoptosis was occurring in an NF-κB– dependent manner, IκBα depletion would be expected to result in decreased apoptosis in

PMX205-treated cells. We indeed observed that, following RT, IκBα depletion attenuated the apoptotic response (Figure 3E and Supplemental Figure 3, Q and R). IκBα depletion did not have a dramatic effect on apoptosis levels in the vehicle- and RT-treated

cells. We hypothesize this is because IκBα levels are reduced by

DNA-damaging agents, and NF-κB signaling is already high in these cells. We also depleted RelA and found that, while RelA depletion increased apoptosis levels in RT- and vehicle-treated cells (as expected), there was no further increase in apoptosis in RT- and PMX205-treated cells (presumably because these cells already have reduced "active" RelA) (Supplemental Figure 3, S and T). Furthermore, interrogation of The Cancer Genome Atlas (TCGA) patient data sets in which high C5aR1 mRNA expression was associated with poor outcome identified that C5aR1 expression was positively and significantly correlated with prosurvival/antiapoptosis

genes, including NF-κB target genes in the BCL2 family (Figure 3,

F–J, and Supplemental Table 6). We confirmed these associations in two further independent patient data sets, including biopsies from patients with rectal cancer collected prior to radiotherapy (Figure 3, G–J). Treatment of CRC cells with PMX205 also resulted in reduced mRNA expression of BCL2 (Supplemental Figure 3U).

We next assessed the effects of ERK inhibition on PMX205- induced apoptosis by treating CRC cells with PMX205 and ERK inhibitor selumetinib. As expected, PMX205 and selumetinib alone resulted in enhanced apoptosis following RT, with PMX205 displaying the most significant effects (Supplemental Figure 3, V and W). A moderate (yet not significant) increase in apoptosis was also observed when both compounds were combined (Supplemental Figure 3, V and W). These data suggest that although attenuated ERK may contribute to apoptosis following PMX205 treatment, it is unlikely to be a main driver of the apoptotic

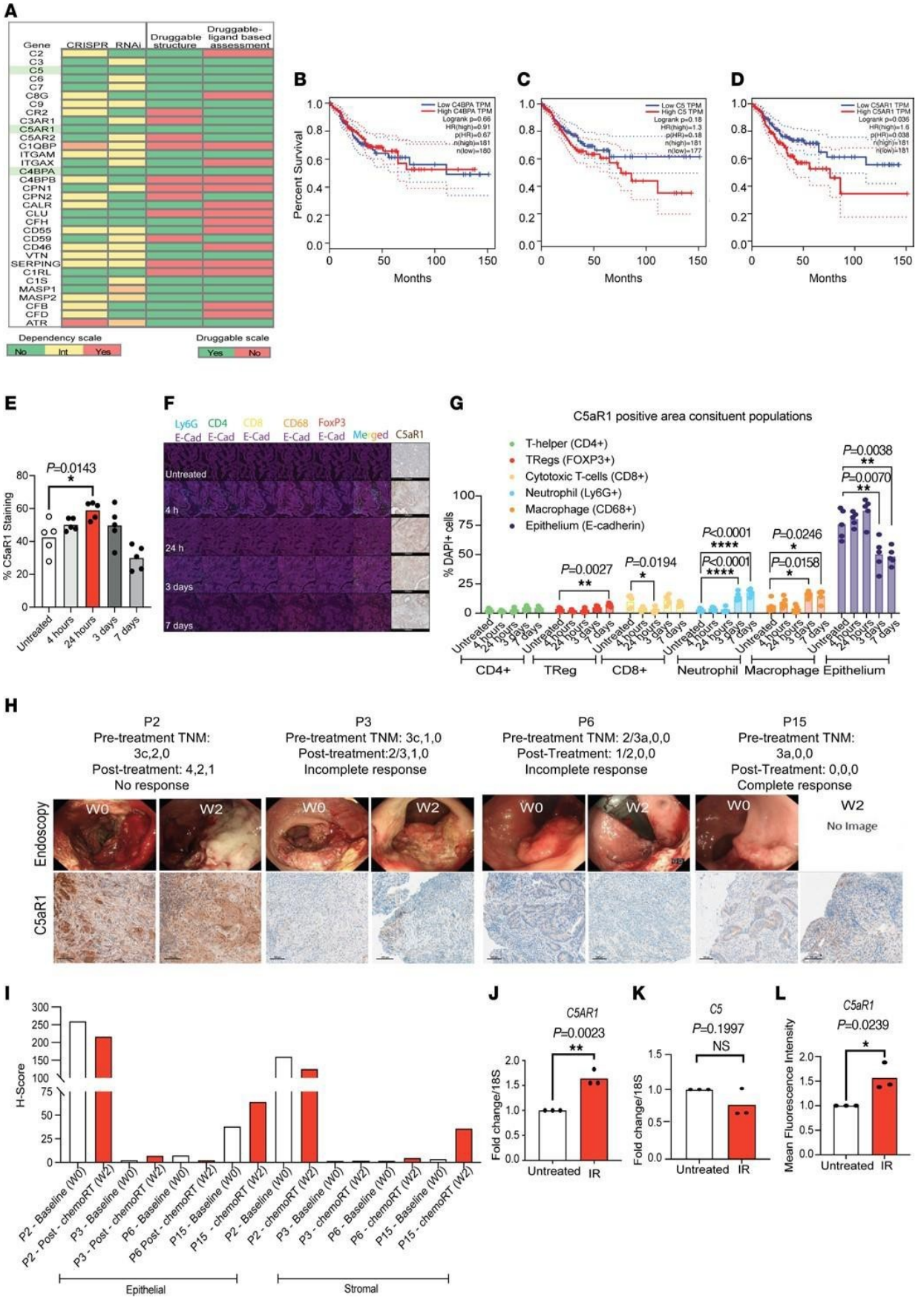

A
Gene
CRISPR
RNAi
Druggable structure
Druggable-ligand based assessment
C2
C3
C5
C6
C7
C8G
C9
CR2
C3AR1
C5AR1
C5AR2
C1QBP
ITGAM
ITGAX
C4BPA
C4BPB
CPN1
CPN2
CALR
CLU
CFH
CD55
CD59
CD46
VTN
SERPING
C1RL
C1S
MASP1
MASP2
CFB
CFD
ATR
Dependency scale
No
Int
Yes
Druggable scale
Yes
No
B
Low C4BPA TPM
High C4BPA TPM
Logrank p=0.66
HR(high)=0.91
p(HR)=0.67
n(high)=181
n(low)=180
Percent Survival
Months
C
Low C5 TPM
High C5 TPM
Logrank p=0.18
HR(high)=1.3
p(HR)=0.18
n(high)=181
n(low)=177
Months
D
Low C5AR1 TPM
High C5AR1 TPM
Logrank p=0.036
HR(high)=1.6
p(HR)=0.038
n(high)=181
n(low)=181
Months
E
P=0.0143
% C5aR1 Staining
Untreated
4 hours
24 hours
3 days
7 days
F
Ly6G E-Cad
CD4 E-Cad
CD8 E-Cad
CD68 E-Cad
FoxP3 E-Cad
Merged
C5aR1
Untreated
4 h
24 h
3 days
7 days
G
C5aR1 positive area consituent populations
T-helper (CD4+)
TRegs (FOXP3+)
Cytotoxic T-cells (CD8+)
Neutrophil (Ly6G+)
Macrophage (CD68+)
Epithelium (E-cadherin)
% DAPI+ cells
P=0.0027
P=0.0194
P<0.0001
P<0.0001
P=0.0246
P=0.0158
P=0.0038
P=0.0070
CD4+
TReg
CD8+
Neutrophil
Macrophage
Epithelium
H
P2
Pre-treatment TNM: 3c,2,0
Post-treatment: 4,2,1
No response
P3
Pre-treatment TNM: 3c,1,0
Post-treatment:2/3,1,0
Incomplete response
P6
Pre-treatment TNM: 2/3a,0,0
Post-Treatment: 1/2,0,0
Incomplete response
P15
Pre-treatment TNM: 3a,0,0
Post-Treatment: 0,0,0
Complete response
W0
W2
No Image
Endoscopy
C5aR1
I
H-Score
P2 - Baseline (W0)
P2 - Post - chemoRT (W2)
P3 - Baseline (W0)
P3 - Post - chemoRT (W2)
P6 - Baseline (W0)
P6 Post - chemoRT (W2)
P15 - Baseline (W0)
P15 - chemoRT (W2)
P2 - Baseline (W0)
P2 - chemoRT (W2)
P3 - Baseline (W0)
P3 - chemoRT (W2)
P6 - Baseline (W0)
P6 - chemoRT (W2)
P15 - Baseline (W0)
P15 - chemoRT (W2)
Epithelial
Stromal
J
C5AR1
P=0.0023
Fold change/18S
Untreated
IR
K
C5
P=0.1997
NS
Fold change/18S
Untreated
IR
L
C5aR1
P=0.0239
Mean Fluorescence Intensity
Untreated
IR

Figure 2. C5aR1 is a radiation-responsive druggable target. (**A**) Essential genes are shown in red. Nonessential genes are shown in green. Yellow/ Orange indicates intermediate dependence or essentiality. For target tractability, green corresponds with druggable structure = Yes and druggable by ligand-based assessment = Yes. Red corresponds to druggable structure = No and druggable by ligand-based assessment = No. (**B**) Kaplan- Meier (KM) curve for disease-free survival (dfs) of TCGA patients with CRC with high (red) or low (blue) C4BPA mRNA expression. For all KM curves, group cutoff = median (http://gepia.cancer-pku.cn). (**C**) KM curve for dfs of TCGA patients with CRC with high (red) or low (blue) C5 mRNA expression. (**D**) KM curve for dfs of TCGA CRC with high (red) or low (blue) C5AR1 mRNA expression. (**E**) Quantification of C5aR1 immunohistochemistry staining in AKPT tumors. $^{*}P < 0.05$, ordinary 1-way ANOVA, Dunnett's multiple comparisons. All other comparisons relative to untreated were not significant. $n = 5$. (**F**) Representative images of multiplex and C5aR1 IHC staining in AKPT tumors (original magnification, ×40) Scale bar: 500 μm. (**G**) Proximity-based machine learning quantification of the percentage of C5aR1 staining in the epithelium and stroma of AKPT tumors. $^{*}P < 0.05$, $^{**}P < 0.01$, $^{****}P < 0.0001$, ordinary 1-way ANOVA with Tukey's multiple comparisons. All other comparisons relative to untreated were not significant. $n = 5$. (**H**) Endoscopy images and representative examples of C5aR1 staining at baseline (W0) compared with W2 in longitudinal biopsies from patients with rectal adenocarcinoma. W2, week 2 after treatment. Numbers refer to patient number, week after treatment, or TNM stage. Scale bar: 100 mm. (**I**) H-Scores of C5aR1 staining in epithelial and stromal areas of cancerous tissue from rectal adenocarcinoma longitudinal biopsies taken at W0 compared with W2. (**J**) mRNA expression of *C5AR1*/housekeeping in HCT116 cells treated with either 0 or 9 Gy. $n = 3$. $^{**}P < 0.01$, 2-tailed *t* test. (**K**) mRNA expression of *C5*/housekeeping in HCT116 cells treated as in **J**. $n = 3$. Two-tailed *t* test. (**L**) C5aR1 median fluorescence intensity in HCT116 cells treated with either 0 or 9 Gy. $n = 3$. $^{*}P < 0.05$, 2-tailed *t* test.

effect observed. Together, these data suggest that C5aR1 mediates tumor cell prosurvival signaling, with NF-κB acting as a key regulator of this response. In support of this conclusion, increased cell death following PMX205 treatment occurs downstream of attenuated NF-κB signaling.

C5aR1 deficiency does not result in increased apoptosis in healthy intestinal epithelium. To assess whether the cell-intrinsic effects of complement were specific to malignant cells, we first considered if organoids derived from different genotypes expressed complement genes when grown in vitro (and therefore in the absence of systemic complement or TME-derived complement). Interestingly, following RNA-Seq, we found that complement genes were significantly differentially expressed in both AKPT tumor organoids as well as organoids derived from *villin*Cre^{ER}; *Kras*$^{G12D/+}$; *Trp53*$^{fl/fl}$ Rosa26$^{N1icd/+}$ (KPN) mice (compared with untransformed WT organoids). Over 74% of the complement genes queried were expressed at significantly higher levels in the AKPT organoids compared with the WT organoids (including C5aR1), suggesting that increased cell-intrinsic complement expression is a malignant cell- associated phenomenon (Figure 4, A and B).

To investigate whether targeting C5aR1 might alter prosurvival signaling in healthy tissues, we assessed RelA and ERK phosphorylation in untransformed intestinal organoids. We noted that, while ERK phosphorylation was reduced following PMX205 treatment, RelA phosphorylation was not affected (Supplemental Figure 4A). We also performed RNA-Seq in intestinal untransformed organoids treated with or without PMX205 and with or without RT. Following gene ontology analysis, as expected, genes within the GPCR activity pathway were among those differentially expressed (downregulated) in untransformed organoids treated with PMX205 (Supplemental Figure 4, B and C). In line with the lack of RelA phosphorylation changes observed by Western blotting, we noted that

transcriptional NF-κB target genes were not differentially expressed in PMX205- and RT-treated versus RT-treated organoids (Supplemental Figure 4D). Similarly, in vivo, small intestines did not show significant transcriptional changes in antiapoptotic target genes in the BCL2 family with deletion of C5aR1 (following RT) (Figure

4C). These data suggest that changes in NF-κB antiapoptotic signaling downstream of C5aR1 do not occur in the untransformed intestinal epithelium. In line with these signaling changes, we did not observe an increase in apoptosis in small intestines following PMX205 treatment or C5aR1 loss (Figure 4, D–F). In fact, small intestinal crypts in vivo had significantly reduced apoptosis following PMX205 treatment or C5aR1 loss following total abdominal RT (Figure 4, D–F). Together, these data indicate that C5aR1 attenuates stress-induced apoptosis in malignant but not nontransformed epithelial cells.

C5aR1 inhibition improves tumor radiation response. To assess whether targeting C5aR1 could improve radiation responses in vivo, we treated MC38 subcutaneous tumors with PMX205 and no RT, fractionated RT (3 × 4.45 Gy), or single-dose RT (9 Gy) (Figure 5A and Supplemental Figure 5A). PMX205 treatment in the absence of RT did not have significant effects on tumor response (Figure 5B and Supplemental Figure 5B). PMX205 treatment also had no negative effects on mouse weight (Supplemental Figure 5A). However, following treatment with either single-dose or equivalent

fractionation regimens (equivalent assuming an α/β ratio of 5.06) (26) PMX205 treatment significantly improved radiation response (Figure 5, C and D, and Supplemental Figure 5, C and D).

Targeting C5aR1 does not increase the percentage of $CD8^+$ T cells in the tumor following RT. Targeting C5aR1 as a means of reinvigorating antitumor $CD8^+$ T cell responses has undergone clinical testing (27). Because we had observed stromal C5aR1 expression in irradiated tumors, we next investigated immune infiltration changes in tumor draining lymph nodes and tumors following PMX205 and RT (Figure 6A). Interestingly, no significant changes in CD3, CD4, NK, or B cells were found in the tumor draining lymph nodes across treatment groups (Figure 6, B–E, and Supplemental Figure 6A). Mice treated with PMX205 alone, however, displayed a higher percentage of $CD8^+$ T cells compared with those treated with PMX205 and RT (Figure 6F). Mice treated with PMX205 alone also had a reduced percentage of Tregs

compared with vehicle-treated mice (Figure 6G). However, these changes did not correlate with altered functionality/effector functions

of CD8+ T cells, which showed comparable expression of IFN-γ,

GrzB, and TNF-α across all treatment groups (Figure 6, H–L). In the tumor, we found that, although RT, as expected, significantly increased levels of $CD3^+$ and $CD8^+$ T cells, treatment with PMX205 did not further increase the percentage of these cells (Figure 6, M and N, and Supplemental Figure 6B). In fact, the percentage of $CD8^+$ T cells was significantly reduced in tumors after PMX205 and RT treatment when compared with RT vehicle-treated mice (Figure 6N). This was surprising, given the improved tumor regression previously observed in these models (Figure 5D). No significant changes in NK cells or either monocytic or granulocytic myeloid derived suppressor cells were observed across

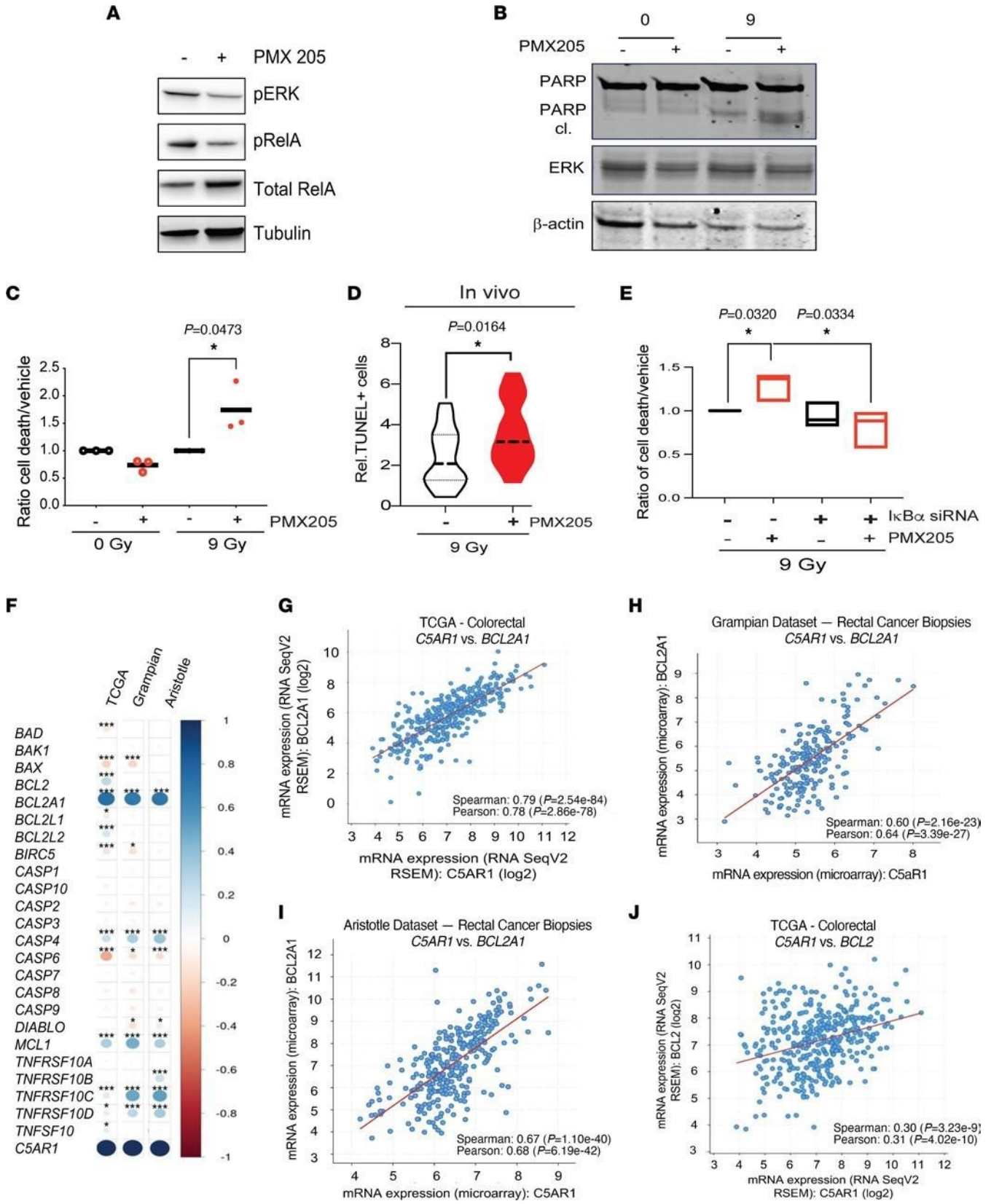


Figure 3. C5aR1 regulates tumor cell survival under stress. (**A**) HCT116 cells were treated with either vehicle or PMX205 (10 mg/mL) for 48 hours. Western blotting was carried with the antibodies indicated. (**B**) HCT116

cells were treated with 0 or 9 Gy and either vehicle or PMX205 for 1 hour before RT. Cells were harvested 48 hours after RT. Western blotting was carried with the antibodies indicated. (**C**) The ratio of dead (apoptotic)

cells/nonapoptotic cells as a percentage of the whole population relative to vehicle-treated cells. $n = 3$. $^*P < 0.05$, 2-tailed t test. (**D**) TUNEL$^+$ cells per field of view of sections from HCT116 subcutaneous tumors. Mice were treated with 9 Gy and either vehicle or PMX205 (10 mg/kg) for 3 doses flanking RT. $^*P < 0.05$, 2-tailed t test. (**E**) The number of dead(apoptotic)/ nonapoptotic cells as a percentage of the whole population for HCT116 cells transfected with either Scr or IκBα siRNA and treated with either vehicle or PMX205 for 1 hour before RT. Cells were harvested 48 hours after RT. Independent fields of view from a representative experiment are shown, $n = 3$. $^*P < 0.05$, 2-tailed t test. (**F**) Pearson's correlation of mRNA expression of pro- and antiapoptotic genes with C5aR1 in TCGA samples from patients with CRC and rectal cancer biopsies from Grampian and Aristotle. $^*P < 0.05$, $^{***}P < 0.001$, $^{****}P < 0.0001$. All TCGA data were accessed through cBioPortal (http://www.cbioportal.org/). All Grampian and Aristotle data were accessed through SCORT (stratification in colorectal cancer, http://www.cbioportal.org/). (**G**) Correlation of *BCL2A1* and *C5AR1* mRNA expression in TCGA CRC samples. (**H**) Correlation of *BCL2A1* and *C5AR1* mRNA expression in Grampian rectal cancer biopsies. (**I**) Correlation of *BCL2A1* and *C5AR1* mRNA expression in Aristotle rectal cancer biopsies. (**J**) Correlation of *BCL2* and *C5AR1* mRNA expression in TCGA CRC samples.

treatments (Supplemental Figure 6, C–F). These data indicated that improved radiation responses following PMX205 treatment can occur despite reduced tumor CD8$^+$ T cell infiltration changes.

C5aR1 inhibition can improve radiotherapy in tumors with an immunosuppressive microenvironment. The improved tumor responses observed in the context of reduced tumor CD8$^+$ T cell numbers made us question whether PMX205 could be used to improve radiation responses in models displaying low CD8$^+$ T cell infiltration. We, therefore, next asked whether PMX205 could improve response in the AKPT model where we had previously observed robust C5aR1 expression and low CD8$^+$ T cell tumor infiltration. In support of C5aR1 having cell-intrinsic effects, we observed that, in vitro, PMX205 reduced survival of AKPT organoids upon treatment with increasing RT doses (Figure 7A). We also observed reduced RelA (and Erk) phosphorylation by Western blotting in PMX205-treated AKPT organoids (Supplemental Figure 7A). When these organoids were grown as subcutaneous tumors, PMX205 alone had no significant effect on tumor growth (as previously observed in the MC38 model) (Figure 7, B and C, and Supplemental Figure 7B). However, combination treatment with PMX205 and RT resulted in a significant tumor growth delay, increased apoptosis, and dramatic improvement in tumor-free survival, with 20% of mice having impalpable tumors at the end of the experiment (Figure 7, D–F, and Supplemental Figure 7B). To investigate the T cell dependence of these effects, we repeated the AKPT subcutaneous experiment in athymic nude mice. We noted that improve tumor response and survival was maintained in this model (Figure 7, G–I, and Supplemental Figure 7C). Together, our data indicate that targeting C5aR1 can improve radiation response even in models with low (or absent) tumor CD8$^+$ T cell infiltration. Importantly, improved responses are associated with increased tumor cell apoptosis and without concomitant increases in healthy intestinal epithelial cell apoptosis (Figure 7J).

Discussion

Identifying tumor-promoting components of the TME presents therapeutic opportunities. However, expression of these components can be extremely dynamic and may be governed by selective pressures, such as those posed by treatment-induced stress responses. The effects of these selective pressures on dysregulation of complement components and their evolving functions in the TME is unclear. Here, we report that complement gene expression was induced after RT in murine tumor models that recapitulate features of human tumors displaying the worse outcomes. Importantly, a significant enrichment in complement gene signatures was also found when analyzing biopsies from patients with rectal adenocarcinoma during and after CRT. Among these genes, C5aR1 expression was transiently induced following radiotherapy, likely as a stress response mounted to promote tumor cell survival. Interestingly, in AKPT tumor models, C5aR1 was expressed by both the tumor epithelium and stroma. We found that epithelial expression was more prominent at baseline and early time points after RT, while stromal expression dominated at later time points. Increased C5aR1 stromal expression at later time points may reflect recruitment of C5aR1 expressing immune cells following RT (as indicated in Figure 1C and Supplemental Figure 1, A–G). Interestingly, in patients with rectal cancer, we found that those classified as CMS4 have the highest levels of C5aR1 expression compared with the other subtypes. Analysis of C5aR1 expression in rectal adenocarcinoma biopsies also points to a potential "Goldilocks" effect to C5aR1 expression. In the samples analyzed, very high baseline expression was observed in the patient displaying overt radiation resistance and tumor progression during treatment, low expression was observed in both patients with partial responses, while intermediate epithelial expression (concomitant with increased stromal expression following treatment) was observed in the patient with exquisite radiation sensitivity and a complete response. Future studies with additional samples will be necessary to fully investigate these associations and how to use this information clinically. Together, our data indicate that patients with tumors displaying immunosuppressive features and high C5aR1 expression could represent populations most likely to benefit from C5aR1-targeting therapy.

Previous reports investigating the effects of complement inhibition on radiotherapy response have focused on complement's role in modulating antitumor immunity, albeit with conflicting results (28, 29). Furthermore, whether targeting complement protein would have the same effects in tumor and normal tissues had, until this study, remained unexplored to our knowledge. Using a combination of RNA-Seq and in silico mining of DepMap, CanSAR, and patient data sets, we identified C5aR1 as a druggable target for enhancing stress-specific cancer cell death. Our data indicate that C5aR1 negatively regulates apoptosis in cancer cells by modulating cell survival pathways, such as NF-κB, and that attenuating such prosurvival signaling can render cancer cells more susceptible to death following RT. Importantly, in the normal intestine, targeting C5aR1 does not result in increased apoptosis, and, in fact, C5aR1

deficiency appears to confer a protective phenotype. Why or how C5aR1 may differentially regulate signaling in normal and

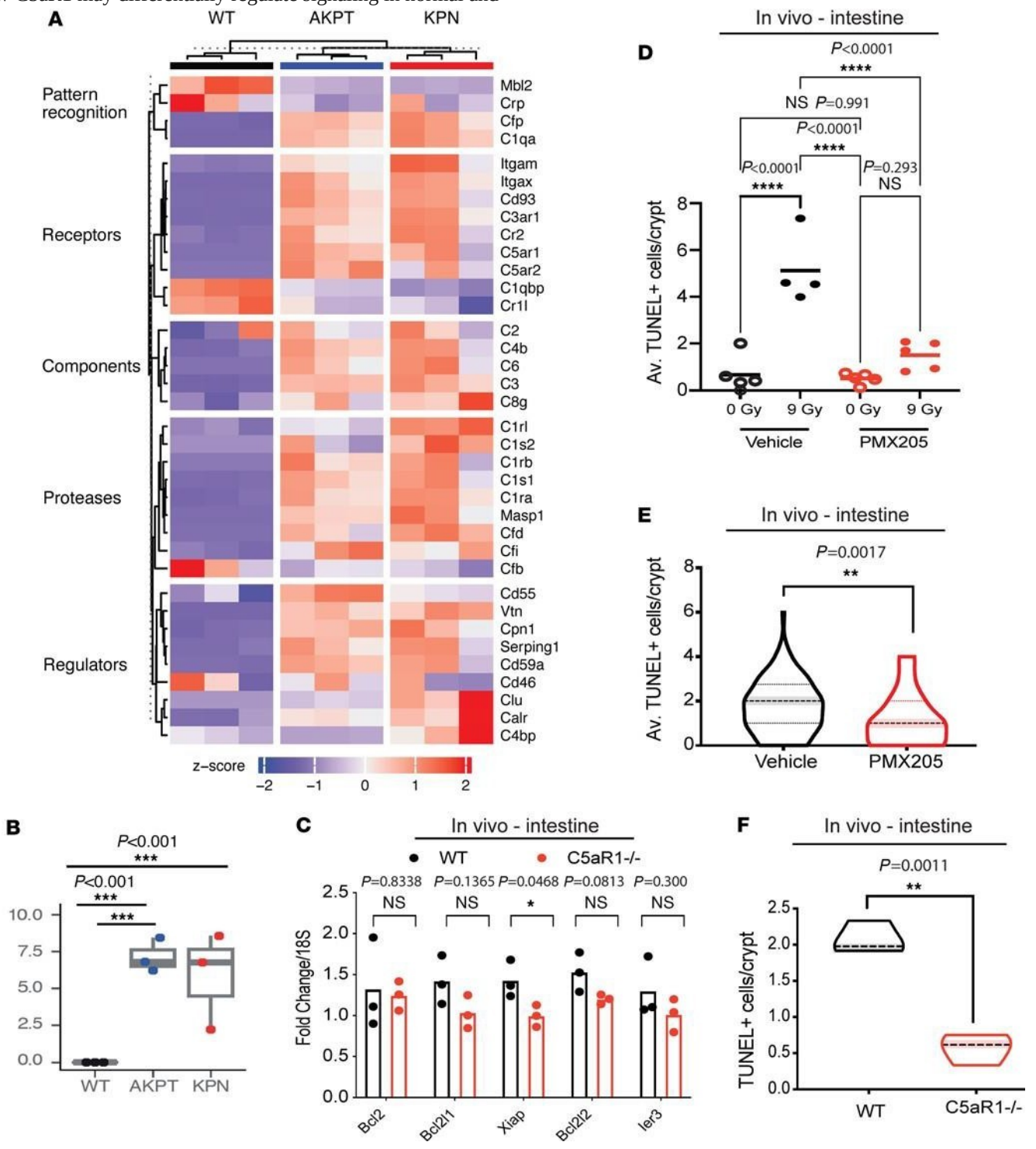


Figure 4. C5aR1 deficiency does not result in increased apoptosis in healthy intestinal epithelium. (**A**) Heatmap of complement genes differentially
expressed by RNA-Seq in WT, AKPT, or KPN organoids grown in vitro. Upregulation is shown in red, as per Z-score indicated below. Data for 3 independent samples is shown from data deposited at the ArrayExpress database under accession

number E-MTAB-11769 (46). (**B**) C5aR1 expression (CPM) assessed by RNA-Seq in WT, AKPT, or KPN organoids grown in vitro as in **A**. ***$P < 0.001$, empirical Bayes moderated t-statistic test. (**C**) mRNA expression of *Bcl2*,

Bcl2l1, *Bcl2l2*, *Ier3*, and *Xiap* in WT or C5aR1$^{-/-}$ mice treated with 9 Gy. Points indicate individual mice per group. n = 3. *P = 0.0468, unpaired 2-tailed t test.

(**D**) The average TUNEL^{+} cells/crypt of BALBc/J mice treated with either 0 or 9 Gy and either vehicle or PMX205. Intestines were harvested 72 hours after RT. n = 4/5 mice per group. ****P < 0.0001, by ordinary 1-way ANOVA with Tukey's multiple comparisons.

(**E**) The average TUNEL^{+} cells/crypt of C57BL/6 mice treated with 9 Gy and either vehicle or PMX205. Intestines were harvested 72 hours after RT. n = 3 mice per group. **P < 0.01, 2-tailed t test. (**F**) The average number of TUNEL^{+} cells of WT or C5aR1$^{-/-}$ mice treated with 9 Gy. Intestines were harvested 48 hours after RT. n = 3 mice per group. *P < 0.05, 2-tailed t test.

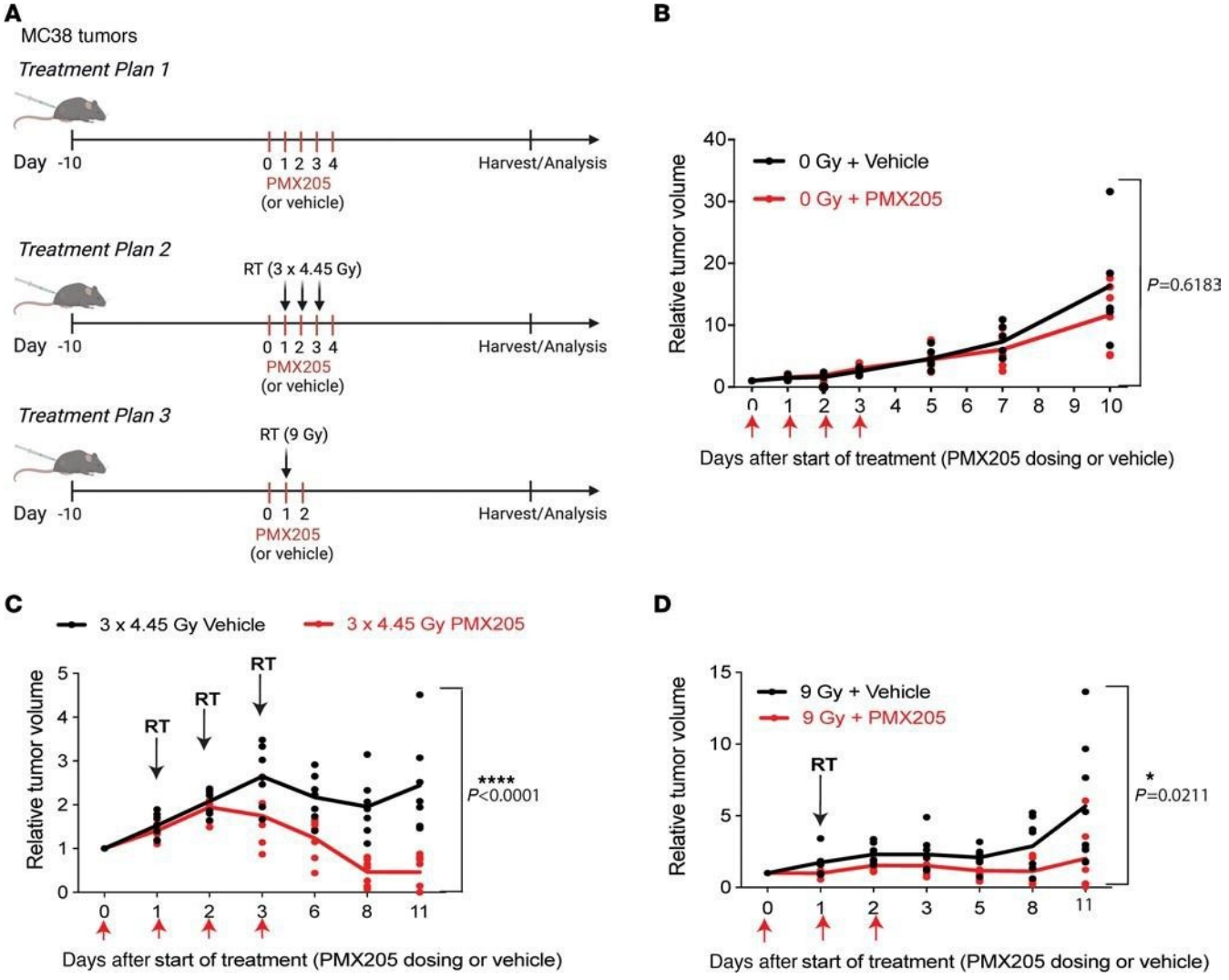


Figure 5. C5aR1 inhibition improves tumor radiation response. (**A**) Schematic representation of the treatment schemes followed. Created with BioRender.com. (**B**) Relative tumor growth curves are shown for MC38 subcutaneous tumors treated with either vehicle or PMX205 treatment for 3 doses (on day 0, 1, and 2). P = 0.6183 by repeated measures 2-way ANOVA (with Geisser-Greanhouse correction). n = 7 for PMX205; n = 6 for vehicle. (**C**) Relative tumor growth curves are shown for MC38 subcutaneous tumors treated with 3 × 4.45 Gy and either vehicle or PMX205 treatment for 3 doses flanking RT. Individual points represent individual mice per group. ****P < 0.0001 by repeated measures 2-way ANOVA (with Geisser-Greanhouse correction); P = 0.0073 for day 3; P = 0.0048 for day 6; P = <0.0001 for day 8 and 11 with Šídák's multiple comparison test. n = 7 for both groups. (**D**) Relative tumor growth curves are shown for MC38 subcutaneous tumors treated with single-dose 9 Gy and either vehicle or

PMX205 treatment for 3 doses flanking RT. Individual points represent individual mice per group. *P* = 0.0211 by repeated measures 2-way ANOVA (with Geisser-Greanhouse correction); *P* = 0.0001 for day 11 with Šídák's multiple comparison test. *n* = 7 for PMX205; *n* = 8 for vehicle.

malignant cells remains to be elucidated. However, divergent consequences of autocrine complement signaling between cell lines have been previously reported (30). To therapeutically target C5aR1, we used the specific antagonist PMX205, which has FDA and EMA "orphan drug" designation for ALS, allowing accelerated progression to clinical trials (31). This class of cyclic peptides have minimal penetrance into the cell (32) and should therefore primarily impact cell-surface C5aR1. This is important because recent reports indicate that C5aR1 intracellular pools are present in tumor cells where they contribute to tumorigenesis through β-catenin stabilization (33).

We have compared, for the first time to our knowledge, single and equivalent fractionation doses in CRC models to specifically assess the effect of targeting C5aR1. In both settings, we observed

that PMX205 improves radiation response, although, interestingly, the effect appeared more pronounced in the fractionated setting. We propose that increased PMX205-mediated cell death is a mechanism that can be exploited to improve responses, even in tumors displaying immunosuppressive features. The importance of modulating antitumor immune host responses following C5aR1 targeting has been highlighted in previous studies, and ourselves and others have observed reduced tumor burden in C5aR1$^{-/-}$ mice (data not shown) (28, 33, 34). The defect in tumor uptake displayed by C5aR1$^{-/-}$ mice complicates the investigation of radiation responses in this model and might have contributed to some of the previous conflicting reports. The reduced tumor CD8^{+} T cell infiltration observed here, however, is in line with reports, indicating that

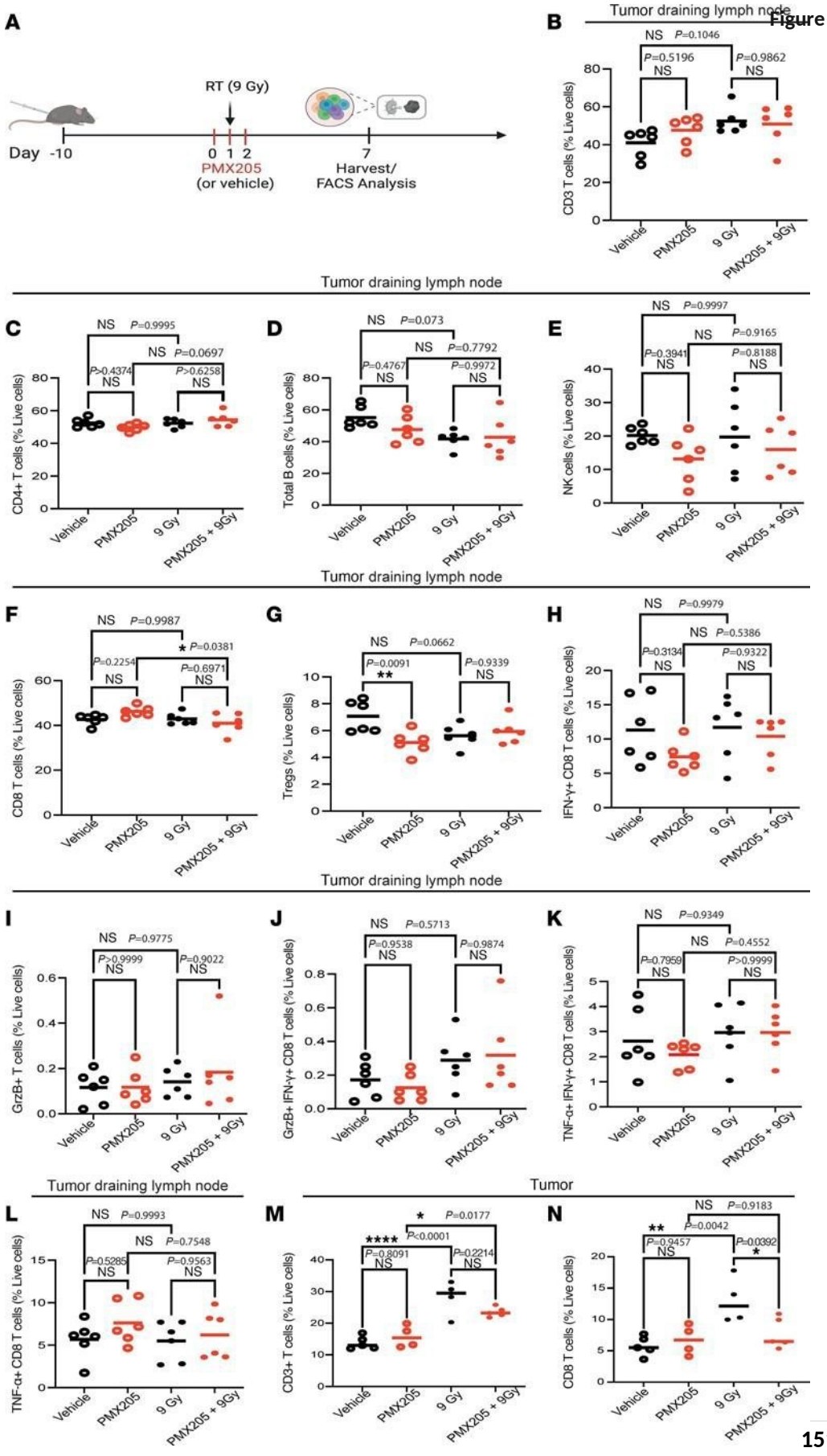
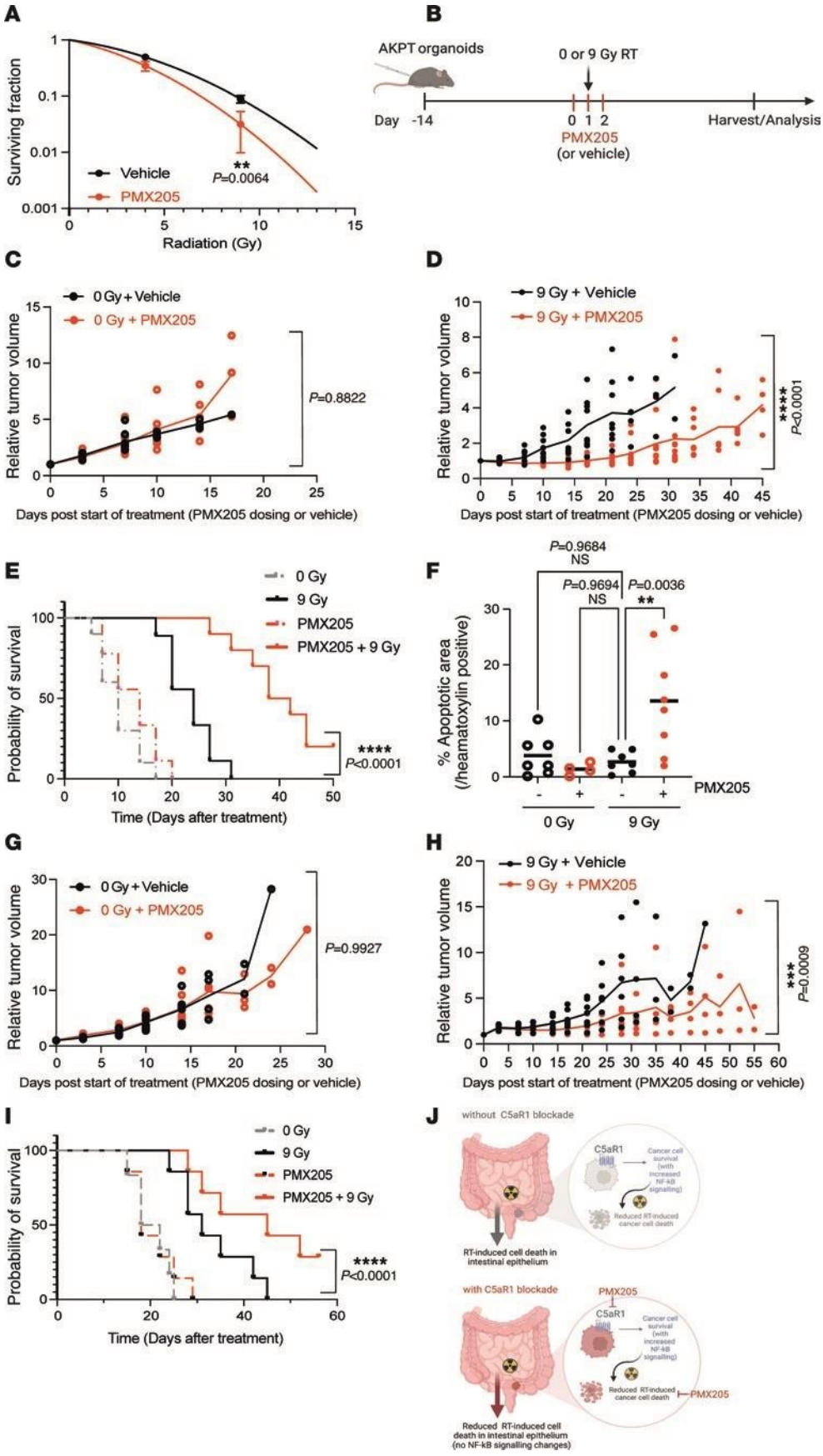


Figure 6. Targeting C5aR1 does not



increase the percentage of CD8$^+$ T cells in the tumor following RT.

(**A**) Schematic representation of the experimental design for **B**–**N**. Created with BioRender.com. (**B**) CD3$^+$ T cells in tumor draining lymph nodes following the dosing scheme shown in **A**. Tumors were harvested 7 days after RT. Ordinary 1-way ANOVA with Tukey's multiple comparisons test. *n* = 5. (**C**) CD4$^+$ T cells in tumor draining lymph nodes following the dosing scheme, harvesting schedule, and statistical analysis shown in **B.** *n* = 5.

(**D**) Total B cells in tumor draining lymph nodes following the dosing scheme, harvesting schedule, and statistical analysis shown in **B**. *n* = 5. (**E**) Total NK cells in tumor draining lymph nodes following the dosing scheme, harvesting schedule, and statistical analysis shown in **B**. *n* = 5. (**F**) CD8$^+$ T cells in tumor draining lymph nodes following the dosing scheme, harvesting schedule, and statistical analysis shown in **B**. *n* = 5. (**G**) Tregs in tumor draining lymph nodes following the dosing scheme, harvesting schedule, and statistical analysis shown in **B**. *n* = 5. (**H**) IFN-γ$^+$ CD8 T cells in tumor draining lymph nodes following the dosing scheme, harvesting schedule, and statistical analysis shown in **B**. *n* = 5.

(**I**) GrzB$^+$CD8 T cells in tumor draining lymph nodes following the dosing scheme, harvesting schedule,

and statistical analysis shown in **B**. *n* = 5. (**J**) GrzB$^+$IFN-γ$^+$ CD8 T cells in tumor draining lymph nodes following the dosing scheme, harvesting schedule, and statistical analysis shown in **B**. *n* = 5. (**K**) TNF-α$^+$ IFN-γ$^+$ CD8 T cells in tumor draining lymph nodes following the dosing scheme, harvesting schedule, and statistical analysis shown in **B**. *n* = 5. (**L**) TNF-α$^+$ CD8 T cells in tumor draining lymph nodes following the dosing scheme, harvesting schedule, and statistical analysis shown in **B**. *n* = 5. (**M**) CD3$^+$ T cells in tumors following the dosing scheme, harvesting schedule, and statistical analysis shown in **B**. *n* = 5. (**N**) CD8$^+$ T cells in tumors following the dosing scheme, harvesting schedule, and statistical analysis shown in **B**. *n* = 5.

Figure 7. C5aR1 inhibition can improve radiotherapy in tumors with an immunosuppressive microenvironment.

(**A**) Curves show counted viable AKPT organoids vs. RT dose following

local production of anaphylatoxins C3a and C5a and signaling through their receptors is required for dendritic cell maturation and $CD8^+$ T cell activation (28). We acknowledge, however, that more

treatment with vehicle or PMX205. **P < 0.01, Welch's t test. Data are shown as the mean. Error bars represent standard deviation. (**B**) Schematic representation of experimental design for **C**–**F**. Created with BioRender.com. (**C**) Tumor growth curves for AKPT organoids grown subcutaneously and treated with 0 Gy and vehicle or PMX205. Comparisons were not significant (P = >0.05) by repeated measures 2-way ANOVA (with Geisser-Greanhouse correction). n = 7 mice/group. (**D**) Tumor growth curves for AKPT organoids grown subcutaneously and treated with 9 Gy and vehicle or PMX205 flanking RT. ****P < 0.0001 by repeated measures 2- way ANOVA (with Geisser-Greanhouse correction); P < 0.05 for day 10, 14, and 17 with Šídák's comparison test. n = 7 mice/group. (**E**) Probability of survival for tumor-bearing mice from **C** and **D**. ****P < 0.0001, logrank. n = 7 mice/group. (**F**) The percentage of apoptotic (TUNEL$^+$) area/ hematoxylin$^+$ area in mice from **C** and **D**. **P < 0.01, ordinary 1-way ANOVA with Dunnett's multiple comparisons test. n = 4–8 mice/group. (**G**) Tumor growth curves for AKPT organoids grown subcutaneously in athymic nude mice and treated with 0 Gy and vehicle or PMX205. Comparisons were not significant (P > 0.05) by repeated measures 2-way ANOVA (with Geisser-Greanhouse correction). n = 7 mice/group. (**H**) Tumor growth curves for AKPT organoids grown subcutaneously in athymic nude mice and treated with 9 Gy and vehicle or PMX205 flanking RT. ***P < 0.001, repeated measures 2-way ANOVA (with Geisser-Greanhouse correction); ***P < 0.001 for day 24, Šídák's comparison test. n = 7 mice/group. (**I**) Probability of survival for mice from **G** and **H**. ****P < 0.0001, log-rank. n = 7/ group (n = 6 for 0 Gy vehicle). (**J**) Working model: C5aR1 attenuates RT-induced tumor cell death via increased prosurvival signaling (including NF-κB). Upon C5aR1 blockade, tumor cells undergo increased RT-induced cell death, which is not observed in the intestinal epithelium. Created with BioRender.com.

extensive immunophenotyping at different time points following both single and fractionated RT would be required to fully

understand the effects of C5aR1 targeting on modulating antitumor immune host responses.

Overall, this study indicates that increased complement gene expression is part of the stress response mounted by irradiated tumors to sustain survival via C5aR1 signaling. These data therefore indicate that, beyond its previously described functions, C5aR1 can also sustain tumor cell survival in a cell-intrinsic manner. Consequently, targeting C5aR1 can improve radiotherapy, even in tumors displaying reduced $CD8^+$ T cell infiltration. Importantly, C5aR1's prosurvival functions appear to be malignant cell specific, because increased apoptosis was not observed in the normal intestinal epithelium following C5aR1 loss. This work is relevant since identifying targets that specifically modulate cancer cell radiosensitivity and can do so even in the absence of robust tumor $CD8^+$ T cell infiltration could lead the way to improving treatment outcomes for the most difficult to treat tumors.

Methods

Cell lines and treatments. HCT116 male adult human epithelial CRC cells and HT-29 female adult CRC cells originally purchased from ATCC were used. MC38 murine C57BL6 colon adenocarcinoma cells were provided in-house. Cells were grown in DMEM with 10% FBS, in a standard humidified incubator at 37°C and 5% CO_2. All cell lines were routinely tested for mycoplasma and found to be negative. Oxaliplatin (Sigma-Aldrich) and 5-FU (Cayman Chemical Company) were used at

40 μM. RT treatment in vitro was carried out using a Gamma Service GSR D1 irradiator containing a Cs137 source. The dose rates of the system, as determined by the supplier, were 1.938 Gy/min and 1.233 Gy/min, depending on the distance from the source.

AKPT organoid culture. Organoids were sourced from Eoghan Mulholland (Wellcome Trust Centre Human Genetics, University of Oxford), working within the ACRCelerator: Colorectal Cancer Stratified Medicine Network (A:CCSMN). These were generated from male mice with tumors from liver metastasis formed from a tamoxifen-

induced CRC mouse model. Organoids were grown within 35 μL

Matrigel and DMEM/F12 media mixture (2:1) with 500 μL media overlaid within each well of a 24-well plate. Overlaid medium was supplemented with epidermal growth factor (EGF) and noggin at a concentration of 100 ng/mL and 50 ng/mL, respectively. Organoids were maintained through passaging every 3 days.

For survival fraction studies, organoids were used 24 hours after passaging and plated into a 24-well plate. Vehicle or PMX205 treatment was added into the surrounding media 1 hour before RT. RT was carried out using an X-ray irradiator with lead shielding, allowing for cumulative doses across a single plate. Organoids were imaged using a 4× objective over 3 days with a JuLi stage Real-Time Cell History recorder (NanoEnTek Inc.). Organoids were manually counted at day 0 and 3, with a surviving fraction subsequently calculated.

Mouse intestinal organoids. Establishment and culture of mouse intestinal organoids was carried out as previously described with some modifications (35, 36). Briefly, approximately 2 mm intestinal pieces were rinsed twice with cold PBS and transferred into a 50 mL falcon tube with 30 mL 10% FBS/PBS solution. The tube was shaken

forcefully, and the 10% FBS/PBS solution was replaced with 25 mL of HBSS/ EDTA solution (without Ca^{2+} and Mg^{2+}, Thermo Fisher Scientific). The tube was incubated in 37°C water bath for 10 minutes and shaken forcefully several times every 2–3 minutes. The supernatants containing the isolated crypts were collected, and the procedure was repeated twice. After filtration, centrifugation and washing of isolated crypts, the supernatant was removed and pellets were resuspended in cold Cultrex UltiMatrix Reduced Growth Factor (RGF) BME (Bio-

Techne). The BME was then solidified and overlaid with 500 μL complete mouse organoid media (1× DMEM/F-12 [Thermo Fisher Scientific], 1× GlutaMAX [Thermo Fisher Scientific], 10 mM HEPES

[Lonza], 10 μg/ mL Primocin [InvivoGen], 1× N-2 Supplement [Thermo Fisher Scientific], 1× B-27 Plus Supplement [Gibco], 0.1% BSA, 25% R-spondin-1 conditioned medium [Trevigen], 10 ng/mL mouse EGF

[PeproTech], 100 ng/mL mouse noggin [PeproTech], and 3 μM CHIR

99021 [Tocris]) with 10 μM Y-27632. Complete media was subsequently refreshed every two days. Organoids were passaged every 5–10 days by a mechanical approach using Gentle Cell Dissociation Reagent (STEMCELL).

PMX205 treatment. For all in vitro experiments, cells were treated with 10 mg/mL PMX205 (Tocris, 5196) dissolved in 20% ethanol/ water. Vehicle control in these experiments refers to 20% ethanol/ water or water alone. Cells were pretreated for 1 hour before RT.

Animal studies. For all studies, animals were randomly divided into groups using a computer-based random order generator. Blinding during data collection and analysis was carried out whenever possible. For Figure 5; Figure 6, M and N; and Supplemental Figure 6, B–F, MC38 cells (5×10^5) were injected subcutaneously into 6- to 8-weekold female C57BL/6 mice (JAX) at a single dorsal site. Animals with growing tumors (average, 80–100 mm^3) were included in the study and treated with either 9 Gy as a single dose or 3 × 4.45 Gy and either vehicle or PMX205 for the days flanking RT. For RT, mice were anesthetized in a knockdown chamber with a mixture of 3% isoflurane and 100% O_2 and placed inside the irradiator cabinet on the subject stage. Anesthesia was maintained using 1.5% isoflurane in O_2 delivered via a nose cone. The X-Rad SmART (Precision X-Ray Inc.) was used. RT was performed using an X-ray energy of 22 5kVp, a current of 13 mA, a power of 3,000 watts, and a beam filter of 0.3 mm Cu, producing a dose rate of approximately 300 cGy/min at the isocenter. Treatment X-ray beams were shaped using a 10 or 15 mm collimator to selectively irradiate the target while sparing adjacent tissue. Pretreatment CT images were acquired, using a beam energy of 40 kVp, a beam filter of 2 mm Al, and a voxel size of 0.2 or 0.1 mm. The open- source RT_ Image software package, version 3.13.1, running on IDL version 8.5.1 was used to visualize CT images and perform treatment planning (37).

Subcutaneous tumors were measured with the use of calipers, and volumes were calculated by the ellipsoid estimation method as previously described (38). Mice were euthanized as per Stanford University's Administrative Panel on Laboratory Animal Care (APLAC) guidelines in a CO_2 chamber and by cervical dislocation.

For analysis of immune populations in tumor draining lymph nodes, 5×10^5 MC38 cells were injected into the flank of 8-week-old female C57BL/6 mice. When tumors were approximately 50 mm^3 in volume, the

mice were treated via oral gavage, as described in Figure 6. Tumor-bearing mice were anesthetized with ketamine/xylazine (80 mg/Kg/10 mg/Kg), and a dose of 9 Gy was delivered using a Varian TrueBeam 2041 clinical linear accelerator.

For heterotopic AKPT organoid-derived tumor models, female C57BL/6 or athymic nude (Crl:NU(NCr)-*Foxn1*^{nu}) mice were purchased from Charles River at 5 to 6 weeks of age. AKPT organoids were suspended in a PBS and Matrigel mixture (1:1) prior to subcutaneous injection. Resulting tumors were monitored once a day, and their volume was determined from the following formula: length × width × height ×
0.52 using caliper measurements. The Gulmay Medical RS320 irradiator (300 kV, 10 mA, 1.81 Gy/min) was used for RT. For experiments shown in Figures 1 and 2, animals with growing tumors were included in the study. Once the mean tumor volume across mice was 150–200 mm^3, mice were randomly divided into groups (as described above). For the experiments shown in Figure 7, animals with growing tumors were included in the study. Once mean tumor volume for all mice reached 100 mm^3, PMX205/vehicle was delivered by oral gavage once a day for 3 days. Once tumor size reached a length by width 1.2 cm geometric mean mice were euthanized by a Schedule 1 method (in line with the UK Animals [Scientific Procedures] Act 1986 [ASPA]).

For normal tissue studies, animals with stable body weights were included in the study. Total abdominal RT of either C57BL/6 (JAX) (treated with vehicle or PMX205) or WT and C5aR1$^{-/-}$ BALBc/J (JAX) mice was performed on anesthetized animals (with the use of ketamine 100 mg/kg/xylazine 20 mg/kg) and using a 225 kVp cabinet X-ray system filtered with 0.5 mm Cu (at Comparative Medicine Unit). Total abdominal RTs were also occasionally carried out using the X-Rad SmART irradiator with the 20 mm collimator with 2 beams (0 and 180 degrees). Mice were euthanized as per Stanford University APLAC guidelines in a CO_2 chamber and by cervical dislocation.

For in vivo experiments involving PMX205 treatment, 10 mg/ kg PMX205 (Tocris, 5196, or synthesized and purified as previously described, ref. 25) was administered to mice orally. Vehicle in these experiments refers to 20% ethanol/water.

Cell cycle analysis. Cells were harvested with trypsin, washed in PBS, and fixed in 1 mL 70% ethanol. Following a 30-minute incubation on ice, cells were washed twice in PBS. Cell pellets were treated with 50 μL PureLink RNase A (Invitrogen, 12091-021, 100 μg/mL) before adding 400

μL propidium iodide solution (Invitrogen, 00-6990-50, 50 μg/ mL) in PBS. Following a 10-minute incubation at room temperature, cell cycle was analyzed with CytoFLEX Flow Cytometer (Beckman Coulter Inc.), and data analysis was performed using FlowJo Software (version 10.7.2, Tree Star Inc.).

Proliferation assays. HCT116 or MC38 cells were seeded at the indicated concentration. Cells were treated with 10 mg/mL PMX205 (or RNAse-Free water as vehicle). On day 2, cells were counted using a hemocytometer and trypan blue in a 1:1 ratio. On day 3, 10 mg/mL PMX205 (or water) was added to the dishes. On day 4, the cells were counted in the same manner as above. Number of cells were plotted normalized to the seeding density.

Immunohistochemistry. FFPE 4 μm sections of C5aR1–/– BALBc/J intestines were dewaxed in Histoclear (10 minutes × 2) followed by

rehydration in 100% ethanol (5 minutes × 2), 70% ethanol (5 minutes), and 50% ethanol (5 minutes). Sections were then stained with primary C5aR1 antibody (1:1000, Abcam, catalog ab59390) using the EnVision G2 Doublestain System (Dako) according to the manufacturer's instructions. The whole section was scanned and analyzed using the Aperio CS scanner and ImageScope analysis software (Aperio Technologies).

TUNEL assay. ApopTag (Millipore, S7100) was used to stain 4 μm FFPE small intestinal or AKPT tumor sections. Intestine stained slides were scanned with a NanoZoomer 2.0-RS Digital Slide Scanner (Hamamatsu). For small intestines, the number of $TUNEL^+$ cells per crypt (or crypts and villi) was manually counted in at least 10 fields of view per section. Stained slides for AKPT tumors were scanned with a Aperio CS scanner (Aperio Technologies), and images were analyzed with QuPath software. The tumor areas were identified on the basis of the histological structure, and the $TUNEL^+$ areas were then normalized to $hematoxylin^+$ areas to calculate the percentage of $TUNEL^+$ cancer cells.

Apoptosis assessment by morphology was carried out as previously described (39, 40) and Mendeley Data, https://data.mendeley.com).

Annexin V and propidium iodide staining. 1×10^5 to 5×10^5 cells/ condition were collected, centrifuged (400*g* for 5 minutes), and washed once with PBS. Pellets were resuspended in 500 μL Annexin V APC staining solution (Abcam, ab236215) and incubated in the dark at room temperature for 10 minutes. Samples were centrifuged (400*g* for 5 minutes), resuspended in 200 μL 50 μg/mL Propidium Iodide solution (Invitrogen, P3566) in PBS, and incubated in the dark at room temperature for 10–15 minutes. Following incubation, 200 μL PBS was added into each tube. Samples were analyzed using CytoFLEX (Beckman Coulter Inc.) and FlowJo Software.

Multiplex and HALO analysis. Multiplex immunofluorescence staining of AKPT tumors was performed on 4 μm thick FFPE sections using the OPAL protocol (Akoya Biosciences). The Leica BOND RXm autostainer (Leica Microsystems) was used to conduct this staining. Staining cycles were conducted 6 consecutive times using the following primary antibody-Opal fluorophore pairs for the immune panel: (a) Ly6G (1:300, 551459; BD Pharmingen) Opal 540; (b) CD4 (1:500, ab183685; Abcam) Opal 520; (c) CD8 (1:800, 98941; Cell Signaling) Opal 570; (d) CD68 (1:1200, ab125212; Abcam) Opal 620; (e) FoxP3 (1:400, 126553; Cell Signaling) Opal 650; and (f) E-cadherin (1:500, 3195; Cell Signaling) Opal 690. The following primary antibody-Opal fluorophore pairs were used for the stroma panel: (a) Gremlin 1 (1:750, AF956; R&D Systems) Opal 540; (b) CD34 (1:3,000, ab81289; Abcam) Opal 520; (c) CD146 (1:500, ab75769; Abcam) Opal 570; (d) SMA (1:1000, ab5694; Abcam) Opal 620; (e) Periostin (1:1000, ab227049; Abcam) Opal 690; and (f) E-cadherin (1:500, 3195; Cell Signaling) Opal 650.

Tissues sections were incubated for 1 hour in primary antibodies and detected using the BOND Polymer Refine Detection System (DS9800; Leica Biosystems) in accordance with the manufacturer's instructions, substituting DAB for the Opal fluorophores, with a 10-minute incubation time and withholding the hematoxylin step. Antigen retrieval at 100°C for 20 minutes, in accordance with standard Leica protocol, with Epitope Retrieval Solution one or two (AR9961; Leica Biosystems) was

performed prior to each primary antibody being applied. Sections were then incubated for 10 minutes with spectral DAPI (FP1490, Akoya Biosciences), and the slides were mounted with VECTASHIELD Vibrance Antifade Mounting Medium (H-170010; Vector Laboratories). Whole slide scans and multispectral images (MSI) were obtained on the Akoya Biosciences Vectra Polaris. Batch analysis of the MSIs from each case was performed with the inForm 2.4.8 software provided. Finally, batched analyzed MSIs were fused in HALO (Indica Labs) to produce a spectrally unmixed reconstructed whole-tissue image. Cell density analysis was performed for each cell phenotype across the 3 MPIF panels using HALO. HALO Image Analysis Platform version 3.5.3577 and HALO AI version 3.5.3577 (Indica Labs Inc.) were used. Analysis modules "Area Quantification 2.4.2", "HighPlex FL 4.2.3" and "Random Forest Classifier" were used.

Cover slips were lifted after multiplex staining and C5aR1 (1:1000, Abcam, catalog ab59390) was stained for chromogenically on the Leica BOND autostainer. Antigen retrieval was carried out at 100°C for 20 minutes with Epitope Retrieval Solution two. Primary antibody incubation at 1:250 dilution for 30 minutes was followed by detection using the BOND Polymer Refine Detection System (DS9800, Leica Biosystems) as per manufacturer's instructions.

Immunoblotting. Cells were lysed in UTB (9 M urea; 75 mM

TrisHCl, pH 7.5; and 0.15 M β-mercaptoethanol) and sonicated briefly before quantification, as described in detail (https://data.mendeley.com). For intestinal organoid experiments, harvesting was carried out in Corning Cell Recovery Solution at 4°C for 30 minutes. Samples were then washed with cold PBS, pelleted (700*g*, 3 minutes, 4°C), and lysed immediately in RIPA buffer (Sigma-Aldrich) containing 1:100 protease inhibitor cocktail (Sigma-Aldrich) and 1:100 phosphatase inhibitor cocktail two (Sigma-Aldrich). Proteins were quantified with the Pierce BCA Protein Assay Kit (Thermo Fisher Scientific), using a BSA standard curve (20–2,000 μg/mL).

4%–20% polyacrylamide gels (Bio-Rad) were used for protein separation. Proteins were blotted onto a nitrocellulose membrane (BioRad). The Bio-Rad Chemidoc XRS system or LI-COR Odyssey imaging system was used. In each case, experiments were carried out in triplicate, and a representative blot is shown unless otherwise stated. See supplemental material for full, uncut gels.

Antibodies used were was follows: β-actin (Sigma-Aldrich, A5441), hFAB Rhodamine Anti-Tubulin (Bio-Rad, 12004166), RelA/ p65 (Cell Signaling, 3034), pRelA/p65-S536 (Cell Signaling, 3033T), total AKT (Cell Signaling, 2920), AKT-T308 (Cell Signaling, 13038), p44/p42 (Cell Signaling, 4696), phospho p44/p42 (Cell Signaling, 4376), and

γH2AX (Millipore, 05-636-1).

RPPA. RPPA was performed by the University of Texas MD Anderson RPPA core as described in a published protocol (https:// www.mdanderson.org/research/research-resources/core-facilities/ functional-proteomics-rppa-core.html). For statistical analysis on differently expressed proteins, linearized (standard curve) normalized (to protein loading) relative protein levels were analyzed using 2-tailed Student's *t* test (t.test()) in R.

Immunofluorescence. Staining was carried out as previously described (41). For 53BPI foci studies, 53BP1 antibody (Cell Signaling

Technology, 4937) and secondary anti-Rabbit, Alexa Fluor 594 (Thermo Fisher Scientific, A32754) were used. For C5aR1-GFP overexpression studies, cells were transfected with C5AR1_OHu107216C_pcDNA3.1(+)-C-eGFP or empty vector (GenScript) using Lipofectamine 3000 as per the manufacturer's instructions (Invitrogen). 24 hours later slides were fixed in 4% PFA for 15 minutes at room temperature. Phalloidin 647 (1:1,000 dilution, A22287) was added to each coverslip and left in a 37°C oven for 1 hour in a humidified chamber. For both 53BP1 foci and C5aR1 overexpression studies, coverslips were mounted onto microscope slides using ProLong Mounting Medium with DAPI Stain (P36931, Thermo Fisher Scientific) and were imaged on the Zeiss LSM 710 Confocal Microscope.

Flow cytometry analyses. One week after RT, the mice were sacrificed and tumor draining lymph nodes were collected. Cells were incubated with anti-FcR antibody (clone 24G2) and stained with the following surface antibodies: anti-CD45.2 (clone 104, eBioscience), CD3 (clone 17A2, eBioscience), CD4 (cloneRM4-5), CD8a (clone 53- 6-7), B220 (clone RA3-6B2), CD25 (clone PC61), a-CD49b (clone DX5), anti–IFN-γ (clone XMG1.2), anti-FoxP3 (clone FJK-16s, eBioscience), anti–TNF-α (clone MP6-XT22), anti-Granzyme B (clone BG11, BioLegend). Dead cells were stained using a Fixable Viability Dye eFluor 506 (eBioscience). For cytokine staining, cells were stimulated for 4 hours with 50 ng/mL PMA and 500 ng/mL Ionomycin (Sigma-Aldrich), washed, and after surface staining, permeabilized with Cytofix/Cytoperm buffer according to manufacturer instructions. FoxP3 permeabilization buffer (eBioscience) was used for FoxP3 staining. All antibodies were purchased from BD Pharmingen unless otherwise specified. Samples were acquired with Fortessa LSR (BD Bioscience) and analyzed with FlowJo software.

For analysis of tumor immune infiltration, female C57BL/6 MC38 tumor tissue was digested into a single suspension using the murine tumor dissociation kit from Miltenyi Biotech as per the manufacturer's protocol. After RBC lysis, cells were resuspended in PBS, counted, and then stained with Zombie NIR (BioLegend) for live/dead cell discrimination. Nonspecific binding was blocked using an anti-mouse CD16/32 (BioLegend) antibody, following which, cell surface staining was performed using fluorophore-conjugated anti-mouse CD45.1 (30F11), CD11b (M1/70), CD11c (N418), Ly6G (1A8), Ly6C (HK1.4), and CD8 (53-6.7), all from Biolegend. Cell acquisition was performed with FACSDiva software on an LSR II flow cytometer (BD Biosciences) and analyzed with FlowJo software. Compensations were attained using anti- rat and anti-hamster compensation beads (BD Biosciences). For fixable live/dead staining, compensation was performed using ArC amine reactive compensation beads (BD Biosciences).

The gating schemes of dissociated tissues were as follows: immune cells ($ZNIR^{-}CD45^{+}$), CD8 T cells ($ZNIR^{-}CD45^{+}CD8^{+}$), neutrophils ($ZNIR^{-}CD45^{+}CD11b^{+}Ly6G^{+}$), and monocytes ($ZNIR^{-}CD45^{+}CD11b^{+}Ly6C^{+}$).

For C5aR1 expression analysis in cell lines, 1×10^6 cells (either HCT116 or MC38 as indicated in figures) were collected into each tube, centrifuged at 400*g* for 5 minutes, and washed once with PBS. Pellets were resuspended in 100 μL Zombie Green Fixable Viability Kit (BioLegend, 423111) or Zombie NIR (BioLegend, 423105) diluted 1:5,000 and

incubated in the dark at room temperature for 15–30 minutes. Following incubation, cells were washed once in buffer containing 0.5% BSA. Cells were resuspended in PE/Cyanine7 anti-mouse CD88 antibody (BioLegend, 135810) or BD OptiBuild BV421 Mouse Anti-Human CD88 (BD Biosciences, 742315) at 1 μg per million cells in 100 μL volume.

PE/Cyanine7 Rat IgG2b, κ Isotype Ctrl Antibody (BioLegend, 400618) and BD Horizon BV421 Mouse IgG1, k Isotype Control (BD Biosciences, 562438) were also used at 1 μg per million cells in 100 μL volume. Samples were analyzed using CytoFLEX (Beckman Coulter Inc.). Data analysis was done using FlowJo Software (version 10.7.2).

qRT-PCR. RNA was extracted using Trizol (Invitrogen/Life Technologies, 15596018). The iScript cDNA synthesis kit (Bio-Rad, 1708891) or Verso cDNA Synthesis kit (Thermo Fisher Scientific, AB- 1453/B) was used to reverse transcribe cDNA from total RNA according to manufacturer's instructions. Relative mRNA levels were calculated using the dCt methodology using a 7900HT Fast RealTime PCR System. Primers used were as follows: ACTB forward, ACATCCGCAAAGACCTCTACG, ACTB reverse, TTGCTGATCCA- CATCTGCTGG; C5AR1 forward, TCCTTCAATTATACCACCCCTGA, C5AR1 reverse, ACGCAGCGTGTTAGAAGTTTTAT; BCL2 forward, TTGCCAGCCGGAACCTATG, BCL2 reverse, CGAAGGCGACCAGCAATGATA; C5 forward, CTCCTCAGGCCATGTTCATT; C5 reverse, TCTTTTGGCTGGCTTCAAGT; 18s forward, GTGGAG- CGATTTGTCTGGTT, 18s reverse, ACGCTGAGCCAGTCAGTGTA; C5ar1 forward, ACATGGACCCCATAGATAAC, C5ar1 reverse, ACCACCGAGTAGATGATAAG; c5 forward, TACCAATGCCAACCTGGTGAAAGG, c5 reverse, TCTGCAGAACCTCTTTGCCCATGA; Bcl2 forward, GTCGCTACCGTCGTGACTTC, Bcl2 reverse, CAGA- CATGCACCTACCCAGC, Bcl2l1 forward, GACAAGGAGATGCAGGTATTGG, bcl2l1 reverse, TCCCGTAGAGATCCACAAAAGT, and Xiap1 forward, CGAGCTGGGTTTCTTTATACCG, Xiap1 reverse, GCAATTTGGGGATATTCTCCTGT.

siRNA transfection. NFKBIA (L-004765-00), RelA (L-003533-00), C5aR1 (L-005442-00), or nontargeting RNAi negative control (Scramble, D-001810-10) (all from Dharmacon) were transfected into HCT116 cells using Lipofectamine RNAiMax transfection reagent (Invitrogen, 13778075) at a final concentration of 50 nM, according to the manufacturers' instructions. Cells were harvested 72 hours after transfection.

In silico screen. Data were accessed through the DepMap portal (https://depmap.org/portal/, September 10, 2020). Essentiality scores were calculated by dividing the number of dependent cell lines for each gene/total number of cell lines in either CRISPR/Cas9 and RNAi screens. To identify stress- and cancer-specific dependencies, we looked for genes that were deemed nonessential across all cell lines (genes that when knocked out/down under baseline conditions do not alter cell survival) while still being expressed across cell lines. Genes described as complement system components, receptors, proteases, and regulators (as reported in ref. 17) were queried. The calculated essentiality score was presented as a color in the heatmap. *ATR* was included in the screen a

positive control. Target tractability was assessed by accessing CanSAR data, as displayed on the DepMap portal. A gene was only considered a hit if it was "druggable" based on structural and ligand-based assessment. C1R and CF1 were not included in the heatmap due to lack of CRISPR/Cas9 or RNAi data. C4A, C4B, VSIG4, C8A, C8B, CD93, and
CR1 were not included due to their very low expression in the majority of tissues.

RNA-Seq. Transcriptomic profiling of mouse tumor tissues was carried out by 3′RNA-Seq. Extracted RNA was quantified using RiboGreen (Invitrogen) on the FLUOstar OPTIMA plate reader (BMG Labtech), and the size profiles and integrity were analyzed on the TapeStation (Agilent, RNA ScreenTape). Libraries were prepared using the Lexogen QuantSeq 3′mRNA-Seq kit FWD kit (Lexogen, 015.2 × 96) and the Lexogen UMI Second strand synthesis module for QuantSeq FWD (Lexogen, 81.96) following the manufacturer's instructions. Individual libraries were quantified using a Qubit Fluorometer (Invitrogen), and the size profiles were analyzed on the Agilent TapeStation. Individual libraries were normalized and pooled accordingly to multiplex for sequencing. Libraries were sequenced on a NextSeq 500 instrument (Illumina) as 75 bp single-end reads.

Raw sequence reads were subjected to adapter trimming using *BBduk* (BBTools ver. 38.46) Trimmed reads were aligned to the Genome Reference Consortium mouse genome build 38 (GRCm38) of the mouse reference using *STAR* (ver. 2.7.0f). Ensembl 96 annotations were used for alignment and subsequent quantifications. Gene expression was quantified using *featureCounts* (ver. 1.6.4). Further analyses of RNA-Seq data were carried out in the R statistical environment (ver. 4.0.3). Differential expression analyses were performed using the *limma* (ver. 3.46) package. Gene set enrichment analyses (GSEA) were performed using the *fgsea* package (ver. 1.16).

Organoids RNA extraction for sequencing. Organoids were harvested by direct incubation in 350 μL RLT plus lysis buffer (Qiagen RNeasy Plus Micro kit) for 5 minutes. RNA was extracted using the Qiagen RNeasy Plus Micro kit according to the manufacturer's protocol. RNA quality and concentration were measured with Bioanalyzer 2100 (Agilent) and Nanodrop (Thermo Fisher Scientific), respectively. RNA library preparation, sequencing, and data analysis were outsourced to Novogene.

CMS in rectal tumors. The Grampian cohort profiled by the S:CORT consortium was used. Pretreatment rectal tumor biopsies from patients treated with radiotherapy and capecitabine were selected (n = 129). Xcell array data were normalized and CMS was called using the R tool CMScaller (42). Patients gave consent to biobank their samples in the Grampian Biorepository (ref no. TR000028, 1/10/2014) with release of linked anonymized clinical data for ethically approved research projects. *Analysis on longitudinal biopsies*. Patients received nCRT as part of their standard-of-care management. The gross rectal tumor and tumor involved lymph nodes were irradiated to a dose 50 Gy in 25 fractions, and pelvis nodes to a dose of 45 Gy in 25 fractions, over 5 weeks, concurrently with capecitabine chemotherapy at 900 mg/m^2. Patients underwent sigmoidoscopy at the described time points with direct visualization and biopsies of the tumor.

RNA-Seq of longitudinal biopsies. The Partek Flow server was used to process FASTQ files by adapter trimming, quality control alignment

to the genome, and abundance estimation. R version 4.1.2. was used to perform all exploratory analysis. R package "DESeq2" was used to calculate differentially expressed genes between baseline and after treatment time points (43). Genes with *P* values of less than 0.05 were considered significantly different between time points, and a positive $\log_2$ fold change was indicative of a gene with greater expression after the start of treatment. Differentially expressed genes were visualized using a custom volcano plot produced using "ggplot2"; complement- associated genes were annotated on the volcano plot (17). Genes ranked by Wald statistic were used to perform pairwise GSEA using the "fgsea" package, mSigDB Hallmark signature set, and the complement signature from Ricklin et al. 2010 (17, 44, 45). To gauge the relative enrichment of the "Hallmark Complement" gene set, the signatures within the mSigDB Hallmark set were ranked by normalized enrichment score.

Staining and analysis of longitudinal biopsies. C5aR1 staining was performed as above. For analysis, the Indica Labs HALO image analysis software (v3.6.4134.137 and HALO AI 3.6.4134) was used. Sections were manually annotated by a trained pathologist as cancer, normal/reactive, or ulcer/granulation tissue. DenseNet V2 (HALO AI) was then "taught" to discriminate among epithelium, stroma, and glass. Within each annotation region, stroma and epithelium tissue compartments were analyzed separately for (a) general tissue DAB intensity using "Indica Labs Area Quantification v2.4.2" and (b) cell localized DAB intensity using "Indica Labs Multiplex IHC v3.4.9." Both analyses yielded the same overall results. H-scores are presented in this manuscript.

Statistics. Statistical analysis was carried out using Graphpad Prism software (version 9.2.0). *P* values were used to determine significance of differences, and *P* values of less than 0.05 were considered significant. Two-tailed Student's *t* test and 1- or 2-way ANOVA were used as appropriate and as specified in each figure legend.

Study approval. This study involved human participants, and all samples were obtained following individual informed consent for research projects and subsequent ethical approval by the National Research Ethics Service in the UK (REC ref. 15/EE/0241, IRAS ref 169363, and REC ref 18WS00031). Experimental procedures were carried out under a project license issued by the UK Home Office under the UK Animals (Scientific Procedures) Act of 1986; under approved protocols by the Institutional Animal Care and Use Committee at Medical University of South Carolina; or in accordance with the NIH guidelines for the use and care of live animals (approved by the Stanford University Institutional Animal Care and Use Committee). Animal Research Reporting of In vivo Experiments guidelines were used.

Data availability. The RNA-Seq data generated for this paper have been deposited at the ArrayExpress database at EMBL-EBI (https:// www.ebi.ac.uk/biostudies/arrayexpress) and are publicly available. The data from the time-course study after radiation treatment of heterotopic AKPT organoid-derived tumors are available under accession E-MTAB-12538, and the data from the intestinal organoids treated with PMX205 and/or RT are available under accession E-MTAB-12548. Publicly available data were analyzed in this paper. The analysis of WT, AKPT, and KPN intestinal organoids used data deposited at the ArrayExpress database under accession E-MTAB-11769 (46). Underlying data can also be accessed in the Supporting Data Values file or from the corresponding author upon request.

Author contributions

CB, D MacLean, D Majorova, SM, DKN, RKK, SG, GNV, MDD,
TS, AE, DJ, YJ, ED, and MMO provided methodology. MMO wrote the original draft of the manuscript. MMO, D MacLean, AJG, DKN, SG, GNV, MDD, AE, ED, EJM, YJ, SJAB, MS, SJL, QTL, TMW,
and SMO reviewed and edited the manuscript. MMO and AJG conceptualized the study. CB, D MacLean, D Majorova, SM, DKN, RKK, SG, CK, GNV, TS, MDD, ED, YJ, EJM, DJ, AKM, KP, and
MMO provided investigation. MMO, DKN,
RKK, CB, D MacLean, D Majorova, ED, DJ, SG, GNV, LVSH, and RKM provided formal analysis. MMO, AJG, TMW, SJAB, SJL, QTL, EGG, SG, ACK, CSR, and MS provided resources. MMO, AJG, SJL, TM, QTL, SMO, JE, and CSR provided supervision.

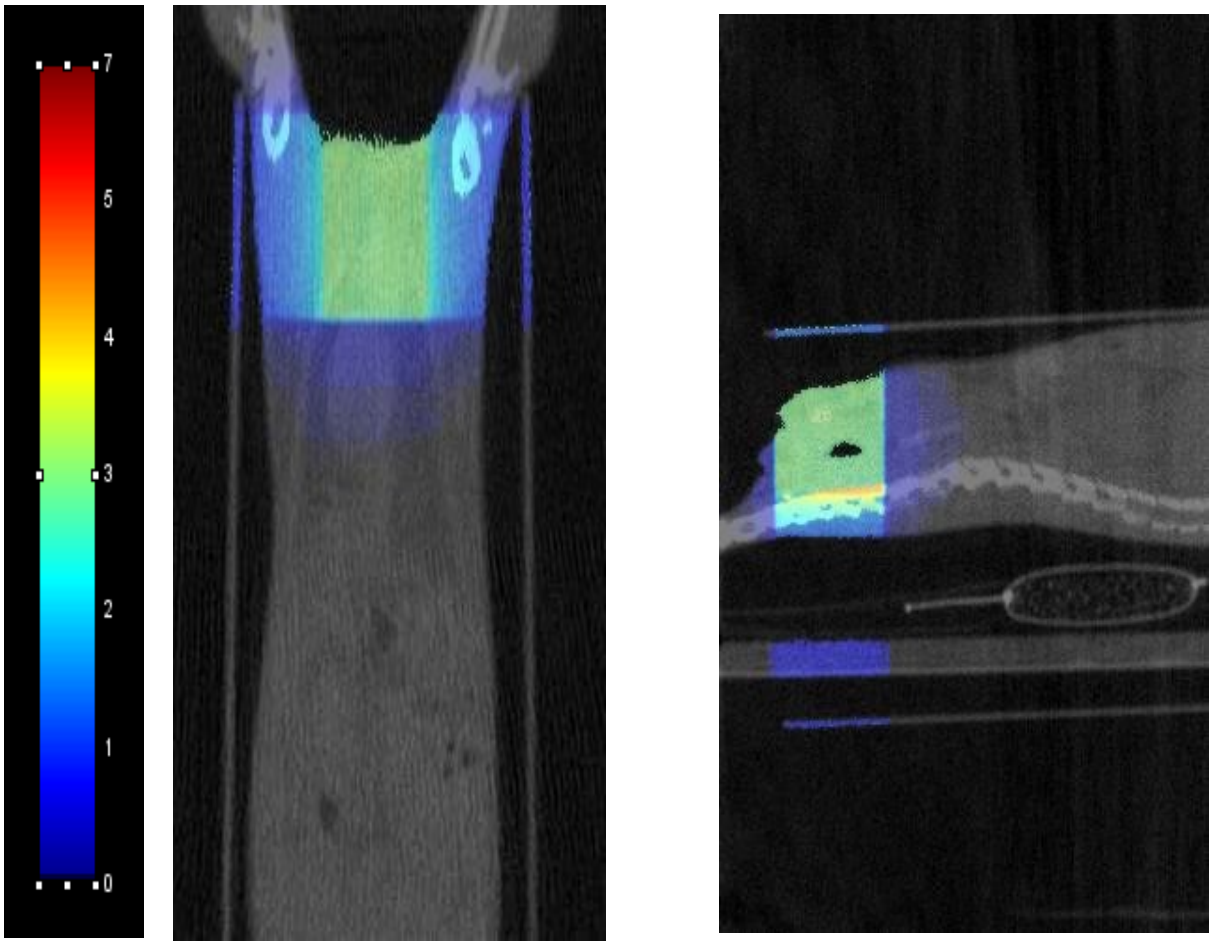
MMO, AJG, SJL, CSR, and MS acquired funding. Co–first authors are listed in alphabetical order.

Acknowledgments

This work was supported by the Medical Research Council (MRC) (MC_UU_00001/10); NIH grants CA257907-01A1, CA-67166, and
CA-197713; the Silicon Valley Foundation; the Sydney Frank Foundation and the Kimmelman Fund (to AJG); the Academy of Medical Sciences (AMS); the Wellcome Trust; the Government Department of Business, Energy and Industrial Strategy; the British Heart Foundation and Diabetes UK through an AMS Springboard (ref SBF008/1156, awarded to MMO); the Gray
Trust; Cancer Research UK grant C5255/A18085, through the Cancer Research UK Oxford Centre and the Beatson Cancer Charity. MMO was a Cancer Research Institute Irvington Fellow, supported by the Cancer Research Institute and Stiftung für Forschung, Medical Faculty, UZH. This research was also supported by an International Accelerator Award, ACRCelerate, jointly funded by Cancer Research UK (A26825 and A28223), FC AECC (GEACC18004TAB), and
AIRC (22795). This research was also supported by MRC funding (MC_PC_21042). TS is supported by Takeda Science Foundation and the British Council Japan Association Scholarship Scheme. RKK was supported by Stanford ChEM-H Undergraduate Scholars Program. MS and MMO were supported by a project grant from the Swiss National Foundation (31003A_163141). ED is supported by the S:CORT Consortium, which is funded by a grant from the MRC and CR-UK. TMW is supported by a fellowship from the National Health and Medical Research Council (2009957). CSR is funded by a CSO fellowship. QTL, DKN, AJG, EJM, YJ, and MMO are supported by NIH grant 1P01CA257907. QTL and DKN are supported by NIH grant 1R01DE029672. We would also like to acknowledge the Tissue Histopathology Laboratory (University of Oxford) and, in particular, Leticia Campo Urriza and Molly Browne.

Appendix B

CT scan treatment planning to aim radiation dose to rectum in orthotopic AKPT model



Radiation (Gy)

Radiation delivered in an arc rotating -180° to 180°. Mice inverted, and biological landmarks used to focus radiation toward the rectum containing orthotopic AKPT tumours. Landmarks included spine vertebrate and the bladder.

References

Adjemian, S., Oltean, T., Martens, S., Wiernicki, B., Goossens, V., Vanden Berghe, T., Cappe, B., Ladik, M., Riquet, F. B., Heyndrickx, L., Bridelance, J., Vuylsteke, M., Vandecasteele, K., & Vandenabeele, P. (2020). Ionizing radiation results in a mixture of cellular outcomes including mitotic catastrophe, senescence, methuosis, and iron-dependent cell death. *Cell Death & Disease*, *11*(11), 1003. https://doi.org/10.1038/s41419-020-03209-y

Aguirre, J. E., Beswick, E. J., Grim, C., Uribe, G., Tafoya, M., Chacon Palma, G., Samedi, V., McKee, R., Villeger, R., Fofanov, Y., Cong, Y., Yochum, G., Koltun, W., Powell, D., & Pinchuk, I. V. (2019). Matrix metalloproteinases cleave membrane-bound PD-L1 on CD90+ (myo-)fibroblasts in Crohn's disease and regulate Th1/Th17 cell responses. *International Immunology*, *32*(1), 57–68. https://doi.org/10.1093/intimm/dxz060

Ajona, D., Ortiz-Espinosa, S., & Pio, R. (2019). Complement anaphylatoxins C3a and C5a: Emerging roles in cancer progression and treatment. *Seminars in Cell & Developmental Biology*, *85*, 153–163. https://doi.org/10.1016/j.semcdb.2017.11.023

Alcindor, T., & Beauger, N. (2011). Oxaliplatin: A review in the era of molecularly targeted therapy. *Current Oncology*, *18*(1), 18–25.

Alderdice, M., Richman, S. D., Gollins, S., Stewart, J. P., Hurt, C., Adams, R., McCorry, A. M., Roddy, A. C., Vimalachandran, D., Isella, C., Medico, E., Maughan, T., McArt, D. G., Lawler, M., & Dunne, P. D. (2018). Prospective patient stratification into robust cancer-cell intrinsic subtypes from colorectal cancer biopsies. *The Journal of Pathology*, *245*(1), 19–28. https://doi.org/10.1002/path.5051

Al-Mterin, M. A., Murshed, K., Alsalman, A., Abu-Dayeh, A., & Elkord, E. (2022). Associations of different immune checkpoints-expressing CD4+ Treg/ T cell subsets with disease-free survival in colorectal cancer patients. *BMC Cancer*, *22*(1), 601. https://doi.org/10.1186/s12885-022-09710-1

Althumairi, A. A., & Gearhart, S. L. (2015). Local excision for early rectal cancer: Transanal endoscopic microsurgery and beyond. *Journal of Gastrointestinal Oncology*, *6*(3), 296–306. https://doi.org/10.3978/j.issn.2078-6891.2015.022

Antonia, S. J., Villegas, A., Daniel, D., Vicente, D., Murakami, S., Hui, R., Yokoi, T., Chiappori, A., Lee, K. H., de Wit, M., Cho, B. C., Bourhaba, M., Quantin, X., Tokito, T., Mekhail, T., Planchard, D., Kim, Y.-C., Karapetis, C. S., Hiret, S., … PACIFIC Investigators. (2017b). Durvalumab after Chemoradiotherapy in Stage III Non-Small-Cell Lung Cancer. *The New England Journal of Medicine*, *377*(20), 1919–1929. https://doi.org/10.1056/NEJMoa1709937

Appelt, A. L., Pløen, J., Vogelius, I. R., Bentzen, S. M., & Jakobsen, A. (2013). Radiation dose-response model for locally advanced rectal cancer after pre-operative chemoradiotherapy. *International Journal of Radiation Oncology, Biology, Physics*, *85*(1), 74–80. https://doi.org/10.1016/j.ijrobp.2012.05.017

Aristin Revilla, S., Kranenburg, O., & Coffer, P. J. (2022a). Colorectal Cancer-Infiltrating Regulatory T Cells: Functional Heterogeneity, Metabolic Adaptation, and Therapeutic Targeting. *Frontiers in Immunology*, *13*. https://www.frontiersin.org/articles/10.3389/fimmu.2022.903564

Aschele, C., Cionini, L., Lonardi, S., Pinto, C., Cordio, S., Rosati, G., Artale, S., Tagliagambe, A., Ambrosini, G., Rosetti, P., Bonetti, A., Negru, M. E., Tronconi, M. C., Luppi, G., Silvano, G., Corsi, D. C., Bochicchio, A. M., Chiaulon, G., Gallo, M., & Boni, L. (2011). Primary tumor response to preoperative chemoradiation with or without oxaliplatin in locally advanced rectal cancer: Pathologic results of the STAR-01 randomized phase III trial. *Journal of Clinical Oncology: Official Journal of the American Society of Clinical Oncology*, *29*(20), 2773–2780. https://doi.org/10.1200/JCO.2010.34.4911

Aubert, M., Mege, D., & Panis, Y. (2020). Total mesorectal excision for low and middle rectal cancer: Laparoscopic versus transanal approach-a meta-analysis. *Surgical Endoscopy*, *34*(9), 3908–3919. https://doi.org/10.1007/s00464-019-07160-8

Azwar, S., Seow, H. F., Abdullah, M., Faisal Jabar, M., & Mohtarrudin, N. (2021). Recent Updates on Mechanisms of Resistance to 5-Fluorouracil and Reversal Strategies in Colon Cancer Treatment. *Biology*, *10*(9), Article 9. https://doi.org/10.3390/biology10090854

Baba, A. B., Rah, B., Bhat, G. R., Mushtaq, I., Parveen, S., Hassan, R., Hameed Zargar, M., & Afroze, D. (2022). Transforming Growth Factor-Beta (TGF-β) Signaling in Cancer-A Betrayal Within. *Frontiers in Pharmacology*, *13*. https://doi.org/10.3389/fphar.2022.791272

Bahadoer, R. R., Dijkstra, E. A., Etten, B. van, Marijnen, C. A. M., Putter, H., Kranenbarg, E. M.-K., Roodvoets, A. G. H., Nagtegaal, I. D., Beets-Tan, R. G. H., Blomqvist, L. K., Fokstuen, T., Tije, A. J. ten, Capdevila, J., Hendriks, M. P., Edhemovic, I., Cervantes, A., Nilsson, P. J., Glimelius, B., Velde, C. J. H. van de, … Silviera, M. L. (2021). Short-course radiotherapy followed by chemotherapy before total mesorectal excision (TME) versus preoperative chemoradiotherapy, TME, and optional adjuvant chemotherapy in locally advanced rectal cancer (RAPIDO): A randomised, open-label, phase 3 trial. *The Lancet Oncology*, *22*(1), 29–42. https://doi.org/10.1016/S1470-2045(20)30555-6

Bailey, C. E., Hu, C.-Y., You, Y. N., Bednarski, B. K., Rodriguez-Bigas, M. A., Skibber, J. M., Cantor, S. B., & Chang, G. J. (2015). Increasing Disparities in Age-Related Incidence of Colon and Rectal Cancer in the United States, 1975-2010. *JAMA Surgery*, *150*(1), 17–22. https://doi.org/10.1001/jamasurg.2014.1756

Baker, L., Robinson, N., Wilson, D., Tabaqchali, M., & Leaper, D. (2019). Vascular endothelial growth factor in colorectal cancer pathology, survival and treatment. *Annals of Oncology*, *30*, v12. https://doi.org/10.1093/annonc/mdz238.039

Balogh, A., Persa, E., Bogdándi, E. N., Benedek, A., Hegyesi, H., Sáfrány, G., & Lumniczky, K. (2013). The effect of ionizing radiation on the homeostasis and functional integrity of murine splenic regulatory T cells. *Inflammation Research: Official Journal of the European Histamine Research Society ... [et Al.]*, *62*(2), 201–212. https://doi.org/10.1007/s00011-012-0567-y

Bang, A., Wilhite, T. J., Pike, L. R. G., Cagney, D. N., Aizer, A. A., Taylor, A., Spektor, A., Krishnan, M., Ott, P. A., Balboni, T. A., Hodi, F. S., & Schoenfeld, J. D. (2017). Multicenter Evaluation of the Tolerability of Combined Treatment With PD-1 and CTLA-4 Immune Checkpoint Inhibitors and Palliative Radiation Therapy. *International Journal of Radiation Oncology, Biology, Physics*, *98*(2), 344–351. https://doi.org/10.1016/j.ijrobp.2017.02.003

Bao, S., Jiang, X., Jin, S., Tu, P., & Lu, J. (2021). TGF-β1 Induces Immune Escape by Enhancing PD-1 and CTLA-4 Expression on T Lymphocytes in Hepatocellular Carcinoma. *Frontiers in Oncology*, *11*. https://www.frontiersin.org/articles/10.3389/fonc.2021.694145

Barker, H. E., Paget, J. T. E., Khan, A. A., & Harrington, K. J. (2015). The Tumour Microenvironment after Radiotherapy: Mechanisms of Resistance and Recurrence. *Nature Reviews. Cancer*, *15*(7), 409–425. https://doi.org/10.1038/nrc3958

Bashir, M., Damineni, S., Mukherjee, G., & Kondaiah, P. (2015). Activin-A signaling promotes epithelial–mesenchymal transition, invasion, and metastatic growth of breast cancer. *NPJ Breast Cancer*, *1*, 15007. https://doi.org/10.1038/npjbcancer.2015.7

Baskar, R. (2010a). Emerging role of radiation induced bystander effects: Cell communications and carcinogenesis. *Genome Integrity*, *1*(1), 13. https://doi.org/10.1186/2041-9414-1-13

Battaglia, A., Buzzonetti, A., Baranello, C., Fanelli, M., Fossati, M., Catzola, V., Scambia, G., & Fattorossi, A. (2013). Interleukin-21 (IL-21) synergizes with IL-2 to enhance T-cell receptor-induced human T-cell proliferation and counteracts IL-2/transforming growth factor-β-induced regulatory T-cell development. *Immunology*, *139*(1), 109–120. https://doi.org/10.1111/imm.12061

Bazarbashi, S., Omar, A., Aljubran, A., Alzahrani, A., Alsanea, N., Abduljabbar, A., Alhomoud, S., Ashari, L., Balaraj, K., Soudy, H., Neimatallah, M., & Fagih, M. (2016). Pre-operative chemoradiotherapy using capecitabine and cetuximab followed by definitive surgery in patients with operable rectal cancer. *Hematology/Oncology and Stem Cell Therapy*, *9*(4), 147–153. https://doi.org/10.1016/j.hemonc.2016.08.004

Beach, C., MacLean, D., Majorova, D., Arnold, J. N., & Olcina, M. M. (2022a). The effects of radiation therapy on the macrophage response in cancer. *Frontiers in Oncology*, *12*. https://doi.org/10.3389/fonc.2022.1020606

Beach, C., MacLean, D., Majorova, D., Melemenidis, S., Nambiar, D. K., Kim, R. K., Valbuena, G. N., Guglietta, S., Krieg, C., Darvish-Damavandi, M., Suwa, T., Easton, A., Hillson, L.

V. S., McCulloch, A. K., McMahon, R. K., Pennel, K., Edwards, J., O'Cathail, S. M., Roxburgh, C. S., … Olcina, M. M. (2023a). Improving radiotherapy in immunosuppressive microenvironments by targeting complement receptor C5aR1. *The Journal of Clinical Investigation*, *133*(23). https://doi.org/10.1172/JCI168277

Beach, C., Mul, E., Belnoue-Davis, H., Valbuena, G., Molino, M. O. del, Maughan, T., & Leedham, S. (2022). O40 Impact of TGFβ inhibition and radiotherapy in a heterotopic rectal cancer mouse model. *Gut*, *71*(Suppl 1), A24–A24. https://doi.org/10.1136/gutjnl-2022-BSG.40

Becherini, C., Lancia, A., Detti, B., Lucidi, S., Scartoni, D., Ingrosso, G., Carnevale, M. G., Roghi, M., Bertini, N., Orsatti, C., Mangoni, M., Francolini, G., Marani, S., Giacomelli, I., Loi, M., Pergolizzi, S., Bonzano, E., Aristei, C., & Livi, L. (2023). Modulation of tumor-associated macrophage activity with radiation therapy: A systematic review. *Strahlentherapie Und Onkologie*, *199*(12), 1173–1190. https://doi.org/10.1007/s00066-023-02097-3

Becht, E., de Reyniès, A., Giraldo, N. A., Pilati, C., Buttard, B., Lacroix, L., Selves, J., Sautès-Fridman, C., Laurent-Puig, P., & Fridman, W. H. (2016). Immune and Stromal Classification of Colorectal Cancer Is Associated with Molecular Subtypes and Relevant for Precision Immunotherapy. *Clinical Cancer Research: An Official Journal of the American Association for Cancer Research*, *22*(16), 4057–4066. https://doi.org/10.1158/1078-0432.CCR-15-2879

Bonavita, E., Gentile, S., Rubino, M., Maina, V., Papait, R., Kunderfranco, P., Greco, C., Feruglio, F., Molgora, M., Laface, I., Tartari, S., Doni, A., Pasqualini, F., Barbati, E., Basso, G., Galdiero, M. R., Nebuloni, M., Roncalli, M., Colombo, P., … Mantovani, A. (2015). PTX3 Is an Extrinsic Oncosuppressor Regulating Complement-Dependent Inflammation in Cancer. *Cell*, *160*(4), 700–714. https://doi.org/10.1016/j.cell.2015.01.004

Bose, D., Banerjee, S., Chatterjee, N., Das, S., Saha, M., & Saha, K. D. (2019). Inhibition of TGF-β induced lipid droplets switches M2 macrophages to M1 phenotype. *Toxicology in Vitro*, *58*, 207–214. https://doi.org/10.1016/j.tiv.2019.03.037

Brisset, M., Mehlen, P., Meurette, O., & Hollande, F. (2023). Notch receptor/ligand diversity: Contribution to colorectal cancer stem cell heterogeneity. *Frontiers in Cell and Developmental Biology*, *11*, 1231416. https://doi.org/10.3389/fcell.2023.1231416

Budhu, S., Schaer, D. A., Li, Y., Toledo-Crow, R., Panageas, K., Yang, X., Zhong, H., Houghton, A. N., Silverstein, S. C., Merghoub, T., & Wolchok, J. D. (2017). Blockade of surface-bound TGF-β on regulatory T cells abrogates suppression of effector T cell function in the tumor microenvironment. *Science Signaling*, *10*(494), eaak9702. https://doi.org/10.1126/scisignal.aak9702

Bujko, K., Nowacki, M. P., Nasierowska-Guttmejer, A., Michalski, W., Bebenek, M., & Kryj, M. (2006). Long-term results of a randomized trial comparing preoperative short-course radiotherapy with preoperative conventionally fractionated chemoradiation for rectal cancer. *The British Journal of Surgery*, *93*(10), 1215–1223. https://doi.org/10.1002/bjs.5506

Bujko, K., Wyrwicz, L., Rutkowski, A., Malinowska, M., Pietrzak, L., Kryński, J., Michalski, W., Olędzki, J., Kuśnierz, J., Zając, L., Bednarczyk, M., Szczepkowski, M., Tarnowski, W., Kosakowska, E., Zwoliński, J., Winiarek, M., Wiśniowska, K., Partycki, M., Bęczkowska, K., … Polish Colorectal Study Group. (2016). Long-course oxaliplatin-based preoperative chemoradiation versus 5 × 5 Gy and consolidation chemotherapy for cT4 or fixed cT3 rectal cancer: Results of a randomized phase III study. *Annals of Oncology: Official Journal of the European Society for Medical Oncology*, *27*(5), 834–842. https://doi.org/10.1093/annonc/mdw062

Burnette, B., Liang, H., Lee, Y., Chlewicki, L., Khodarev, N. N., Weichselbaum, R. R., Fu, Y.-X., & Auh, S. L. (2011). The Efficacy of Radiotherapy Relies Upon Induction of Type I Interferon-Dependent Innate and Adaptive Immunity. *Cancer Research*, *71*(7), 2488–2496. https://doi.org/10.1158/0008-5472.CAN-10-2820

Byun, H. K., & Koom, W. S. (2023). A practical review of watch-and-wait approach in rectal cancer. *Radiation Oncology Journal*, *41*(1), 4–11. https://doi.org/10.3857/roj.2023.00038

C5aR is frequently expressed in metastatic renal cell carcinoma and plays a crucial role in cell invasion via the ERK and PI3 kinase pathways. (n.d.). Retrieved 11 December 2023, from https://www.spandidos-publications.com/or/33/4/1844

Calon, A., Lonardo, E., Berenguer-Llergo, A., Espinet, E., Hernando-Momblona, X., Iglesias, M., Sevillano, M., Palomo-Ponce, S., Tauriello, D. V. F., Byrom, D., Cortina, C., Morral, C., Barceló, C., Tosi, S., Riera, A., Attolini, C. S.-O., Rossell, D., Sancho, E., & Batlle, E. (2015). Stromal gene expression defines poor-prognosis subtypes in colorectal cancer. *Nature Genetics*, *47*(4), 320–329. https://doi.org/10.1038/ng.3225

Cancer Genome Atlas Network. (2012). Comprehensive molecular characterization of human colon and rectal cancer. *Nature*, *487*(7407), 330–337. https://doi.org/10.1038/nature11252

Cerami, E., Gao, J., Dogrusoz, U., Gross, B. E., Sumer, S. O., Aksoy, B. A., Jacobsen, A., Byrne, C. J., Heuer, M. L., Larsson, E., Antipin, Y., Reva, B., Goldberg, A. P., Sander, C., & Schultz, N. (2012). The cBio cancer genomics portal: An open platform for exploring multidimensional cancer genomics data. *Cancer Discovery*, *2*(5), 401–404. https://doi.org/10.1158/2159-8290.CD-12-0095

Cercek, A., Lumish, M., Sinopoli, J., Weiss, J., Shia, J., Lamendola-Essel, M., El Dika, I. H., Segal, N., Shcherba, M., Sugarman, R., Stadler, Z., Yaeger, R., Smith, J. J., Rousseau, B., Argiles, G., Patel, M., Desai, A., Saltz, L. B., Widmar, M., … Diaz, L. A. (2022). PD-1 Blockade in Mismatch Repair–Deficient, Locally Advanced Rectal Cancer. *New England Journal of Medicine*, *386*(25), 2363–2376. https://doi.org/10.1056/NEJMoa2201445

Charan, J., & Kantharia, N. D. (2013). How to calculate sample size in animal studies? *Journal of Pharmacology & Pharmacotherapeutics*, *4*(4), 303–306. https://doi.org/10.4103/0976-500X.119726

Chen, H. H. W., & Kuo, M. T. (2017). Improving radiotherapy in cancer treatment: Promises and challenges. *Oncotarget*, *8*(37), 62742–62758. https://doi.org/10.18632/oncotarget.18409

Chen, H., Xu, L., Li, L., Liu, X., Gao, J., & Bai, Y. (2018). Inhibiting the CD8+ T cell infiltration in the tumor microenvironment after radiotherapy is an important mechanism of radioresistance. *Scientific Reports*, *8*, 11934. https://doi.org/10.1038/s41598-018-30417-6

Chen, M.-L., Pittet, M. J., Gorelik, L., Flavell, R. A., Weissleder, R., von Boehmer, H., & Khazaie, K. (2005). Regulatory T cells suppress tumor-specific CD8 T cell cytotoxicity through TGF-beta signals in vivo. *Proceedings of the National Academy of Sciences of the United States of America*, *102*(2), 419–424. https://doi.org/10.1073/pnas.0408197102

Chen, Q., Sun, L., & Chen, Z. J. (2016). Regulation and function of the cGAS-STING pathway of cytosolic DNA sensing. *Nature Immunology*, *17*(10), 1142–1149. https://doi.org/10.1038/ni.3558

Chen, W. (2023). TGF-β Regulation of T Cells. *Annual Review of Immunology*, *41*(1), 483–512. https://doi.org/10.1146/annurev-immunol-101921-045939

Chen, W., Jin, W., Hardegen, N., Lei, K.-J., Li, L., Marinos, N., McGrady, G., & Wahl, S. M. (2003). Conversion of peripheral CD4+CD25- naive T cells to CD4+CD25+ regulatory T cells by TGF-beta induction of transcription factor Foxp3. *The Journal of Experimental Medicine*, *198*(12), 1875–1886. https://doi.org/10.1084/jem.20030152

Chen, Y., Zhao, H., Feng, Y., Ye, Q., Hu, J., Guo, Y., & Feng, Y. (2021). Pan-Cancer Analysis of the Associations of TGFBI Expression With Prognosis and Immune Characteristics. *Frontiers in Molecular Biosciences*, *8*, 745649. https://doi.org/10.3389/fmolb.2021.745649

Chiavarina, B., Costanza, B., Ronca, R., Blomme, A., Rezzola, S., Chiodelli, P., Giguelay, A., Belthier, G., Doumont, G., Van Simaeys, G., Lacroix, S., Yokobori, T., Erkhem-Ochir, B., Balaguer, P., Cavailles, V., Fabbrizio, E., Di Valentin, E., Gofflot, S., Detry, O., … Turtoi, A. (2021). Metastatic colorectal cancer cells maintain the TGFβ program and use TGFBI to fuel angiogenesis. *Theranostics*, *11*(4), 1626–1640. https://doi.org/10.7150/thno.51507

Chiriva-Internati, M., Grizzi, F., Pinkston, J., Morrow, K. J., D'Cunha, N., Frezza, E. E., Muzzio, P. C., Kast, W. M., & Cobos, E. (2006). Gamma-radiation upregulates MHC class I/II and ICAM-I molecules in multiple myeloma cell lines and primary tumors. *In Vitro Cellular & Developmental Biology. Animal*, *42*(3–4), 89–95. https://doi.org/10.1290/0508054.1

Cho, M. Y., Siegel, D. A., Demb, J., Richardson, L. C., & Gupta, S. (2022). Increasing Colorectal Cancer Incidence Before and After Age 50: Implications for Screening Initiation and Promotion of "On-Time" Screening. *Digestive Diseases and Sciences*, *67*(8), 4086–4091. https://doi.org/10.1007/s10620-021-07213-w

Clayton, S. W., Ban, G. I., Liu, C., & Serra, R. (2020). Canonical and noncanonical TGF-β signaling regulate fibrous tissue differentiation in the axial skeleton. *Scientific Reports*, *10*(1), Article 1. https://doi.org/10.1038/s41598-020-78206-4

Coates, P. J., Rundle, J. K., Lorimore, S. A., & Wright, E. G. (2008). Indirect macrophage responses to ionizing radiation: Implications for genotype-dependent bystander signaling. *Cancer Research*, *68*(2), 450–456. https://doi.org/10.1158/0008-5472.CAN-07-3050

Cohen, J. (1988). *Statistical Power Analysis for the Behavioral Sciences* (2nd ed.). Routledge. https://doi.org/10.4324/9780203771587

Cohen–Jonathan, E., Bernhard, E. J., & McKenna, W. G. (1999). How does radiation kill cells? *Current Opinion in Chemical Biology*, *3*(1), 77–83. https://doi.org/10.1016/S1367-5931(99)80014-3

Cordes, N., & Meineke, V. (2004). Integrin signalling and the cellular response to ionizing radiation. *Journal of Molecular Histology*, *35*(3), 327–337. https://doi.org/10.1023/b:hijo.0000032364.43566.3a

Cornel, A. M., Mimpen, I. L., & Nierkens, S. (2020). MHC Class I Downregulation in Cancer: Underlying Mechanisms and Potential Targets for Cancer Immunotherapy. *Cancers*, *12*(7), 1760. https://doi.org/10.3390/cancers12071760

Daugan, M. V., Revel, M., Russick, J., Dragon-Durey, M.-A., Gaboriaud, C., Robe-Rybkine, T., Poillerat, V., Grunenwald, A., Lacroix, G., Bougouin, A., Meylan, M., Verkarre, V., Oudard, S. M., Mejean, A., Vano, Y. A., Perkins, G., Validire, P., Cathelineau, X., Sanchez-Salas, R., … Roumenina, L. T. (2021). Complement C1s and C4d as Prognostic Biomarkers in Renal Cancer: Emergence of Noncanonical Functions of C1s. *Cancer Immunology Research*, *9*(8), 891–908. https://doi.org/10.1158/2326-6066.CIR-20-0532

D'Costa, Z., Jones, K., Azad, A., van Stiphout, R., Lim, S. Y., Gomes, A. L., Kinchesh, P., Smart, S. C., Gillies McKenna, W., Buffa, F. M., Sansom, O. J., Muschel, R. J., O'Neill, E., & Fokas, E. (2017). Gemcitabine-Induced TIMP1 Attenuates Therapy Response and Promotes Tumor Growth and Liver Metastasis in Pancreatic Cancer. *Cancer Research*, *77*(21), 5952–5962. https://doi.org/10.1158/0008-5472.CAN-16-2833

de Andrade Carvalho, H., & Villar, R. C. (2018). Radiotherapy and immune response: The systemic effects of a local treatment. *Clinics*, *73*(Suppl 1), e557s. https://doi.org/10.6061/clinics/2018/e557s

de Bruijn, I., Kundra, R., Mastrogiacomo, B., Tran, T. N., Sikina, L., Mazor, T., Li, X., Ochoa, A., Zhao, G., Lai, B., Abeshouse, A., Baiceanu, D., Ciftci, E., Dogrusoz, U., Dufilie, A., Erkoc, Z., Garcia Lara, E., Fu, Z., Gross, B., … Schultz, N. (2023). Analysis and Visualization of Longitudinal Genomic and Clinical Data from the AACR Project GENIE Biopharma Collaborative in cBioPortal. *Cancer Research*, *83*(23), 3861–3867. https://doi.org/10.1158/0008-5472.CAN-23-0816

Demaria, S., Coleman, C. N., & Formenti, S. C. (2016). Radiotherapy: Changing the Game in Immunotherapy. *Trends in Cancer*, *2*(6), 286–294. https://doi.org/10.1016/j.trecan.2016.05.002

Demaria, S., Guha, C., Schoenfeld, J., Morris, Z., Monjazeb, A., Sikora, A., Crittenden, M., Shiao, S., Khleif, S., Gupta, S., Formenti, S. C., Vikram, B., Coleman, C. N., & Ahmed, M. M. (2021). Radiation dose and fraction in immunotherapy: One-size regimen does not fit all settings, so how does one choose? *Journal for Immunotherapy of Cancer*, *9*(4), e002038. https://doi.org/10.1136/jitc-2020-002038

Demyan, L., Habowski, A. N., Plenker, D., King, D. A., Standring, O. J., Tsang, C., St Surin, L., Rishi, A., Crawford, J. M., Boyd, J., Pasha, S. A., Patel, H., Galluzzo, Z., Metz, C., Gregersen, P. K., Fox, S., Valente, C., Abadali, S., Matadial-Ragoo, S., … Weiss, M. J. (2022). Pancreatic Cancer Patient-derived Organoids Can Predict Response to Neoadjuvant Chemotherapy. *Annals of Surgery*, *276*(3), 450–462. https://doi.org/10.1097/SLA.0000000000005558

Deng, X., Ao, S., Hou, J., Li, Z., Lei, Y., & Lyu, G. (2019). Prognostic significance of periostin in colorectal cancer. *Chinese Journal of Cancer Research*, *31*(3), 547–556. https://doi.org/10.21147/j.issn.1000-9604.2019.03.16

Deng, Y., Chi, P., Lan, P., Wang, L., Chen, W., Cui, L., Chen, D., Cao, J., Wei, H., Peng, X., Huang, Z., Cai, G., Zhao, R., Huang, Z., Xu, L., Zhou, H., Wei, Y., Zhang, H., Zheng, J., … Wang, J. (2016). Modified FOLFOX6 With or Without Radiation Versus Fluorouracil and Leucovorin With Radiation in Neoadjuvant Treatment of Locally Advanced Rectal Cancer: Initial Results of the Chinese FOWARC Multicenter, Open-Label, Randomized

Three-Arm Phase III Trial. *Journal of Clinical Oncology: Official Journal of the American Society of Clinical Oncology*, *34*(27), 3300–3307. https://doi.org/10.1200/JCO.2016.66.6198

Ding, H., Chen, J., Qin, J., Chen, R., & Yi, Z. (2021). TGF-β-induced α-SMA expression is mediated by C/EBPβ acetylation in human alveolar epithelial cells. *Molecular Medicine*, *27*(1), 22. https://doi.org/10.1186/s10020-021-00283-6

Ding, P., Li, L., Li, L., Lv, X., Zhou, D., Wang, Q., Chen, J., Yang, C., Xu, E., Dai, W., Zhang, X., Wang, N., Wang, Q., Zhang, W., Zhang, L., Zhou, Y., Gu, H., Lei, Q., Zhou, X., & Hu, W. (2020). C5aR1 is a master regulator in Colorectal Tumorigenesis via Immune modulation. *Theranostics*, *10*(19), 8619–8632. https://doi.org/10.7150/thno.45058

Ding, P., Xu, Y., Li, L., Lv, X., Li, L., Chen, J., Zhou, D., Wang, X., Wang, Q., Zhang, W., Liao, T., Ji, Q.-H., Lei, Q.-Y., & Hu, W. (2022). Intracellular complement C5a/C5aR1 stabilizes β-catenin to promote colorectal tumorigenesis. *Cell Reports*, *39*(9), 110851. https://doi.org/10.1016/j.celrep.2022.110851

DiToro, D., & Basu, R. (2021). Emerging Complexity in CD4+T Lineage Programming and Its Implications in Colorectal Cancer. *Frontiers in Immunology*, *12*. https://www.frontiersin.org/articles/10.3389/fimmu.2021.694833

Domingo, E., Rathee, S., Blake, A., Samuel, L., Murray, G., Sebag-Montefiore, D., Gollins, S., West, N. P., Begum, R., Richman, S., Quirke, P., Redman, K., Chatzpili, A., Barberis, A., Hassanieh, S., Mahmoud, U., Youdell, M., Mcdermot, U., Koelzer, V. H., … Consortium, S. (2022b). *A Machine Learning Model of Complete Response to Radiation in Rectal Cancer Reveals Immune Infiltrate and TGFβ Signalling as Key Predictors* (SSRN Scholarly Paper 4267509). https://doi.org/10.2139/ssrn.4267509

Dorafshan, S., Razmi, M., Safaei, S., Gentilin, E., Madjd, Z., & Ghods, R. (2022). Periostin: Biology and function in cancer. *Cancer Cell International*, *22*(1), 315. https://doi.org/10.1186/s12935-022-02714-8

Dovedi, S. J., Adlard, A. L., Lipowska-Bhalla, G., McKenna, C., Jones, S., Cheadle, E. J., Stratford, I. J., Poon, E., Morrow, M., Stewart, R., Jones, H., Wilkinson, R. W., Honeychurch, J., & Illidge, T. M. (2014). Acquired resistance to fractionated radiotherapy can be overcome by concurrent PD-L1 blockade. *Cancer Research*, *74*(19), 5458–5468. https://doi.org/10.1158/0008-5472.CAN-14-1258

Dufour, A. M., Alvarez, M., Russo, B., & Chizzolini, C. (2018). Interleukin-6 and Type-I Collagen Production by Systemic Sclerosis Fibroblasts Are Differentially Regulated by Interleukin-17A in the Presence of Transforming Growth Factor-Beta 1. *Frontiers in Immunology*, *9*, 1865. https://doi.org/10.3389/fimmu.2018.01865

Dunkelberger, J., Zhou, L., Miwa, T., & Song, W.-C. (2012). C5aR expression in a novel GFP reporter gene knockin mouse: Implications for the mechanism of action of C5aR signaling in T cell immunity. *Journal of Immunology (Baltimore, Md.: 1950)*, *188*(8), 4032–4042. https://doi.org/10.4049/jimmunol.1103141

Dunn, G. P., Old, L. J., & Schreiber, R. D. (2004). The immunobiology of cancer immunosurveillance and immunoediting. *Immunity*, *21*(2), 137–148. https://doi.org/10.1016/j.immuni.2004.07.017

Egorshina, A. Yu., Zamaraev, A. V., Kaminskyy, V. O., Radygina, T. V., Zhivotovsky, B., & Kopeina, G. S. (2022). Necroptosis as a Novel Facet of Mitotic Catastrophe. *International Journal of Molecular Sciences*, *23*(7), 3733. https://doi.org/10.3390/ijms23073733

Elvington, M., Scheiber, M., Yang, X., Lyons, K., Jacqmin, D., Wadsworth, C., Marshall, D., Vanek, K., & Tomlinson, S. (2014a). Complement-Dependent Modulation of Antitumor Immunity following Radiation Therapy. *Cell Reports*, *8*(3), 818–830. https://doi.org/10.1016/j.celrep.2014.06.051

Elvington, M., Scheiber, M., Yang, X., Lyons, K., Jacqmin, D., Wadsworth, C., Marshall, D., Vanek, K., & Tomlinson, S. (2014b). Complement-dependent modulation of antitumor immunity following radiation therapy. *Cell Reports*, *8*(3), 818–830. https://doi.org/10.1016/j.celrep.2014.06.051

Emons, G., Spitzner, M., Reineke, S., Möller, J., Auslander, N., Kramer, F., Hu, Y., Beissbarth, T., Wolff, H. A., Rave-Fränk, M., Heßmann, E., Gaedcke, J., Ghadimi, B. M., Johnsen, S. A., Ried, T., & Grade, M. (2017). Chemoradiotherapy Resistance in Colorectal Cancer Cells is Mediated by Wnt/β-catenin Signaling. *Molecular Cancer Research: MCR*, *15*(11), 1481–1490. https://doi.org/10.1158/1541-7786.MCR-17-0205

Fan, Z., Qin, J., Wang, D., & Geng, S. (2019). Complement C3a promotes proliferation, migration and stemness in cutaneous squamous cell carcinoma. *Journal of Cellular and Molecular Medicine*, *23*(5), 3097–3107. https://doi.org/10.1111/jcmm.13959

Fang, Z., Li, P., Du, F., Shang, L., & Li, L. (2023). The role of organoids in cancer research. *Experimental Hematology & Oncology*, *12*(1), 69. https://doi.org/10.1186/s40164-023-00433-y

Fantini, M. C., Becker, C., Monteleone, G., Pallone, F., Galle, P. R., & Neurath, M. F. (2004). Cutting edge: TGF-beta induces a regulatory phenotype in CD4+CD25- T cells through Foxp3 induction and down-regulation of Smad7. *Journal of Immunology (Baltimore, Md.: 1950)*, *172*(9), 5149–5153. https://doi.org/10.4049/jimmunol.172.9.5149

Faul, F., Erdfelder, E., Lang, A.-G., & Buchner, A. (2007). G*Power 3: A flexible statistical power analysis program for the social, behavioral, and biomedical sciences. *Behavior Research Methods*, *39*(2), 175–191. https://doi.org/10.3758/bf03193146

Fearon, E. R., & Vogelstein, B. (1990b). A genetic model for colorectal tumorigenesis. *Cell*, *61*(5), 759–767. https://doi.org/10.1016/0092-8674(90)90186-I

Feeney, G., Sehgal, R., Sheehan, M., Hogan, A., Regan, M., Joyce, M., & Kerin, M. (2019). Neoadjuvant radiotherapy for rectal cancer management. *World Journal of Gastroenterology*, *25*(33), 4850–4869. https://doi.org/10.3748/wjg.v25.i33.4850

Feng, L., Zhao, K., Sun, L., Yin, X., Zhang, J., Liu, C., & Li, B. (2021). SLC7A11 regulated by NRF2 modulates esophageal squamous cell carcinoma radiosensitivity by inhibiting ferroptosis. *Journal of Translational Medicine*, *19*(1), 367. https://doi.org/10.1186/s12967-021-03042-7

Feng, S., Li, Z., Liu, M., Ye, Q., Xue, T., & Yan, B. (2023). Postoperative serum interleukin-6 levels correlate with survival in stage I-III colorectal cancer. *BMC Gastroenterology*, *23*(1), 156. https://doi.org/10.1186/s12876-023-02800-9

Ferlay, J., Colombet, M., Soerjomataram, I., Dyba, T., Randi, G., Bettio, M., Gavin, A., Visser, O., & Bray, F. (2018). Cancer incidence and mortality patterns in Europe: Estimates for 40 countries and 25 major cancers in 2018. *European Journal of Cancer (Oxford, England: 1990)*, *103*, 356–387. https://doi.org/10.1016/j.ejca.2018.07.005

Fishelson, Z., & Kirschfink, M. (2019). Complement C5b-9 and Cancer: Mechanisms of Cell Damage, Cancer Counteractions, and Approaches for Intervention. *Frontiers in Immunology*, *10*. https://www.frontiersin.org/articles/10.3389/fimmu.2019.00752

Fisher, B., Wolmark, N., Rockette, H., Redmond, C., Deutsch, M., Wickerham, D. L., Fisher, E. R., Caplan, R., Jones, J., Lerner, H., Gordon, P., Feldman, M., Cruz, A., Legault-Poisson, S., Wexler, M., Lawrence, W., Robidoux, A., & Other NSABP Investigators. (1988). Postoperative Adjuvant Chemotherapy or Radiation Therapy for Rectal Cancer: Results From NSABP Protocol R-0112. *JNCI: Journal of the National Cancer Institute*, *80*(1), 21–29. https://doi.org/10.1093/jnci/80.1.21

Formenti, S. C., & Demaria, S. (2013). Combining radiotherapy and cancer immunotherapy: A paradigm shift. *Journal of the National Cancer Institute*, *105*(4), 256–265. https://doi.org/10.1093/jnci/djs629

Fridlender, Z. G., Sun, J., Kim, S., Kapoor, V., Cheng, G., Ling, L., Worthen, G. S., & Albelda, S. M. (2009). Polarization of Tumor-Associated Neutrophil (TAN) Phenotype by TGF-β: "N1" versus "N2" TAN. *Cancer Cell*, *16*(3), 183–194. https://doi.org/10.1016/j.ccr.2009.06.017

Fridman, W. H., Zitvogel, L., Sautès–Fridman, C., & Kroemer, G. (2017). The immune contexture in cancer prognosis and treatment. *Nature Reviews Clinical Oncology*, *14*(12), Article 12. https://doi.org/10.1038/nrclinonc.2017.101

G, I., Hv, N., S, I., & B, Z. (2011). Chromosomal breaks during mitotic catastrophe trigger γH2AX-ATM-p53-mediated apoptosis. *Journal of Cell Science*, *124*(Pt 17). https://doi.org/10.1242/jcs.081612

Gabay, M., Li, Y., & Felsher, D. W. (2014). MYC Activation Is a Hallmark of Cancer Initiation and Maintenance. *Cold Spring Harbor Perspectives in Medicine*, *4*(6), a014241. https://doi.org/10.1101/cshperspect.a014241

Gadwa, J., Bickett, T. E., Darragh, L. B., Knitz, M. W., Bhatia, S., Piper, M., Van Court, B., Bhuvane, S., Nguyen, D., Nangia, V., Kleczko, E. K., Nemenoff, R. A., & Karam, S. D. (2021). Complement C3a and C5a receptor blockade modulates regulatory T cell conversion in head and neck cancer. *Journal for Immunotherapy of Cancer*, *9*(3), e002585. https://doi.org/10.1136/jitc-2021-002585

Gaipl, U. S., Multhoff, G., Scheithauer, H., Lauber, K., Hehlgans, S., Frey, B., & Rödel, F. (2014). Kill and spread the word: Stimulation of antitumor immune responses in the context of radiotherapy. *Immunotherapy*, *6*(5), 597–610. https://doi.org/10.2217/imt.14.38

Galluzzi, L., Buqué, A., Kepp, O., Zitvogel, L., & Kroemer, G. (2017). Immunogenic cell death in cancer and infectious disease. *Nature Reviews. Immunology*, *17*(2), 97–111. https://doi.org/10.1038/nri.2016.107

Galluzzi, L., Vitale, I., Aaronson, S. A., Abrams, J. M., Adam, D., Agostinis, P., Alnemri, E. S., Altucci, L., Amelio, I., Andrews, D. W., Annicchiarico-Petruzzelli, M., Antonov, A. V., Arama, E., Baehrecke, E. H., Barlev, N. A., Bazan, N. G., Bernassola, F., Bertrand, M. J. M., Bianchi, K., … Kroemer, G. (2018). Molecular mechanisms of cell death: Recommendations of the Nomenclature Committee on Cell Death 2018. *Cell Death and Differentiation*, *25*(3), 486. https://doi.org/10.1038/s41418-017-0012-4

Gao, J., Aksoy, B. A., Dogrusoz, U., Dresdner, G., Gross, B., Sumer, S. O., Sun, Y., Jacobsen, A., Sinha, R., Larsson, E., Cerami, E., Sander, C., & Schultz, N. (2013). Integrative analysis of complex cancer genomics and clinical profiles using the cBioPortal. *Science Signaling*, *6*(269), pl1. https://doi.org/10.1126/scisignal.2004088

Garcia-Lora, A., Algarra, I., & Garrido, F. (2003). MHC class I antigens, immune surveillance, and tumor immune escape. *Journal of Cellular Physiology*, *195*(3), 346–355. https://doi.org/10.1002/jcp.10290

Gavaruzzi, T., Lotto, L., Giandomenico, F., Perin, A., & Pucciarelli, S. (2014). Patient-reported outcomes after neoadjuvant therapy for rectal cancer: A systematic review. *Expert Review of Anticancer Therapy*, *14*(8), 901–918. https://doi.org/10.1586/14737140.2014.911090

Gérard, J.-P., Azria, D., Gourgou-Bourgade, S., Martel-Lafay, I., Hennequin, C., Etienne, P.-L., Vendrely, V., François, E., de La Roche, G., Bouché, O., Mirabel, X., Denis, B., Mineur, L., Berdah, J.-F., Mahé, M.-A., Bécouarn, Y., Dupuis, O., Lledo, G., Seitz, J.-F., … Conroy, T. (2012). Clinical outcome of the ACCORD 12/0405 PRODIGE 2 randomized trial in rectal cancer. *Journal of Clinical Oncology: Official Journal of the American Society of Clinical Oncology*, *30*(36), 4558–4565. https://doi.org/10.1200/JCO.2012.42.8771

Gérard, J.-P., Azria, D., Gourgou-Bourgade, S., Martel-Laffay, I., Hennequin, C., Etienne, P.-L., Vendrely, V., François, E., de La Roche, G., Bouché, O., Mirabel, X., Denis, B., Mineur, L., Berdah, J.-F., Mahé, M. A., Bécouarn, Y., Dupuis, O., Lledo, G., Montoto-Grillot, C., & Conroy, T. (2010). Comparison of two neoadjuvant chemoradiotherapy regimens for locally advanced rectal cancer: Results of the phase III trial ACCORD 12/0405-Prodige 2. *Journal of Clinical Oncology: Official Journal of the American Society of Clinical Oncology*, *28*(10), 1638–1644. https://doi.org/10.1200/JCO.2009.25.8376

Glynne-Jones, R., Wyrwicz, L., Tiret, E., Brown, G., Rödel, C., Cervantes, A., Arnold, D., & ESMO Guidelines Committee. (2017). Rectal cancer: ESMO Clinical Practice Guidelines for diagnosis, treatment and follow-up. *Annals of Oncology: Official Journal of the European Society for Medical Oncology*, *28*(suppl_4), iv22–iv40. https://doi.org/10.1093/annonc/mdx224

Goedegebuure, R. S. A., de Klerk, L. K., Bass, A. J., Derks, S., & Thijssen, V. L. J. L. (2019). Combining Radiotherapy With Anti-angiogenic Therapy and Immunotherapy; A Therapeutic Triad for Cancer? *Frontiers in Immunology*, *9*. https://doi.org/10.3389/fimmu.2018.03107

Golden, E. B., & Apetoh, L. (2015). Radiotherapy and immunogenic cell death. *Seminars in Radiation Oncology*, *25*(1), 11–17. https://doi.org/10.1016/j.semradonc.2014.07.005

Gollins, S., West, N., Sebag-Montefiore, D., Myint, A. S., Saunders, M., Susnerwala, S., Quirke, P., Essapen, S., Samuel, L., Sizer, B., Worlding, J., Southward, K., Hemmings, G., Tinkler-Hundal, E., Taylor, M., Bottomley, D., Chambers, P., Lawrie, E., Lopes, A., & Beare, S. (2017). Preoperative chemoradiation with capecitabine, irinotecan and cetuximab in rectal cancer: Significance of pre-treatment and post-resection RAS mutations. *British Journal of Cancer*, *117*(9), 1286–1294. https://doi.org/10.1038/bjc.2017.294

Gong, Y., Scott, E., Lu, R., Xu, Y., Oh, W. K., & Yu, Q. (2013). TIMP-1 Promotes Accumulation of Cancer Associated Fibroblasts and Cancer Progression. *PLoS ONE*, *8*(10), e77366. https://doi.org/10.1371/journal.pone.0077366

Gonzalez, H., Hagerling, C., & Werb, Z. (2018). Roles of the immune system in cancer: From tumor initiation to metastatic progression. *Genes & Development*, *32*(19–20), 1267–1284. https://doi.org/10.1101/gad.314617.118

Grauel, A. L., Nguyen, B., Ruddy, D., Laszewski, T., Schwartz, S., Chang, J., Chen, J., Piquet, M., Pelletier, M., Yan, Z., Kirkpatrick, N. D., Wu, J., deWeck, A., Riester, M., Hims, M., Geyer, F. C., Wagner, J., MacIsaac, K., Deeds, J., … Cremasco, V. (2020). TGFβ-blockade uncovers stromal plasticity in tumors by revealing the existence of a subset of interferon-licensed fibroblasts. *Nature Communications*, *11*(1), Article 1. https://doi.org/10.1038/s41467-020-19920-5

Gros, P., Milder, F. J., & Janssen, B. J. C. (2008). Complement driven by conformational changes. *Nature Reviews. Immunology*, *8*(1), 48–58. https://doi.org/10.1038/nri2231

Grotendorst, G. R., Smale, G., & Pencev, D. (1989). Production of transforming growth factor beta by human peripheral blood monocytes and neutrophils. *Journal of Cellular Physiology*, *140*(2), 396–402. https://doi.org/10.1002/jcp.1041400226

Guinney, J., Dienstmann, R., Wang, X., de Reyniès, A., Schlicker, A., Soneson, C., Marisa, L., Roepman, P., Nyamundanda, G., Angelino, P., Bot, B. M., Morris, J. S., Simon, I. M., Gerster, S., Fessler, E., De Sousa E Melo, F., Missiaglia, E., Ramay, H., Barras, D., … Tejpar, S. (2015). The consensus molecular subtypes of colorectal cancer. *Nature Medicine*, *21*(11), 1350–1356. https://doi.org/10.1038/nm.3967

Gunderson, A. J., Yamazaki, T., McCarty, K., Fox, N., Phillips, M., Alice, A., Blair, T., Whiteford, M., O'Brien, D., Ahmad, R., Kiely, M. X., Hayman, A., Crocenzi, T., Gough, M. J., Crittenden, M. R., & Young, K. H. (2020b). TGFβ suppresses CD8+ T cell expression of CXCR3 and tumor trafficking. *Nature Communications*, *11*(1), Article 1. https://doi.org/10.1038/s41467-020-15404-8

Gupta, A., Probst, H. C., Vuong, V., Landshammer, A., Muth, S., Yagita, H., Schwendener, R., Pruschy, M., Knuth, A., & van den Broek, M. (2012). Radiotherapy Promotes Tumor-Specific Effector CD8+ T Cells via Dendritic Cell Activation. *The Journal of Immunology*, *189*(2), 558–566. https://doi.org/10.4049/jimmunol.1200563

Hallmarks of Cancer: The Next Generation: Cell. (n.d.). Retrieved 17 November 2023, from https://www.cell.com/fulltext/S0092-8674(11)00127-9#bib93

Hamada, S., Masamune, A., Yoshida, N., Takikawa, T., & Shimosegawa, T. (2016). IL-6/STAT3 Plays a Regulatory Role in the Interaction Between Pancreatic Stellate Cells and Cancer Cells. *Digestive Diseases and Sciences*, *61*(6), 1561–1571. https://doi.org/10.1007/s10620-015-4001-5

Hanahan, D., & Weinberg, R. A. (2000). The hallmarks of cancer. *Cell*, *100*(1), 57–70. https://doi.org/10.1016/s0092-8674(00)81683-9

Hanahan, D., & Weinberg, R. A. (2011). Hallmarks of Cancer: The Next Generation. *Cell*, *144*(5), 646–674. https://doi.org/10.1016/j.cell.2011.02.013

Haustermans, K., Schmoll, H. J., Price, T., Nordlinger, B., Hofheinz, R. D., Daisne, J. F., Janssens, J., Schmidt, P., Reinel, H., & Cutsem, E. V. (2014a). OC-0250: First results of the PETACC-6 randomized phase III trial in locally advanced rectal cancer. *Radiotherapy and Oncology*, *111*, S96. https://doi.org/10.1016/s0167-8140(15)30355-8

Heald, R. J., Husband, E. M., & Ryall, R. D. (1982). The mesorectum in rectal cancer surgery—The clue to pelvic recurrence? *The British Journal of Surgery*, *69*(10), 613–616. https://doi.org/10.1002/bjs.1800691019

Hellevik, T., & Martinez-Zubiaurre, I. (2014). Radiotherapy and the tumor stroma: The importance of dose and fractionation. *Frontiers in Oncology*, *4*, 1. https://doi.org/10.3389/fonc.2014.00001

Hellevik, T., Pettersen, I., Berg, V., Winberg, J. O., Moe, B. T., Bartnes, K., Paulssen, R. H., Busund, L.-T., Bremnes, R., Chalmers, A., & Martinez-Zubiaurre, I. (2012). Cancer-associated fibroblasts from human NSCLC survive ablative doses of radiation but their invasive capacity is reduced. *Radiation Oncology*, *7*(1), 59. https://doi.org/10.1186/1748-717X-7-59

Hermans, D., Gautam, S., García-Cañaveras, J. C., Gromer, D., Mitra, S., Spolski, R., Li, P., Christensen, S., Nguyen, R., Lin, J.-X., Oh, J., Du, N., Veenbergen, S., Fioravanti, J., Ebina-Shibuya, R., Bleck, C., Neckers, L. M., Rabinowitz, J. D., Gattinoni, L., & Leonard, W. J. (2020). Lactate dehydrogenase inhibition synergizes with IL-21 to promote CD8+ T cell stemness and antitumor immunity. *Proceedings of the National Academy of Sciences*, *117*(11), 6047–6055. https://doi.org/10.1073/pnas.1920413117

Ho, A. Y., Barker, C. A., Arnold, B. B., Powell, S. N., Hu, Z. I., Gucalp, A., Lebron-Zapata, L., Wen, H. Y., Kallman, C., D'Agnolo, A., Zhang, Z., Flynn, J., Dunn, S. A., & McArthur, H. L. (2020). A phase 2 clinical trial assessing the efficacy and safety of pembrolizumab

and radiotherapy in patients with metastatic triple-negative breast cancer. *Cancer*, *126*(4), 850–860. https://doi.org/10.1002/cncr.32599

Hofmeyer, T., Schmelz, S., Degiacomi, M. T., Dal Peraro, M., Daneschdar, M., Scrima, A., van den Heuvel, J., Heinz, D. W., & Kolmar, H. (2013). Arranged sevenfold: Structural insights into the C-terminal oligomerization domain of human C4b-binding protein. *Journal of Molecular Biology*, *425*(8), 1302–1317. https://doi.org/10.1016/j.jmb.2012.12.017

Hu, L., Huang, S., Chen, G., Li, B., Li, T., Lin, M., Huang, Y., Xiao, Z., Shuai, X., & Su, Z. (2022). Nanodrugs Incorporating LDHA siRNA Inhibit M2-like Polarization of TAMs and Amplify Autophagy to Assist Oxaliplatin Chemotherapy against Colorectal Cancer. *ACS Applied Materials & Interfaces*, *14*(28), 31625–31633. https://doi.org/10.1021/acsami.2c05841

Improved Survival with Preoperative Radiotherapy in Resectable Rectal Cancer. (1997). *New England Journal of Medicine*, *336*(14), 980–987. https://doi.org/10.1056/NEJM199704033361402

Imreh, G., Norberg, H. V., Imreh, S., & Zhivotovsky, B. (2011). Chromosomal breaks during mitotic catastrophe trigger γH2AX–ATM–p53-mediated apoptosis. *Journal of Cell Science*, *124*(17), 2951–2963. https://doi.org/10.1242/jcs.081612

Intracellular complement C5a/C5aR1 stabilizes β-catenin to promote colorectal tumorigenesis—ScienceDirect. (n.d.). Retrieved 11 December 2023, from https://www.sciencedirect.com/science/article/pii/S2211124722006246

Isella, C., Brundu, F., Bellomo, S. E., Galimi, F., Zanella, E., Porporato, R., Petti, C., Fiori, A., Orzan, F., Senetta, R., Boccaccio, C., Ficarra, E., Marchionni, L., Trusolino, L., Medico, E., & Bertotti, A. (2017b). Selective analysis of cancer-cell intrinsic transcriptional traits defines novel clinically relevant subtypes of colorectal cancer. *Nature Communications*, *8*, 15107. https://doi.org/10.1038/ncomms15107

Isella, C., Terrasi, A., Bellomo, S. E., Petti, C., Galatola, G., Muratore, A., Mellano, A., Senetta, R., Cassenti, A., Sonetto, C., Inghirami, G., Trusolino, L., Fekete, Z., De Ridder, M., Cassoni, P., Storme, G., Bertotti, A., & Medico, E. (2015). Stromal contribution to the colorectal cancer transcriptome. *Nature Genetics*, *47*(4), 312–319. https://doi.org/10.1038/ng.3224

Jackstadt, R., van Hooff, S. R., Leach, J. D., Cortes-Lavaud, X., Lohuis, J. O., Ridgway, R. A., Wouters, V. M., Roper, J., Kendall, T. J., Roxburgh, C. S., Horgan, P. G., Nixon, C., Nourse, C., Gunzer, M., Clark, W., Hedley, A., Yilmaz, O. H., Rashid, M., Bailey, P., … Sansom, O. J. (2019). Epithelial NOTCH Signaling Rewires the Tumor Microenvironment of Colorectal Cancer to Drive Poor-Prognosis Subtypes and Metastasis. *Cancer Cell*, *36*(3), 319-336.e7. https://doi.org/10.1016/j.ccell.2019.08.003

Jiang, K., Lu, S., Li, D., Liu, M., Jin, H., Lei, B., Wang, S., Long, K., He, S., & Zhong, F. (2023). Blockade of C5aR1 alleviates liver inflammation and fibrosis in a mouse model of NASH by regulating TLR4 signaling and macrophage polarization. *Journal of Gastroenterology*, *58*(9), 894–907. https://doi.org/10.1007/s00535-023-02002-w

Jie, J., Hao, S., Hongxiu, Y., Huiying, Y., Jun, M., Chenji, W., Mingjie, Y., & Yong, M. (2007). Evaluation of Cu in hepatocellular carcinoma by particle induced X-ray emission. *Journal of Trace Elements in Medicine and Biology: Organ of the Society for Minerals and Trace Elements (GMS)*, *21*(4), 255–260. https://doi.org/10.1016/j.jtemb.2007.06.004

Jin, W.-J., Xu, J.-M., Xu, W.-L., Gu, D.-H., & Li, P.-W. (2014). Diagnostic value of interleukin-8 in colorectal cancer: A case-control study and meta-analysis. *World Journal of Gastroenterology : WJG*, *20*(43), 16334–16342. https://doi.org/10.3748/wjg.v20.i43.16334

Jin, X., Cai, Y., Xue, G., Que, J., Cheng, R., Yang, Y., Xiao, L., Lin, X., Xu, C., Wang, P., Xu, Z., Nie, H., & Jiang, Q. (2023). Identification of shared characteristics in tumor-infiltrating T cells across 15 cancers. *Molecular Therapy - Nucleic Acids*, *32*, 189–202. https://doi.org/10.1016/j.omtn.2023.03.007

Jung, S. Y., Hwang, S., Clarke, J. M., Bauer, T. M., Keedy, V. L., Lee, H., Park, N., Kim, S.-J., & Lee, J. I. (2020). Pharmacokinetic characteristics of vactosertib, a new activin receptor-like kinase 5 inhibitor, in patients with advanced solid tumors in a first-in-human phase 1 study. *Investigational New Drugs*, *38*(3), 812–820. https://doi.org/10.1007/s10637-019-00835-y

Kamphorst, J. J., Cross, J. R., Fan, J., de Stanchina, E., Mathew, R., White, E. P., Thompson, C. B., & Rabinowitz, J. D. (2013). Hypoxic and Ras-transformed cells support growth by scavenging unsaturated fatty acids from lysophospholipids. *Proceedings of the National Academy of Sciences of the United States of America*, *110*(22), 8882–8887. https://doi.org/10.1073/pnas.1307237110

Kanthou, C., & Tozer, G. (2019b). Targeting the vasculature of tumours: Combining VEGF pathway inhibitors with radiotherapy. *The British Journal of Radiology*, *92*(1093), 20180405. https://doi.org/10.1259/bjr.20180405

Kapiteijn, E., Marijnen, C. A., Nagtegaal, I. D., Putter, H., Steup, W. H., Wiggers, T., Rutten, H. J., Pahlman, L., Glimelius, B., van Krieken, J. H., Leer, J. W., van de Velde, C. J., & Dutch Colorectal Cancer Group. (2001). Preoperative radiotherapy combined with total mesorectal excision for resectable rectal cancer. *The New England Journal of Medicine*, *345*(9), 638–646. https://doi.org/10.1056/NEJMoa010580

Karsten, C. M., Laumonnier, Y., Eurich, B., Ender, F., Bröker, K., Roy, S., Czabanska, A., Vollbrandt, T., Figge, J., & Köhl, J. (2015). Monitoring and cell-specific deletion of C5aR1 using a novel floxed GFP-C5aR1 reporter knock-in mouse. *Journal of Immunology (Baltimore, Md.: 1950)*, *194*(4), 1841–1855. https://doi.org/10.4049/jimmunol.1401401

Katz, L. H., Li, Y., Chen, J.-S., Muñoz, N. M., Majumdar, A., Chen, J., & Mishra, L. (2013). Targeting TGF-β signaling in cancer. *Expert Opinion on Therapeutic Targets*, *17*(7), 743–760. https://doi.org/10.1517/14728222.2013.782287

Kaur, P., & Asea, A. (2012). Radiation-induced effects and the immune system in cancer. *Frontiers in Oncology*, *2*. https://doi.org/10.3389/fonc.2012.00191

Kdimati, S., Bürtin, F., Linnebacher, M., & Mullins, C. S. (2023). Patient-Derived Organoids for In Vivo Validation of In Vitro Data. *Methods in Molecular Biology (Clifton, N.J.)*, *2589*, 111–126. https://doi.org/10.1007/978-1-0716-2788-4_8

Kepp, O., Senovilla, L., & Kroemer, G. (2014a). Immunogenic cell death inducers as anticancer agents. *Oncotarget*, *5*(14), 5190–5191. https://doi.org/10.18632/oncotarget.2266

Khan, U., Chowdhury, S., Billah, M. M., Islam, K. M. D., Thorlacius, H., & Rahman, M. (2021). Neutrophil Extracellular Traps in Colorectal Cancer Progression and Metastasis. *International Journal of Molecular Sciences*, *22*(14), 7260. https://doi.org/10.3390/ijms22147260

Kitakaze, M., Uemura, M., Hara, T., Chijimatsu, R., Motooka, D., Hirai, T., Konno, M., Okuzaki, D., Sekido, Y., Hata, T., Ogino, T., Takahashi, H., Miyoshi, N., Ofusa, K., Mizushima, T., Eguchi, H., Doki, Y., & Ishii, H. (2023). Cancer-specific tissue-resident memory T-cells express ZNF683 in colorectal cancer. *British Journal of Cancer*, *128*(10), 1828–1837. https://doi.org/10.1038/s41416-023-02202-4

Klug, F., Prakash, H., Huber, P. E., Seibel, T., Bender, N., Halama, N., Pfirschke, C., Voss, R. H., Timke, C., Umansky, L., Klapproth, K., Schäkel, K., Garbi, N., Jäger, D., Weitz, J., Schmitz-Winnenthal, H., Hämmerling, G. J., & Beckhove, P. (2013). Low-dose irradiation programs macrophage differentiation to an iNOS^{+}/M1 phenotype that orchestrates effective T cell immunotherapy. *Cancer Cell*, *24*(5), 589–602. https://doi.org/10.1016/j.ccr.2013.09.014

Kochanek, D. M., Ghouse, S. M., Karbowniczek, M. M., & Markiewski, M. M. (2018). Complementing Cancer Metastasis. *Frontiers in Immunology*, *9*. https://www.frontiersin.org/articles/10.3389/fimmu.2018.01629

Kolev, M., & Markiewski, M. M. (2018). Targeting complement-mediated immunoregulation for cancer immunotherapy. *Seminars in Immunology*, *37*, 85–97. https://doi.org/10.1016/j.smim.2018.02.003

Kondělková, K., Vokurková, D., Krejsek, J., Borská, L., Fiala, Z., & Ctirad, A. (2010). Regulatory T cells (TREG) and their roles in immune system with respect to immunopathological disorders. *Acta Medica (Hradec Kralove)*, *53*(2), 73–77. https://doi.org/10.14712/18059694.2016.63

Krieg, C., Weber, L. M., Fosso, B., Marzano, M., Hardiman, G., Olcina, M. M., Domingo, E., El Aidy, S., Mallah, K., Robinson, M. D., & Guglietta, S. (2022). Complement downregulation promotes an inflammatory signature that renders colorectal cancer susceptible to immunotherapy. *Journal for Immunotherapy of Cancer*, *10*(9), e004717. https://doi.org/10.1136/jitc-2022-004717

Kroemer, G., Galluzzi, L., Kepp, O., & Zitvogel, L. (2013). Immunogenic Cell Death in Cancer Therapy. *Annual Review of Immunology*, *31*(Volume 31, 2013), 51–72. https://doi.org/10.1146/annurev-immunol-032712-100008

Krook, J. E., Moertel, C. G., Gunderson, L. L., Wieand, H. S., Collins, R. T., Beart, R. W., Kubista, T. P., Poon, M. A., Meyers, W. C., Mailliard, J. A., Twito, D. I., Morton, R. F., Veeder, M. H., Witzig, T. E., Cha, S., & Vidyarthi, S. C. (1991a). Effective Surgical Adjuvant Therapy for High-Risk Rectal Carcinoma. *New England Journal of Medicine*, *324*(11), 709–715. https://doi.org/10.1056/NEJM199103143241101

Krysko, O., Aaes, T. L., Kagan, V. E., D'Herde, K., Bachert, C., Leybaert, L., Vandenabeele, P., & Krysko, D. V. (2017a). Necroptotic cell death in anti-cancer therapy. *Immunological Reviews*, *280*(1), 207–219. https://doi.org/10.1111/imr.12583

Kumar, V., Lee, J. D., Clark, R. J., Noakes, P. G., Taylor, S. M., & Woodruff, T. M. (2020b). Preclinical Pharmacokinetics of Complement C5a Receptor Antagonists PMX53 and PMX205 in Mice. *ACS Omega*, *5*(5), 2345–2354. https://doi.org/10.1021/acsomega.9b03735

Ladoire, S., Martin, F., & Ghiringhelli, F. (2011). Prognostic role of FOXP3+ regulatory T cells infiltrating human carcinomas: The paradox of colorectal cancer. *Cancer Immunology, Immunotherapy: CII*, *60*(7), 909–918. https://doi.org/10.1007/s00262-011-1046-y

Landry, J. C., Feng, Y., Cohen, S. J., Staley, C. A., Whittington, R., Sigurdson, E. R., Nimeiri, H., Verma, U., Prabhu, R. S., & Benson, A. B. (2013). Phase 2 study of preoperative radiation with concurrent capecitabine, oxaliplatin, and bevacizumab followed by surgery and postoperative 5-fluorouracil, leucovorin, oxaliplatin (FOLFOX), and bevacizumab in patients with locally advanced rectal cancer: ECOG 3204. *Cancer*, *119*(8), 1521–1527. https://doi.org/10.1002/cncr.27890

Lauber, K., Ernst, A., Orth, M., Herrmann, M., & Belka, C. (2012). Dying cell clearance and its impact on the outcome of tumor radiotherapy. *Frontiers in Oncology*, *2*, 116. https://doi.org/10.3389/fonc.2012.00116

Lawrence, T. S., Blackstock, A. W., & McGinn, C. (2003). The mechanism of action of radiosensitization of conventional chemotherapeutic agents. *Seminars in Radiation Oncology*, *13*(1), 13–21. https://doi.org/10.1053/srao.2003.50002

Lee, H.-J. (2020). Recent Advances in the Development of TGF-β Signaling Inhibitors for Anticancer Therapy. *Journal of Cancer Prevention*, *25*(4), 213–222. https://doi.org/10.15430/JCP.2020.25.4.213

Lei, G., Mao, C., Yan, Y., Zhuang, L., & Gan, B. (2021). Ferroptosis, radiotherapy, and combination therapeutic strategies. *Protein & Cell*, *12*(11), 836–857. https://doi.org/10.1007/s13238-021-00841-y

Levine, M. S., & Holland, A. J. (2018). The impact of mitotic errors on cell proliferation and tumorigenesis. *Genes & Development*, *32*(9–10), 620–638. https://doi.org/10.1101/gad.314351.118

Li, B., Zhang, S., Huang, N., Chen, H., Wang, P., Yang, J., & Li, Z. (2019). CCL9/CCR1 induces myeloid-derived suppressor cell recruitment to the spleen in a murine H22 orthotopic hepatoma model. *Oncology Reports*, *41*(1), 608–618. https://doi.org/10.3892/or.2018.6809

Li, D., Jiao, Y., Gao, W., Hu, S., Li, D., Zhao, W., Chen, P., Jin, L., Zhao, Y., Ma, Z., Wu, X., Yan, Y., Sun, W., Du, X., & Dong, G. (2022). Comprehensive analysis of the prognostic and immunotherapeutic implications of STAT family members in human colorectal cancer. *Frontiers in Genetics*, *13*, 951252. https://doi.org/10.3389/fgene.2022.951252

Li, M., Bolduc, A. R., Hoda, M. N., Gamble, D. N., Dolisca, S.-B., Bolduc, A. K., Hoang, K., Ashley, C., McCall, D., Rojiani, A. M., Maria, B. L., Rixe, O., MacDonald, T. J., Heeger, P. S., Mellor, A. L., Munn, D. H., & Johnson, T. S. (2014). The indoleamine 2,3-dioxygenase pathway controls complement-dependent enhancement of chemo-radiation therapy against murine glioblastoma. *Journal for ImmunoTherapy of Cancer*, *2*(1), 21. https://doi.org/10.1186/2051-1426-2-21

Lin, C., Ballah, T., Nottage, M., Hay, K., Chua, B., Kenny, L., Thomas, P., Teng, M., Keller, J., Le, T., Edmunds, J., & Hughes, B. (2021). A prospective study investigating the efficacy and toxicity of definitive ChemoRadiation and ImmunOtherapy (CRIO) in locally and/or regionally advanced unresectable cutaneous squamous cell carcinoma. *Radiation Oncology (London, England)*, *16*(1), 69. https://doi.org/10.1186/s13014-021-01795-5

Lin, Y. H., Duong, H. G., Limary, A. E., Kim, E. S., Hsu, P., Patel, S. A., Wong, W. H., Indralingam, C. S., Liu, Y. C., Yao, P., Chiang, N. R., Vandenburgh, S. A., Anderson, T. R.,

Olvera, J. G., Ferry, A., Takehara, K. K., Jin, W., Tsai, M. S., Yeo, G. W., … Chang, J. T. (2023). Small intestine and colon tissue-resident memory CD8+ T cells exhibit molecular heterogeneity and differential dependence on Eomes. *Immunity*, *56*(1), 207-223.e8. https://doi.org/10.1016/j.immuni.2022.12.007

Liu, J., Lin, F., Strainic, M. G., An, F., Miller, R. H., Altuntas, C. Z., Heeger, P. S., Tuohy, V. K., & Medof, M. E. (2008). IFN-gamma and IL-17 production in experimental autoimmune encephalomyelitis depends on local APC-T cell complement production. *Journal of Immunology (Baltimore, Md.: 1950)*, *180*(9), 5882–5889. https://doi.org/10.4049/jimmunol.180.9.5882

Liu, M., Wang, X., Wang, L., Ma, X., Gong, Z., Zhang, S., & Li, Y. (2018). Targeting the IDO1 pathway in cancer: From bench to bedside. *Journal of Hematology & Oncology*, *11*(1), 100. https://doi.org/10.1186/s13045-018-0644-y

Liu, S., Sun, X., Luo, J., Zhu, H., Yang, X., Guo, Q., Song, Y., & Sun, X. (2015). Effects of radiation on T regulatory cells in normal states and cancer: Mechanisms and clinical implications. *American Journal of Cancer Research*, *5*(11), 3276–3285.

Liu, T., Han, C., Wang, S., Fang, P., Ma, Z., Xu, L., & Yin, R. (2019). Cancer-associated fibroblasts: An emerging target of anti-cancer immunotherapy. *Journal of Hematology & Oncology*, *12*(1), 86. https://doi.org/10.1186/s13045-019-0770-1

Liu, Y., Zhang, Q., Xing, B., Luo, N., Gao, R., Yu, K., Hu, X., Bu, Z., Peng, J., Ren, X., & Zhang, Z. (2022). Immune phenotypic linkage between colorectal cancer and liver metastasis. *Cancer Cell*, *40*(4), 424-437.e5. https://doi.org/10.1016/j.ccell.2022.02.013

Liu, Y.-T., & Sun, Z.-J. (2021). Turning cold tumors into hot tumors by improving T-cell infiltration. *Theranostics*, *11*(11), 5365–5386. https://doi.org/10.7150/thno.58390

Long, Z., Wang, B., Tao, D., Huang, Y., & Tao, Z. (2014). Hypofractionated radiotherapy induces miR-34a expression and enhances apoptosis in human nasopharyngeal carcinoma cells. *International Journal of Molecular Medicine*, *34*(5), 1388–1394. https://doi.org/10.3892/ijmm.2014.1937

Lu, G., Shi, W., & Zhang, Y. (2021a). Prognostic Implications and Immune Infiltration Analysis of ALDOA in Lung Adenocarcinoma. *Frontiers in Genetics*, *12*, 721021. https://doi.org/10.3389/fgene.2021.721021

Lu, G., Shi, W., & Zhang, Y. (2021b). Prognostic Implications and Immune Infiltration Analysis of ALDOA in Lung Adenocarcinoma. *Frontiers in Genetics*, *12*, 721021. https://doi.org/10.3389/fgene.2021.721021

Lu, Y., Gu, D., Zhao, C., Sun, Y., Li, W., He, L., Wang, X., Kou, Z., Su, J., & Guo, F. (2023). Genomic landscape and expression profile of consensus molecular subtype four of colorectal cancer. *Frontiers in Immunology*, *14*, 1160052. https://doi.org/10.3389/fimmu.2023.1160052

Lu, Y., Zhang, Y., Wang, X., Zhang, H., Zhu, Y., Zhang, J., Sha, H., Zou, R., Gan, Y., Sui, Y., Wang, J., Du, T., Wu, J., & Feng, J. (2023). Aldolase A Promotes Colorectal Cancer Progression through Targeting COPS6 and Regulating MAPK Signaling Pathway. *Disease Markers*, *2023*, 1702125. https://doi.org/10.1155/2023/1702125

Lv, Y., Ma, X., Ma, Y., Du, Y., & Feng, J. (2023). A new emerging target in cancer immunotherapy: Galectin-9 (LGALS9). *Genes & Diseases*, *10*(6), 2366–2382. https://doi.org/10.1016/j.gendis.2022.05.020

MacFarlane, J. K., Ryall, R. D. H., & Heald, R. J. (1993). Mesorectal excision for rectal cancer. *The Lancet*, *341*(8843), 457–460. https://doi.org/10.1016/0140-6736(93)90207-W

Macor, P., Capolla, S., & Tedesco, F. (2018). Complement as a Biological Tool to Control Tumor Growth. *Frontiers in Immunology*, *9*. https://www.frontiersin.org/articles/10.3389/fimmu.2018.02203

Maeda, Y., Kawano, Y., Wada, Y., Yatsuda, J., Motoshima, T., Murakami, Y., Kikuchi, K., Imamura, T., & Eto, M. (2015). C5aR is frequently expressed in metastatic renal cell carcinoma and plays a crucial role in cell invasion via the ERK and PI3 kinase pathways. *Oncology Reports*, *33*(4), 1844–1850. https://doi.org/10.3892/or.2015.3800

Malek, E., Rana, P. S., Swamydas, M., Daunov, M., Miyagi, M., Murphy, E., Ignatz-Hoover, J. J., Metheny, L., Seong Jin, K., & Driscoll, J. J. (2023). Vactosertib, a novel TGF-β1 type I receptor kinase inhibitor, improves T-cell fitness: A single-arm, phase 1b trial in relapsed/refractory multiple myeloma. *Research Square*, rs.3.rs-3112163. https://doi.org/10.21203/rs.3.rs-3112163/v1

Mao, X., Xu, J., Wang, W., Liang, C., Hua, J., Liu, J., Zhang, B., Meng, Q., Yu, X., & Shi, S. (2021). Crosstalk between cancer-associated fibroblasts and immune cells in the

tumor microenvironment: New findings and future perspectives. *Molecular Cancer*, *20*(1), 131. https://doi.org/10.1186/s12943-021-01428-1

Mardis, E. R. (2019). Neoantigens and genome instability: Impact on immunogenomic phenotypes and immunotherapy response. *Genome Medicine*, *11*(1), 71. https://doi.org/10.1186/s13073-019-0684-0

Marin, I., Boix, O., Garcia-Garijo, A., Sirois, I., Caballe, A., Zarzuela, E., Ruano, I., Attolini, C. S.-O., Prats, N., López-Domínguez, J. A., Kovatcheva, M., Garralda, E., Muñoz, J., Caron, E., Abad, M., Gros, A., Pietrocola, F., & Serrano, M. (2023). Cellular Senescence Is Immunogenic and Promotes Antitumor Immunity. *Cancer Discovery*, *13*(2), 410–431. https://doi.org/10.1158/2159-8290.CD-22-0523

Marisa, L., Blum, Y., Taieb, J., Ayadi, M., Pilati, C., Le Malicot, K., Lepage, C., Salazar, R., Aust, D., Duval, A., Blons, H., Taly, V., Gentien, D., Rapinat, A., Selves, J., Mouillet-Richard, S., Boige, V., Emile, J.-F., de Reyniès, A., & Laurent-Puig, P. (2021). Intratumor CMS Heterogeneity Impacts Patient Prognosis in Localized Colon Cancer. *Clinical Cancer Research*, *27*(17), 4768–4780. https://doi.org/10.1158/1078-0432.CCR-21-0529

Marsh, P. J., James, R. D., & Schofield, P. F. (1994). Adjuvant preoperative radiotherapy for locally advanced rectal carcinoma. Results of a prospective, randomized trial. *Diseases of the Colon and Rectum*, *37*(12), 1205–1214. https://doi.org/10.1007/BF02257783

Martling, A., Holm, T., Rutqvist, L. E., Johansson, H., Moran, B. J., Heald, R. J., & Cedermark, B. (2005). Impact of a surgical training programme on rectal cancer outcomes in Stockholm. *The British Journal of Surgery*, *92*(2), 225–229. https://doi.org/10.1002/bjs.4834

Massard, C., Cassier, P., Bendell, J. C., Marie, D. B., Blery, M., Morehouse, C., Ascierto, M., Zerbib, R., Mitry, E., & Tolcher, A. W. (2019). 1203P - Preliminary results of STELLAR-001, a dose escalation phase I study of the anti-C5aR, IPH5401, in combination with durvalumab in advanced solid tumours. *Annals of Oncology*, *30*, v492. https://doi.org/10.1093/annonc/mdz253.029

Matsumura, S., Wang, B., Kawashima, N., Braunstein, S., Badura, M., Cameron, T. O., Babb, J. S., Schneider, R. J., Formenti, S. C., Dustin, M. L., & Demaria, S. (2008). Radiation-induced CXCL16 release by breast cancer cells attracts effector T cells. *Journal of Immunology (Baltimore, Md.: 1950)*, *181*(5), 3099–3107. https://doi.org/10.4049/jimmunol.181.5.3099

Mattes, M. D., Eubank, T. D., Almubarak, M., Wen, S., Marano, G. D., Jacobson, G. M., & Ma, P. C. (2021). A Prospective Trial Evaluating the Safety and Systemic Response From the Concurrent Use of Radiation Therapy with Checkpoint Inhibitor Immunotherapy in Metastatic Non-Small Cell Lung Cancer. *Clinical Lung Cancer*, *22*(4), 268–273. https://doi.org/10.1016/j.cllc.2021.01.012

Mc Gee, M. M. (2015). Targeting the Mitotic Catastrophe Signaling Pathway in Cancer. *Mediators of Inflammation*, *2015*, 146282. https://doi.org/10.1155/2015/146282

McCorry, A. M., Loughrey, M. B., Longley, D. B., Lawler, M., & Dunne, P. D. (2018). Epithelial-to-mesenchymal transition signature assessment in colorectal cancer quantifies tumour stromal content rather than true transition. *The Journal of Pathology*, *246*(4), 422–426. https://doi.org/10.1002/path.5155

McGill, M. R., & Jaeschke, H. (2019). Animal models of drug-induced liver injury. *Biochimica et Biophysica Acta (BBA) - Molecular Basis of Disease*, *1865*(5), 1031–1039. https://doi.org/10.1016/j.bbadis.2018.08.037

Melzer, C., Hass, R., von der Ohe, J., Lehnert, H., & Ungefroren, H. (2017). The role of TGF-β and its crosstalk with RAC1/RAC1b signaling in breast and pancreas carcinoma. *Cell Communication and Signaling: CCS*, *15*(1), 19. https://doi.org/10.1186/s12964-017-0175-0

Mempel, T. R., Pittet, M. J., Khazaie, K., Weninger, W., Weissleder, R., von Boehmer, H., & von Andrian, U. H. (2006). Regulatory T cells reversibly suppress cytotoxic T cell function independent of effector differentiation. *Immunity*, *25*(1), 129–141. https://doi.org/10.1016/j.immuni.2006.04.015

Meziani, L., Deutsch, E., & Mondini, M. (2018). Macrophages in radiation injury: A new therapeutic target. *Oncoimmunology*, *7*(10), e1494488. https://doi.org/10.1080/2162402X.2018.1494488

Minsky, B. D. (2012). Short-Course Radiation Versus Long-Course Chemoradiation for Rectal Cancer: Making Progress. *Journal of Clinical Oncology*, *30*(31), 3777–3778. https://doi.org/10.1200/JCO.2012.45.0551

Monteran, L., Ershaid, N., Doron, H., Zait, Y., Scharff, Y., Ben-Yosef, S., Avivi, C., Barshack, I., Sonnenblick, A., & Erez, N. (2022). Chemotherapy-induced complement signaling modulates immunosuppression and metastatic relapse in breast cancer. *Nature Communications*, *13*(1), Article 1. https://doi.org/10.1038/s41467-022-33598-x

Mortezaee, K., & Najafi, M. (2021). Immune system in cancer radiotherapy: Resistance mechanisms and therapy perspectives. *Critical Reviews in Oncology/Hematology*, *157*, 103180. https://doi.org/10.1016/j.critrevonc.2020.103180

Mukherjee, P., Winter, S. L., & Alexandrow, M. G. (2010). Cell cycle arrest by transforming growth factor beta1 near G1/S is mediated by acute abrogation of prereplication complex activation involving an Rb-MCM interaction. *Molecular and Cellular Biology*, *30*(3), 845–856. https://doi.org/10.1128/MCB.01152-09

Murao, A., Aziz, M., Wang, H., Brenner, M., & Wang, P. (2021). Release mechanisms of major DAMPs. *Apoptosis*, *26*(3), 152–162. https://doi.org/10.1007/s10495-021-01663-3

Muroyama, Y., Nirschl, T. R., Kochel, C. M., Lopez-Bujanda, Z., Theodros, D., Mao, W., Carrera-Haro, M. A., Ghasemzadeh, A., Marciscano, A. E., Velarde, E., Tam, A. J., Thoburn, C. J., Uddin, M., Meeker, A. K., Anders, R. A., Pardoll, D. M., & Drake, C. G. (2017). Stereotactic Radiotherapy Increases Functionally Suppressive Regulatory T Cells in the Tumor Microenvironment. *Cancer Immunology Research*, *5*(11), 992–1004. https://doi.org/10.1158/2326-6066.CIR-17-0040

Nagarsheth, N., Wicha, M. S., & Zou, W. (2017). Chemokines in the cancer microenvironment and their relevance in cancer immunotherapy. *Nature Reviews. Immunology*, *17*(9), 559–572. https://doi.org/10.1038/nri.2017.49

Nakayama, M., Wang, D., Kok, S. Y., Oshima, H., & Oshima, M. (2022). Genetic Alterations and Microenvironment that Drive Malignant Progression of Colorectal Cancer: Lessons from Mouse and Organoid Models. *Journal of Cancer Prevention*, *27*(1), 1–6. https://doi.org/10.15430/JCP.2022.27.1.1

Ngan, S. Y., Burmeister, B., Fisher, R. J., Solomon, M., Goldstein, D., Joseph, D., Ackland, S. P., Schache, D., McClure, B., McLachlan, S.-A., McKendrick, J., Leong, T., Hartopeanu, C., Zalcberg, J., & Mackay, J. (2012). Randomized trial of short-course radiotherapy versus long-course chemoradiation comparing rates of local recurrence in patients with T3 rectal cancer: Trans-Tasman Radiation Oncology Group trial 01.04. *Journal of Clinical Oncology: Official Journal of the American Society of Clinical Oncology*, *30*(31), 3827–3833. https://doi.org/10.1200/JCO.2012.42.9597

Ngwa, W., Irabor, O. C., Schoenfeld, J. D., Hesser, J., Demaria, S., & Formenti, S. C. (2018). Using immunotherapy to boost the abscopal effect. *Nature Reviews. Cancer*, *18*(5), 313–322. https://doi.org/10.1038/nrc.2018.6

Nishishita, R., Morohashi, S., Seino, H., Wu, Y., Yoshizawa, T., Haga, T., Saito, K., Hakamada, K., Fukuda, S., & Kijima, H. (2018). Expression of cancer-associated fibroblast markers in advanced colorectal cancer. *Oncology Letters*, *15*(5), 6195–6202. https://doi.org/10.3892/ol.2018.8097

O'Brien, R. M., Lynam-Lennon, N., & Olcina, M. M. (2023). Thinking inside the box: Intracellular roles for complement system proteins come into focus. *British Journal of Cancer*, *128*(2), Article 2. https://doi.org/10.1038/s41416-022-02116-7

O'Connell, M. J., Colangelo, L. H., Beart, R. W., Petrelli, N. J., Allegra, C. J., Sharif, S., Pitot, H. C., Shields, A. F., Landry, J. C., Ryan, D. P., Parda, D. S., Mohiuddin, M., Arora, A., Evans, L. S., Bahary, N., Soori, G. S., Eakle, J., Robertson, J. M., Moore, D. F., … Wolmark, N. (2014). Capecitabine and oxaliplatin in the preoperative multimodality treatment of rectal cancer: Surgical end points from National Surgical Adjuvant Breast and Bowel Project trial R-04. *Journal of Clinical Oncology: Official Journal of the American Society of Clinical Oncology*, *32*(18), 1927–1934. https://doi.org/10.1200/JCO.2013.53.7753

Olcina, M. M., Stavros, M., Nambiar, D. K., Kim, R. K., Casey, K. M., Rie, V. E., Woodruff, T. M., Graves, E. G., Quynh-Thu, L., Manuel, S., & Giaccia, A. J. (2020). *Targeting C5aR1 Increases the Therapeutic Window of Radiotherapy*. https://doi.org/10.1101/2020.10.27.358036

Oliveri, V. (2022). Selective Targeting of Cancer Cells by Copper Ionophores: An Overview. *Frontiers in Molecular Biosciences*, *9*, 841814. https://doi.org/10.3389/fmolb.2022.841814

Opzoomer, J. W., Anstee, J. E., Dean, I., Hill, E. J., Bouybayoune, I., Caron, J., Muliaditan, T., Gordon, P., Sosnowska, D., Nuamah, R., Pinder, S. E., Ng, T., Dazzi, F., Kordasti, S., Withers, D. R., Lawrence, T., & Arnold, J. N. (2021). Macrophages orchestrate the

expansion of a proangiogenic perivascular niche during cancer progression. *Science Advances*, *7*(45), eabg9518. https://doi.org/10.1126/sciadv.abg9518

Padovan, E., Spagnoli, G. C., Ferrantini, M., & Heberer, M. (2002). IFN-alpha2a induces IP-10/CXCL10 and MIG/CXCL9 production in monocyte-derived dendritic cells and enhances their capacity to attract and stimulate CD8+ effector T cells. *Journal of Leukocyte Biology*, *71*(4), 669–676.

Pan, J., Ma, Z., Liu, B., Qian, H., Shao, X., Liu, J., Wang, Q., & Xue, W. (2023). Identification of cancer-associated fibroblasts subtypes in prostate cancer. *Frontiers in Immunology*, *14*, 1133160. https://doi.org/10.3389/fimmu.2023.1133160

Pang, N., Alimu, X., Chen, R., Muhashi, M., Ma, J., Chen, G., Zhao, F., Wang, L., Qu, J., & Ding, J. (2021). Activated Galectin-9/Tim3 promotes Treg and suppresses Th1 effector function in chronic lymphocytic leukemia. *FASEB Journal: Official Publication of the Federation of American Societies for Experimental Biology*, *35*(7), e21556. https://doi.org/10.1096/fj.202100013R

Pappou, E. P., Temple, L. K., Patil, S., Smith, J. J., Wei, I. H., Nash, G. M., Guillem, J. G., Widmar, M., Weiser, M. R., Paty, P. B., Schrag, D., & Garcia-Aguilar, J. (2022). Quality of life and function after rectal cancer surgery with and without sphincter preservation. *Frontiers in Oncology*, *12*, 944843. https://doi.org/10.3389/fonc.2022.944843

Park, J.-H., Kim, Y.-H., Shim, S., Kim, A., Jang, H., Lee, S.-J., Park, S., Seo, S., Jang, W. I., Lee, S. B., & Kim, M.-J. (2021). Radiation-Activated PI3K/AKT Pathway Promotes the Induction of Cancer Stem-Like Cells via the Upregulation of SOX2 in Colorectal Cancer. *Cells*, *10*(1), 135. https://doi.org/10.3390/cells10010135

Pawlik, T. M., & Keyomarsi, K. (2004). Role of cell cycle in mediating sensitivity to radiotherapy. *International Journal of Radiation Oncology, Biology, Physics*, *59*(4), 928–942. https://doi.org/10.1016/j.ijrobp.2004.03.005

Pennel, K. A. F., Hatthakarnkul, P., Wood, C. S., Lian, G.-Y., Al-Badran, S. S. F., Quinn, J. A., Legrini, A., Inthagard, J., Alexander, P. G., van Wyk, H., Kurniawan, A., Hashmi, U., Gillespie, M. A., Mills, M., Ammar, A., Hay, J., Andersen, D., Nixon, C., Rebus, S., … Edwards, J. (2024). JAK/STAT3 represents a therapeutic target for colorectal cancer patients with stromal-rich tumors. *Journal of Experimental & Clinical Cancer Research*, *43*(1), 64. https://doi.org/10.1186/s13046-024-02958-4

Pine, J. K., Morris, E., Hutchins, G. G., West, N. P., Jayne, D. G., Quirke, P., & Prasad, K. R. (2015). Systemic neutrophil-to-lymphocyte ratio in colorectal cancer: The relationship to patient survival, tumour biology and local lymphocytic response to tumour. *British Journal of Cancer*, *113*(2), 204–211. https://doi.org/10.1038/bjc.2015.87

Pinto, C., Di Bisceglie, M., Di Fabio, F., Bochicchio, A., Latiano, T., Cordio, S., Rosati, G., Aschele, C., Marino, A., Bergamo, F., Bustreo, S., Frassineti, L., Ciardiello, F., Damato, A., Giaquinta, S., Baldari, D., & Boni, L. (2018). Phase II Study of Preoperative Treatment with External Radiotherapy Plus Panitumumab in Low-Risk, Locally Advanced Rectal Cancer (RaP Study/STAR-03). *The Oncologist*, *23*(8), 912–918. https://doi.org/10.1634/theoncologist.2017-0484

Pio, R., Corrales, L., & Lambris, J. D. (2014). The role of complement in tumor growth. *Advances in Experimental Medicine and Biology*, *772*, 229–262. https://doi.org/10.1007/978-1-4614-5915-6_11

Plitas, G., & Rudensky, A. Y. (2016). Regulatory T Cells: Differentiation and Function. *Cancer Immunology Research*, *4*(9), 721–725. https://doi.org/10.1158/2326-6066.CIR-16-0193

Prame Kumar, K., Nicholls, A. J., & Wong, C. H. Y. (2018). Partners in crime: Neutrophils and monocytes/macrophages in inflammation and disease. *Cell and Tissue Research*, *371*(3), 551–565. https://doi.org/10.1007/s00441-017-2753-2

Putra, A., Alif, I., Hamra, N., Santosa, O., Kustiyah, A. R., Muhar, A. M., & Lukman, K. (2020). MSC-released TGF-β regulate α-SMA expression of myofibroblast during wound healing. *Journal of Stem Cells & Regenerative Medicine*, *16*(2), 73–79. https://doi.org/10.46582/jsrm.1602011

Qiu, W., Kuo, C.-Y., Tian, Y., & Su, G. H. (2021). Dual Roles of the Activin Signaling Pathway in Pancreatic Cancer. *Biomedicines*, *9*(7), 821. https://doi.org/10.3390/biomedicines9070821

Qiu, X., Quan, G., Ou, W., Wang, P., Huang, X., Li, X., Shen, Y., Yang, W., Wang, J., & Wu, X. (2023). Unraveling TIMP1: A multifaceted biomarker in colorectal cancer. *Frontiers in Genetics*, *14*, 1265137. https://doi.org/10.3389/fgene.2023.1265137

Reardon, D. A., Brandes, A. A., Omuro, A., Mulholland, P., Lim, M., Wick, A., Baehring, J., Ahluwalia, M. S., Roth, P., Bähr, O., Phuphanich, S., Sepulveda, J. M., De Souza, P., Sahebjam, S., Carleton, M., Tatsuoka, K., Taitt, C., Zwirtes, R., Sampson, J., & Weller, M. (2020). Effect of Nivolumab vs Bevacizumab in Patients With Recurrent Glioblastoma: The CheckMate 143 Phase 3 Randomized Clinical Trial. *JAMA Oncology*, *6*(7), 1003–1010. https://doi.org/10.1001/jamaoncol.2020.1024

Regal, J. F., Dornfeld, K. J., & Fleming, S. D. (2016). Radiotherapy: Killing with complement. *Annals of Translational Medicine*, *4*(5), 94. https://doi.org/10.21037/atm.2015.12.46

Reibman, J., Meixler, S., Lee, T. C., Gold, L. I., Cronstein, B. N., Haines, K. A., Kolasinski, S. L., & Weissmann, G. (1991). Transforming growth factor beta 1, a potent chemoattractant for human neutrophils, bypasses classic signal-transduction pathways. *Proceedings of the National Academy of Sciences of the United States of America*, *88*(15), 6805–6809.

Reits, E. A., Hodge, J. W., Herberts, C. A., Groothuis, T. A., Chakraborty, M., Wansley, E. K., Camphausen, K., Luiten, R. M., de Ru, A. H., Neijssen, J., Griekspoor, A., Mesman, E., Verreck, F. A., Spits, H., Schlom, J., van Veelen, P., & Neefjes, J. J. (2006). Radiation modulates the peptide repertoire, enhances MHC class I expression, and induces successful antitumor immunotherapy. *The Journal of Experimental Medicine*, *203*(5), 1259–1271. https://doi.org/10.1084/jem.20052494

Ricklin, D., Hajishengallis, G., Yang, K., & Lambris, J. D. (2010a). Complement—A key system for immune surveillance and homeostasis. *Nature Immunology*, *11*(9), 785–797. https://doi.org/10.1038/ni.1923

Rockey, D. C., Weymouth, N., & Shi, Z. (2013). Smooth muscle α actin (Acta2) and myofibroblast function during hepatic wound healing. *PloS One*, *8*(10), e77166. https://doi.org/10.1371/journal.pone.0077166

Rödel, C., Graeven, U., Fietkau, R., Hohenberger, W., Hothorn, T., Arnold, D., Hofheinz, R.-D., Ghadimi, M., Wolff, H. A., Lang-Welzenbach, M., Raab, H.-R., Wittekind, C., Ströbel, P., Staib, L., Wilhelm, M., Grabenbauer, G. G., Hoffmanns, H., Lindemann, F., Schlenska-Lange, A., … German Rectal Cancer Study Group. (2015). Oxaliplatin added to fluorouracil-based preoperative chemoradiotherapy and postoperative chemotherapy of locally advanced rectal cancer (the German CAO/ARO/AIO-04 study): Final results of the multicentre, open-label, randomised, phase 3 trial. *The Lancet. Oncology*, *16*(8), 979–989. https://doi.org/10.1016/S1470-2045(15)00159-X

Rodriguez-Ruiz, M. E., Garasa, S., Rodriguez, I., Solorzano, J. L., Barbes, B., Yanguas, A., Teijeira, A., Etxeberria, I., Aristu, J. J., Halin, C., Melero, I., & Rouzaut, A. (2017). Intercellular Adhesion Molecule-1 and Vascular Cell Adhesion Molecule Are Induced by Ionizing Radiation on Lymphatic Endothelium. *International Journal of Radiation Oncology, Biology, Physics*, *97*(2), 389–400. https://doi.org/10.1016/j.ijrobp.2016.10.043

Roper, J., Tammela, T., Cetinbas, N. M., Akkad, A., Roghanian, A., Rickelt, S., Almeqdadi, M., Wu, K., Oberli, M. A., Sánchez-Rivera, F. J., Park, Y. K., Liang, X., Eng, G., Taylor, M. S., Azimi, R., Kedrin, D., Neupane, R., Beyaz, S., Sicinska, E. T., … Yilmaz, Ö. H. (2017). In vivo genome editing and organoid transplantation models of colorectal cancer and metastasis. *Nature Biotechnology*, *35*(6), 569–576. https://doi.org/10.1038/nbt.3836

Ross, G. M. (1999). Induction of cell death by radiotherapy. *Endocrine-Related Cancer*, *6*(1), 41–44. https://doi.org/10.1677/erc.0.0060041

Ross, S. H., & Cantrell, D. A. (2018). Signaling and Function of Interleukin-2 in T Lymphocytes. *Annual Review of Immunology*, *36*, 411–433. https://doi.org/10.1146/annurev-immunol-042617-053352

Roudko, V., Cimen Bozkus, C., Greenbaum, B., Lucas, A., Samstein, R., & Bhardwaj, N. (2021). Lynch Syndrome and MSI-H Cancers: From Mechanisms to “Off-The-Shelf” Cancer Vaccines. *Frontiers in Immunology*, *12*. https://doi.org/10.3389/fimmu.2021.757804

Roumenina, L. T., Daugan, M. V., Noé, R., Petitprez, F., Vano, Y. A., Sanchez-Salas, R., Becht, E., Meilleroux, J., Clec’h, B. L., Giraldo, N. A., Merle, N. S., Sun, C.-M., Verkarre, V., Validire, P., Selves, J., Lacroix, L., Delfour, O., Vandenberghe, I., Thuilliez, C., … Fridman, W. H. (2019). Tumor Cells Hijack Macrophage-Produced Complement C1q to Promote Tumor Growth. *Cancer Immunology Research*, *7*(7), 1091–1105. https://doi.org/10.1158/2326-6066.CIR-18-0891

Rückert, M., Flohr, A.-S., Hecht, M., & Gaipl, U. S. (2021). Radiotherapy and the immune system: More than just immune suppression. *STEM CELLS*, *39*(9), 1155–1165. https://doi.org/10.1002/stem.3391

Salas-Benito, D., Vercher, E., Conde, E., Glez-Vaz, J., Tamayo, I., & Hervas-Stubbs, S. (2020). Inflammation and immunity in ovarian cancer. *EJC Supplements*, *15*, 56–66. https://doi.org/10.1016/j.ejcsup.2019.12.002

Sarkar, T., Dhar, S., & Sa, G. (2021). Tumor-infiltrating T-regulatory cells adapt to altered metabolism to promote tumor-immune escape. *Current Research in Immunology*, *2*, 132–141. https://doi.org/10.1016/j.crimmu.2021.08.002

Satorres, C., García-Campos, M., & Bustamante-Balén, M. (2021). Molecular Features of the Serrated Pathway to Colorectal Cancer: Current Knowledge and Future Directions. *Gut and Liver*, *15*(1), 31–43. https://doi.org/10.5009/gnl19402

Sauer, R., Becker, H., Hohenberger, W., Rödel, C., Wittekind, C., Fietkau, R., Martus, P., Tschmelitsch, J., Hager, E., Hess, C. F., Karstens, J.-H., Liersch, T., Schmidberger, H., Raab, R., & German Rectal Cancer Study Group. (2004). Preoperative versus postoperative chemoradiotherapy for rectal cancer. *The New England Journal of Medicine*, *351*(17), 1731–1740. https://doi.org/10.1056/NEJMoa040694

Schoenhals, J. E., Cushman, T. R., Barsoumian, H. B., Li, A., Cadena, A. P., Niknam, S., Younes, A. I., Caetano, M. da S., Cortez, M. A., & Welsh, J. W. (2018). Anti-glucocorticoid-induced Tumor Necrosis Factor-Related Protein (GITR) Therapy Overcomes Radiation-Induced Treg Immunosuppression and Drives Abscopal Effects. *Frontiers in Immunology*, *9*, 2170. https://doi.org/10.3389/fimmu.2018.02170

Schoeps, B., Eckfeld, C., Prokopchuk, O., Böttcher, J., Häußler, D., Steiger, K., Demir, I. E., Knolle, P., Soehnlein, O., Jenne, D. E., Hermann, C. D., & Krüger, A. (2021). TIMP1 Triggers Neutrophil Extracellular Trap Formation in Pancreatic Cancer. *Cancer Research*, *81*(13), 3568–3579. https://doi.org/10.1158/0008-5472.CAN-20-4125

Schrag, D., Shi, Q., Weiser, M. R., Gollub, M. J., Saltz, L. B., Musher, B. L., Goldberg, J., Al Baghdadi, T., Goodman, K. A., McWilliams, R. R., Farma, J. M., George, T. J., Kennecke, H. F., Shergill, A., Montemurro, M., Nelson, G. D., Colgrove, B., Gordon, V., Venook, A. P., … Mamon, H. J. (2023). Preoperative Treatment of Locally Advanced Rectal Cancer. *New England Journal of Medicine*, *389*(4), 322–334. https://doi.org/10.1056/NEJMoa2303269

Schrag, D., Weiser, M. R., Goodman, K. A., Gonen, M., Hollywood, E., Cercek, A., Reidy-Lagunes, D. L., Gollub, M. J., Shia, J., Guillem, J. G., Temple, L. K. F., Paty, P. B., & Saltz, L. B. (2014). Neoadjuvant chemotherapy without routine use of radiation therapy for patients with locally advanced rectal cancer: A pilot trial. *Journal of Clinical Oncology: Official Journal of the American Society of Clinical Oncology*, *32*(6), 513–518. https://doi.org/10.1200/JCO.2013.51.7904

Schrantz, N., Bourgeade, M. F., Mouhamad, S., Leca, G., Sharma, S., & Vazquez, A. (2001). P38-mediated regulation of an Fas-associated death domain protein-independent pathway leading to caspase-8 activation during TGFbeta-induced apoptosis in human Burkitt lymphoma B cells BL41. *Molecular Biology of the Cell*, *12*(10), 3139–3151. https://doi.org/10.1091/mbc.12.10.3139

Sebag-Montefiore, D., Adams, R., Gollins, S., Samuel, L. M., Glynne-Jones, R., Harte, R., West, N., Quirke, P., Myint, A. S., Bach, S. P., Parsons, P., Falk, S., Dhadda, A. S., Misra, V., Brown, N., Brown, G., Harrison, M., White, L., Duggan, M., & Lopes, A. (2020). ARISTOTLE: A phase III trial comparing concurrent capecitabine with capecitabine and irinotecan (Ir) chemoradiation as preoperative treatment for MRI-defined locally advanced rectal cancer (LARC). *Journal of Clinical Oncology*, *38*(15_suppl), 4101–4101. https://doi.org/10.1200/JCO.2020.38.15_suppl.4101

Sebag-Montefiore, D., Stephens, R. J., Steele, R., Monson, J., Grieve, R., Khanna, S., Quirke, P., Couture, J., de Metz, C., Myint, A. S., Bessell, E., Griffiths, G., Thompson, L. C., & Parmar, M. (2009). Preoperative radiotherapy versus selective postoperative chemoradiotherapy in patients with rectal cancer (MRC CR07 and NCIC-CTG C016): A multicentre, randomised trial. *Lancet (London, England)*, *373*(9666), 811–820. https://doi.org/10.1016/S0140-6736(09)60484-0

Shen, L., Smith, J. M., Shen, Z., Eriksson, M., Sentman, C., & Wira, C. R. (2007). Inhibition of human neutrophil degranulation by transforming growth factor-beta1. *Clinical and Experimental Immunology*, *149*(1), 155–161. https://doi.org/10.1111/j.1365-2249.2007.03376.x

Soruri, A., Kim, S., Kiafard, Z., & Zwirner, J. (2003). Characterization of C5aR expression on murine myeloid and lymphoid cells by the use of a novel monoclonal antibody. *Immunology Letters*, *88*(1), 47–52. https://doi.org/10.1016/s0165-2478(03)00052-x

Spaas, M., Sundahl, N., Hulstaert, E., Kruse, V., Rottey, S., De Maeseneer, D., Surmont, V., Meireson, A., Brochez, L., Reynders, D., Goetghebeur, E., Van den Begin, R., Van Gestel, D., Renard, V., Dirix, P., Mestdagh, P., & Ost, P. (2021). Checkpoint inhibition in combination with an immunoboost of external beam radiotherapy in solid tumors (CHEERS): Study protocol for a phase 2, open-label, randomized controlled trial. *BMC Cancer*, *21*(1), 514. https://doi.org/10.1186/s12885-021-08088-w

Spigel, D. R., Faivre-Finn, C., Gray, J. E., Vicente, D., Planchard, D., Paz-Ares, L., Vansteenkiste, J. F., Garassino, M. C., Hui, R., Quantin, X., Rimner, A., Wu, Y.-L., Özgüroğlu, M., Lee, K. H., Kato, T., de Wit, M., Kurata, T., Reck, M., Cho, B. C., … Antonia, S. J. (2022). Five-Year Survival Outcomes From the PACIFIC Trial: Durvalumab After Chemoradiotherapy in Stage III Non-Small-Cell Lung Cancer. *Journal of Clinical Oncology: Official Journal of the American Society of Clinical Oncology*, *40*(12), 1301–1311. https://doi.org/10.1200/JCO.21.01308

Spitzner, M., Roesler, B., Bielfeld, C., Emons, G., Gaedcke, J., Wolff, H. A., Rave-Fränk, M., Kramer, F., Beissbarth, T., Kitz, J., Wienands, J., Ghadimi, B. M., Ebner, R., Ried, T., & Grade, M. (2014). STAT3 inhibition sensitizes colorectal cancer to chemoradiotherapy in vitro and in vivo. *International Journal of Cancer*, *134*(4), 997–1007. https://doi.org/10.1002/ijc.28429

Srinivas, U. S., Tan, B. W. Q., Vellayappan, B. A., & Jeyasekharan, A. D. (2019). ROS and the DNA damage response in cancer. *Redox Biology*, *25*, 101084. https://doi.org/10.1016/j.redox.2018.101084

Strainic, M. G., Shevach, E. M., An, F., Lin, F., & Medof, M. E. (2013c). Absence of signaling into $CD4^+$ cells via C3aR and C5aR enables autoinductive TGF-β1 signaling and induction of $Foxp3^+$ regulatory T cells. *Nature Immunology*, *14*(2), 162–171. https://doi.org/10.1038/ni.2499

Surace, L., Lysenko, V., Fontana, A. O., Cecconi, V., Janssen, H., Bicvic, A., Okoniewski, M., Pruschy, M., Dummer, R., Neefjes, J., Knuth, A., Gupta, A., & van den Broek, M. (2015). Complement Is a Central Mediator of Radiotherapy-Induced Tumor-Specific Immunity and Clinical Response. *Immunity*, *42*(4), 767–777. https://doi.org/10.1016/j.immuni.2015.03.009

Suzuki, H., Chikazawa, N., Tasaka, T., Wada, J., Yamasaki, A., Kitaura, Y., Sozaki, M., Tanaka, M., Onishi, H., Morisaki, T., & Katano, M. (2010). Intratumoral CD8(+) T/FOXP3 (+) cell ratio is a predictive marker for survival in patients with colorectal cancer. *Cancer Immunology, Immunotherapy: CII*, *59*(5), 653–661. https://doi.org/10.1007/s00262-009-0781-9

Swedish Rectal Cancer Trial, Cedermark, B., Dahlberg, M., Glimelius, B., Påhlman, L., Rutqvist, L. E., & Wilking, N. (1997). Improved survival with preoperative radiotherapy in resectable rectal cancer. *The New England Journal of Medicine*, *336*(14), 980–987. https://doi.org/10.1056/NEJM199704033361402

Tabasso, A. F. S., Jones, D. J. L., Jones, G. D. D., & Macip, S. (2019). Radiotherapy-Induced Senescence and its Effects on Responses to Treatment. *Clinical Oncology (Royal College of Radiologists (Great Britain))*, *31*(5), 283–289. https://doi.org/10.1016/j.clon.2019.02.003

Takeshima, T., Pop, L. M., Laine, A., Iyengar, P., Vitetta, E. S., & Hannan, R. (2016). Key role for neutrophils in radiation-induced antitumor immune responses: Potentiation with G-CSF. *Proceedings of the National Academy of Sciences*, *113*(40), 11300–11305. https://doi.org/10.1073/pnas.1613187113

Tan, G., Lin, C., Huang, C., Chen, B., Chen, J., Shi, Y., & Zhi, F. (2022). Radiosensitivity of colorectal cancer and radiation-induced gut damages are regulated by gasdermin E. *Cancer Letters*, *529*, 1–10. https://doi.org/10.1016/j.canlet.2021.12.034

Tanaka, A., & Sakaguchi, S. (2017). Regulatory T cells in cancer immunotherapy. *Cell Research*, *27*(1), Article 1. https://doi.org/10.1038/cr.2016.151

Tauriello, D. V. F., Palomo-Ponce, S., Stork, D., Berenguer-Llergo, A., Badia-Ramentol, J., Iglesias, M., Sevillano, M., Ibiza, S., Cañellas, A., Hernando-Momblona, X., Byrom, D., Matarin, J. A., Calon, A., Rivas, E. I., Nebreda, A. R., Riera, A., Attolini, C. S.-O., & Batlle, E. (2018). TGFβ drives immune evasion in genetically reconstituted colon cancer metastasis. *Nature*, *554*(7693), Article 7693. https://doi.org/10.1038/nature25492

ten Hoorn, S., de Back, T. R., Sommeijer, D. W., & Vermeulen, L. (2021). Clinical Value of Consensus Molecular Subtypes in Colorectal Cancer: A Systematic Review and Meta-

Analysis. *JNCI Journal of the National Cancer Institute*, *114*(4), 503–516. https://doi.org/10.1093/jnci/djab106

Terada, H., Urano, T., & Konno, H. (2005). Association of interleukin-8 and plasminogen activator system in the progression of colorectal cancer. *European Surgical Research. Europaische Chirurgische Forschung. Recherches Chirurgicales Europeennes*, *37*(3), 166–172. https://doi.org/10.1159/000085964

Thomas, D. A., & Massagué, J. (2005). TGF-β directly targets cytotoxic T cell functions during tumor evasion of immune surveillance. *Cancer Cell*, *8*(5), 369–380. https://doi.org/10.1016/j.ccr.2005.10.012

Thomas, P. R. M., & Lindblad, A. S. (1988). Adjuvant postoperative radiotherapy and chemotherapy in rectal carcinoma: A review of the gastrointestinal tumor study group experience. *Radiotherapy and Oncology*, *13*(4), 245–252. https://doi.org/10.1016/0167-8140(88)90219-8

Tian, W., Zhou, J., Chen, M., Qiu, L., Li, Y., Zhang, W., Guo, R., Lei, N., & Chang, L. (2022). Bioinformatics analysis of the role of aldolase A in tumor prognosis and immunity. *Scientific Reports*, *12*, 11632. https://doi.org/10.1038/s41598-022-15866-4

Transforming growth factor beta induces fibroblasts to express and release the immunomodulatory protein PD-L1 into extracellular vesicles. (n.d.). https://doi.org/10.1096/fj.201902354R

Trowell, O. A. (1952). The sensitivity of lymphocytes to ionising radiation. *The Journal of Pathology and Bacteriology*, *64*(4), 687–704. https://doi.org/10.1002/path.1700640403

Tuveson, D., & Clevers, H. (2019). Cancer modeling meets human organoid technology. *Science (New York, N.Y.)*, *364*(6444), 952–955. https://doi.org/10.1126/science.aaw6985

Ubink, I., Elias, S. G., Moelans, C. B., Laclé, M. M., van Grevenstein, W. M. U., van Diest, P. J., Borel Rinkes, I. H. M., & Kranenburg, O. (2017). A Novel Diagnostic Tool for Selecting Patients With Mesenchymal-Type Colon Cancer Reveals Intratumor Subtype Heterogeneity. *JNCI: Journal of the National Cancer Institute*, *109*(7), djw303. https://doi.org/10.1093/jnci/djw303

Vadrevu, S. K., Chintala, N. K., Sharma, S. K., Sharma, P., Cleveland, C., Riediger, L., Manne, S., Fairlie, D. P., Gorczyca, W., Almanza, O., Karbowniczek, M., & Markiewski, M. M. (2014). Complement C5a Receptor Facilitates Cancer Metastasis by Altering T-Cell Responses in the Metastatic Niche. *Cancer Research*, *74*(13), 3454–3465. https://doi.org/10.1158/0008-5472.CAN-14-0157

van Gijn, W., Marijnen, C. A. M., Nagtegaal, I. D., Kranenbarg, E. M.-K., Putter, H., Wiggers, T., Rutten, H. J. T., Påhlman, L., Glimelius, B., van de Velde, C. J. H., & Dutch Colorectal Cancer Group. (2011). Preoperative radiotherapy combined with total mesorectal excision for resectable rectal cancer: 12-year follow-up of the multicentre, randomised controlled TME trial. *The Lancet. Oncology*, *12*(6), 575–582. https://doi.org/10.1016/S1470-2045(11)70097-3

Vaquero-Siguero, N., Schleussner, N., Volk, J., Mastel, M., Meier, J., & Jackstadt, R. (2022). Modeling Colorectal Cancer Progression Reveals Niche-Dependent Clonal Selection. *Cancers*, *14*(17), 4260. https://doi.org/10.3390/cancers14174260

Vasquez-Dunddel, D., Pan, F., Zeng, Q., Gorbounov, M., Albesiano, E., Fu, J., Blosser, R. L., Tam, A. J., Bruno, T., Zhang, H., Pardoll, D., & Kim, Y. (2013). STAT3 regulates arginase-I in myeloid-derived suppressor cells from cancer patients. *The Journal of Clinical Investigation*, *123*(4), 1580–1589. https://doi.org/10.1172/JCI60083

Vesely, M. D., Kershaw, M. H., Schreiber, R. D., & Smyth, M. J. (2011). Natural innate and adaptive immunity to cancer. *Annual Review of Immunology*, *29*, 235–271. https://doi.org/10.1146/annurev-immunol-031210-101324

Vitale, I., Galluzzi, L., Castedo, M., & Kroemer, G. (2011). Mitotic catastrophe: A mechanism for avoiding genomic instability. *Nature Reviews. Molecular Cell Biology*, *12*(6), 385–392. https://doi.org/10.1038/nrm3115

Vuik, F. E., Nieuwenburg, S. A., Bardou, M., Lansdorp-Vogelaar, I., Dinis-Ribeiro, M., Bento, M. J., Zadnik, V., Pellisé, M., Esteban, L., Kaminski, M. F., Suchanek, S., Ngo, O., Májek, O., Leja, M., Kuipers, E. J., & Spaander, M. C. (2019). Increasing incidence of colorectal cancer in young adults in Europe over the last 25 years. *Gut*, *68*(10), 1820–1826. https://doi.org/10.1136/gutjnl-2018-317592

Walko, C. M., & Lindley, C. (2005). Capecitabine: A review. *Clinical Therapeutics*, *27*(1), 23–44. https://doi.org/10.1016/j.clinthera.2005.01.005

Wang, H., Li, S., Wang, Q., Jin, Z., Shao, W., Gao, Y., Li, L., Lin, K., Zhu, L., Wang, H., Liao, X., & Wang, D. (2021). Tumor immunological phenotype signature-based high-throughput screening for the discovery of combination immunotherapy compounds. *Science Advances*, *7*(4), eabd7851. https://doi.org/10.1126/sciadv.abd7851

Wang, J., Kang, M., Wen, Q., Qin, Y.-T., Wei, Z.-X., Xiao, J.-J., & Wang, R.-S. (2017). Berberine sensitizes nasopharyngeal carcinoma cells to radiation through inhibition of Sp1 and EMT. *Oncology Reports*, *37*(4), 2425–2432. https://doi.org/10.3892/or.2017.5499

Wang, J., Xu, Z., Wang, Z., Du, G., & Lun, L. (2021). TGF-beta signaling in cancer radiotherapy. *Cytokine*, *148*, 155709. https://doi.org/10.1016/j.cyto.2021.155709

Wang, J., Zhao, X., & Wan, Y. Y. (2023). Intricacies of TGF-β signaling in Treg and Th17 cell biology. *Cellular & Molecular Immunology*, *20*(9), Article 9. https://doi.org/10.1038/s41423-023-01036-7

Wang, L., Li, H., Zhang, Y., Santella, R. M., & Weinstein, I. B. (2009). HINT1 INHIBITS β-CATENIN/TCF4, USF2 AND NFκB ACTIVITY IN HUMAN HEPATOMA CELLS. *International Journal of Cancer. Journal International Du Cancer*, *124*(7), 1526–1534. https://doi.org/10.1002/ijc.24072

Wang, M., Wang, L., He, X., Zhang, J., Zhu, Z., Zhang, M., & Li, X. (2020). lncRNA CCAT2 promotes radiotherapy resistance for human esophageal carcinoma cells via the miR-145/p70S6K1 and p53 pathway. *International Journal of Oncology*, *56*(1), 327–336. https://doi.org/10.3892/ijo.2019.4929

Wang, X., Schoenhals, J. E., Valdecanas, D. R., Li, A., Ye, H., Zhang, F., Tang, M., Tang, C., Liu, C. G., Liu, X., Komaki, R. U., Gomez, D. R., Chang, J. Y., Cortez, M. A., & Welsh, J. W. (2016). Suppression of Major Histocompatibility Complex (MHC) Class I and II Mediates Resistance to Anti-PD-1 in Lung Adenocarcinoma Tumors That Can Be Overcome by Radiation Therapy. *International Journal of Radiation Oncology, Biology, Physics*, *96*(2), S89. https://doi.org/10.1016/j.ijrobp.2016.06.224

Wang, Z., Tang, Y., Tan, Y., Wei, Q., & Yu, W. (2019). Cancer-associated fibroblasts in radiotherapy: Challenges and new opportunities. *Cell Communication and Signaling: CCS*, *17*(1), 47. https://doi.org/10.1186/s12964-019-0362-2

Ward, J. F. (1988b). DNA damage produced by ionizing radiation in mammalian cells: Identities, mechanisms of formation, and reparability. *Progress in Nucleic Acid Research and Molecular Biology*, *35*, 95–125. https://doi.org/10.1016/s0079-6603(08)60611-x

Wasmuth, H. H., Faerden, A. E., Myklebust, T. Å., Pfeffer, F., Norderval, S., Riis, R., Olsen, O. C., Lambrecht, J. R., Kørner, H., Larsen, S. G., Norwegian TaTME Collaborative Group, on behalf of the Norwegian Colorectal Cancer Group, Forsmo, H. M., Baekkelund, O., Lavik, S., Knapp, J. C., Sjo, O., & Rashid, G. (2020a). Transanal total mesorectal excision for rectal cancer has been suspended in Norway. *The British Journal of Surgery*, *107*(1), 121–130. https://doi.org/10.1002/bjs.11459

Wasmuth, H. H., Faerden, A. E., Myklebust, T. Å., Pfeffer, F., Norderval, S., Riis, R., Olsen, O. C., Lambrecht, J. R., Kørner, H., Larsen, S. G., Norwegian TaTME Collaborative Group, on behalf of the Norwegian Colorectal Cancer Group, Forsmo, H. M., Baekkelund, O., Lavik, S., Knapp, J. C., Sjo, O., & Rashid, G. (2020b). Transanal total mesorectal excision for rectal cancer has been suspended in Norway. *The British Journal of Surgery*, *107*(1), 121–130. https://doi.org/10.1002/bjs.11459

Welsh, J. W., Heymach, J. V., Guo, C., Menon, H., Klein, K., Cushman, T. R., Verma, V., Hess, K. R., Shroff, G., Tang, C., Skoulidis, F., Jeter, M., Comeaux, N., Patel, R. R., Chen, D., Ozgen, T., Nguyen, Q.-N., Chang, J. Y., Altan, M., … Glisson, B. (2020). Phase 1/2 Trial of Pembrolizumab and Concurrent Chemoradiation Therapy for Limited-Stage SCLC. *Journal of Thoracic Oncology: Official Publication of the International Association for the Study of Lung Cancer*, *15*(12), 1919–1927. https://doi.org/10.1016/j.jtho.2020.08.022

Werfel, T., Oppermann, M., Schulze, M., Krieger, G., Weber, M., & Götze, O. (1992). Binding of fluorescein-labeled anaphylatoxin C5a to human peripheral blood, spleen, and bone marrow leukocytes. *Blood*, *79*(1), 152–160.

Windhagen, A., Scholz, C., Höllsberg, P., Fukaura, H., Sette, A., & Hafler, D. A. (1995). Modulation of cytokine patterns of human autoreactive T cell clones by a single amino acid substitution of their peptide ligand. *Immunity*, *2*(4), 373–380. https://doi.org/10.1016/1074-7613(95)90145-0

Wo, J. Y., Anker, C. J., Ashman, J. B., Bhadkamkar, N. A., Bradfield, L., Chang, D. T., Dorth, J., Garcia-Aguilar, J., Goff, D., Jacqmin, D., Kelly, P., Newman, N. B., Olsen, J., Raldow, A.

C., Ruiz-Garcia, E., Stitzenberg, K. B., Thomas, C. R., Wu, Q. J., & Das, P. (2021). Radiation Therapy for Rectal Cancer: Executive Summary of an ASTRO Clinical Practice Guideline. *Practical Radiation Oncology*, *11*(1), 13–25. https://doi.org/10.1016/j.prro.2020.08.004

Wrana, J. L., & Attisano, L. (2000). The Smad pathway. *Cytokine & Growth Factor Reviews*, *11*(1), 5–13. https://doi.org/10.1016/S1359-6101(99)00024-6

Wu, Q., Allouch, A., Martins, I., Modjtahedi, N., Deutsch, E., & Perfettini, J.-L. (2017). Macrophage biology plays a central role during ionizing radiation-elicited tumor response. *Biomedical Journal*, *40*(4), 200–211. https://doi.org/10.1016/j.bj.2017.06.003

Wynn, T. A., & Barron, L. (2010). Macrophages: Master Regulators of Inflammation and Fibrosis. *Seminars in Liver Disease*, *30*(3), 245–257. https://doi.org/10.1055/s-0030-1255354

Xi, Y., & Xu, P. (2021). Global colorectal cancer burden in 2020 and projections to 2040. *Translational Oncology*, *14*(10), 101174. https://doi.org/10.1016/j.tranon.2021.101174

Xu, D., Li, M., Ran, L., Li, X., Sun, X., & Yin, T. (2023a). C5aR1 promotes the progression of colorectal cancer by EMT and activating Wnt/β-catenin pathway. *Clinical & Translational Oncology*, *25*(2), 440–446. https://doi.org/10.1007/s12094-022-02956-y

Xu, D., Li, M., Ran, L., Li, X., Sun, X., & Yin, T. (2023b). C5aR1 promotes the progression of colorectal cancer by EMT and activating Wnt/β-catenin pathway. *Clinical & Translational Oncology*, *25*(2), 440–446. https://doi.org/10.1007/s12094-022-02956-y

Xu, W., Yang, Z., & Lu, N. (2015). A new role for the PI3K/Akt signaling pathway in the epithelial-mesenchymal transition. *Cell Adhesion & Migration*, *9*(4), 317–324. https://doi.org/10.1080/19336918.2015.1016686

Xue, J., Schmidt, S. V., Sander, J., Draffehn, A., Krebs, W., Quester, I., De Nardo, D., Gohel, T. D., Emde, M., Schmidleithner, L., Ganesan, H., Nino-Castro, A., Mallmann, M. R., Labzin, L., Theis, H., Kraut, M., Beyer, M., Latz, E., Freeman, T. C., … Schultze, J. L. (2014). Transcriptome-Based Network Analysis Reveals a Spectrum Model of Human Macrophage Activation. *Immunity*, *40*(2), 274–288. https://doi.org/10.1016/j.immuni.2014.01.006

Xue, X., & Shah, Y. M. (2013). In vitro Organoid Culture of Primary Mouse Colon Tumors. *Journal of Visualized Experiments : JoVE*, *75*, 50210. https://doi.org/10.3791/50210

Yahyanejad, S., Theys, J., & Vooijs, M. (2015b). Targeting Notch to overcome radiation resistance. *Oncotarget*, *7*(7), 7610–7628. https://doi.org/10.18632/oncotarget.6714

Yang, C., Liang, Y., Liu, N., & Sun, M. (2023). Role of the cGAS-STING pathway in radiotherapy for non-small cell lung cancer. *Radiation Oncology*, *18*(1), 145. https://doi.org/10.1186/s13014-023-02335-z

Yang, J., Luo, Y., Tian, T., Dong, P., & Fu, Z. (2022). Effects of Neoadjuvant Radiotherapy on Postoperative Complications in Rectal Cancer: A Meta-Analysis. *Journal of Oncology*, *2022*, 8197701. https://doi.org/10.1155/2022/8197701

Yang, R., Sun, L., Li, C.-F., Wang, Y.-H., Yao, J., Li, H., Yan, M., Chang, W.-C., Hsu, J.-M., Cha, J.-H., Hsu, J. L., Chou, C.-W., Sun, X., Deng, Y., Chou, C.-K., Yu, D., & Hung, M.-C. (2021). Galectin-9 interacts with PD-1 and TIM-3 to regulate T cell death and is a target for cancer immunotherapy. *Nature Communications*, *12*(1), Article 1. https://doi.org/10.1038/s41467-021-21099-2

Yang, X.-Z., Chen, X.-M., Zeng, L.-S., Deng, J., Ma, L., Jin, C., Wang, R., Wang, M.-H., Wen, Y.-F., Wu, X.-L., Wang, H.-Y., & Cui, S.-Z. (2020). Rab1A promotes cancer metastasis and radioresistance through activating GSK-3β/Wnt/β-catenin signaling in nasopharyngeal carcinoma. *Aging*, *12*(20), 20380–20395. https://doi.org/10.18632/aging.103829

Yang, Y., Wu, M., Cao, D., Yang, C., Jin, J., Wu, L., Hong, X., Li, W., Lu, L., Li, J., Wang, X., Meng, X., Zhang, Z., Cheng, J., Ye, Y., Xiao, H., Yu, J., & Deng, L. (2021). ZBP1-MLKL necroptotic signaling potentiates radiation-induced antitumor immunity via intratumoral STING pathway activation. *Science Advances*, *7*(41), eabf6290. https://doi.org/10.1126/sciadv.abf6290

Yao, H., Wang, H., Li, C., Fang, J.-Y., & Xu, J. (2018). Cancer Cell-Intrinsic PD-1 and Implications in Combinatorial Immunotherapy. *Frontiers in Immunology*, *9*, 1774. https://doi.org/10.3389/fimmu.2018.01774

Ying, H., Kimmelman, A. C., Lyssiotis, C. A., Hua, S., Chu, G. C., Fletcher-Sananikone, E., Locasale, J. W., Son, J., Zhang, H., Coloff, J. L., Yan, H., Wang, W., Chen, S., Viale, A., Zheng, H., Paik, J., Lim, C., Guimaraes, A. R., Martin, E. S., … DePinho, R. A. (2012).

Oncogenic Kras maintains pancreatic tumors through regulation of anabolic glucose metabolism. *Cell*, *149*(3), 656–670. https://doi.org/10.1016/j.cell.2012.01.058

Yu, L., Guo, Q., Luo, Z., Wang, Y., Weng, J., Chen, Y., Liang, W., Li, Y., Zhang, Y., Chen, K., Chen, Z., Ding, Y., & Zhang, Y. (2022). TXN inhibitor impedes radioresistance of colorectal cancer cells with decreased ALDH1L2 expression via TXN/NF-κB signaling pathway. *British Journal of Cancer*, *127*(4), Article 4. https://doi.org/10.1038/s41416-022-01835-1

Yuan, Z., Fernandez, D., Dhillon, J., Abraham-Miranda, J., Awasthi, S., Kim, Y., Zhang, J., Jain, R., Serna, A., Pow-Sang, J. M., Poch, M., Li, R., Manley, B., Fink, A., Naghavi, A., Torres-Roca, J. F., Grass, G. D., Kim, S., Latifi, K., … Yamoah, K. (2021). Proof-of-principle Phase I results of combining nivolumab with brachytherapy and external beam radiation therapy for Grade Group 5 prostate cancer: Safety, feasibility, and exploratory analysis. *Prostate Cancer and Prostatic Diseases*, *24*(1), 140–149. https://doi.org/10.1038/s41391-020-0254-y

Zhan, T., Rindtorff, N., & Boutros, M. (2017). Wnt signaling in cancer. *Oncogene*, *36*(11), 1461–1473. https://doi.org/10.1038/onc.2016.304

Zhang, C., Cao, K., Yang, M., Wang, Y., He, M., Lu, J., Huang, Y., Zhang, G., & Liu, H. (n.d.). C5aR1 blockade reshapes immunosuppressive tumor microenvironment and synergizes with immune checkpoint blockade therapy in high-grade serous ovarian cancer. *Oncoimmunology*, *12*(1), 2261242. https://doi.org/10.1080/2162402X.2023.2261242

Zhang, F., Wang, H., Wang, X., Jiang, G., Liu, H., Zhang, G., Wang, H., Fang, R., Bu, X., Cai, S., & Du, J. (2016). TGF-β induces M2-like macrophage polarization via SNAIL-mediated suppression of a pro-inflammatory phenotype. *Oncotarget*, *7*(32), 52294–52306. https://doi.org/10.18632/oncotarget.10561

Zhang, L., Zhao, Y., Dai, Y., Cheng, J.-N., Gong, Z., Feng, Y., Sun, C., Jia, Q., & Zhu, B. (2018). Immune Landscape of Colorectal Cancer Tumor Microenvironment from Different Primary Tumor Location. *Frontiers in Immunology*, *9*, 1578. https://doi.org/10.3389/fimmu.2018.01578

Zhang, P., Gu, Y., Wang, J., Lv, K., Lin, C., Zhang, H., Li, H., He, H., Li, R., Liu, H., & Xu, J. (2023). Complement receptor C5aR1 blockade reprograms tumor-associated macrophages and synergizes with anti-PD-1 therapy in gastric cancer. *International Journal of Cancer*, *153*(1), 224–237. https://doi.org/10.1002/ijc.34474

Zhang, R., Liu, Q., Li, T., Liao, Q., & Zhao, Y. (2019). Role of the complement system in the tumor microenvironment. *Cancer Cell International*, *19*(1), 300. https://doi.org/10.1186/s12935-019-1027-3

Zhang, T., Wu, D.-M., Luo, P.-W., Liu, T., Han, R., Deng, S.-H., He, M., Zhao, Y.-Y., & Xu, Y. (2022). CircNEIL3 mediates pyroptosis to influence lung adenocarcinoma radiotherapy by upregulating PIF1 through miR-1184 inhibition. *Cell Death & Disease*, *13*(2), 167. https://doi.org/10.1038/s41419-022-04561-x

Zhang, Y., Alexander, P. B., & Wang, X.-F. (2017). TGF-β Family Signaling in the Control of Cell Proliferation and Survival. *Cold Spring Harbor Perspectives in Biology*, *9*(4), a022145. https://doi.org/10.1101/cshperspect.a022145

Zhang, Y., Lv, N., Li, M., Liu, M., & Wu, C. (2023c). Cancer-associated fibroblasts: Tumor defenders in radiation therapy. *Cell Death & Disease*, *14*(8), Article 8. https://doi.org/10.1038/s41419-023-06060-z

Zhao, F., Evans, K., Xiao, C., DeVito, N., Theivanthiran, B., Holtzhausen, A., Siska, P. J., Blobe, G. C., & Hanks, B. A. (2018). Stromal Fibroblasts Mediate Anti–PD-1 Resistance via MMP-9 and Dictate TGFβ Inhibitor Sequencing in Melanoma. *Cancer Immunology Research*, *6*(12), 1459–1471. https://doi.org/10.1158/2326-6066.CIR-18-0086

Zhao, Z., Chen, X., Dowbaj, A. M., Sljukic, A., Bratlie, K., Lin, L., Fong, E. L. S., Balachander, G. M., Chen, Z., Soragni, A., Huch, M., Zeng, Y. A., Wang, Q., & Yu, H. (2022). Organoids. *Nature Reviews Methods Primers*, *2*(1), Article 1. https://doi.org/10.1038/s43586-022-00174-y

Zheng, Z., Wieder, T., Mauerer, B., Schäfer, L., Kesselring, R., & Braumüller, H. (2023). T Cells in Colorectal Cancer: Unravelling the Function of Different T Cell Subsets in the Tumor Microenvironment. *International Journal of Molecular Sciences*, *24*(14), Article 14. https://doi.org/10.3390/ijms241411673

Zhong, W., Myers, J. S., Wang, F., Wang, K., Lucas, J., Rosfjord, E., Lucas, J., Hooper, A. T., Yang, S., Lemon, L. A., Guffroy, M., May, C., Bienkowska, J. R., & Rejto, P. A. (2020a). Comparison of the molecular and cellular phenotypes of common mouse syngeneic

models with human tumors. *BMC Genomics*, *21*(1), 2. https://doi.org/10.1186/s12864-019-6344-3

Zhong, W., Myers, J. S., Wang, F., Wang, K., Lucas, J., Rosfjord, E., Lucas, J., Hooper, A. T., Yang, S., Lemon, L. A., Guffroy, M., May, C., Bienkowska, J. R., & Rejto, P. A. (2020b). Comparison of the molecular and cellular phenotypes of common mouse syngeneic models with human tumors. *BMC Genomics*, *21*(1), 2. https://doi.org/10.1186/s12864-019-6344-3

Zhou, J., Lyu, N., Wang, Q., Yang, M., Kimchi, E. T., Cheng, K., Joshi, T., Tukuli, A. R., Staveley-O'Carroll, K. F., & Li, G. (2023). A novel role of TGFBI in macrophage polarization and macrophage-induced pancreatic cancer growth and therapeutic resistance. *Cancer Letters*, *578*, 216457. https://doi.org/10.1016/j.canlet.2023.216457

Zhou, S., Zhang, M., Zhou, C., Wang, W., Yang, H., & Ye, W. (2020). The role of epithelial-mesenchymal transition in regulating radioresistance. *Critical Reviews in Oncology/Hematology*, *150*, 102961. https://doi.org/10.1016/j.critrevonc.2020.102961

Zwirner, J., Fayyazi, A., & Götze, O. (1999). Expression of the anaphylatoxin C5a receptor in non-myeloid cells. *Molecular Immunology*, *36*(13), 877–884. https://doi.org/10.1016/S0161-5890(99)00109-1